Theoretical and experimental study of flow in annular vaneless diffusers.

El-Geresy, B. A.

Award date:
1982

Awarding institution:
University of Bath

THEORETICAL AND EXPERIMENTAL STUDY OF FLOW

IN ANNULAR VANELESS DIFFUSERS

Submitted by : B.A. El-Geresy
for the degree of Ph.D
of the University of Bath
1982

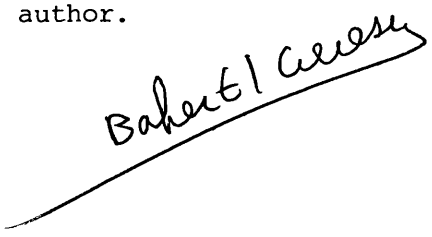

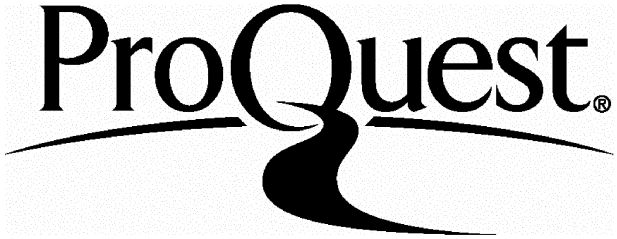

To my Family

SOURAYA

MAI, TAREK and KAREEM

ACKNOWLEDGEMENTS

The author wishes to acknowledge his very deep gratitude to Professor F.J. Wallace for his valuable guidance and to Dr. A. Whitfield for his thorough and helpful supervision during the performing and writing up of this work.

The author is indebted to Dr. T. David for his assistance in boundary-layer analysis reported in this thesis.

Acknowledgement is also due to the staff of the School of Engineering workshop and laboratories, University of Bath.

The author would also like to thank Mrs. H.J. Ford for her patience in typing the thesis.

Finally, the author wishes to express his sincere appreciation to his wife, Souraya, for her encouragement, patience and support.

SUMMARY

Annular vaneless diffusers have been studied both experimentally and theoretically to investigate their flow behaviour and performance.

The experimental work was carried out on large models of a conical diffuser and a curved diffuser with initial contraction. Besides steady inlet conditions a simulated impeller discharge flow with a jet-wake pattern was investigated. For both conditions of steady and unsteady flow the curved diffuser gave better performance and improved stability. The jet-wake flow proved to have no significant effect upon the performance of either diffuser.

The conical diffuser exhibited reversed flow on the hub which increased with mass flow reduction, and when the mass flow was low separation extended from outlet to inlet and strong low frequency pulsations of the flow were initiated. This pulsating flow phenomenon was explained as a rotating stall. Large areas of reversed flow or any flow pulsations were not detected in case of the curved diffuser.

An analytical direct solution of the inviscid flow through annular vaneless diffusers of any geometry was developed on the basis of the streamline curvature approach. The solution was obtained under the assumption of a linear distribution of flow parameters. The direct solution agreed quite well with known numerical methods and with experimental results up to separation. While separation itself was well predicted, the solution failed to predict any decrease in flow distortion which was observed experimentally; this was due to the nature of the assumptions within the inviscid analysis.

The direct inviscid solution was combined with a boundary layer calculation method from the literature to provide a simultaneous solution of the inviscid core and boundary layer interaction. The calculation method gave good results in the case of non-separated flows. It is felt that this calculation method could be further improved by the inclusion of separation and curvature effects in the boundary layer equations.

CONTENTS

NOMENCLATURE

A	cross-sectional area
AR	area ratio
b	diffuser width
b'	fluid width after separation eq.(2.29)
B	blockage factor eq.(1.11)
C	absolute velocity
C_f	wall shear stress coefficient $\tau_w/\frac{1}{2}\rho C^2$
C_K	twice the mean meridional velocity eq.(2.21)
C_p	pressure recovery coefficient
C_{p_i}	ideal pressure recovery coefficient
h	enthalpy
h_1,h_2,h_3	metric coefficients
H	boundary layer shape factor δ_1^*/θ_{11}
K_i,K_{ij}	curvature parameters eq.(B.9) (i=1,3), (j=1,3)
K1,K2,K3	calibration factors eq.(3.2,3.3 and 3.4)
K_s	coefficient of separation eq.(D.22)
m	meridional distance
$\dot{m},\dot{M}$	mass flow rate
n	normal distance
n	power-law velocity profile shape parameter
p	pressure
P_R	curvature parameter eq.(2.3)
q	dynamic pressure
r,R	radius
r_s	radius of separation eq.(2.28)
R_c	radius of curvature
RR	radius ratio
t	time
T	temperature
$\bar{V}$	velocity vector
α	slope of stream surface
α	coefficient of kinetic energy flux
β	skew angle
ψ	flow angle measured from meridional direction
γ	flow angle at the wall = $\psi + \beta$
λ	whirl = $C_\theta.r$

NOMENCLATURE cont'd

ρ	density
δ	boundary layer thickness
δ^*	displacement thickness
θ	momentum thickness
ε	residue eq.(2.32)
ζ	non-dimensional width $b/\bar{R}_c$
ξ	diffuser effectiveness eq.(1.8)
μ	dynamic viscosity
ν	kinematic viscosity
$\bar{\omega}$	loss coefficient eq.(1.6)
ϕ	diffuser cone angle
τ	shear stress

Subscripts

e	edge of boundary layer
J	normal line position
m	meridional
n	normal
r	radial
X	axial
θ	tangential
1	hub
2	shroud
$1'$	inlet
$2'$	outlet
S	streamwise
N	normal to streamline direction in stream surface plane
o	total or stagnation condition
s	static condition

Superscripts

$\overline{\quad}$	mean value
$'$	fluctuating value

Co-ordinate Systems

X,r,θ	cylindrical co-ordinate
X,Y,Z	curvilinear co-ordinate
u,v,w	velocities in boundary layer in X,Y,Z directions
U_e,V_e,W_e	velocities at the edge of boundary layer in X,Y,Z directions

CHAPTER 1 : INTRODUCTION AND LITERATURE REVIEW

1.1 Introduction

The diffuser is a fluid flow device used to convert kinetic energy into static pressure. The reduction in kinetic energy between inlet and outlet is transformed into static pressure and used to overcome losses due to turbulence and friction.

Whether the velocity reduction or static pressure rise is the primary objective of the diffuser will depend on the particular application. The use of the diffuser to increase pressure can be found in centrifugal compressor applications to increase stage efficiency, and downstream of a turbine to reduce back pressure, hence increase work output. If a diffuser is installed between a compressor and a burner of a gas turbine engine, its primary objective will be to reduce the velocity level of the stream to prevent the blowing out of the flame. In a closed circuit wind tunnel a diffuser is used to give a lower dynamic head, which in turn will reduce losses in downstream components.

To achieve its objective, the diffuser utilizes the principles of conservation of energy, mass and angular momentum. The difference in static pressure and kinetic energy between inlet and outlet will account for losses. One dimensional flow is diffused by increasing the cross-sectional area of the diffuser, i.e. utilizing conservation of mass principles. If the flow has a high degree of swirl, such as that at the discharge of a centrifugal compressor, the diffusion process can be achieved by increasing radius, thus utilizing the conservation of angular momentum with or without an increase in area.

The diffuser in a flow system may take any shape of wall and cross-section. Usually diffusers are classified according to their cross sectional geometry into the following :

(I) Two-dimensional (plane-walled) diffuser
(II) Conical diffusers
(III) Annular diffusers

The annular diffusers are mainly used in turbomachinery applications. For axial machines where the swirl is moderate or weak the cone angle is usually small, while for centrifugal compressors a high swirl is involved and diffusion is mainly due to a reduction in swirl velocity component, hence a large cone angle (180^{o} in radial diffuser) is used.

Different types of diffusers are shown in fig. 1.1. The geometrical relationship of two-dimensional and conical diffusers involves three parameters; area ratio, divergence angle ϕ and non dimensional length (L/W_i or N/W_i for two-dimensional diffusers and L/R_i for conical diffusers). For annular diffusers with different hub and casing cone angles two more parameters are needed. The latter fact makes systematic experimental investigation of the effect of geometrical parameters on annular diffusers a much more difficult task than for the other two types.

1.2 Evaluation of Diffuser Performance

Theoretical prediction of flow behaviour is possible for straight-wall diffusers having low-speed incompressible flow where the pressure gradient is moderate and the flow can mainly be considered potential. In engineering practice conditions usually encountered are more complicated, hence there is a need for more experimental investigations to establish diffuser performance and stability limit and to provide detailed experimental data from which a better understanding of the diffuser flow will be developed, which in turn, will help in constructing more complicated and realistic mathematical models for theoretical predictions.

1.2.1 Performance parameters

The usual measure of diffuser performance is the pressure recovery coefficient defined as the ratio of the rise in static pressure to the inlet kinetic energy. For a one dimensional flow through a straight-wall diffuser, the static pressure can be assumed constant through any cross-section. In that case the pressure recovery is

$$cp = \frac{P_2' - P_1'}{\frac{1}{2}\rho \bar{C}_1'^2} \qquad 1.1$$

where $\bar{C}_1'$ = mean inlet velocity.

To estimate how 'effective' a certain diffuser is, it is compared to an ideal diffuser with the same geometry. For these conditions the ideal pressure recovery is

$$cp_i = 1 - \frac{1}{AR^2} \qquad 1.2$$

and diffuser effectiveness ξ is defined as

$$\xi = \frac{c_p}{c_{p_i}} \qquad 1.3$$

In the more common case of a distorted inlet flow, while the mean velocity $\bar{C}$ will satisfy the continuity equation, it will not satisfy the energy equation and the kinetic energy flux co-efficient is usually introduced as

$$\alpha = \frac{1}{A} \frac{\int C^3 dA}{\bar{C}^3} \qquad 1.4$$

The energy equation is then

$$P_1' + \frac{\rho}{2} \alpha_1' \bar{C}_1'^2 = P_2' + \frac{\rho}{2} \alpha_2' \bar{C}_2'^2 + \text{losses} \qquad 1.5$$

and a loss parameter can be defined as

$$\bar{\omega}_{1-2}' = \frac{P_{O1}' - P_{O2}'}{\rho/2 \; \bar{C}_1'^2} \qquad 1.6$$

Substituting between equations 1.1, 1.5 and 1.6 yields the pressure recovery coefficient as

$$cp = \alpha_1' \left(1 - \frac{\alpha_2'/\alpha_1'}{AR^2}\right) - \bar{\omega}_{1-2}' \qquad 1.7$$

and the effectiveness as

$$\xi = \frac{\alpha_1' \left(1 - \frac{\alpha_2'/\alpha_1'}{AR^2}\right)}{1 - \frac{1}{AR^2}} - \frac{\bar{\omega}_{1-2}''}{1 - \frac{1}{AR^2}} \qquad 1.8$$

Sovran and Klomp (1) showed that $\xi < 1.0$ can result from either or both of :-

(I) $\alpha_2'/\alpha_1' > 1.0$ which represents the reduction in effectiveness due to insufficient diffusion.

(II) $\bar{\omega}_{1-2}' > 0.0$ which represents the reduction in effectiveness due to inefficient diffusion.

In centrifugal compressor diffusers the flow usually has a high swirling component and a major part of the diffusion process is achieved through the reduction of this velocity component. Schneider (2) and Wallace et al (3) showed that the ideal pressure recovery coefficient for swirling flow is given by

$$Cp_i = \cos^2 \bar{\psi}_1' \left(1 - \frac{1}{AR^2}\right) + \sin^2 \bar{\psi}_1' \left(1 - \frac{1}{RR^2}\right) \qquad 1.9$$

where RR is the radius ratio.

It can be seen that the coefficient of recovery is composed of two terms, one due to the meridional flow normal to the cross section and the other due to the component of velocity in the tangential direction. Fig. 1.2 shows a plot of equation 1.9 for inlet swirl angles of 40 and 70 degrees (3). When losses and flow distortion are included equation 1.9 becomes

$$Cp = \cos^2 \bar{\psi}_1' \alpha_1' \left(1 - \frac{\alpha_2'/\alpha_1'}{AR^2}\right) + \sin^2 \bar{\psi}_1' \alpha_1' \left(1 - \frac{\alpha_2'/\alpha_1'}{RR^2}\right) - \bar{\omega}_{1-2}' \qquad 1.10$$

Maps for diffuser performance were established through extensive experimental work. Fig. 1.3a represents a map for two dimensional diffusers by Reneau et al (4), Fig.1.3b for conical diffusers by Cockrell and Markland (5) and fig. 1.4a for annular conical diffusers by Sovran and Klomp (1).

The optimum pressure recovery lines Cp* and Cp** are defined as follows :

Cp* is the locus of points which define the diffuser area ratio producing maximum pressure recovery for a constant non-dimensional length.

Cp** is the locus of points which define the diffuser non-dimensional length producing maximum pressure recovery for a constant area ratio.

Fig. 1.4b compares these optimum lines for various diffuser types (1).

1.2.2 Flow regimes and stability

Another feature which is important in most diffuser applications is the steadiness and uniformity of diffuser discharge flow. Separation affects diffuser performance also because of the losses that are usually associated with it. A particular example where steadiness of discharge flow is important can be found in cases where a compressor is located near the diffuser discharge since the performance of the compressor is sensitive to inlet flow conditions.

Kline et al (6) identified four flow regimes for two dimensional diffusers. Later Reneau et al (4) presented flow regimes as function of overall diffuser geometry as shown in fig. 1.5a. These regimes are :

(I) Region below a-a line represents steady flow with no appreciable stall.

(II) Region between line a-a and line b-b where unsteady flow with large transitory stall exists.

(III) Region between line b-b and d-d where steady fully developed two dimensional stall dominates.

(IV) Region above line c-c represents jet flow.

The region between line d-d and c-c represents a hystrises zone. Line a-a is called "line of first appreciable stall". A comparison of location of a-a line and Cp* line between two dimensional and

conical diffuser was done by McDonald and Fox (7) and shown in fig. 1.5b. It can be seen from the figure that the Cp* line lies close to the a-a line which means that for the two kinds of diffusers maximum recovery is achieved where conditions are close to stall conditions. However, similar data for annular diffusers is not available.

1.3 Review of Experimental Investigation

While two-dimensional and conical diffusers enjoyed extensive experimental investigation, annular diffuser investigations lacked the same systematic and detailed study until a decade ago. This is attributed to the extensive experimental work required for systematic testing of the many geometric and flow parameters involved. The interest in designing more efficient turbomachinery stages, especially centrifugal and axial flow compressors, stimulated more research to be focused on this type of diffusers.

The main effort in this review will be devoted to annular diffusers of axial and centrifugal flow. A good summary of the available data on two-dimensional and conical diffusers can be found in the work of Cockrell and Markland (5) and Runstadler et al (8). McDonald and Runstadler (9) tried to relate available design information on diffusers to problems encountered by designers using the two-dimensional diffuser as a "base line" for their assessment.

A diffuser can be considered as an element having two main input parameter groups :

(1) Geometric parameters
(2) Inlet flow parameters

These two input parameters affect diffuser behaviour measured by the two output parameters.

(1) Performance
(2) Flow regimes and stability.

Boundary layer control can be considered as another parameter

affecting diffuser behaviour. Fig. 1.6 shows a detailed account of various parameters. An interaction will take place between all parameters with a feedback effect which is difficult to isolate, hence it will be included in this review implicitly.

1.3.1 Geometric parameters

A detailed systematic treat of annular diffusers of axial flow type is given by Sovran Klomp (1) to assess the effect of geometric parameters on performance. A typical performance map is shown in fig. 1.4a. Flow regimes of axial flow annular diffusers were investigated by Howard et al (10) for fully developed inlet flow. For convergent centre body diffusers, the line of first appreciable stall was close to that for two dimensional diffusers, while its fully developed stall line lay significantly lower. The stall lines for a diffuser with a constant diameter centre body were located between those of conical and two-dimensional diffusers.

The use of a curved rather than a straight wall diffuser stems from (i) mechanical construction requirements, if the diffused flow is carried around bends, (ii) from consideration of overall axial length or (iii) to modify the flow behaviour using streamline curvature effects. A typical curved annular diffuser application is that installed prior to a gas turbine combustion system. Stevens and Fry (11) found that, for an annular diffuser, the inlet bend distorted the velocity profile which was distorted further by the diffusion process. Thayer (12) showed that a short diffuser employing curved annular walls following a turbine can have high performance besides acting as a shield for hot engine parts to reduce vulnerability of military aircraft to a heat-seeking missile.

Centrifugal compressors usually utilize either a vaned or vaneless diffuser. Vaned diffusers are more efficient than vaneless ones but they do not offer as wide a flow range as the vaneless diffusers, so efficiency, in some cases, is traded for a wider range of operation.

For vaned diffusers, the similarity in behaviour between the well

established two-dimensional and conical diffusers and the channel diffusers of the vaned space gives the designer a valuable guide for vaned diffuser design. In vaneless diffusers no such resemblance exists and separate investigations had to be carried out.

One of the early attempts in investigating geometric effects of the vaneless diffuser of centrifugal compressors is due to Barina (13) who showed that conical and curved diffusers will have similar performance. Sakai et al (14) obtained the same results and showed that while performance was very similar, flow regimes were completely different. A conical diffuser had separation only on the hub side, while the curved diffuser exhibited a flow pattern with separation on both hub and shroud walls occurring alternatively.

The problem of separation in centrifugal compressor diffusers is a main concern because of increased losses and unsteady operation associated with it. Polyakov and Bukatykh (15) tried to define an optimum radial vaneless diffuser profile theoretically to give separation-free flow. The proposed profile had a constant width at entry followed by a converging part.

The idea of having a radial diffuser with non-parallel walls simulated many research programs resulting in some contradicting conclusions. Brown and Bradshaw (16) first suggested a configuration having a converging inlet section to accelerate jet-wake mixing into a steady uniform flow, followed by a second diverging part to increase the diffusion process. Sherstyuk and Kosmin (17) showed that a contracting inlet was beneficial for radial diffusers especially if profiled, and an optimum contraction value existed for maximum stage efficiency. Watson and Ingham (18) investigated different radial diffuser profiles having convergent-divergent, convergent-parallel, or parallel walls. While all configurations gave similar pressure recovery, the parallel walled diffuser gave a more uniform outlet velocity profile. However, theoretical investigations by Volov and Shakhov (19) suggested that a convergent or convergent-divergent walled diffuser would give better performance than a parallel one.

Combining contraction with curvature was investigated by Whitfield

et al (20), for a mixed flow compressor. The diffuser with initial contraction gave better stage efficiency at optimum operating conditions over the constant width diffuser. That conclusion was supported theoretically by an inviscid analysis developed by Wallace et al (21) and experimentally by testing six-times full size models of the above mentioned curved diffusers by Barbotin (22), although the inlet flow for the latter diffuser models was severely distorted owing to the test rig design.

For two dimensional diffusers Carlson et al (23) showed that contouring the walls offered little advantage. Fox and Kline (24) and Sagi and Johnston (25) investigated curved two dimensional diffusers and found a rapid drop in allowable area ratio as the turning angle was increased (24). It was also concluded that the performance of a curved diffuser is below that of a straight walled one having the same area ratio and L_{in}/W_1, where L_{in} is the length of inner wall and W_1 is the width of the diffuser between diverging walls at inlet, even for similar observed flow pattern (25).

1.3.2 Inlet flow parameters

Diffusers performance and flow regimes were mainly assessed as a function of gross geometrical parameters as shown in figs. 1.3a, 1.3b, 1.4a, 1.5a and 1.5b. However, to assume that diffusers designed from these maps will always give good results is not true since inlet flow conditions can also have marked effects on diffuser stability and performance.

The following inlet flow parameters will be considered

(i) spatial distortion
(ii) swirl
(iii) temporal distortion
(iv) Reynolds number, Mach number, turbulence level and mixing.

(i) Spatial distortion

The through flow in a diffuser can be divided into a boundary

layer and a centre inviscid core flow. A distortion in inlet flow will occur due to the boundary layer build up along the walls plus any core flow distortion. The two distortions can be expressed as a velocity profile distortion.

(a) Boundary layer thickness can be seen as if the diffuser was partially blocked and its walls were contracted to carry the same mass flow rate at a uniform maximum inlet velocity. Blockage factor B is defined as a ratio of cross sectional area which is considered blocked due to the boundary layer effect to the geometrical area

$$B = \frac{\text{Blockage Area}}{\text{Geometrical Area}} = 1 - \frac{\text{Effective area}}{\text{Geometrical area}}$$

$$B = \frac{A_B}{A} = 1 - \frac{A_E}{A} \qquad 1.11$$

Increased blockage was usually associated with a deterioration in performance as reported by Waitman et al (26), and Runstadler et al (8) for two dimensional and conical diffuser and Moller (27) for radial diffusers. However, some investigators found that trend reversed in some cases. Coladipietro et al (28) found that a short annular conical diffuser gave better formance for thin inlet boundary layers, while for a long diffuser thick inlet boundary layers gave better performance than thin boundary layers. Bradshaw (29) suggested as an explanation for a similar trend reported by Cockrell and Markland (30) that when the entry boundary layer is fully developed, the flow is more capable of radial momentum transference far down the diffuser than when the entry boundary layer is thin and thus the downstream velocity profile is improved giving better performance. For two dimensional stalled diffusers Johnston and Powers (31) noticed the same phenomena. Eckert et al (32) found for annular conical diffusers that the blockage versus pressure recovery curve was parabolic having double values as shown in fig. 1.7. Two levels of radial distortion as seen from the figure can produce the same pressure recovery. Earlier observation of this trend was reported by Tyler and Williamson (33) for conical diffusers.

(b) Core distortion

While boundary layer distortion is commonly expressed by the blockage factor, there is no similar parameter to express the core flow distortion alone. The kinetic energy flux coefficient α will account for the overall velocity profile distortion. One can express a core distortion by the ratio of its maximum to its mean velocity, but in this case one may consider "equal" two profiles which might give totally different behaviour, such as a jet profile and a wake profile. Usually distortion of the core is expressed in a qualitative rather than a quantitative manner, e.g. descriptions such as uniform, shear, step shear, jet and wake flow are used.

The diffusion process is usually considered to accentuate any velocity profile distortion. Using an inviscid analysis and assuming static pressure to be constant across any cross-section, to achieve a certain pressure rise the flow along each streamline must offer the same amount of kinetic energy reduction. If two fluid elements on two streamlines a and b start with a certain velocity difference at location 1, and end up at location 2 then

$$P_{o_a} = P_{1_a} + \rho/2 \; C_{1_a}^2 = P_{2_a} + \rho/2 \; C_{2_a}^2$$

$$P_{o_b} = P_{1_b} + \rho/2 \; C_{1_b}^2 = P_{2_b} + \rho/2 \; C_{2_b}^2$$

where $P_{o_a} > P_{o_b}$, $P_{1_a} = P_{1_b}$, $P_{2_a} = P_{2_b}$ (constant pressure)

$$\therefore \; P_{2_a} - P_{1_a} = P_{2_b} - P_{1_b}$$

$$\therefore \; \rho/2 \; (C_{1_a}^2 - C_{2_a}^2) = \rho/2 \; (C_{1_b}^2 - C_{2_b}^2)$$

$$(C_{1_a}^2 - C_{1_b}^2) = (C_{2_a}^2 - C_{2_b}^2)$$

$$\therefore \; (C_{1_a} - C_{1_b}) \; (C_{1_a} + C_{1_b}) = (C_{2_a} - C_{2_b}) (C_{2_a} + C_{2_b}) \qquad 1.12$$

for a diffusion process $(C_{1_a} + C_{1_b}) > (C_{2_a} + C_{2_b})$

and it then follows that

$$(C_{2_a} - C_{2_b}) > (C_{1_a} - C_{1_b}) \qquad 1.13$$

This shows that a distorted velocity profile will be accentuated by diffusion. Referring to equation 1.7 this means α_2' will be higher than α_1', the greater α_2' the less cp will be for a constant α_1' and $\bar{\omega}_{1'-2'}$. Sovran and Klomp (1) argued that the problem of many diffusers is due to insufficient diffusion (i.e. α_2'/α_1' high) rather than to inefficient diffusion (i.e. $\bar{\omega}_{1'-2'}$ high).

If turbulence mixing existed, the inviscid flow analysis is not valid and distortion may in fact be attenuated. Masuda et al (34) studied a shear flow behaviour between the parallel walls of a two dimensional diffuser. Their experimental results showed a constant decay in the velocity profile distortion through the diffuser while the inviscid analysis gave an opposite trend. Quinn (35) and Viets (36) explained this phenomena on basis of a mixing effect. Viets (36) concluded that the diffusion in the plane of the velocity profile inhibits the mixing process while diffusion normal to that plane enhances this mixing process.

The most important inlet distortion in an annular diffuser is the energy or total enthalpy or total pressure gradient. The tendency for separation will be on the wall having low inlet total enthalpy even if the inlet meridional velocity showed initial separation on the other wall at inlet. This effect was confirmed by Ellis (37) who changed the inlet total pressure gradient to a radial diffuser by cutting back the impeller tip, and Sakai et al (14) for a conical mixed flow diffuser by different angled rotating screen. When this gradient was taken into account in an inviscid solution to the flow, separation was well predicted by Rebernik (38) and Ellis (37).

While the above researchers changed inlet conditions by controlling the mass flow rate or the design of the upstream element, other investigators changed inlet conditions by an artificial means called a flow spoiler or a velocity profile

generator. However, any artificial obstacle in the flow path will alter its turbulence structure, increase mixing, and cause losses. Eckert et al (32) found that an artificial flow distortion will degrade an annular conical diffuser performance, while for a straight core annular diffuser Williams (39)using a coarse grid and a flow spoiler at inlet reported favourable effect on stability and performance. Klein et al (40) found the losses associated with a compressor cascade of blades for a dump diffuser increased substantially as distance from the diffuser entrance was reduced. There was an optimum position with minimum losses, and by removing the cascade from that optimum position losses were increased by 30%. However, Eckert et al (32) pointed out that any beneficial effect recorded on performance by means of artificial distortion is apparent rather than real, and a total pressure loss which is created will appear only after complete flow mixing downstream and will offset the gain in pressure recovery.

For two dimensional diffusers, Wolf and Johnston (41)studied the effect of different inlet profiles on performance and stall characteristics. Profiles having a low velocity region near one or both walls such as uniform, step shear and jet flow showed a decrease in performance compared to the uniform inlet profile, while the wake distortion showed an increase in performance. Different profiles showed different stall characteristics, profiles having a high velocity on one wall exhibited a stable stall on the low velocity side. For jet flow bi-stable stall switched from one wall to the other. For large area ratio diffusers the wake profile caused centre stall in the core. Kaiser and McDonald (42) confirmed the effect of wake profile on stall characteristics.

(ii) Swirl

In many turbomachinery applications, particularly radial machines, an annular diffuser will have to handle flow with a swirl component. The swirl angle, measured from the meridional direction can be as high as 70 degrees or more at the inlet of a centrifugal compressor

diffuser. Hoadley (43), Srinath (44), and Kumar and Kumar (45) reported a direct effect of swirl on the stall characteristics in an annular axial flow diffuser. A stall on the shroud was eliminated by introducing swirl and further increases in swirl caused the stall to appear on the hub. This was attributed to a centrifugal force created by the swirl component which pushed the flow towards the shroud or casing. At swirl angles in excess of 70 degrees Jansen (46) reported a rotating stall in a radial vaneless diffuser.

Annular diffuser performance was reported to increase slightly with swirl then decrease with further increase in swirl angle. This was observed by James (47) for radial diffuser over a range of swirl angle from 20° to 70° with optimum performance around 30°. Hoadley (43), Srinath (44), Kumar and Kumar (45), and Japikse and Pampreen (48) reported a similar effect for straight walled annular axial flow diffusers. Gardow (49) reported a decrease in performance for swirl angles between 45° and 65° which agrees with the results of James (47). However Schneider (2) testing equiangular annular diffuser for swirl angles between 0° and 25° reported an opposite trend with the pressure recovery-swirl angle curve having a minimum. For curved diffusers tested by Japikse and Pampreen (48) at similar conditions to the straight wall diffuser, performance showed consistant reduction with swirl.

The cone angle of annular diffuser of axial flow type which will give maximum pressure recovery was reported to increase progressively with swirl angle increasing. Lohman et al (50) and Srinath (44) found optimum conditions when the cone angle was approximately equal to the swirl angle. Lohman et al (50) further observed that the angular momentum of the flow tended to be conserved through the diffuser. The same observation was made by Honami et al (51).

For conical diffusers a general improvement in performance by the introduction of swirl was observed by McDonald et al (52), Neve and Wirasinghe (53) and Senoo et al (54).

(iii) Temporal distortion

In most turbomachinery applications annular diffusers will receive unsteady flow at their inlet with large scale distortions. Most important of these distortions is the impeller blade effect or the jet-wake distortion. If the flow coefficient becomes small, compressor rotating stall can be initiated and presented at the inlet to the diffuser. Rotating stall can be initiated in the diffuser itself and not as an inlet condition.

(a) Jet-wake distortion

The discharge flow from an axial or centrifugal compressor will be characterised by circumferential distortions consisting of regions of high and low relative velocity.

Dean and Senoo (55) and Johnston and Dean (56) developed two different methods to account for the mixing of the jet-wake systems and the losses associated with it. Both models predicted almost similar losses although they were physically different. While Dean and Senoo (55) based their analysis upon reversible work exchange between jet and wake, Johnston and Dean (56) used a sudden expansion process at inlet to account for the losses. Inoue (57) tried to identify differences between these models and showed that the predictions by the two theories were close when the distorted flow pattern was rotating, but if the wakes were stationery, the Johnston and Dean model predicted lower losses than Dean and Senoo model. Later Inoue and Cumpsty (58) constructed a model using a general approach by Baade (59) assuming small disturbancies to the flow equation. Unlike Dean and Senoo they allowed the flow angle to vary circumferentially without imposing an inlet static pressure pattern. They showed that due to the effect of relative flow angle variation, their model gave similar results to that of Dean and Senoo (55) for case of large blade numbers, while for small blade numbers the two models gave different predictions.

While the Dean and Senoo (55) model predicted complete mixing of the jet and wake at a small radius, Mates (60), Baade (59)

Watson and Ingham (18), and Eckardt (61) found experimentally that complete mixing did not occur until a much larger radius.

Baghdadi (62) tried to account for the effect of this non-uniformity on vaned radial diffuser performance. He tested the same diffuser coupled with an impeller, and with a vortex nozzle facility to simulate outlet from the compressor without the jet-wake system. Nearly identical performance in both cases suggested that the effect of rotating wakes on diffuser performance were trivial. In their discussion to that work, Fister and Muller confirmed the author's conclusion by their own experimental findings. The same results were reached by Adenubi (63) for an annular diffuser downstream of an axial compressor.

Senoo and Ishida (64) tried to clarify the mechanism of decay of the rotating wakes in vaneless diffusers by using a severely asymmetric flow created by blocking every other passage of a centrifugal impeller with a punched plate. They observed that the shear force between the jet and wake regions did not contribute much to the decay of the distortion. They concluded that the major part of the total pressure loss was due to wall friction. The reversible work exchange was considered the main factor in the mixing of jet-wake system.

(b) Diffuser rotating stall

The phenomena of rotating stall in a vaneless diffuser will be initiated if the mass flow rate at the inlet to the diffuser is low compared to the design flow. Some reports about this phenomena in vaneless radial diffusers suggested that the phenomena occurs prior to system surge (65, 66). The mechanism of initiation of the phenomena is not clear and various suggestions exist. Jansen (65) suggested that the phenomena will be initiated if a three dimensional flow separation existed in the radial diffuser, while Imaichi and Tsurusaki (67) found that the rotating stall started after the back flow occupied a certain radial portion on the diffuser wall.

Abdel hamid and Bertrand (68) studying the effect of diffuser geometry on the phenomena found that the higher the radius ratio and the smaller the width of the diffuser, the more likely that rotating stall will occur at a given flow rate. An analytical investigation by Senoo and Kinoshita (69) agreed with the results of Abdel hamid and Bertrand. Imaichi and Tsurusaki (67) studied the effect of a hydraulic resistance at the diffuser outlet upon the phenomena. By fitting a wire net of increasing mesh number at the exit of the diffuser, they successfully decreased the critical flow coefficient and when a porous belt was used, they could eliminate the phenomena at any flow rate. The latter indicate the importance of the downstream component on diffuser rotating stall characteristics.

The rotating stall cells varied according to the operating conditions. Jansen reported two cells for inlet flow angles around 70^{o}, and at flow angles approaching 90^{o} the number of cells were reduced to one. Abdel hamid et al (66), (68) observed also cells number between one and two.

The two theoretical attempts to analyse the phenomena are due to Jansen (65) and Abdel hamid (70), both of whom considered the flow as a superposition of a steady inviscid and unsteady one. Senoo and Kinoshita (69) tried to establish a criteria for the phenomena without analyzing it in detail and, as mentioned above, succeeded in predicting the correct geometrical effect.

(iv) Reynolds number, Mach number, turbulence and mixing

The effects of these parameters overlap to a certain degree and may be difficult to isolate. An increase in inlet Reynolds number will increase Mach number, and alter the velocity profile and turbulence structure.

For radial diffuser having radial flow without swirl Moller (27) found that a decrease in Reynolds number will decrease pressure recovery. Runstadler and Dolan (71) arrived at the same conclusion for two dimensional diffusers. Runstadler and Dean (72)

showed that for straight wall diffuser there was no subsonic critical Mach number above which a precipitious decrease in pressure recovery occurs. However, at high Mach number shock and boundary layer interaction will result in boundary layer separation causing a degradation in performance.

While turbulence will enhance mixing, thus improve diffuser performance, artifically created turbulence will create losses which can offset gains from associated mixing as pointed out by Eckert et al (32). However, Williams (39) and Stevens and Williams (73) for annular axial diffusers, Bradley and Cockrel (74) for conical diffusers and Norbury (75) and Livesey and Turner (76) for two dimensional diffusers, reported a favourable effect upon performance of artifically created turbulence and artifically created boundary layers.

1.3.3 Conclusion

From this review it is concluded that, while more research is being done in the annular diffuser field, the majority of these investigations are centred around the axial flow type. Existing reports on annular vaneless diffusers still lack systematic approach and most of them are concentrated on the radial type. Very few reports exist on conical and curved vaneless annular diffusers. The effect of different inlet flow conditions including the effect of the jet-wake pattern is an area which is little explored.

1.4 Review of Calculation Methods for Annular Diffusers Flow

For an annular diffuser downstream of a centrifugal compressor the flow has high swirl, is distorted between the two walls, has a jet-wake pattern circumferentially, and boundary layers developing against a positive pressure gradient which might lead to separation or rotating stall. The nature of this flow is three dimensional, asymmetric, viscous and unsteady. Since no general solution for such complicated flow is available, simplifying assumptions have to be made. The various models available can be classified into two main

categories :-

(i) Inviscid and simple models

(ii) Boundary layer models.

1.4.1 Inviscid and simple models

Since no adequate analytical solution has been found for the inviscid flow through a diffuser, several numerical solutions of the inviscid equations of motion have been developed. Although all methods of numerical solution are physically similar, they differ in the way they treat the equations. Generally, there are two well developed methods, a Matrix method and a streamline curvature method. A comparison between the two methods for axial flow turbomachinery was presented by Davis and Millar (77). In the matrix method a fixed grid is superimposed on the area of interest and finite difference equations are written for each grid point. The resultant set of algebraic equations can then be arranged in a matrix form for the solution. In the streamline curvature method the flow is divided into several stream tubes which are traced through the passage. The streamline grid changes after every iteration. While the equations are generally solved in terms of a stream function in the matrix method, the solution is in terms of velocities in the streamline curvature methods. Examples of the matrix method are due to the work of Ellis (37) and Marsh (78) and of streamline curvature methods due to Wallace et al (21). A different approach in solving inviscid equations was adopted by Rebernik (38) in which the change in flow properties across the diffuser width were expressed in polynomial functions. A finite element approach was developed by Hirsch and Warzee (79) for axial flow machines and proved to predict similar results to the streamline curvature method for a curved annular-axial diffuser. In the discussion of the same work (79) Chen presented a general comparison between streamline curvature, finite difference and finite element methods.

Ellis (37) and Rebernik (38) demonstrated the importance of the total pressure distribution at the diffuser entry by predicting separation correctly. However both of these solutions failed to predict the behaviour of the flow after separation. In both predictions the

distortion of flow field increased continuously after separation, while experimental results indicated a decrease in distortion beyond a certain point which led in some cases to the development of separation on the opposite wall. Hoadley (43) used the Marsh matrix method (78) to predict the swirling flow in an annular diffuser of the axial flow type. While experimental data showed separation on the hub shortly after the inlet, the predicted axial velocity distributions remained almost uniform across the width at all axial positions.

Wallace et al (21) developed a streamline curvature method to predict the inviscid flow behaviour of vaneless diffusers of different geometries. They showed by calculated examples the advantage of curvature and initial contraction on flow stability and the effect of inlet total enthalpy gradient presented by different cut-off impellers designs. These results agreed with those of Rebernik (38) with respect to the effect of inlet total pressure gradient, and were confirmed experimentally by Sakai et al (14). However, the computation method was not capable of calculating the flow field after an inviscid separation and separation itself could not be predicted precisely due to the failure of the computation method to converge when velocities near a wall approached zero.

To account for the effect of wall and internal friction many investigators combine a simple analysis of the flow with a coefficient of friction to calculate mean flow parameters along the diffuser. Bammert et al (80) assumed a dissipation coefficient which consists of a wall friction component and an internal friction component which was assumed as a decay function dependent upon the inlet tangential Mach number. Good prediction of mean flow values was found for cases where the boundary layer did not merge before the exit. Johnston and Dean (56) obtained satisfactory results with one dimensional axisymmetric friction loss analysis for radial diffusers; however they observed that total coefficient of friction varied in real cases between 0.01 and 0.05 and they were not able to give a firm figure to be used. Baghdadi showed in the discussion of the boundary layer method presented by Senoo et al (81) that a simple one

dimensional analysis with friction coefficients can predict pressure recovery as good as a more detailed and complicated boundary layer analysis.

Although these simple methods could predict pressure distribution along the diffuser in most cases, they were not capable of defining flow behaviour and are not satisfactory in the determination of flow distortion or separation. An attempt to do this was carried out by Marsh (78) by specifying loss parameters or changes in entropy and body force in conjunction with the inviscid analysis. Atkey (82) developed a similar computation method using the streamline curvature approach to calculate the non-isentropic flow in centrifugal compressor stages by introducing a dissipative friction force. Friction coefficients were assumed between various stream tubes and between walls and adjacent streamtubes to account for wall and internal friction. Barbotin (22) extended this method and used it for flow analysis of annular vaneless diffusers and was able to predict velocity distribution similar to some of his experimental results. However, the friction coefficient used in these methods had to be adjusted arbitrarily to suit a particular case, and since there was no correlation between the values and inlet and geometric parameters, the use of this method is rather limited.

1.4.2 Boundary layer models

Unlike boundary layer growth in a free stream, the interaction between core flow and boundary layer has to be considered in an internal flow problem such as diffuser flows. All models considered in this review belong to the momentum integral type, they are physically similar, but differ in their auxiliary equations and in the way they consider the interaction with the core flow. From the latter point they can be classified into three main approaches. The first approach is to substitute for the core flow from experimentally specified conditions, hence solve the boundary layer equations only e.g. Hoadley (43). A second approach is to solve the boundary layer equations allowing for the core flow influence by simple relations from either or both of energy and tangential momentum equations, e.g. Voorde and Bos (83), Jansen (46) and Senoo et al (81). The third

approach is to use an iterative solution for complete interaction between core flow and boundary layer flow e.g. Davis (84). Other researchers disregarded the core flow completely by considering the flow after the merging of the boundary layers, but had to assume symmetrical conditions, e.g. Kawaguchi and Furuya (85) and Antonia (86).

Hoadley (43) used an entrainment method with a prescribed static pressure distribution from experimental data and Cole's velocity profile. His results showed good agreement with his experimental results; however, the limitation of the method was clearly in predicting boundary layer growth in a non-specified static pressure field. The possibility of coupling the method with an inviscid solution was, however, mentioned.

The method of Voorde & Bos (83) was also an entrainment one, but for non-swirling flow in radial diffusers. Using Cole's velocity profile, they succeeded in predicting their own experimental results. The method, however, is extremely limited since it could only handle non-swirling flows. Jansen's model (46) could handle a highly swirling flow using a constant power law velocity profile in tangential direction and a radial profile to fit his range of data allowing a change in shape factor. The flow was considered axisymmetric through the diffuser and a condition of wall separation was imposed when the boundary layer filled the passage. The main criticism of this method was laid on the latter assumptions and on the fact that the model did not satisfy the momentum equation in the radial direction. However, a good prediction of the author's experimental results was demonstrated. Senoo et al (81) considered the non-symmetric inlet flow represented by tangential and radial velocity profile gradients assuming linear distributions of velocities in the core. The solution satisfied the energy and conservation of angular momentum equations at the core edges to obtain gradients for the velocities in the core. A power low velocity profile was assumed for the streamwise velocity component with a variable shape parameter which was a function of the boundary layer thickness based upon Reynolds number. A modified Mager (87) profile was used for the cross flow velocity component. The method was capable of predicting oscillating flow between the two walls and by

some assumptions the solution was extended to the region where boundary layers filled the passage. Senoo was able to show good prediction for a number of test cases but his solution for the downstream part where the inviscid core disappears lacked strong physical support. The method was not capable of predicting flow with varying static pressure across the passage and no account was made for the effect of streamline curvature. Generally, the method was limited to highly swirling flow in straight walled radial diffusers.

The possibility of the third approach was investigated by Stastny and Feistauer (88). The prediction of an annular axial - radial diffuser was reasonable for cases of non-separating flow. Davis (84) used a finite difference solution of the inviscid core together with a momentum integral boundary layer calculation based on the entrainment concept. The boundary layer equations were reduced to a set of three ordinary differential equations. Cole's two parameter streamwise velocity profiles were used. The solution of the through-flow in the duct was obtained in an iterative fashion by allowing the core flow to influence the boundary layer growth in one cycle, and in the next cycle the boundary layer was allowed to influence the core flow until convergence of all parameters. The solution of the boundary layer was extended to regions of separation and re-attachment by adjusting some terms in the solution. Although the latter assumptions lacked physical support, the method was capable of calculating a separated and re-attached flow in a return bend. For vaneless radial diffusers good prediction by the iterative solution was demonstrated. However, when the data of Hoadley (43) for an annular conical diffuser of axial flow type was compared to the iterative solution, the separation was predicted far downstream on the casing and not shortly after the inlet on the hub as the expterimental results had shown. With a prescribed static pressure, the non-iterative solution gave good results similar to those of Hoadley (43).

For static pressure prediction in radial diffuser flows where the boundary layer fills the passage, a symmetric solution in which

boundary layer thickness is constant and equal to half the passage width was tried by Kawaguchi and Furuya (85). By assuming the swirl angle to be constant along the diffuser, a relation governing the static pressure variation in the radial direction was obtained by integrating the momentum and continuity equations. Good agreement was found for symmetric flow cases only. Antonia (86) used a similar approach to that of Kawaguchi and Furuya (85) but assumed a weak swirl with free vortex conditions. He obtained a simple expression for static pressure variation which showed reasonable agreement in cases where the assumptions of symmetric flow and weak swirl were sound. These two models were restricted to symmetric flow and are not capable of predicting flow behaviour or the detailed flow field.

1.4.3 Conclusion

From this review it was concluded that :

(a) For inviscid flow solutions ;

(i) the streamline curvature solution reported by Wallace et al (21) was not as reliable as finite difference methods in dealing with separated flows.

(ii) the merits of the inviscid solution after separation are not fully understood where distortion continues to increase downstream of separation (37) and (38).

(iii) there is no general assessment for the effect of the various geometric and inlet flow conditions although some are available from specific examples using a streamline curvature solution (21).

(iv) most of the above difficulties stems from the fact that there is no reliable and simple analytical solution for the inviscid flow.

(b) For boundary layer solutions :

(i) a full interactive solution was attempted by only one investigator (84)

(ii) few models exist that can handle asymmetric flow conditions, most of them are restricted to radial diffusers only.

(iii) no attempt has been made to handle the full interactive solution of the inviscid core and boundary layer simultaneously, hence

reduce computational difficulties and errors in a similar manner to that of Ghoose and Kline (89) for two dimensional diffusers.

(iv) momentum integral solutions in the case of separated, re-attached, and merged boundary layer flows lack generality and strong physical support.

1.5 Main Objectives of the Present Work

The objectives of the investigations carried out in this work :

(i) to investigate the flow behaviour and estimate performance of conical and curved diffusers under highly swirling flow conditions similar to real conditions in centrifugal compressor stages.

(ii) to compare the behaviour of the two diffuser configurations under varying inlet conditions.

(iii) to verify the effect of a jet-wake flow pattern at the inlet upon the performance and flow behaviour of the two configurations.

(iv) in parallel with the test series, to develop a solution to the inviscid flow and couple it with a boundary layer analysis of the momentum integral type in a simultaneous interactive manner.

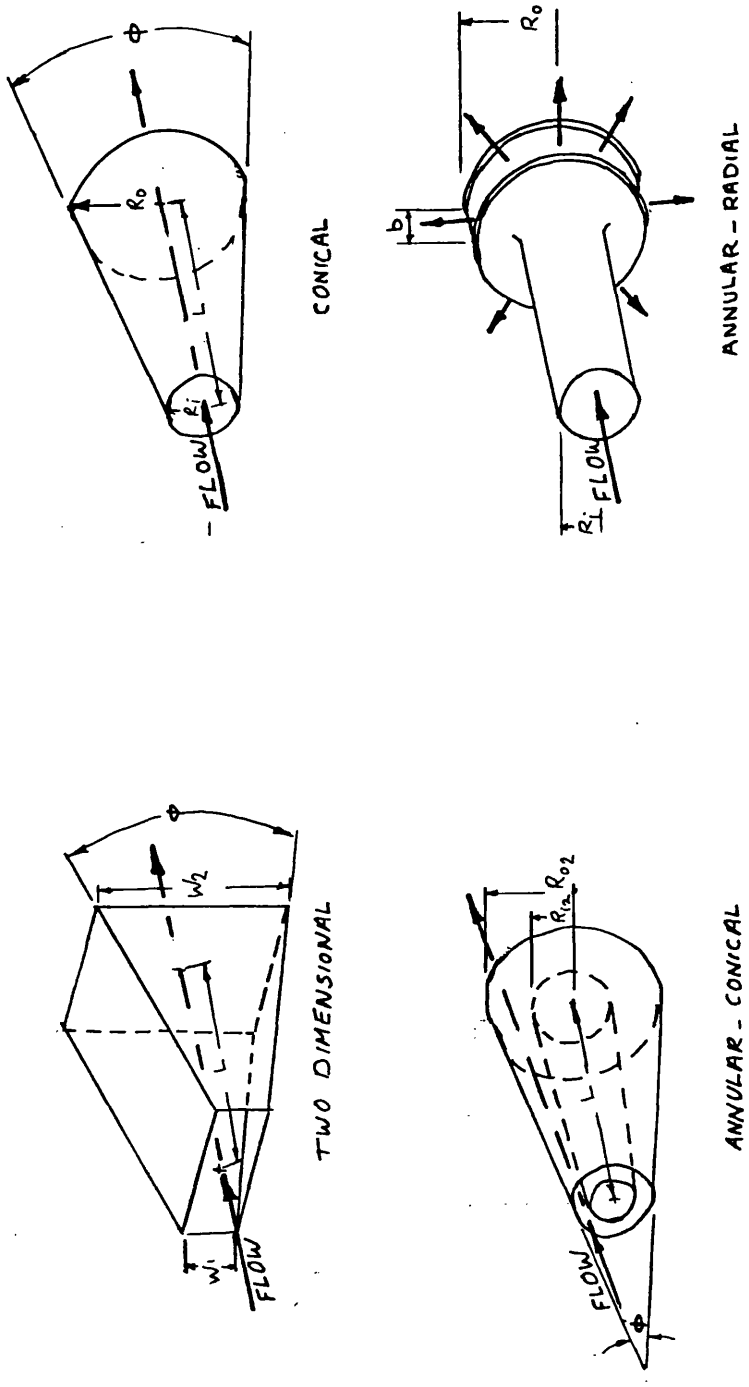

FIG. 1.1 DIFFERENT TYPES OF DIFFUSERS

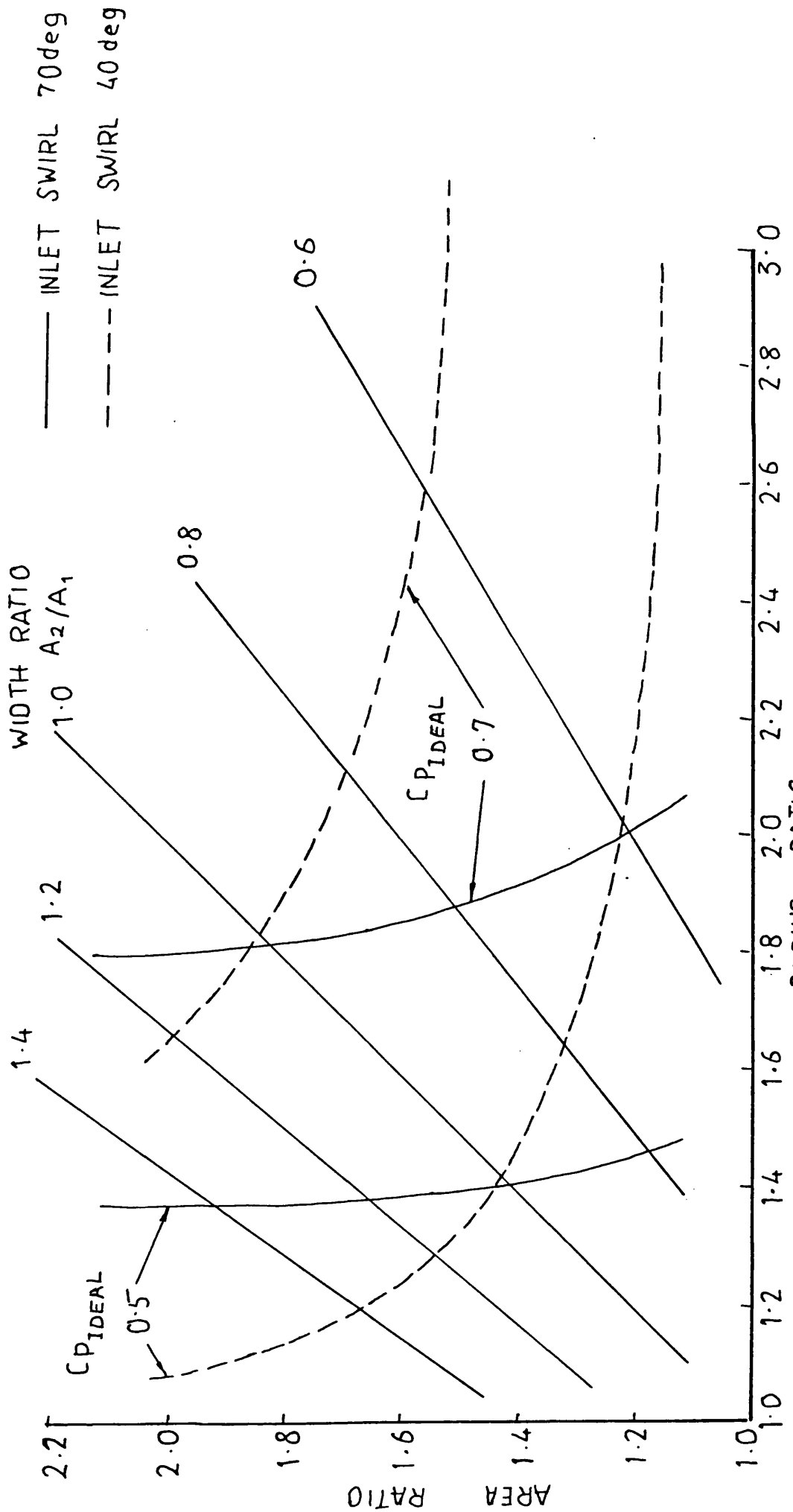

FIG.1.2 IDEAL PRESSURE RECOVERY COEFFICIENTS FOR INLET SWIRL ANGLES OF 70 AND 40 degrees

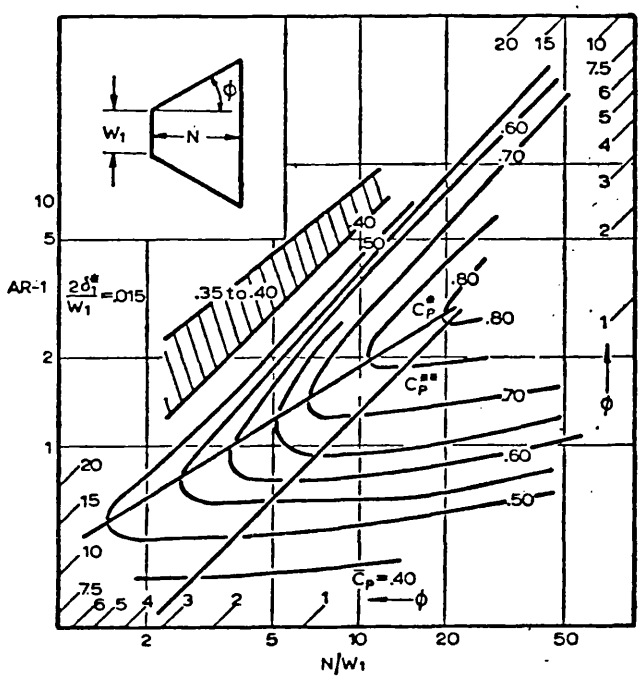

FIG. 1.3a PERFORMANCE MAP FOR TWO DIMENSIONAL DIFFUSERS (FROM REF.4)

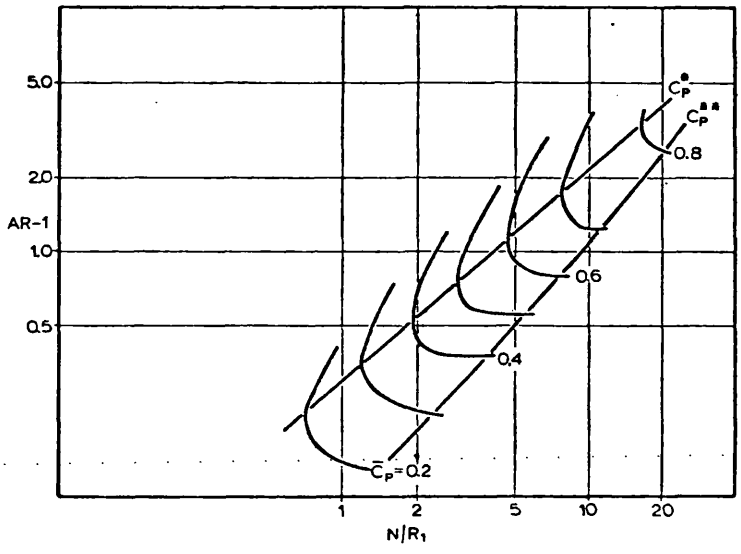

FIG. 1.3b PERFORMANCE MAP FOR CONICAL DIFFUSERS (FROM REF. 5)

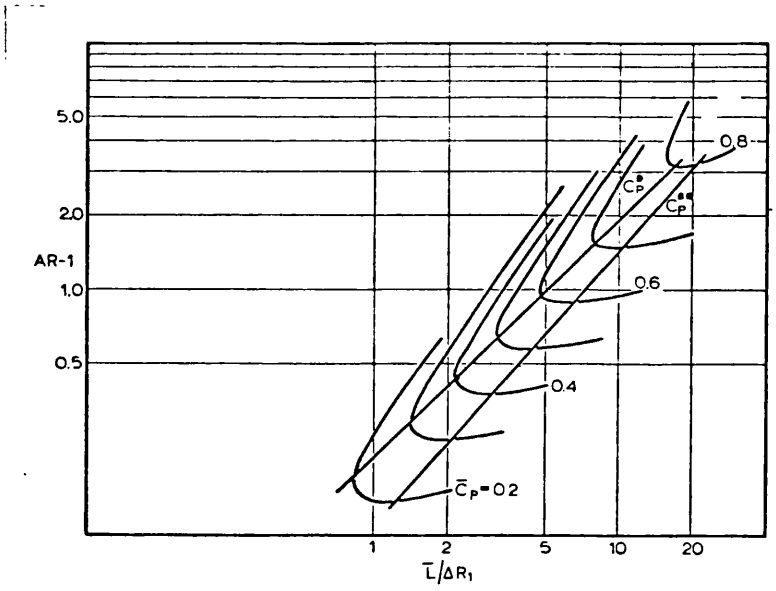

FIG. 1.4a PERFORMANCE MAP FOR ANNULAR CONICAL DIFFUSERS (FROM REF. 1)

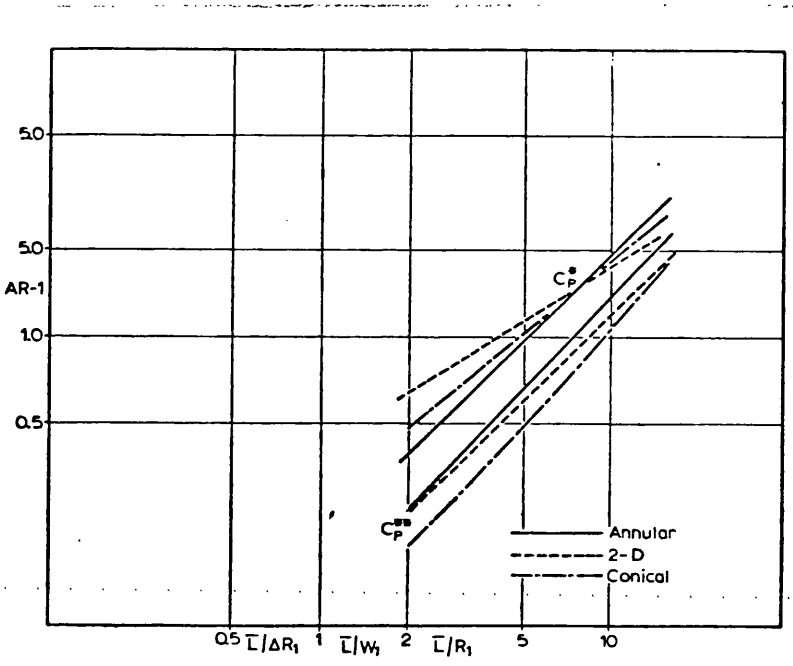

FIG. 1.4b OPTIMUM C_p LINES FOR VARIOUS DIFFUSER TYPES (FROM REF. 1)

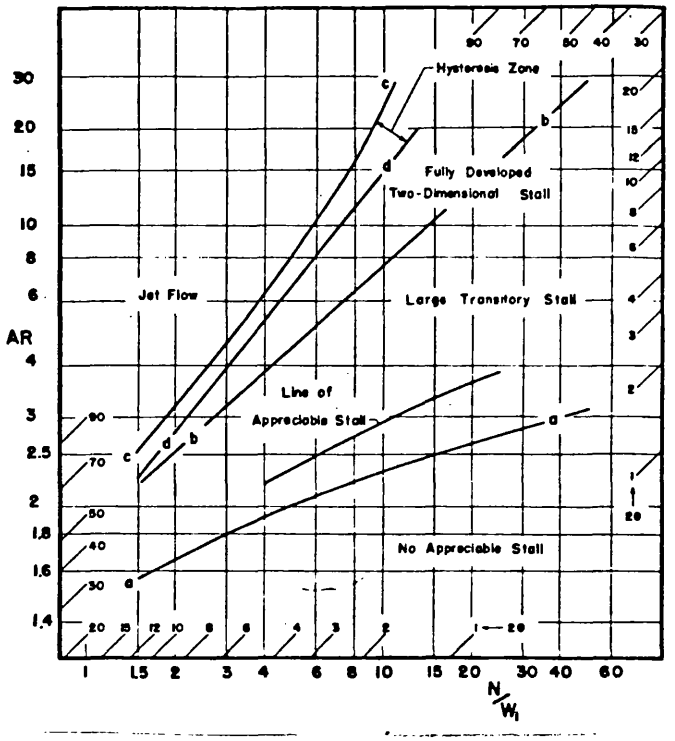

FIG. 1.5a FLOW REGIMES IN TWO DIMENSIONAL DIFFUSERS (FROM REF. 4)

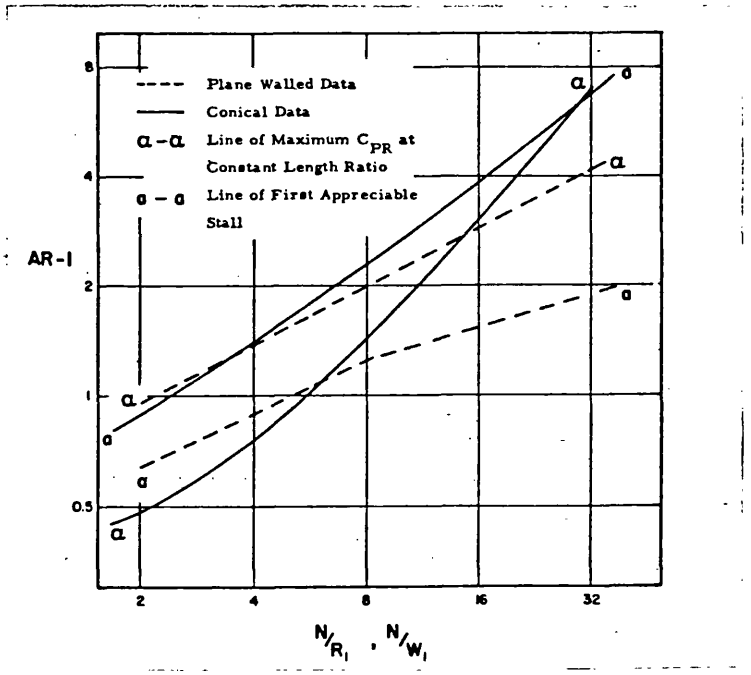

FIG. 1.5b OPTIMUM C_p* LINES AND LINES OF FIRST APPRECIABLE STALL COMPARED FOR CONICAL AND TWO DIMENSIONAL DIFFUSERS (FROM REF.7)

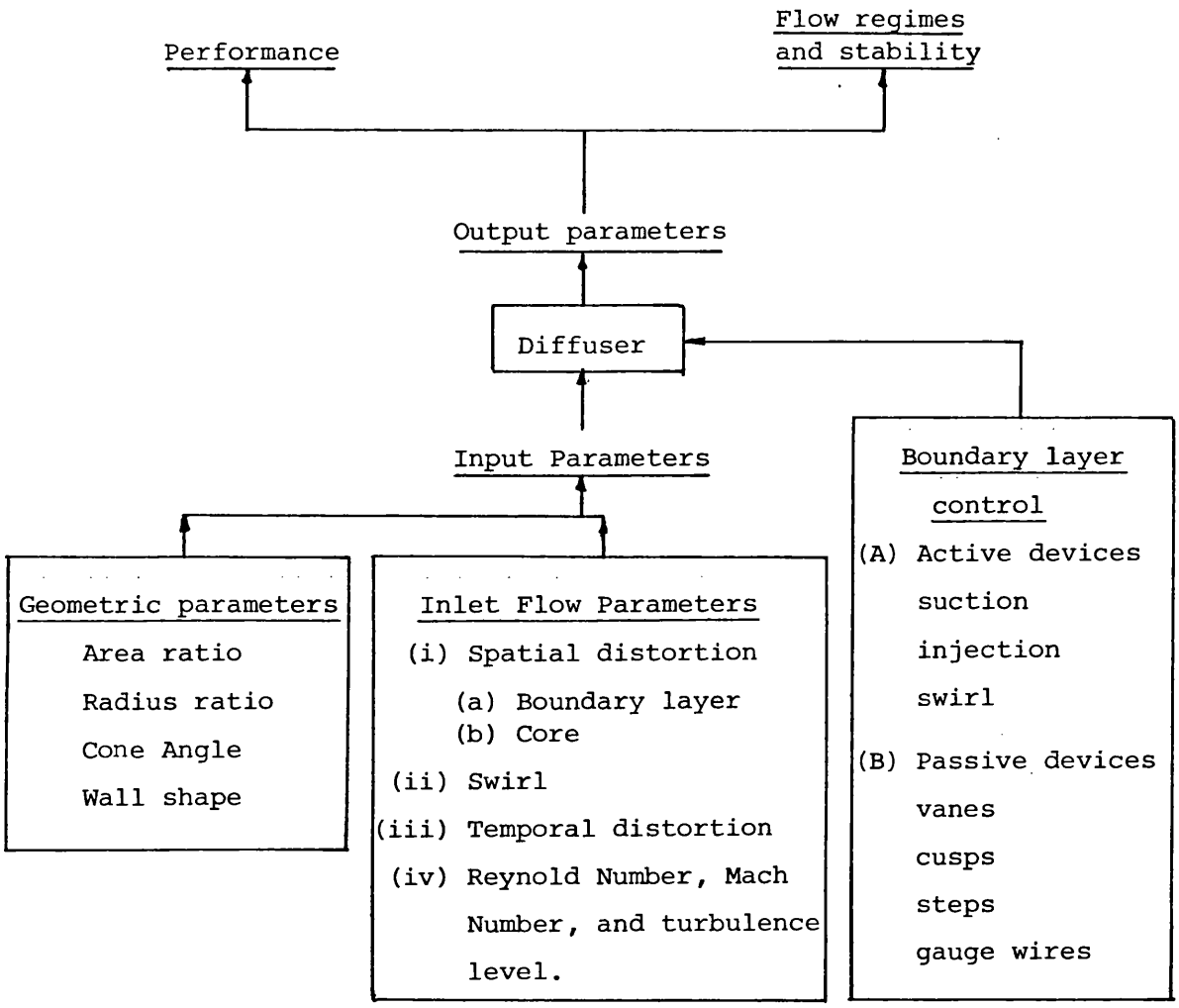

FIG. 1.6 DIFFUSER PARAMETERS DIAGRAM

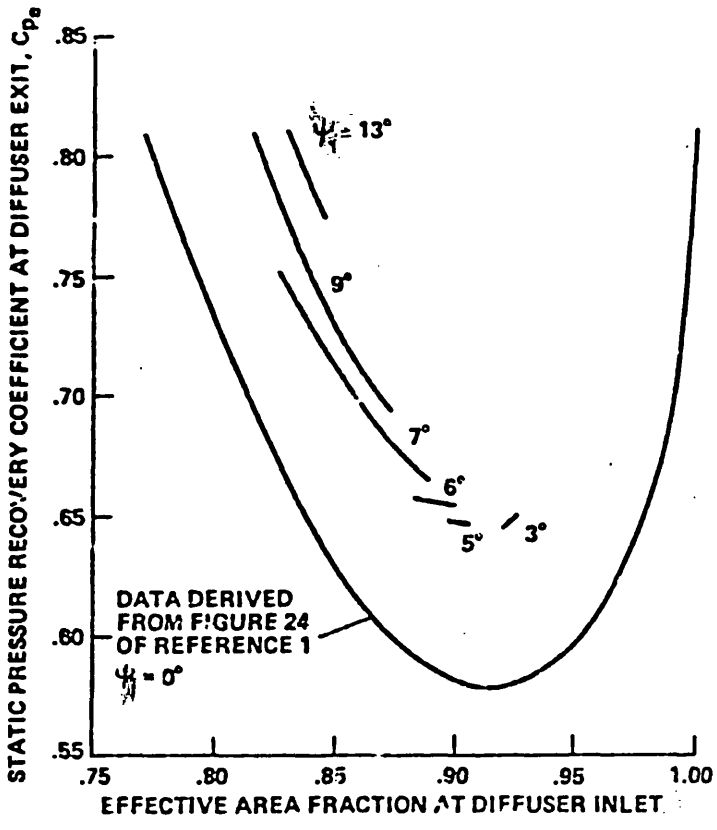

FIG. 1.7 EFFECT OF INLET BLOCKAGE ON ANNULAR DIFFUSER PERFORMANCE (FROM REF.32)

CHAPTER 2 : DEVELOPMENT OF THEORETICAL PROCEDURES FOR THE ANNULAR DIFFUSER FLOW CALCULATION

2.1 Introduction

The existing theoretical analysis procedures for radial flow turbomachines at Bath University are centred around the application of streamline curvature methods. The technique applied to centrifugal compressors and vaneless diffusers was developed by Atkey (82) Barbotin (22) isolated and further extended the application to vaneless diffusers. The main objective of the present work was to develop the technique further so that boundary layer theory could be included. The theoretical procedure was then to be applied in order to be able to assess the effect of inlet flow distortions upon the diffuser performance. A major problem with the earlier methods (21) was that the procedure broke down if any surface velocity approached zero. The first requirement was, therefore, to overcome this difficulty.

Ghoose and Kline (89) whilst developing theoretical procedures for two-dimensional diffusers have concluded that it is unsatisfactory to combine an inviscid and boundary layer approach in an iterative manner, i.e. to perform an inviscid solution, calculate the boundary layer growth, then repeat the inviscid solution with the new boundary. They concluded that it is essential to solve the boundary layer and core flow simultaneously. With this in mind an approximate but direct solution to the inviscid flow problem has been developed in order to combine it with the boundary layer.

2.2 Development of the streamline curvature inviscid flow equations

In order to eliminate the difficulty encountered with the failure of the procedure when low surface velocities were approach, the basic equation which was derived by Wallace, Atkey and Whitfield (21) (see Appendix A)

$$\frac{dC_m}{dn} = \frac{1}{R_c} C_m - \frac{C_\theta}{C_m}\left(\frac{dC_\theta}{dn} + \frac{C_\theta}{r}\cos\alpha\right) + \frac{1}{C_m}\frac{dho}{dn} \qquad 2.1$$

was re-written and solved in terms of C_m^2

$$\frac{dC_m^2}{dn} - \frac{2}{R_c} C_m^2 = 2\left(\frac{dho}{dn} - \frac{1}{2}\frac{d}{dn}(\lambda/r)^2 - (\lambda/r)^2 \frac{d}{dn}\ln r\right) \qquad 2.2a$$

where

$$\lambda = C_\theta . r = \text{constant} \qquad 2.2b$$

and $\cos\alpha = \frac{dr}{dn}$

$$h_o = h_o(n); \quad \lambda = \lambda(n); \quad r = r(n)$$

equation 2.2a is of the standard form

$$\frac{dC_m^2}{dn} + p_R(n)\, C_m^2 = Q(n)$$

which has the solution (90)

$$C_m^2 \; e^{\int_1^n p_R dn} = \int_1^n Q \; e^{\int_1^n p_R dn} dn + C \qquad 2.3$$

where $p_R = -2/R_c$

and $Q = 2\left(\frac{dho}{dn} - \frac{1}{2}\frac{d}{dn}(\lambda/r)^2 - (\lambda/r)^2 \frac{d}{dn}\ln r\right)$

Equation 2.3 can be further simplified by assuming that the radius of curvature R_c is a weak function of the normal distance n and a mean value $\bar{R}_c$ applied

then $\bar{p}_R = -\frac{2}{\bar{R}_c}$

$$\therefore \; C_m^2 \; e^{\bar{p}_R n} = \int_1^n Q \; e^{\bar{p}_R n} \, dn + C$$

at $n = 0$ $\quad C_m^2 = C_{m_1}^2 \quad \therefore \quad C = C_{m_1}^2$

then

$$\therefore \quad C_m^2 = C_{m_1}^2 \; e^{-\bar{p}n_R} + e^{-\bar{p}n_R} \int_1^n Q.e^{\bar{p}n_R}\, dn \qquad 2.4$$

$$\text{Now} \quad \int_1^n Q.e^{\bar{p}n_R}\, dn = 2\int_1^n \left(\frac{dho}{dn} - \frac{1}{2} \frac{d}{dn} (\lambda/r)^2 - (\lambda/r)^2 \frac{d}{dn} \ln r \right) e^{\bar{p}n_R}\, dn$$

$$= 2\left[I_1 - \frac{1}{2} I_2 - I_3 \right]_1^n \qquad 2.5$$

Using generalized integration by parts

$$I_1 = \int e^{\bar{p}n_R} \frac{dho}{dn}\, dn = \frac{e^{\bar{p}n_R}}{\bar{p}_R} \frac{dho}{dn} - \frac{e^{\bar{p}n_R}}{\bar{p}_R^2} \frac{d^2ho}{dn^2}$$

$$+ \frac{e^{\bar{p}n_R}}{\bar{p}_R^3} \frac{d^3ho}{dn^3} - \ldots \qquad 2.6$$

$$I_2 = \int e^{\bar{p}n_R} \frac{d}{dn} (\lambda/r)^2\, dn$$

$$= \frac{e^{\bar{p}n_R}}{\bar{p}_R} \frac{d}{dn} (\lambda/r)^2 - \frac{e^{\bar{p}n_R}}{\bar{p}_R^2} \frac{d^2}{dn^2} (\lambda/r)^2 + \frac{e^{\bar{p}n_R}}{\bar{p}_R^3} \frac{d^3}{dn^3} (\lambda/r)^2 - \ldots$$

2.7

$$I_3 = \int e^{\bar{p}n_R} (\lambda/r)^2 \frac{d}{dn} \ln r\, dn$$

$$= \frac{e^{\bar{p}n_R}}{\bar{p}_R} (\lambda/r)^2 \frac{d}{dn} \ln r - \frac{e^{\bar{p}n_R}}{\bar{p}_R^2} \left((\lambda/r)^2 \frac{d^2}{dn^2} \ln r \right.$$

$$\left. + \frac{d}{dn} \ln r . \frac{d}{dn} (\lambda/r)^2 \right) + \frac{e^{\bar{p}n_R}}{\bar{p}^3} \frac{d^3}{dn^3} \left((\lambda/r)^2 \frac{d}{dn} \ln r \right)$$

$$- \ldots . \qquad 2.8$$

Equation 2.4 represents an analytical solution for equation 2.2. for any distribution of λ and h_o but with the radius of curvature to be considered constant over the width and equal to a mean value. The different integrals are evaluated from equations 2.6, 2.7 and 2.8 for a specified λ and h_o distribution.

In the case of straight streamlines (straight walled diffuser) $\bar{R}_c = \infty$ hence $\bar{p} = 0$ equation 2.4 will be

$$c_m^2 = c_{m_1}^2 + \int_1^n Q \, dn \qquad 2.9$$

$$\int_1^n Q.dn = 2\int_1^n \left(\frac{dho}{dn} - \frac{1}{2}\frac{d}{dn} (\lambda/r)^2 \frac{d}{dn} \ln r \right) dn$$

$$= 2\left(I_1' - \frac{1}{2} I_2' - I_3' \right) \qquad 2.10$$

where

$$I_1' = \int \frac{dho}{dn} \, dn = h_o \qquad 2.11$$

$$I_2' = \int \frac{d}{dn} (\lambda/r)^2 \, dn = (\lambda/r)^2 \qquad 2.12$$

$$I_3' = \int \left((\lambda/r)^2 \frac{d}{dn} \ell nr \right) dn \qquad 2.13$$

Equation 2.9 represents the equivalent solution for the case of a straight walled diffuser for any distribution of λ and h_o.

For the special case of a radial diffuser $I_3' = 0$ then

$$\int_1^n Q.dn = 2\left[h_o - \frac{1}{2} (\lambda/r)^2 \right]_1^n \qquad 2.14$$

2.3 Direct solution of the inviscid equations

The above development of the inviscid equations suggested a further simplification by assuming linear distributions for

λ/r (i.e. C_θ) and h_o. The integrals of equation 2.5 can then be performed. In this case :

$$\left[I_1\right]_1^2 = \int_1^2 e^{\frac{\bar{p}}{\bar{R}}n} \frac{dho}{dn}\, dn = \left[\frac{e^{\frac{\bar{p}}{\bar{R}}n}}{\bar{p}} \frac{dho}{dn}\right]_1^2 = \frac{\Delta ho}{b}\left(\frac{e^{\frac{\bar{p}}{\bar{R}}b}}{\bar{p}} - \frac{1}{\bar{p}}\right)$$

$$= \frac{1}{2}\,\Delta h_o \,\frac{\bar{R}_c}{b}\,(1 - e^{-2\,b/\bar{R}_c}) \qquad 2.15$$

where subscripts 1 and 2 refers to positions on hub and shroud respectively

$$\left[I_2\right]_1^2 = 2\int_1^2 e^{\frac{\bar{p}}{\bar{R}}n}\,(\overline{\lambda/r})\,\frac{d}{dn}\,(\lambda/r)\,dn$$

$$= \bar{C}_\theta\,(C_{\theta 2} - C_{\theta 1})\,(1 - e^{-2b/\bar{R}_c})\,\frac{\bar{R}_c}{b} \qquad 2.16$$

$$\left[I_3\right]_1^2 = \int_1^2 e^{\frac{\bar{p}}{\bar{R}}n}\,(\overline{\lambda/r})^2\,\frac{1}{\bar{r}}\,\frac{d}{dn}\,r.dn$$

$$= \frac{1}{2}\,\bar{C}_\theta^{\,2}\,\frac{1}{\bar{r}}\,(r_2 - r_1)(1 - e^{-2\frac{b}{\bar{R}_c}})\,\frac{\bar{R}_c}{b} \qquad 2.17$$

Parameters C_θ and r outside the derivative

$\frac{d}{dn}$ are replaced by mean values $\bar{C}_\theta$ and $\bar{r}$,

where $\bar{C}_\theta = \dfrac{C_{\theta_1} + C_{\theta_2}}{2}$, $\bar{r} = \dfrac{r_1 + r_2}{2}$

substituting from 2.15, 2.16 and 2.17 into 2.4 and 2.5 yields

$$C_{m_2}^{\,2} = C_{m_1}^{\,2}\, e^{2\,b/\bar{R}_c} + e^{2\,b/\bar{R}_c}\left(\Delta h_o - \frac{C_{\theta_2}^{\,2} - C_{\theta_1}^{\,2}}{2} - \frac{\bar{C}_\theta^{\,2}}{\bar{r}}\,\Delta r\right)$$

$$(1 - e^{-2b/\bar{R}_c}).\,\frac{\bar{R}_c}{b} \qquad 2.18$$

Substituting $\zeta = b/\bar{R}_c$ equation 2.18 becomes

$$C_{m_2}^{\,2} = C_{m_1}^{\,2}\, e^{2\zeta} + D.\frac{(e^{2\zeta}-1)}{\zeta} \qquad 2.19$$

Where

$$D = \Delta h_o - \bar{C}_\theta \Delta C_\theta - \frac{\bar{C}_\theta^2}{\bar{r}} \Delta r$$

Following the same procedure in the case of a straight wall diffuser, equations 2.9, 2.10, 2.11, 2.12 and 2.13 yield

$$C_{m_2}^2 = C_{m_1}^2 + 2D \qquad 2.20$$

Equation 2.19 and 2.20 represent the solution of equations 2.4 for curved and straight wall diffusers respectively. Both equations can also be obtained by integrating equation 2.2a directly.

A full solution of equations 2.19 and 2.20 can be obtained if a linear distribution of the meridional velocity is assumed. In this case the continuity equation is

$$\dot{m} = 2\pi \bar{r}\, b.\rho \frac{C_{m_1} + C_{m_2}}{2}$$

$$\text{i.e. } C_{m_2} = \frac{\dot{m}}{\pi \bar{r} b \rho} - C_{m_1} = C_K - C_{m_1} \qquad 2.21$$

Substituting from 2.21 into 2.19 to eliminate C_{m_2} yields :

$$(e^{2\zeta} - 1) C_{m_1}^2 + 2 C_k C_{m_1} + \frac{(e^{2\zeta} - 1)}{\zeta} D - C_k^2 = 0$$

$$\therefore C_{m_1} = \frac{-C_k \pm \sqrt{C_k^2 - (e^{2\zeta} - 1)\left[\frac{(e^{2\zeta} - 1)}{\zeta} D - C_k^2\right]}}{(e^{2\zeta} - 1)} \qquad 2.22$$

Similarly equation 2.20 and 2.21 yields for a straight wall diffuser :

$$C_{m_1} = \frac{C_k}{2} - \frac{D}{C_k} \qquad 2.23$$

Equations 2.22 for curved and 2.23 for straight wall diffusers, with equations 2.2b and 2.21 gives a direct solution to the inviscid flow problem.

Examination of the above equations reveals the following characteristics of this solution :-

1. The solution is defined by three parameters which decide the meridional velocity gradient, namely C_k, D and ζ for the case of a curved diffuser.

2. C_k is twice the mean meridional velocity and represents the effect of either or both of the mass flow rate $\dot{m}$ and diffuser width b at a particular radius. C_k decreases with radius for increasing cross-sectional area

$$C_k = \frac{\dot{m}}{\pi \bar{r} b . \rho}$$

3. D is a parameter representing the effect of inlet total enthalpy gradient (Δh_o), tangential velocity gradient ($\bar{C}_\theta \Delta C_\theta$) and centrifugal force $\frac{\bar{C}_\theta^2}{\bar{r}} \Delta r$

$$D = (h_{o_2} - h_{o_1}) - \frac{C_{\theta_2}^2 - C_{\theta_1}^2}{2} - \frac{\bar{C}_\theta^2}{\bar{r}} (r_2 - r_1) \qquad 2.24$$

From equation 2.24 it is clear that the total enthalpy gradient effect will be opposed by the two terms involving swirl if the h_o and C_θ gradients are identical in sign. A tangential velocity gradient having the same sign as the meridional velocity gradient will have a favourable effect on delaying separation on the low velocity wall, while a total enthalpy gradient having similar sign will have the opposite effect. In an inviscid analysis Δh_o will remain constant while the absolute value of the swirl terms will decrease with radius. In highly swirling flow, such as that found in centrifugal compressor diffusers, h_o and C_θ gradients will have similar signs, in this case the value of D will increase with radius if Δh_o is positive or decreases with radius if Δh_o is negative.

If at any radius D becomes zero the meridional velocity profile, for a straight wall diffuser, will be uniform, i.e. $C_{m_1} = C_{m_2} = C_k/2$ while for a curved diffuser $C_{m_1} = \frac{C_k}{(e^\zeta + 1)}$ i.e. a distortion is caused by the curvature effect.

If a uniform distribution of λ and h_o is assumed for a straight wall diffuser then from equation 2.24.

$$D = -\frac{C_{\theta_2}^2 - C_{\theta_1}^2}{2} - \frac{C_{\theta}^{-2}}{\bar{r}}(r_2 - r_1)$$

$\lambda_1 = \lambda_2 = \lambda$ i.e. free vortex conditions

$$D = -\frac{\lambda^2}{2}\left[\left(\frac{1}{r_2}\right)^2 - \left(\frac{1}{r_1}\right)^2\right] - \left(\frac{\lambda}{2}\right)^2\left(\frac{1}{r_2} + \frac{1}{r_1}\right)^2 \frac{(r_2 - r_1)}{\frac{1}{2}(r_2 + r_1)}$$

By expanding the second term of this expression it can easily be shown that D = O. Consequently the meridional velocity profile will be uniform at all radial positions if the inlet h_o and λ gradients are zero.

4. ζ is a non-dimensional parameter, $b/\bar{R}_c$. For fixed values of C_k and D two diffusers having different width and radius of curvature but equal ζ, will have identical meridional velocities between hub and shroud. To modify the meridional velocity distribution at a specific radius, it is necessary to alter ζ through a change of width b, or radius of curvature $\bar{R}_c$ or both.

2.3.1 Separation and stability criterion for the direct solution

A criterion for separation can be deduced from equations 2.22 and 2.23. The separation can occur either on the hub or shroud; in this discussion it will be assumed to occur on the hub, while for shroud separation similar substitution will give equivalent conditions.

For a curved diffuser, from equation 2.22, separation occurs when $C_{m_1} = O$

then
$$\frac{-C_k \pm \sqrt{C_k^2 - (e^{2\zeta}-1)\left[\frac{(e^{2\zeta}-1)}{\zeta}D - C_k^2\right]}}{(e^{2\zeta}-1)} = O \qquad 2.25$$

Taking the positive root

$$D = \frac{\zeta}{(e^{2\zeta}-1)} \quad C_k^2 \qquad 2.26$$

Similarly for the straight wall diffuser the condition is

$$D = \frac{C_k^2}{2} \qquad 2.27$$

Equations 2.26 and 2.27 can be solved for the radius at which separation will occur without solving through successive normals.

In the case of a radial diffuser where $r_1 = r_2 = \bar{r} = r$ equation 2.27 after substituting from equation 2.24 yields

$$(h_{o_2} - h_{o_1}) - \frac{C_{\theta_2}^2 - C_{\theta_1}^2}{2} = \frac{1}{2}\left(\frac{\dot{m}}{\pi r b \rho}\right)^2$$

since $C_\theta \cdot r$ = constant = λ

The radius of separation is then given by

$$r_s = \left\{\left[\left(\frac{\dot{m}}{\pi b \rho}\right)^2 + (\lambda_2^2 - \lambda_1^2)\right] / 2\,(h_{o_2} - h_{o_1})\right\}^{\frac{1}{2}} \qquad 2.28$$

The growth of separation downstream of r_s can be calculated from equation 2.27 by solving for values of fluid width b' between one wall and the edge streamline which has separated from the other wall.

For a radial diffuser the position of the edge streamline which has $C_{m_1} = 0$ is given by

$$b' = \left\{\left(\frac{\dot{m}}{\pi \rho}\right)^2 / \left[2(h_{o_2} - h_{o_1})\, r^2 - (\lambda_2^2 - \lambda_1^2)\right]\right\}^{\frac{1}{2}} \qquad 2.29$$

It is clear that the value of b' will decrease continuously with radius. In other words the flow distortion after separation in an inviscid solution will increase continuously with radius. This trend

was observed by Ellis (37) and Rebernik (38) and others using detailed numerical solutions. After separation, however, the streamlines will be curved and equation 2.15 should be used to allow for this curvature, in this case for a radial diffuser.

$$(h_{o_2} - h_{o_1}) - \frac{1}{r^2}\left(\frac{\lambda_2^2 - \lambda_1^2}{2}\right) = \frac{\zeta}{(e^{2\zeta} - 1)}\left(\frac{\dot{m}}{\pi r b \rho}\right)^2$$

Let $E = \left(\frac{\dot{m}}{\pi\rho}\right)^2 = \text{constant}$

$$\text{then } b' = \frac{E}{\left(r^2 \Delta h_o - \frac{\Delta\lambda^2}{2}\right)} \cdot \frac{1}{\left(e^{\frac{2}{\bar{R}_c} b'} - 1\right)\bar{R}_c} \qquad 2.30$$

$$\text{or } b' = X_1 \cdot X_2 \qquad 2.31$$

$$\text{where } X_1 = \frac{E}{\left(r^2 \Delta h_o - \frac{\Delta\lambda^2}{2}\right)} \qquad X_2 = \frac{1}{\left(e^{\frac{2}{\bar{R}_c} b'} - 1\right)\bar{R}_c}$$

It is clear that as the radius increases X_1 decreases, so in order to obtain re-attachment, b' increasing, X_2 must increase continuously with radius. For a re-attaching flow $\bar{R}_c$ is negative, as shown in fig. 2.1. The only way to force X_2 to increase successively with radius is to cause the absolute magnitude of $\bar{R}_c$ to decrease continuously with radius until at a specific value $b' = b$ and re-attachment occurs.

At the point of re-attachment $C_{m_1} = 0$, and beyond this point X_1 will continue to decrease while as the radius of curvature $|\bar{R}_c|$ increases again due to re-attachment X_2 will decrease causing immediate separation as shown in fig. 2.1. This previous argument shows that for an inviscid solution even if re-attachment was forced by adjusting the streamline curvature, the solution will never settle to be a stable attached flow.

To investigate the effect of various parameters on stability consider a diffuser with its flow at the point of separation on the hub.

In this case $D = \frac{C_k^2}{2}$ for straight wall diffuser

and $D = \frac{2\zeta}{(e^{2\zeta}-1)} \cdot \frac{C_k^2}{2}$ for curved diffuser.

After the separation point $D > \frac{C_k^2}{2}$ or $D > \frac{2^{\zeta}}{(e^{2\zeta}-1)} \cdot \frac{C_k^2}{2}$

so let $D = (1 + \varepsilon) \frac{C_k^2}{2}$ 2.32

where ε is a residue that can have positive or negative value.
After separation the streamlines will be curved hence substituting from 2.32 into 2.22

$$C_{m_1} = \frac{- C_k \pm C_k \sqrt{1 - \frac{(e^{2\zeta}-1)}{\zeta}\left[\frac{(e^{2\zeta}-1)}{2}(1 + \varepsilon) - \zeta\right]}}{(e^{2\zeta} - 1)} \qquad 2.33$$

for any diffuser

For re-attachment to occur i.e. $C_{m_1} > 0$

the condition is

$$\begin{aligned} &\frac{(e^{2\zeta}-1)}{2}(1 + \varepsilon) - \zeta \leqslant 0 \quad \text{for } \zeta = +\text{ve} \\ &\frac{(e^{2}-1)}{2}(1 + \varepsilon) - \zeta \geqslant 0 \quad \text{for } \zeta = -\text{ve} \end{aligned} \qquad 2.34$$

i.e. $|\zeta| > \left| \frac{(e^{2\zeta}-1)}{2}(1 + \varepsilon) \right|$

Values of $\frac{(e^{2\zeta}-1)}{2}(1 + \varepsilon)$ versus ζ are plotted in fig. 2.2 for different values of ζ and ε. It can be seen from the figure that for positive values of ε (i.e. straight wall diffuser $D > \frac{C_k^2}{2}$)a re-attachment can occur only for -ve values of ζ. In general ε will increase with radius as D increases successively, and C_k, which is twice the mean meridional velocity, will successively decrease unless the cross sectional area is decreased through contraction. ε can be considered as a criterion for stability, as shown in fig. 2.2 as ε decreases the flow on the considered wall will have higher meridional velocities, hence a change which tends to

decrease ε is a favourable one. From equation 2.32 ε can be decreased by either decreasing D or increasing C_k. It should also be noted that while for a straight wall diffuser no separation is predicted for negative values of ε, for curved diffusers separation is theoretically possible for negative values of ε as shown in fig. 2.2.

The effect of diffuser geometry on stability can be assessed with the aid of fig. 2.2. The actual direct effect of introducing positive curvature at any mean radial position will be unfavourable. However, the stabilizing effect of curvature is due to its effect upon C_θ which leads to a reduction in the magnitude of the parameter D. The introduction of curvature leads to an increase in the magnitude of the term $\left(\frac{\lambda_2^2}{2r_2^2} - \frac{\lambda_1^2}{2r_1^2}\right)$, which in turn reduces the value of D. This will have a moderate effect since the other term involving swirl $\frac{C_\theta^2}{r}(r_2 - r_1)$ will decrease slightly.

A contraction will lead to an improvement in stability due to an increase in the velocity parameter C_k, thereby decreasing ε.

Adopting both contraction and curvature will have a substantial stabilizing effect by reducing D and increasing C_k hence reducing ε markedly, thus equivalent to moving from a to b on fig. 2.2. Previously Wallace et al (21) see figs. 2.3 and 2.4 showed that a change from a conical to a curved configuration delayed separation on the hub slightly, addition of contraction improved the hub velocity further, while a substantial contraction of the curved diffuser eliminated separation totally.

2.3.2 Application of the direct solution by comparison with alternative theoretical techniques

To assess the validity of the proposed direct solution, it was compared to some inviscid computations and some experimental results reported in the literature. To verify the assumption of linearity

of velocity distribution in the inviscid core, available data measured at the inlet to centrifugal compressor diffusers were condensed and presented for the meridional and tangential velocity distributions respectively, see figs. 2.5 and 2.6. In most cases the linear distribution assumption is a good approximation over the central inviscid core. Data from 'isolated' diffusers which were tested with simulated turbomachinery inlet conditions indicated that the assumption is sound for example references (43), (46) and (51).

Figs. 2.7 and 2.8 show a comparison of the direct solution with a detailed streamline curvature computation, (22) and (82), for a curved diffuser as shown in fig. 2.9a. The inlet conditions for both cases are shown in fig. 2.9b. Excellent agreement is shown and the linearity of the parameter distributions were kept even with the inclusion of curvature effects. The agreement between velocity values at both walls demonstrated the accuracy of the direct solution in predicting the meridional velocity gradient. Fig. 2.10 shows a comparison for a conical diffuser using the same streamline curvature procedure. Although the direct solution could not predict the slight curvature in meridional velocity distribution, again the agreement between overall distribution and velocity values at the wall was quite good.

Comparison with results reported by Rebernik (38), fig. 2.11, shows agreement with position and growth of separation. No streamline curvature was assumed after separation for the direct solution and equation 2.29 was used.

As a final example, the direct solution was compared with the results of Hoadley (43), for an axial annular diffuser. In this case, the theoretical results were obtained using the Marsh Matrix program (78). Fig. 2.12 shows the experimental arrangement and theoretical matrix grid used by Hoadley. Fig. 2.13 compares the direct solution with the experimental and theoretical results of Hoadley. It can be seen that while both theoretical solutions yield almost identical uniform velocity distributions between the hub and casing, they did

not show good agreement with the experimental results. The direct solution, however, indicates the steps necessary in order to modify the predicted results. The experimental results presented by Hoadley were, therefore, re-processed in order to estimate the stagnation temperature gradient at diffuser inlet, this was found to be approximately 0.2 K. Whilst this is small and was neglected by Hoadley, it has a marked effect upon the theoretical results as is shown in fig. 2.13. With the inlet enthalpy gradient included the theoretical results show the correct qualitative trends between the hub and the centre of the passage.

These comparisons have, therefore, shown that the direct solution gives good agreement with other but more detailed inviscid solutions, and can therefore form the basis from which an improved theoretical solution, including boundary layers, can be developed.

2.4 The Boundary-layer Analysis

In the previous section, an inviscid core direct solution was developed and was shown to give a good prediction of the flow behaviour. In order to incorporate a boundary layer analysis an integral method, developed by Davis (84) has been chosen. This method is relatively straight forward due to the reduction of the boundary layer equations into a set of ordinary differential equations, yet it retains the significant three-dimensional features of the equation with physical meaningful quantities presented. It therefore offers a straight forward efficient solution which is suitable to be coupled with the direct solution.

2.4.1 Boundary layer equations

The order of magnitude process is applied to the Navier-Stokes equations written in an orthogonal co-ordinate system. The resultant equations are then integrated across the boundary layer using a streamline co-ordinate system shown in fig. 2.14a. The following equations are then obtained :

The incompressible streamwise momentum integral equation

$$\frac{\partial}{\partial S}\cdot(U_e^2\,\theta_{11}) + U_e\frac{\partial U_e}{\partial S}\,\delta_1^* + \frac{\partial}{\partial N}\cdot(U_e^2\,\theta_{12}) + U_e\frac{\partial U_e}{\partial N}\,\delta_2^*$$

$$+ K_1\,U_e^2\,(\theta_{11}-\theta_{12}) + K_3\,U_e^2\,(\theta_{21}+\theta_{12}) = \tau_{ws/\rho} \qquad 2.35a$$

and the incompressible cross-flow momentum integral equation

$$\frac{\partial}{\partial S}\cdot(U_e^2\,\theta_{21}) + \frac{\partial}{\partial N}\cdot(U_e^2\,\theta_{22}) + U_e^2\,K_1\,(\theta_{21}+\theta_{12})$$

$$+ U_e^2\,K_3\,(\theta_{22}-\theta_{11}) + U_e^2\,(K_1\,\delta_2^* - K_3\,\delta_1^*) = \tau_{wN/\rho} \qquad 2.35b$$

The Navier-Stoke equations in curvilinear co-ordinates are given in Appendix B, and derivation of equations 2.35a and 2.35b are given in Appendix C.

The various displacement and momentum thicknesses are defined as :-

$$\delta_1^* = \int_o^\delta \left(1-\frac{u}{U_e}\right)dy$$

$$\delta_2^* = -\int_o^\delta \frac{w}{U_e}\,dy$$

$$\theta_{11} = \int_o^\delta \frac{u}{U_e}\left(1-\frac{u}{U_e}\right)dy \qquad 2.36$$

$$\theta_{12} = \int_o^\delta \frac{w}{U_e}\left(1-\frac{u}{U_e}\right)dy$$

$$\theta_{21} = -\int_o^\delta \frac{uw}{U_e^2}\,dy$$

$$\theta_{22} = -\int_o^\delta \frac{w^2}{U_e^2}\,dy$$

K_1 and K_3 are the rate of divergence of the external or inviscid streamlines and orthogonals respectively. K_1 and K_3 can be related to the rate of change of flow angle and radius.

$$K_1 = - \frac{1}{r \cos \psi_e} \frac{\partial}{\partial S} (r \cos \psi_e)$$

$$K_3 = - \frac{1}{r \sin \psi_e} \frac{\partial}{\partial N} (r \sin \psi_e)$$

If the flow is assumed to be circumferentially symmetric about the meridional direction m, the relation between differentials in the streamline co-ordinate system and meriodional m and tangential T direction is shown in fig. 2.14b to be

$$\frac{\partial}{\partial S} = \cos \psi_e \frac{d}{dm} \quad , \quad \frac{\partial}{\partial N} = - \sin \psi_e \frac{d}{dm}$$

Substituting from the above relations into 2.35a and 2.35b and re-arranging yields :-

$$\frac{d}{dm} U_e^2 (\theta_{11} \cos \psi_e - \theta_{12} \sin \psi_e) + U_e^2 (\theta_{11} \cos \psi_e - \theta_{12} \sin \psi_e)$$

$$\frac{1}{r} \frac{d}{dm} r + U_e (\delta_1^* \cos \psi_e - \delta_2^* \sin \psi_e) \frac{dU_e}{dm} - \frac{\theta_{22} U_e^2}{r} \frac{d}{dm} (r \cos \psi_e)$$

$$- \frac{\theta_{21} U_e^2}{r} \frac{d}{dm} (r \sin \psi_e) = \frac{\tau_{ws}}{\rho} \qquad 2.37a$$

$$\frac{d}{dm} U_e^2 (\theta_{21} \cos \psi_e - \theta_{22} \sin \psi_e) + U_e^2 (\theta_{21} \cos \psi_e - \theta_{22} \sin \psi_e)$$

$$\frac{1}{r} \frac{d}{dm} r + \frac{\theta_{21} U_e^2}{r} \frac{d}{dm} (r \cos \psi_e) + \frac{\theta_{11} U_e^2}{r} \frac{d}{dm} (r \sin \psi_e)$$

$$+ \frac{\delta_1^* U_e^2}{r} (r \sin \psi_e) = \frac{\tau_{wN}}{\rho} \qquad 2.37b$$

Let

$$\theta_o = \theta_{11} \cos \psi_e - \theta_{12} \sin \psi_e$$

$$\delta_m^* = \delta_1^* \cos \psi_e - \delta_2^* \sin \psi_e$$

$$A_1 = \frac{\theta_{22}}{r} \frac{d}{dm} (r \cos \psi_e) + \frac{\theta_{21}}{r} \frac{d}{dm} (r \sin \psi_e)$$

$$\theta_z = \theta_{21} \cos \psi_e - \theta_{22} \sin \psi_e$$

$$A_2 = \frac{\theta_{21}}{r} \frac{d}{dm} (r \cos \psi_e) + \frac{(\theta_{11} + \delta_1^*)}{r} \frac{d}{dm} (r \sin \psi_e)$$

dividing equation 2.37a by $U_e^2 \theta_o$ and equation 2.37b by $U_e^2 \theta_z$, and arranging the results into logarithmic differential form, equation 2.37a and 2.37b become

$$\frac{d}{dm} \ell n \left(U_e^2 r \theta_o \right) = \frac{1}{\theta_o} \left[\frac{C_{f_s}}{2} - \delta_m^* \frac{d}{dm} \ell n U_e + A_1 \right] \qquad 2.38a$$

$$\frac{d}{dm} \ell n \left(U_e^2 r \theta_z \right) = \frac{1}{\theta_z} \left[\frac{C_{f_N}}{2} - A_2 \right] \qquad 2.38b$$

where

$$C_{f_s} = \frac{\tau_{ws}}{\frac{1}{2}\rho U_e^2} \quad , \quad C_{f_N} = \frac{\tau_{wN}}{\frac{1}{2} \rho U_e^2}$$

Equations 2.38a and 2.38b are two ordinary differential equations in the meridional direction.

2.4.2 Boundary layer equations in terms of boundary layer parameters

In order to obtain a solution for equations 2.38a and 2.38b, various boundary layer parameters have to be evaluated by assuming velocity profiles inside the boundary layer and a relation for a wall friction coefficient. Davis (84) used Cole's two-parameter profile for the streamwise boundary layer velocity profile; however Nash and Patel (91) observed that for three-dimensional flows, the simple power law gave better overall agreement with a much wider range of experimental results. Since the simple power law is also mathematically simpler, it was chosen to represent the streamwise velocity profile inside the boundary layer.

$$\frac{u}{U_e} = \left(\frac{y}{\delta}\right)^{\frac{1}{n}} \qquad 2.39a$$

n is related to the shape parameter H by

$$H = \frac{n+2}{n} \qquad \text{where } H = \frac{\delta_1^*}{\theta_{11}}$$

Mager (87) gave the cross-flow boundary layer profile as

$$\frac{w}{U_e} = \left(1 - \frac{y}{\delta}\right)^2 \frac{u}{U_e} \tan\beta \qquad 2.39b$$

where β = angle between the limiting wall streamline and the boundary layer edge streamline fig. 2.13a.

The Ludweig-Tillman (92) skin friction equation is applied to the streamwise velocity profile i.e.

$$C_{f_s} = 0.246 \left(\frac{U_e \theta_{11}}{\nu}\right)^{-0.268} \cdot 10^{-0.678H} \qquad 2.39c$$

and as a consequence of the definition of β

$$C_{f_N} = C_{f_s} \tan\beta \qquad 2.39d$$

Using relations 2.39a and 2.39b, the various integral parameters 2.36 become :

$$\delta_1^* = \delta\left[\frac{1}{n+1}\right] = \delta e_1/n$$

$$\delta_2^* = -\delta\tan\beta\left[\frac{2n^3}{(n+1)(2n+1)(3n+1)}\right] = -\delta\tan\beta\, e_2$$

$$\theta_{11} = \delta\left[\frac{n}{(n+1)(n+2)}\right] = \delta\ell_1$$

$$\theta_{12} = \delta\tan\beta\left[\frac{2n^2}{(n+1)(2n+1)} + \frac{n}{(3n+1)(3n+2)} - \frac{n}{(n+2)}\right] = \delta\tan\beta\ \ell_2 \qquad 2.40$$

$$\theta_{21} = -\delta\tan\frac{n^3}{(n+1)(n+2)(3n+2)} = \delta\tan\beta\ \ell_3$$

$$\theta_{22} = -\delta\tan^2\beta\left[\frac{2n}{(n+1)(3n+2)} + \frac{n}{(5n+2)} - \frac{3n}{(n+2)(2n+1)}\right]$$

$$= \delta\tan^2\beta\ \ell_4$$

Using the definition of θ_o and θ_z together with the integral parameters 2.40, the streamwise and cross flow momentum equations 2.38a and 2.38b can be written as :

$$\frac{d}{dm}\ \ell n\ [\rho\ U_e^2\ r\ \delta(\ell_1\cos\psi_e - \ell_2\sin\psi_e\tan\beta)]$$

$$= \frac{1}{\theta_o}\left[\frac{C_{f_s}}{2} - \delta_m^*\ \frac{d}{dm}\ \ell n\ U_e + A_1\right] = f_1 \qquad 2.41a$$

$$\frac{d}{dm}\ \ell n\ [U_e^2 r\ \delta\tan\beta\ (\ell_3\cos\psi_e - \ell_4\sin\psi_e\tan\beta)]$$

$$= \frac{1}{\theta_z}\left[\frac{C_{f_N}}{2} - A_2\right] = f_2 \qquad 2.41b$$

Since equations 2.41a and 2.41b are non linear it is necessary to integrate them through an iterative procedure by assuming the right hand side to be a known constant, integrate between two meridional stations, improve the estimate of the right hand side and repeat. Doing this equation 2.41a and 2.41b may be written as

$$[U_e^2\, r\, \delta(\ell_1 \cos\psi_e - \ell_2 \sin\psi_e \tan\beta)]_{J+1}$$

$$= [U_e^2\, r\, \delta(\ell_1 \cos\psi_e - \ell_2 \sin\psi_e \tan\beta)]_J . e^{\bar{f}_1 . \Delta m} = F_1 \qquad 2.42a$$

and

$$[U_e^2\, r\, \delta \tan\beta(\ell_3 \cos\psi_e - \ell_4 \sin\psi_e \tan\beta)]_{J+1}$$

$$= [U_e^2\, r\, \delta \tan\beta(\ell_3 \cos\psi_e - \ell_4 \sin\psi_e \tan\beta)]_J . e^{\bar{f}_2 . \Delta m} = F_2 \qquad 2.42b$$

Where $\bar{f}_i = \dfrac{(f_i)_{J+1} + (f_i)_J}{2}$, i = 1,2 and represents the two boundary layers

$$\Delta m = m_{J+1} - m_J$$

With J denoting the meridional station number

From 2.42a

$$\delta_{J+1} = \frac{F_1}{[r\, U_e^2\, (\ell_1 \cos\psi_e - \ell_2 \sin\psi_e \tan\beta)]_{J+1}} \qquad 2.43a$$

Dividing 2.42b by 2.42a gives

$$\tan\beta_{J+1}\, (\ell_3 \cos\psi_e - \ell_4 \sin\psi_e \tan\beta)_{J+1}$$

$$= \frac{F_2}{F_1}\, (\ell_1 \cos\psi_e - \ell_2 \sin\psi_e \tan\beta)_{J+1} \qquad 2.43b$$

which readily gives tanβ as a quadratic solution

2.5 The Full System of Equation for the Core and Boundary Layer Flow

Equations 2.22 or 2.23 and 2.2b together with equations 2.43a and 2.43b represent the core and boundary layer momentum equations. In this case

$$C_k = \frac{\dot{M}_c}{\pi r b \rho}$$

Where $\dot{M}_c$ is the core flow rate given by

$$\dot{M}_c = \dot{M}_{total} - \dot{M}_{\delta_1} - \dot{M}_{\delta_2} \qquad 2.44$$

Where the boundary layer flow is given by

$$\dot{M}_{\delta_i} = \int_0^{\delta} 2\pi r_i \rho \,(u \cos\psi_e - w \sin\psi_e)_i \, dy \qquad 2.45$$

In the case of centrifugal compressor diffusers r is a weak function of y and can be replaced by an averaged value $\bar{r}$ over the boundary layer thickness δ

$$\therefore \dot{M}_{\delta} = 2\pi \bar{r}_i \rho U_{e_i} \delta_i \left[\cos\psi_e \frac{n}{(n+1)} - \sin\psi_e \tan\beta \frac{2n^3}{(n+1)(2n+1)(3n+1)}\right]_i$$

$$\therefore \dot{M}_{\delta_i} = 2\pi \bar{r}_i \rho U_{e_i} \delta_i (e_1 \cos\psi_e - e_2 \sin\psi_e \tan\beta)_i \qquad 2.46$$

It should be noted here that for a curved diffuser the effect of curvature will appear only in the inviscid core equations, the boundary layer equations 2.35a and 2.35b were derived with the assumption that the boundary layer thickness is small in comparison with the principal radii of curvature of the wall i.e. $\frac{\delta}{R_c} << 1.0$. If, however, the order of magnitude of the boundary layer thickness is not small in comparison with the radius of curvature the analysis will not be accurate and may not be applicable.

The system of equations 2.2b (i = 1,2), 2.43a (i = 1,2), 2.43b (i = 1,2), 2.44 and 2.22 or 2.23 represent a closed system of equations in eight unknowns U_e(i = 1,2), ψ_e (i = 1,2), δ (i = 1,2) and β (i = 1,2) for each successive normal position J.

2.5.1 Method of solution

The above mentioned eight unknowns are determined by solving the eight equations simultaneously at each normal position. Since no direct substitution is possible, the solution is achieved in an iterative manner by a computer program. The flow chart of the program is shown in fig. 2.15, the algorithm consists of the following steps to establish flow conditions at meridional station J + 1 assuming conditions at station J are already calculated.

(I) Assume conditions at meridional station J + 1 i.e. $(U_{e_i}, \psi_{e_i}, \beta_i, \delta_i)_{J+1}$

(II) Solve quadratic equation 2.43b to obtain new value for $(\beta_i)_{J+1}$

(III) Solve equation 2.43a to obtain new value for $(\delta_i)_{J+1}$

(IV) Use equations 2.44 and 2.22 or 2.23 to get new values for $(U_{e_i})_{J+1}$

(V) Use relation 2.2b to obtain new values for (ψ_{e_i})

(VI) Check values assumed at step (I) against new values obtained, if in error use new improved values $(U_{e_i}, \psi_{e_i}, \beta_i, \delta_i)_{J+1}$ at (I) and repeat until convergence.

The data required by the program are the diffuser geometry and inlet conditions. Diffuser geometry is arranged as co-ordinates of successive normals or quasi-orthogonals and mean radius of curvature at each normal position. Inlet conditions are inviscid core conditions of meridional and tangential velocities and total enthalpy distributions, together with boundary layer inlet parameters of boundary layer thickness, skew angle and shape parameter H or n. The shape parameter is kept constant for each boundary layer throughout the diffuser.

The iterative method used is Newton-Raphson technique between equations 2.43a, 2.44 and 2.22 or 2.23 with U_{e_i}, δ_i as unknowns. This calculation is included in a second iteration loop for ψ_{e_i} as unknowns. The skew angles β_i (i = 1,2) are calculated within the Newton-Raphson iteration.

2.5.2 Limitation of the method

The method described above has been developed to calculate incompressible flow in vaneless diffusers which consists of turbulent boundary layers developing on smooth impermeable walls of small or zero curvature, and an inviscid core flow with curved or straight streamlines where the flow parameters can be approximated by a linear distribution.

The method will not handle flow after separation or after the boundary layers merge and the inviscid core disappears. The method is not capable of handling a cross-over velocity profile. No change of the shape parameter H is considered although a relation governing that change can easily be added to the system of equations and into the computer program.

Other limitations of the method can be systematically drawn from various equations and relations such that at any instance if

$$\ell_1 \cos \psi_e = \ell_2 \sin \psi_e \tan \beta$$

i.e. if $\tan \beta = \frac{\ell_1}{\ell_2} \frac{1}{\tan \psi_e}$ the program will fail (see equation 2.43a).

The velocity profiles inside the boundary layer are flexible in that no restriction is made for the power n in relation 2.39a. For the cross-flow profile, the relation used in the program is

$$\frac{\omega}{U_e} - (1 - y/\delta)^p \frac{u}{U_e} \tan \beta \qquad 2.47$$

where p can take any value. Calculations in this work used p = 2,

however, the program was arranged so that if p is any other value the various boundary layer parameters involving w are calculated by a numerical integration.

2.5.3 Some flow predictions using the method

The computer program, written in FORTRAN IV, was run to test its validity in prediction and to calculate some theoretical results. The program proved to be fast; on Bath University computer facility of MULTIX the computation time for a typical run was about two seconds. The program itself is amll (less than 500 lines) hence needs very little storage. No convergence problem was experienced in most of the cases due to the advantages of the simultaneous solution of all equations at a specific normal position.

Fig. 2.16 compares the experimental results of Gardow (49) with the theoretical prediction. A very good agreement is evident. Figs. 2.17 and 2.18 represent a comparison with the results of Jansen (46) as tabulated by Wheeler and Johnston (93). The agreement is still good although not as good as those in fig. 2.16. This may be due to the fact that Jansen, while using similar rig facilities as Gardow, used boundary layer suction at the diffuser inlet which resulted in an overall loss coefficient about half the value of that of Gardow, see Johnston and Dean (56).

To investigate the predicted effect of different diffuser geometries and inlet core conditions upon diffuser boundary layer development, three diffuser geometries having similar overall dimensions were compared. The three geometries of radial, conical and curved diffusers are shown in fig. 2.19.

Figs. 2.20 and 2.21 show the predicted development, for the three geometries, of the hub and shroud boundary layer parameters respectively with uniform inlet velocity and flow angle distributions and a zero total enthalpy gradient. Figs. 2.22 and 2.23 represent the same geometries with the same uniform velocities at inlet, but having a total enthalpy difference across the inviscid core equivalent to 0.3K. Figs. 2.24

and 2.25 are the predicted hub and shroud boundary layer parameters with the same inlet total enthalpy gradient as for the latter case, but with non-uniform meridional and tangential velocity profiles, although the flow angle distribution is kept uniform i.e. with non-uniform absolute velocity distribution. From these three cases it can be observed that :-

(a) For uniform inlet conditions figs. 2.20 and 2.21

Since the inlet flow conditions are uniform, the radial diffuser showed symmetric flow indicated by identical hub and shroud boundary layer parameters with a flow angle at the wall γ ($\gamma = \psi_e + \beta$) increasing continuously with radius. The conical diffuser flow, as seen from wall flow angle γ, is more prone to separation at a small radius on the shroud and on the hub at large radius, see figs. 2.20 and 2.21. The curved diffuser has a wall flow angle γ decreasing in the curved contracting section and then increasing in the radial part on both hub and shroud. The boundary layer growth $\delta/_b$, is most rapid in the conical diffuser while the curved diffuser shows the lwest rate of boundary layer growth.

(b) For uniform velocity distribution with total enthalpy gradient at inlet figs. 2.22 and 2.23

The radial diffuser hub flow is predicted to separate early due to the total enthalpy gradient effect which is not opposed by any swirl created centrifugal force in the core (as realistically happens), see equation 2.2.4, this results in much lower boundary layer edge velocities, U_e, on the hub leading to a rapid increase in skew angle β and separation of the boundary layer. Due to the opposing effect between swirl and total enthalpy gradient in the core, the hub flow of the conical diffuser did not separate although it had a similar trend to that of the radial diffuser through half its passage, see fig. 2.22 The curved diffuser showed no change of trend to that shown with a uniform total enthalpy distribution.

(c) For non-uniform inlet conditions, figs. 2.24 and 2.25

The major trend of the radial diffuser flow is similar to that of case (b) with separation occurring at approximately the same radius. The conical diffuser flow indicated separation on the hub half way through

the diffuser. Separation in the case of the conical diffuser is partly due to the increase in inlet flow angle from 60 degrees in case (b) to 65 degrees in case (c) (see fig. 2.24). Again the curved diffuser showed a general pattern of behaviour similar to those of case (a) and (b).

To further investigate the effect of inlet conditions on the curved diffuser, figs. 2.26 and 2.27 show the effect of a swirl angle change from 60 degrees to 70 degrees with $\Delta T_o = 0.0^oK$. Figs. 2.28 and 2.29 compare the effect of an enthalpy gradient for a constant swirl angle. While the general trend remained unchanged for all cases, the change of swirl angle of 10^o had a more profound effect on the boundary layer parameters than a change of total temperature difference of 0.3K.

Figs. 2.30 and 2.31 show the effect of enthalpy difference on the conical diffuser. Although almost similar conditions were predicted at exit for both $\Delta T_o = 0.0K$ and $\Delta T_o = 0.3K$, the flow pattern inside the diffuser is markedly different. With high enthalpy gradients a separation could be expected near the inlet on the hub side.

From the previous theoretical comparisons it can be concluded that the boundary layer analysis supports the suggestion by Wallace et al (21) that a curved diffuser will have a more stable flow over a wide range of inlet conditions.

SIGN CONVENTION FOR THE RADIUS OF CURVATURE R_c

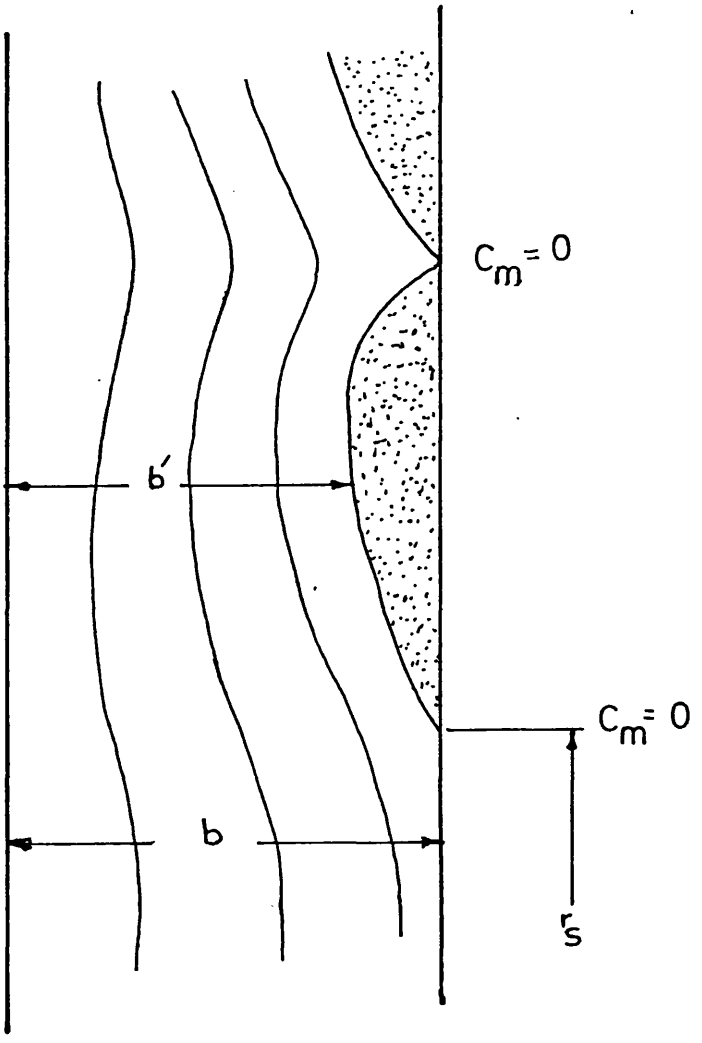

FIG. 2.1 FORCED RE-ATTACHMENT IN AN INVISCID SOLUTION

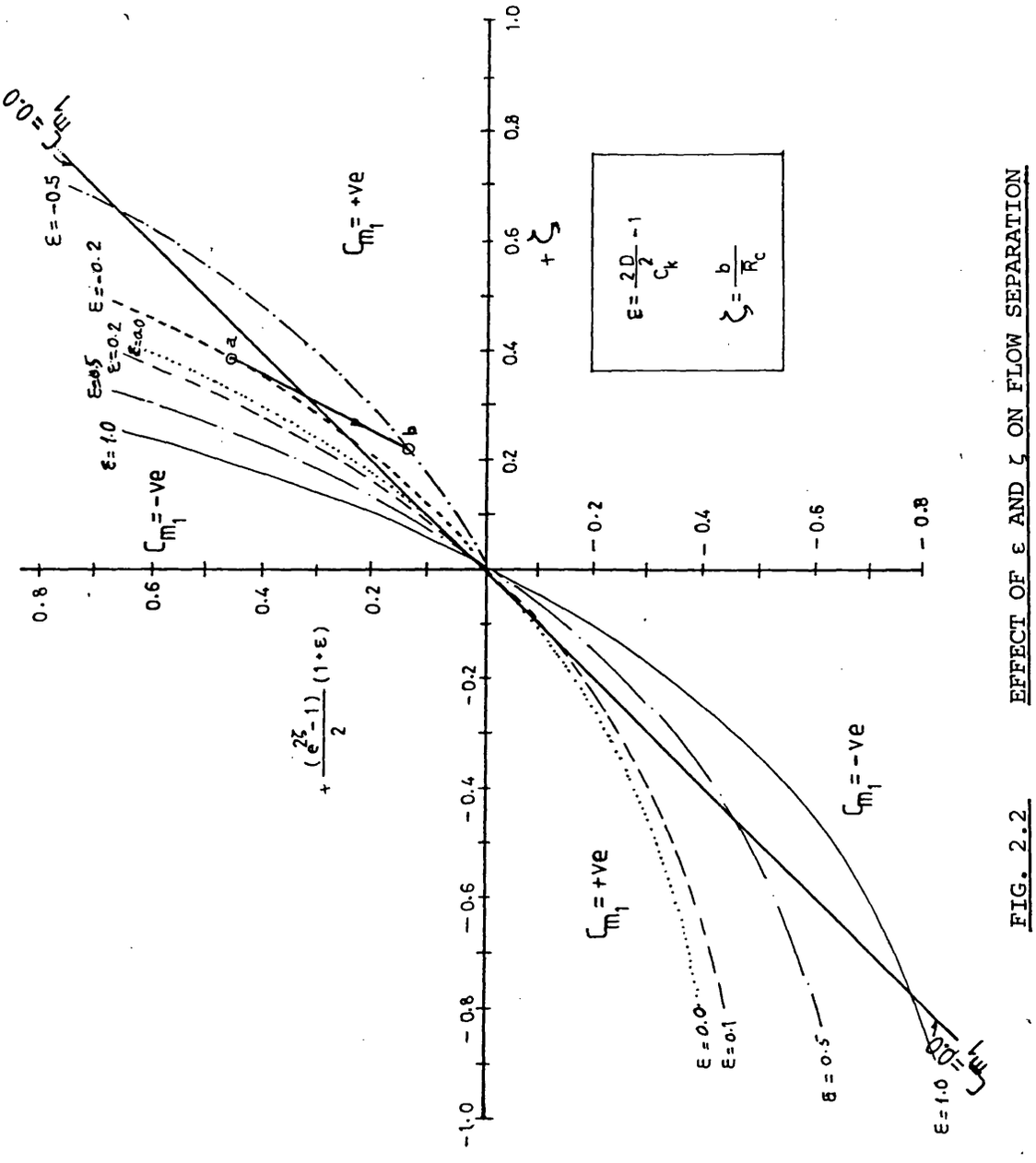

FIG. 2.2 EFFECT OF ε AND ζ ON FLOW SEPARATION

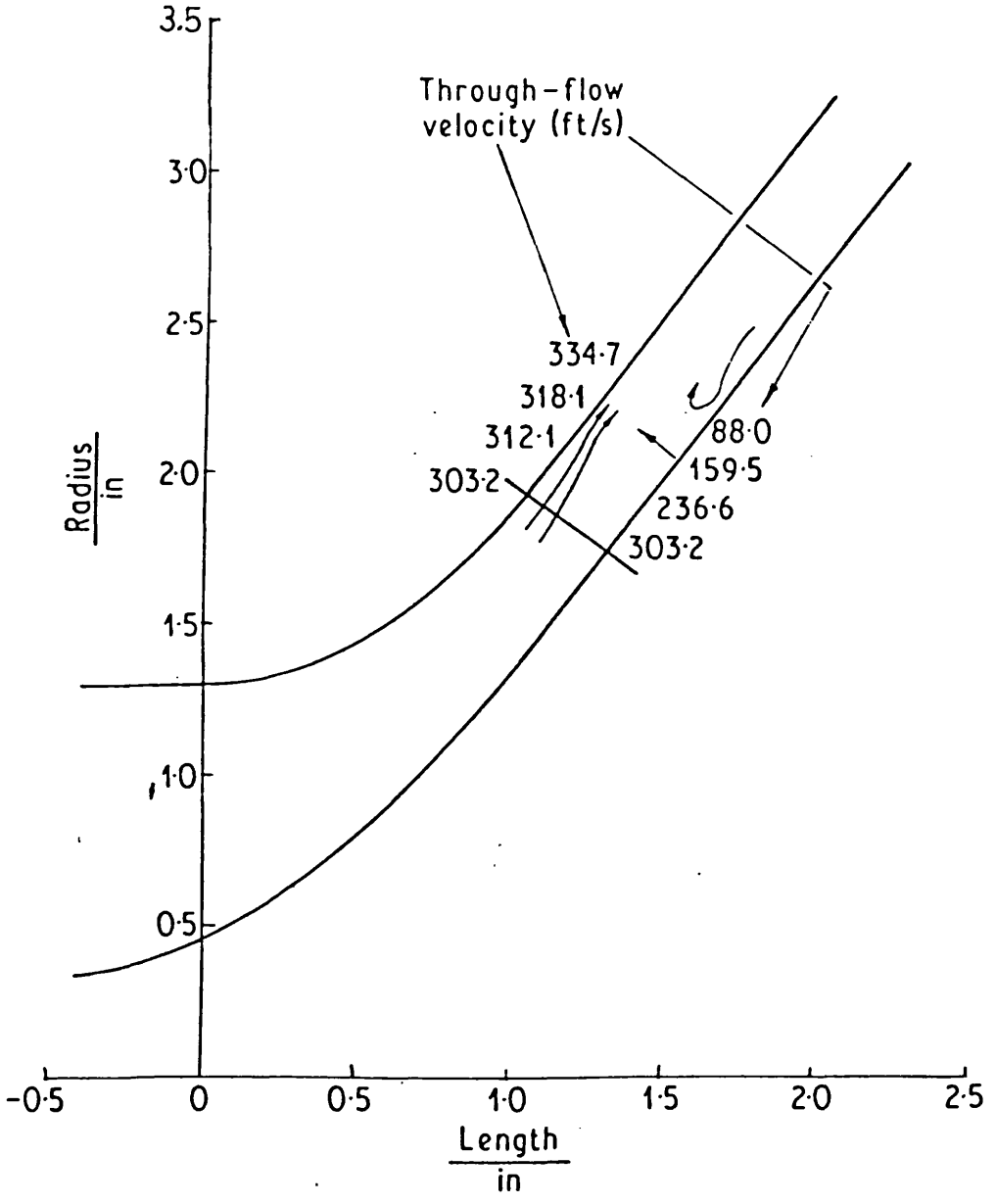

Fig.2.3 *Conical diffuser with angled impeller cut-off*
(REF. 21)

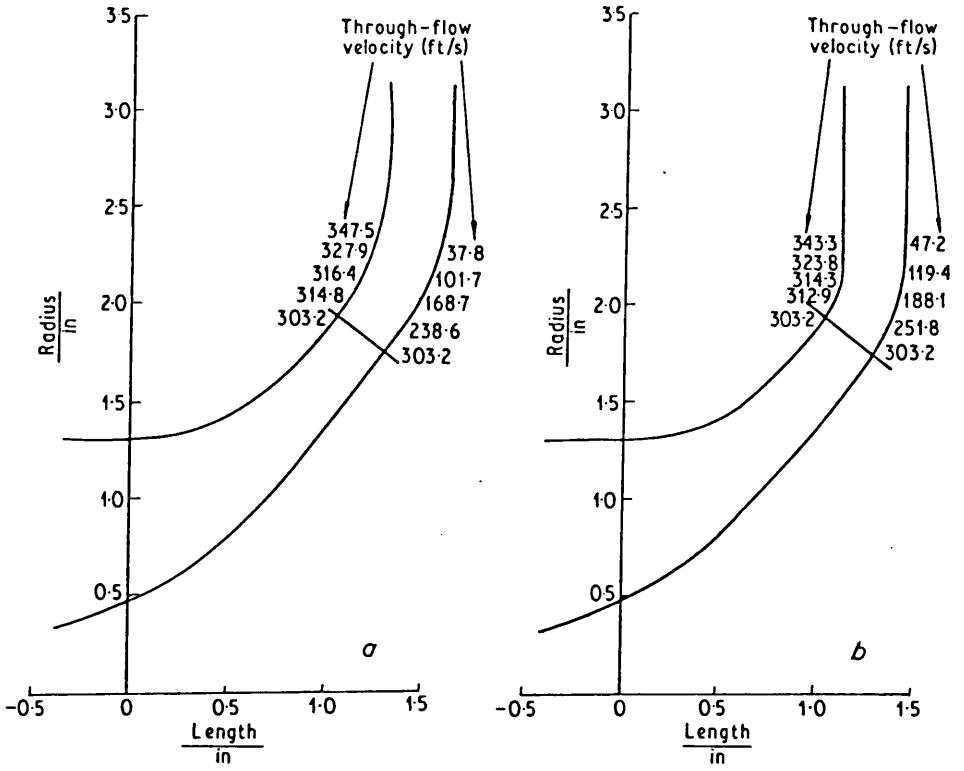

Curved diffusers with zero contraction: (a) mean radius of curvature 1.67 in; (b) mean radius of curvature 0.44 in

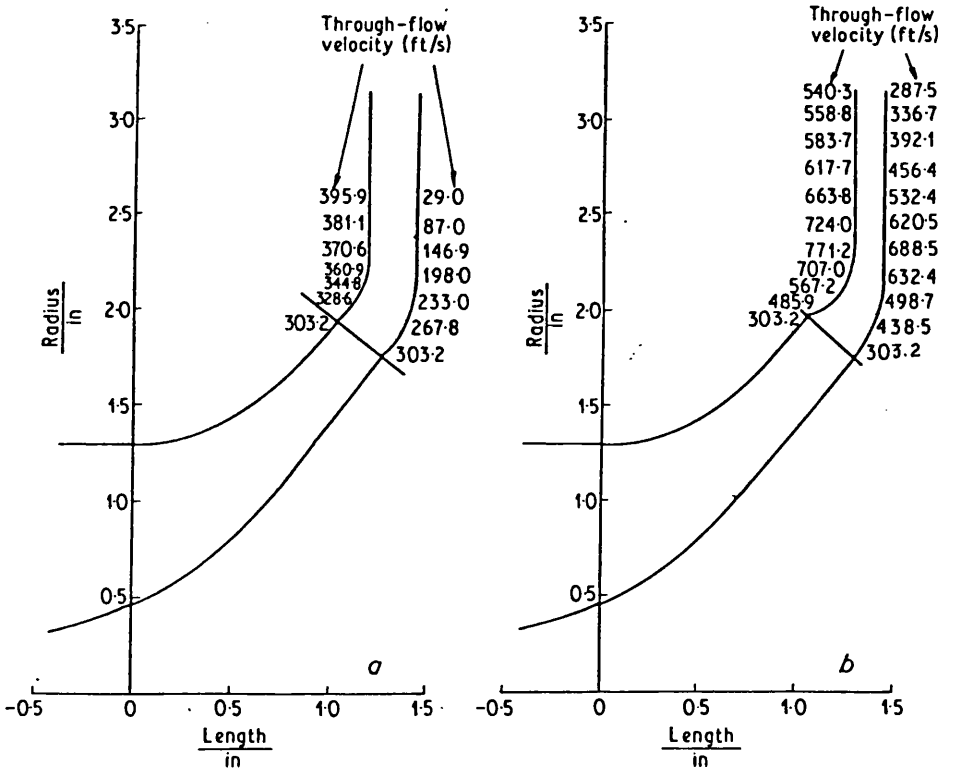

Curved diffusers with initial contraction: (a) contraction ratio 0.885; (b) contraction ratio 0.540

FIG. 2.4 EFFECT OF CURVATURE AND CONTRACTION ON FLOW SEPARATION (FROM REF.21)

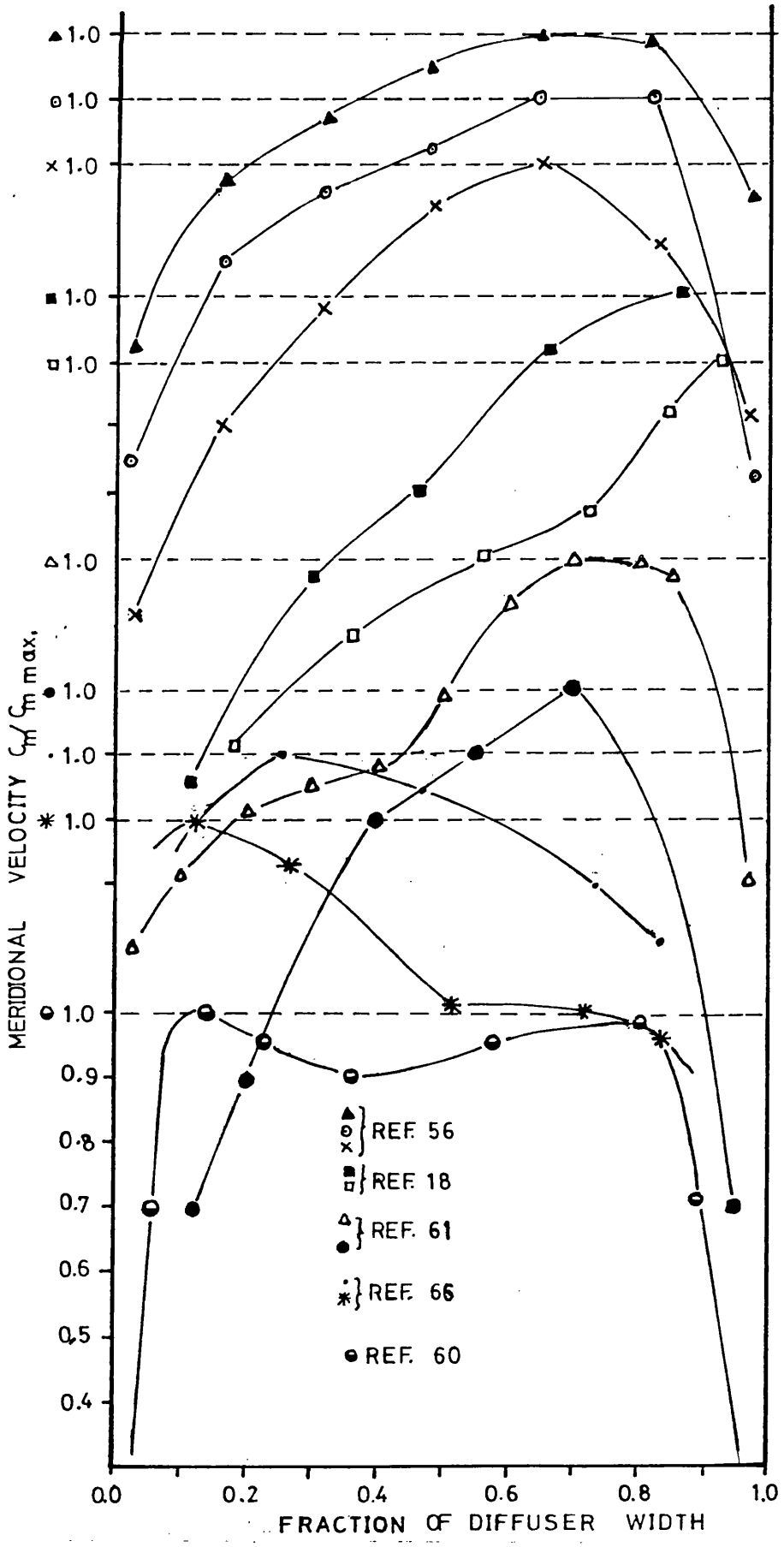

FIG. 2.5 MEASURED MERIDIONAL VELOCITY PROFILES AT THE INLET TO CENTRIFUGAL COMPRESSOR DIFFUSERS FROM THE LITERATURE

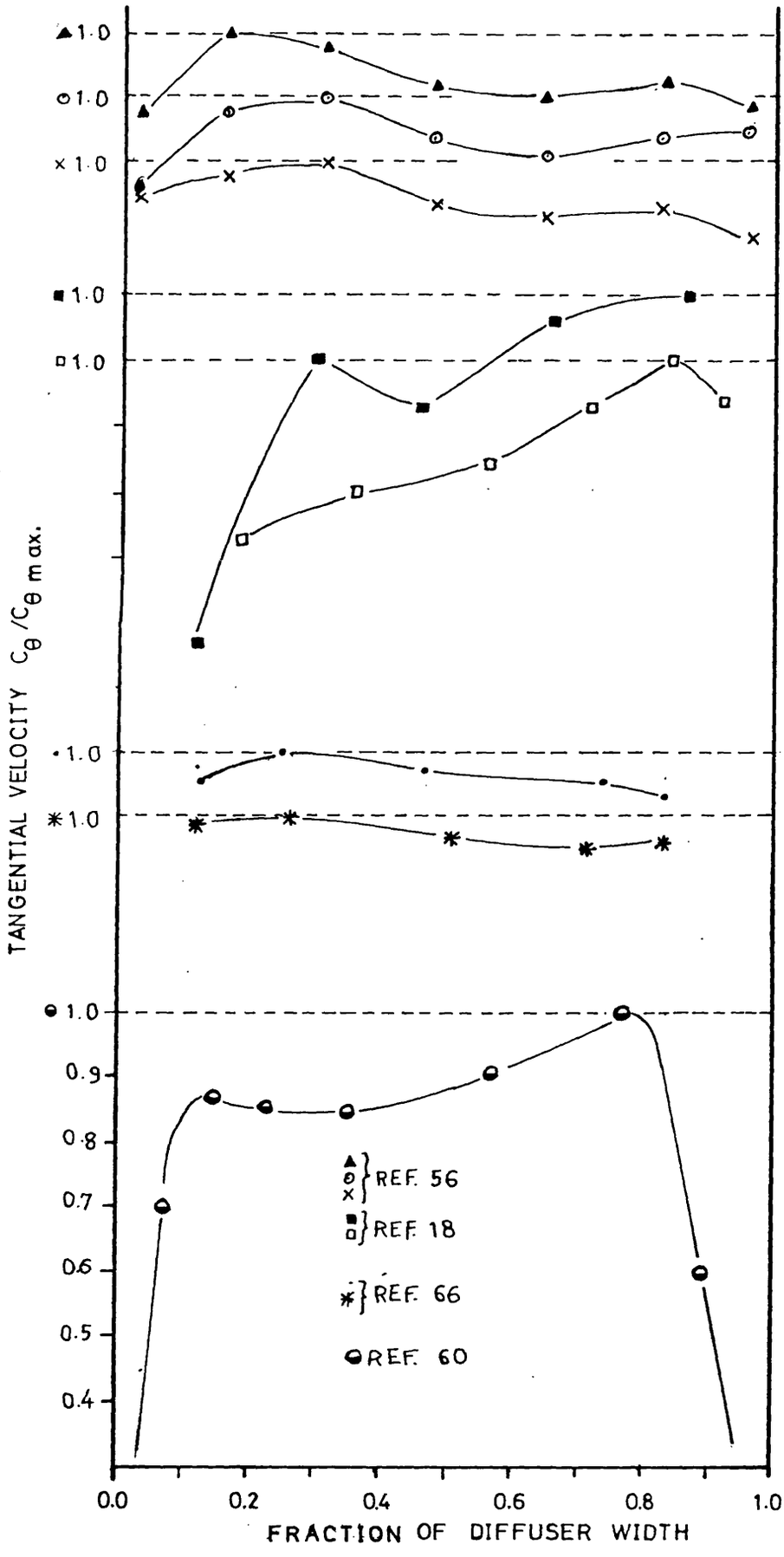

FIG. 2.6 MEASURED TANGENTIAL VELOCITY PROFILES AT THE INLET TO CENTRIFUGAL COMPRESSOR DIFFUSERS FROM THE LITERATURE

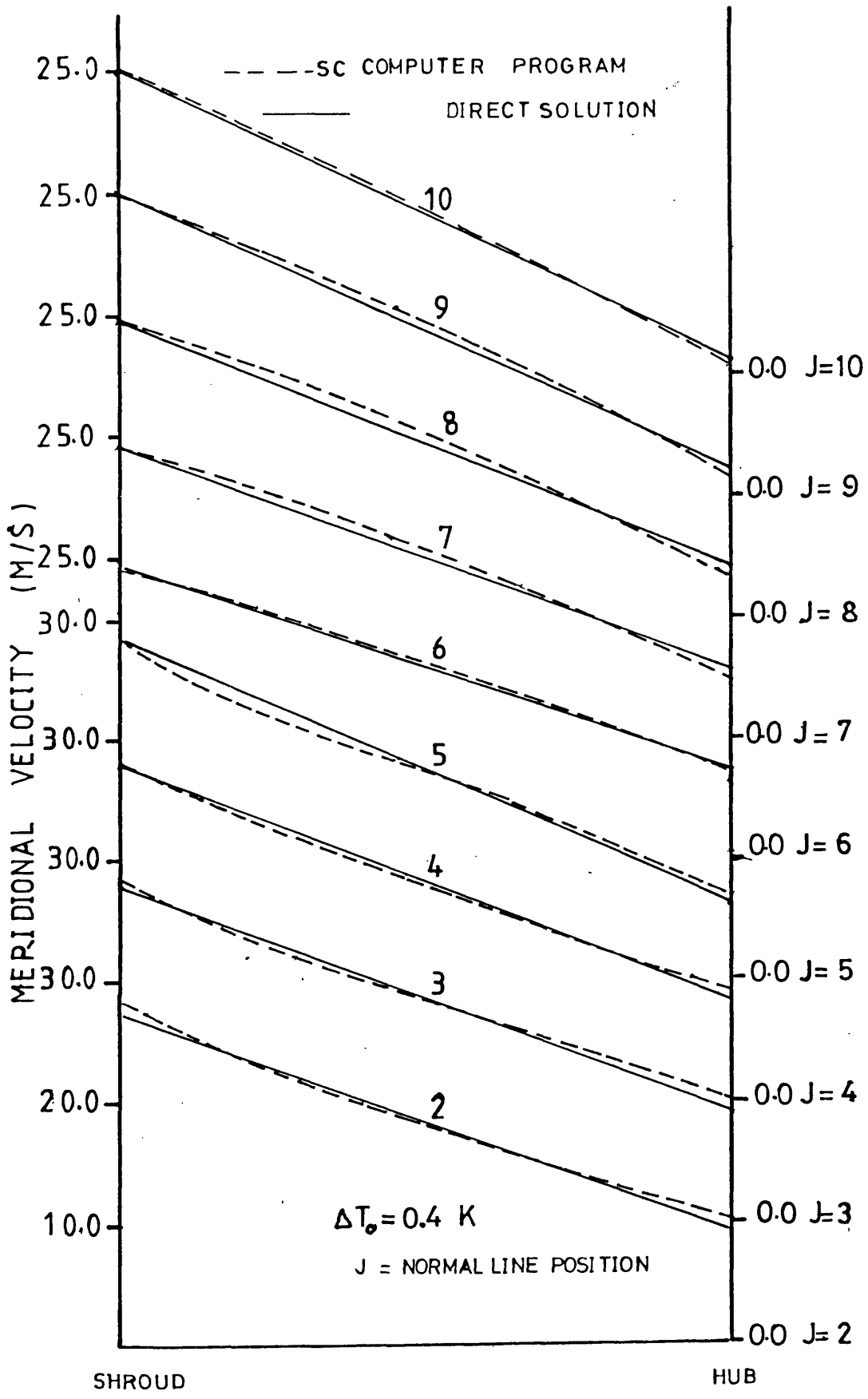

FIG. 2.7 COMPARISON BETWEEN DIRECT ANALYTICAL SOLUTION AND STREAMLINE CURVATURE NUMERICAL SOLUTION (CURVED DIFFUSER)

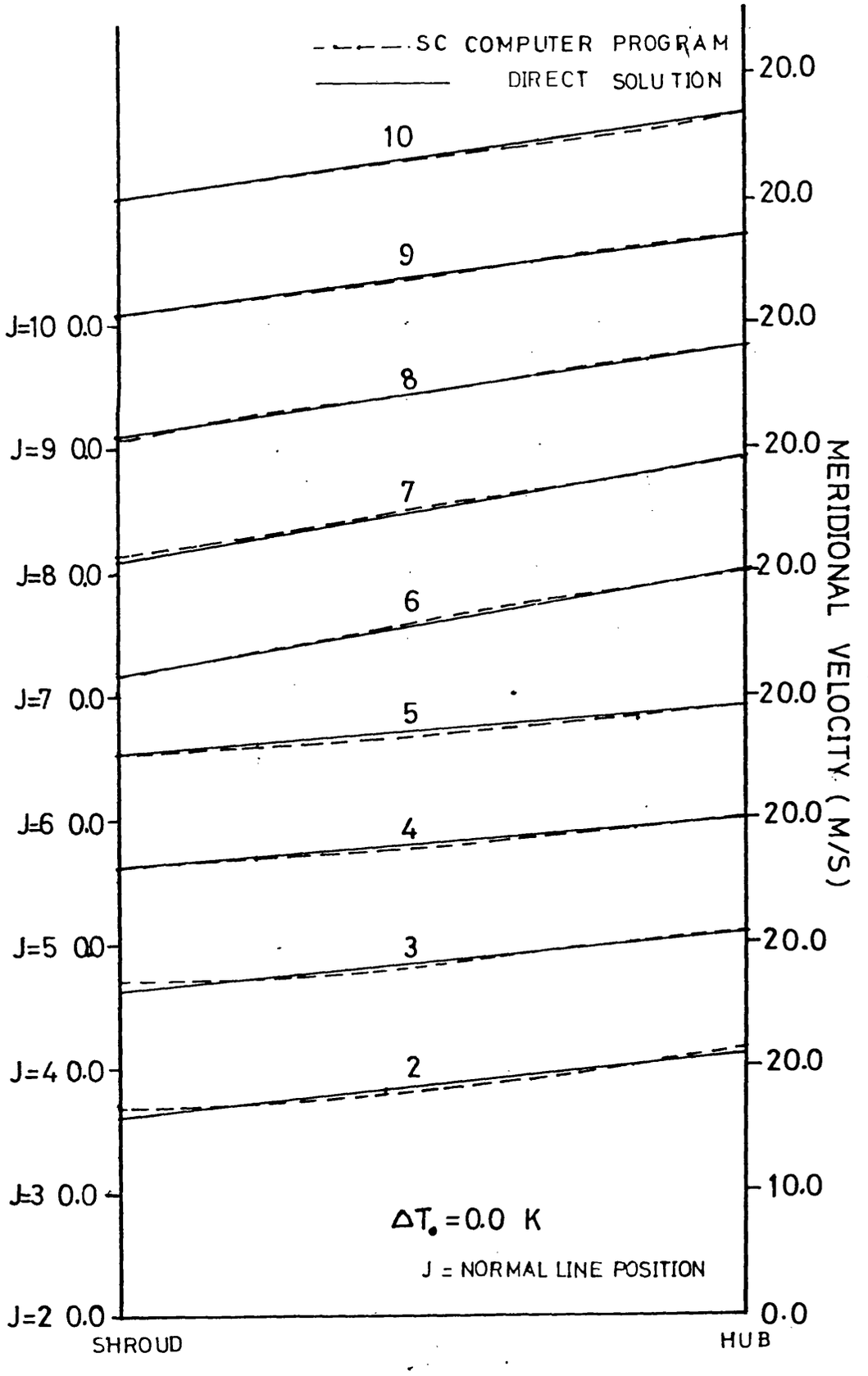

FIG. 2.8 COMPARISON BETWEEN DIRECT ANALYTICAL SOLUTION AND STREAMLINE CURVATURE NUMERICAL SOLUTION (CURVED DIFFUSER)

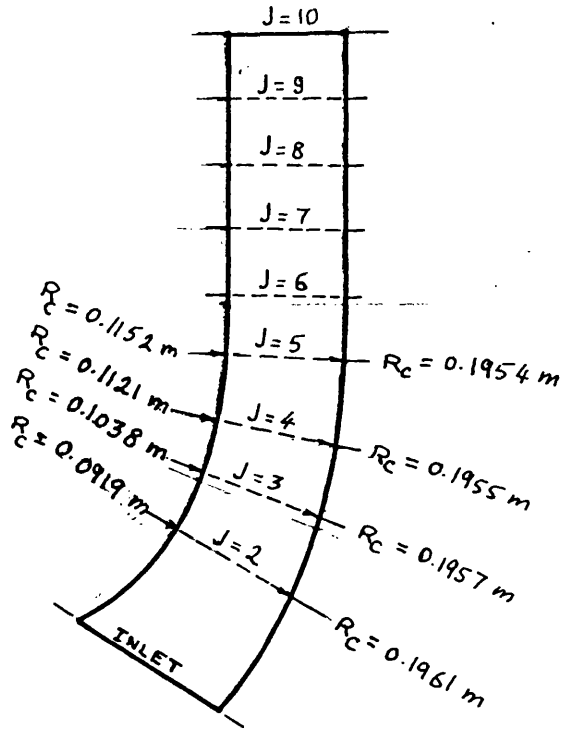

FIG. 2.9a GEOMETRY OF DIFFUSER USED IN CALCULATIONS OF FIGS. 2.7 and 2.8.

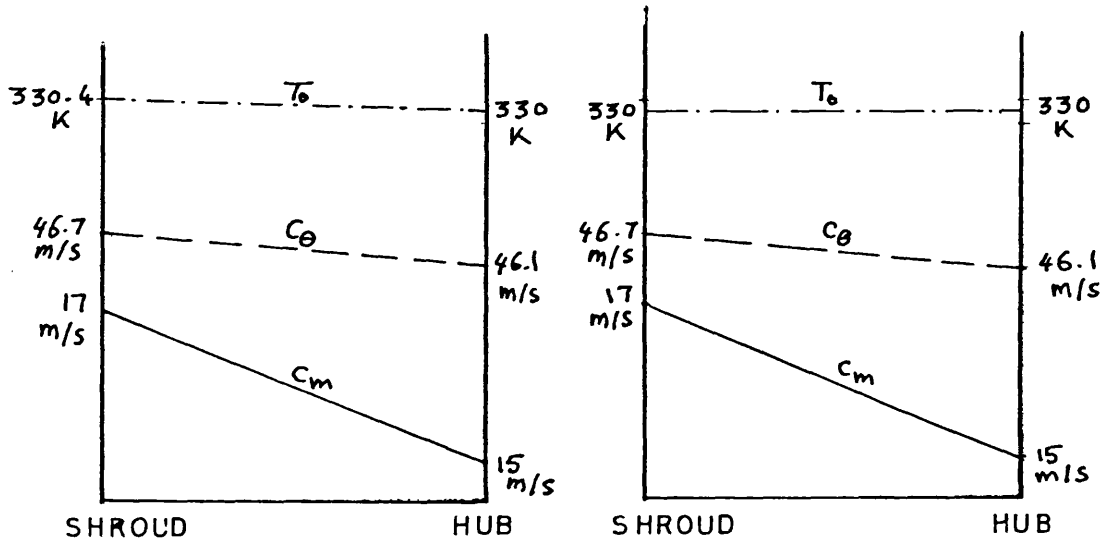

FIG. 2.9b INLET CONDITIONS OF DIFFUSER USED IN CALCULATIONS OF FIGS. 2.7 and 2.8

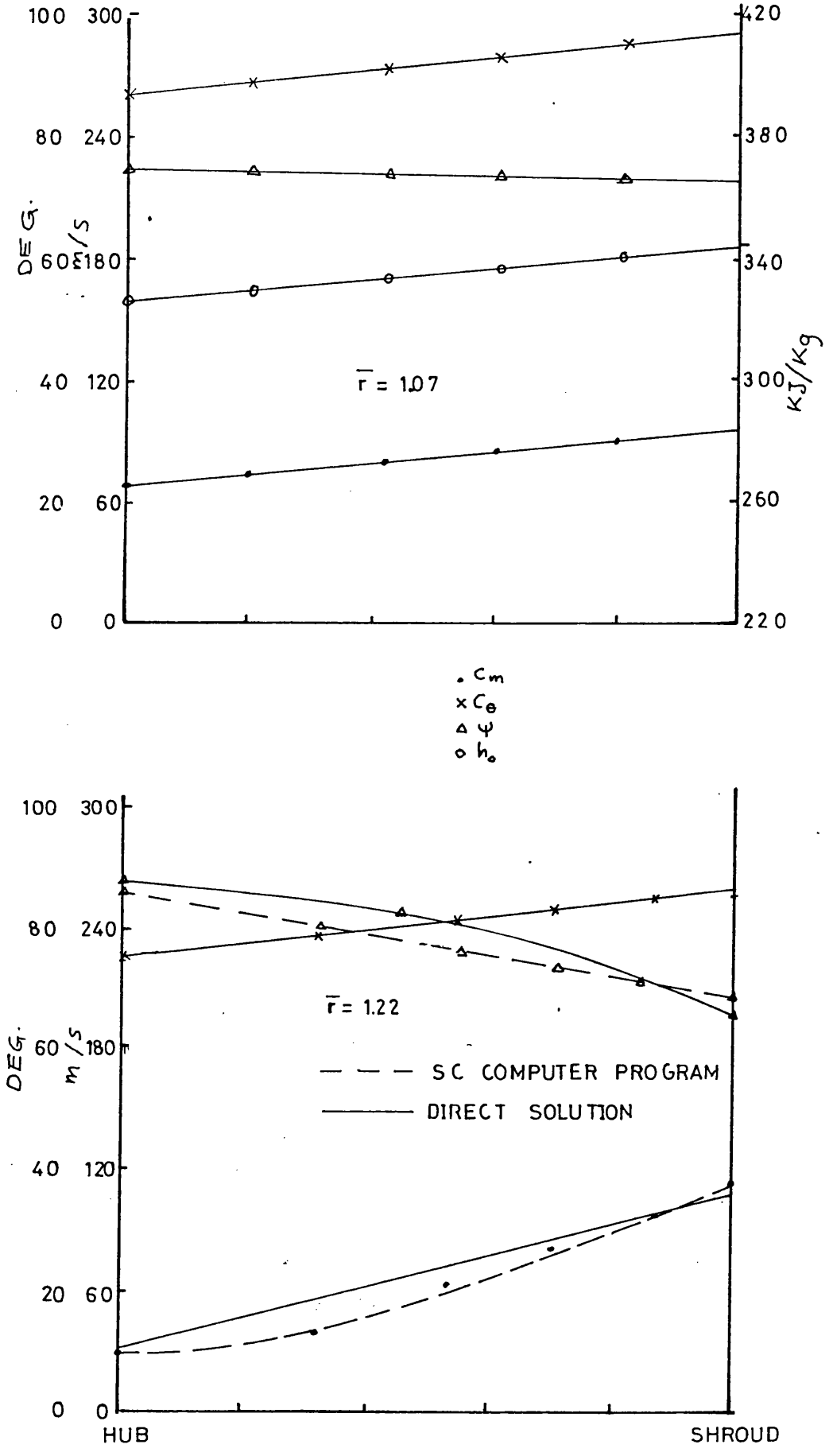

FIG. 2.10 COMPARISON BETWEEN DIRECT ANALYTICAL SOLUTION AND STREAMLINE CURVATURE NUMERICAL SOLUTION (CONICAL DIFFUSER)

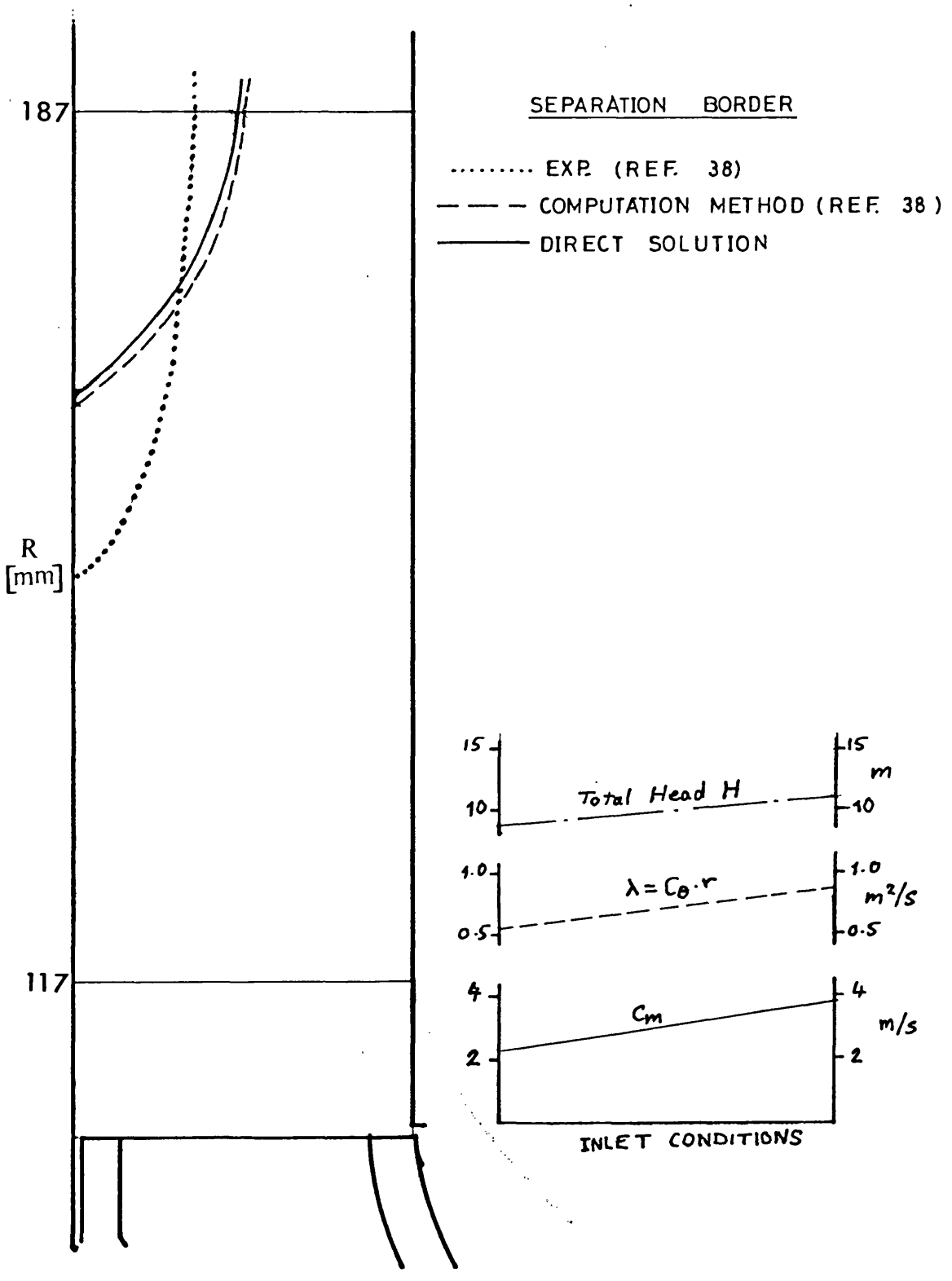

FIG. 2.11 COMPARISON BETWEEN DIRECT ANALYTICAL SOLUTION AND COMPUTATION METHOD OF REF. 38 (RADIAL DIFFUSER)

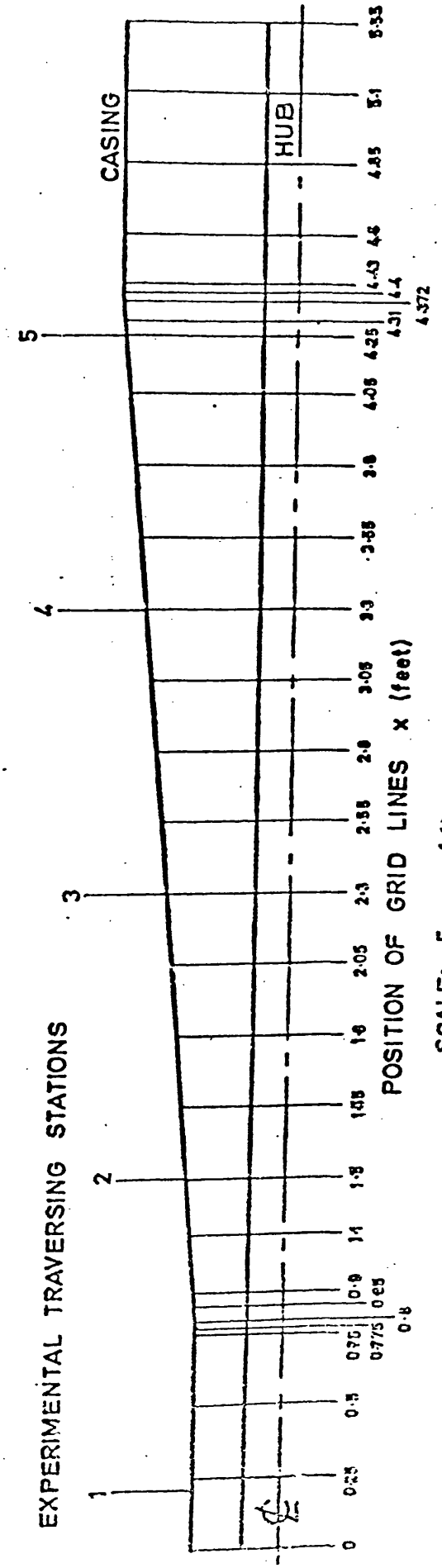

FIG. 2.12 CONICAL DIFFUSER AND THEORETICAL MATRIX GRID USED BY HOADLEY REF. 43.

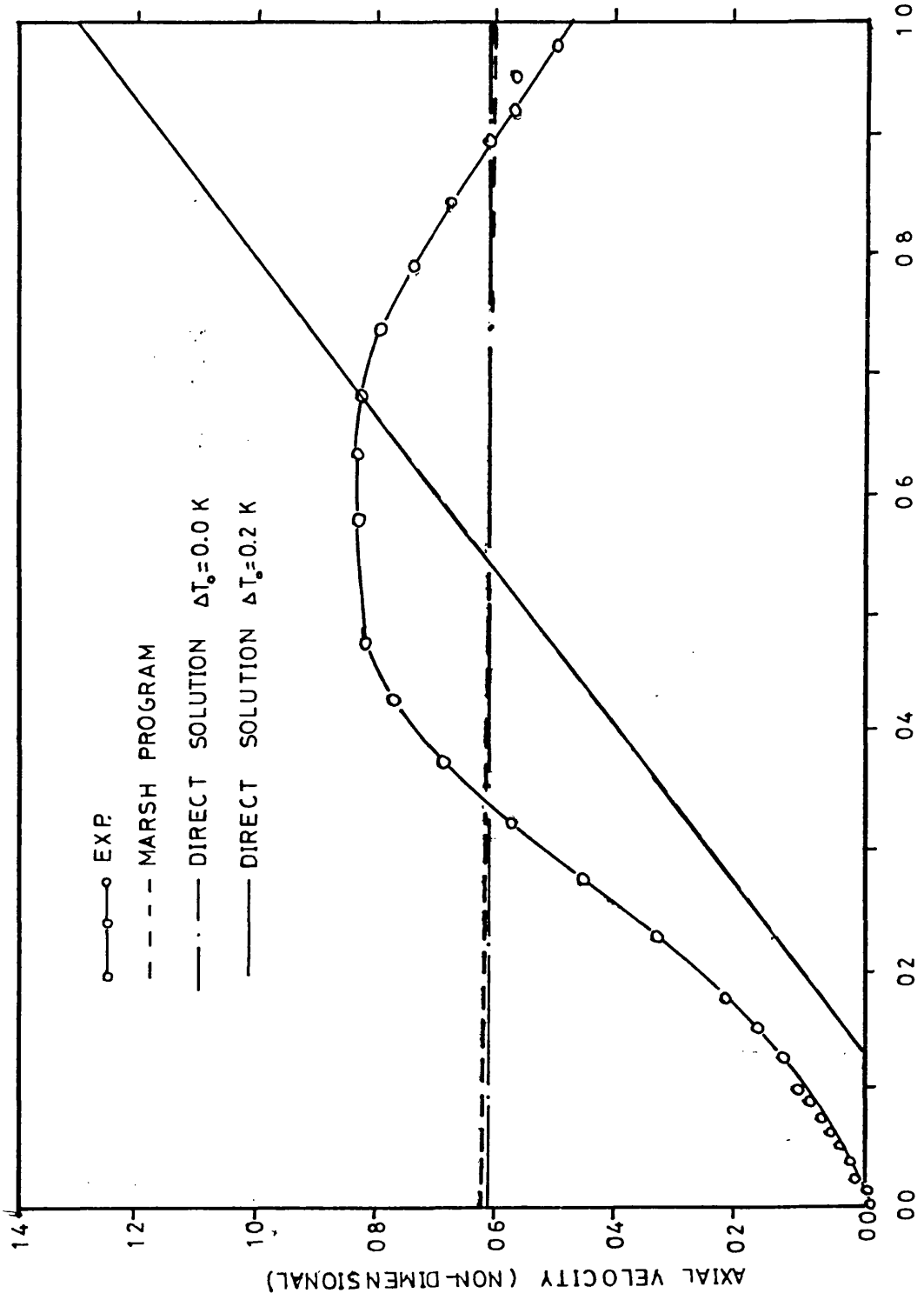

FIG. 2.13 COMPARISON BETWEEN DIRECT ANALYTICAL SOLUTION AND MATRIX METHOD CALCULATION (FROM REF. 43)

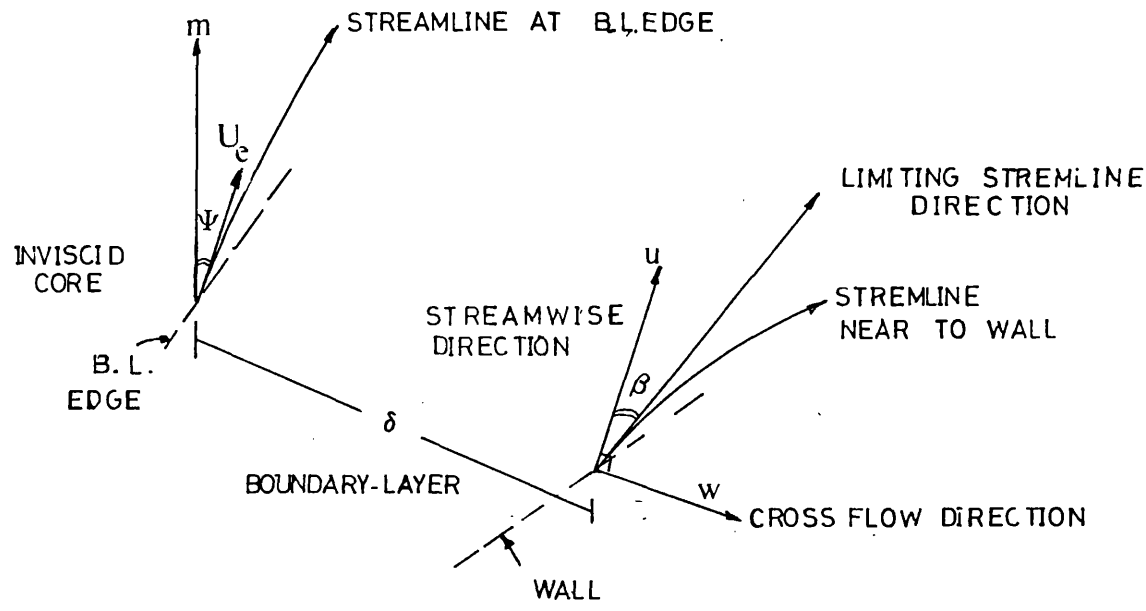

FIG. 2.14a STREAMLINE CO-ORDINATE SYSTEM

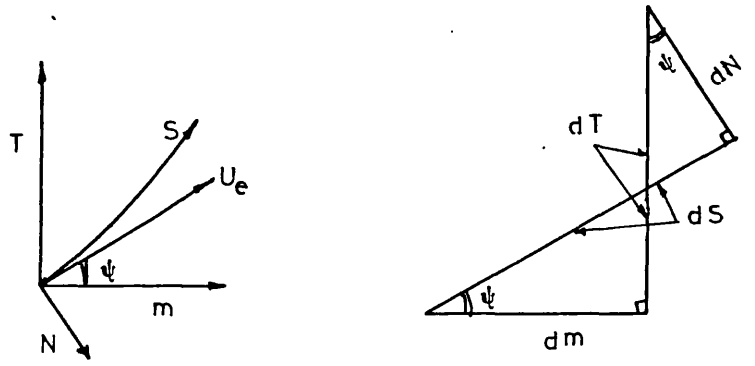

dm = meridional co-ordinate

dT = co-ordinate $\perp$ r to the meridional (tangential)

$dT = ds \sin\psi + dN \cos\psi$

$dm = ds \cos\psi - dN \sin\psi$ if $f(m,T) = f(S,N)$

Eliminating dm and dT and comparing coefficient of ds and dN

$$\cos\psi \frac{\partial}{\partial m} + \sin\psi \frac{\partial}{\partial T} = \frac{\partial}{\partial s}$$

$$\cos\psi \frac{\partial}{\partial T} - \sin\psi \frac{\partial}{\partial m} = \frac{\partial}{\partial N}$$

$\frac{\partial}{\partial T} = 0$ for axisymmetry

FIG. 2.14b RELATION BETWEEN DIFFERENTIALS IN MERIDIONAL AND TANGENTIAL DIRECTION AND IN STREAMLINE CO-ORDINATE

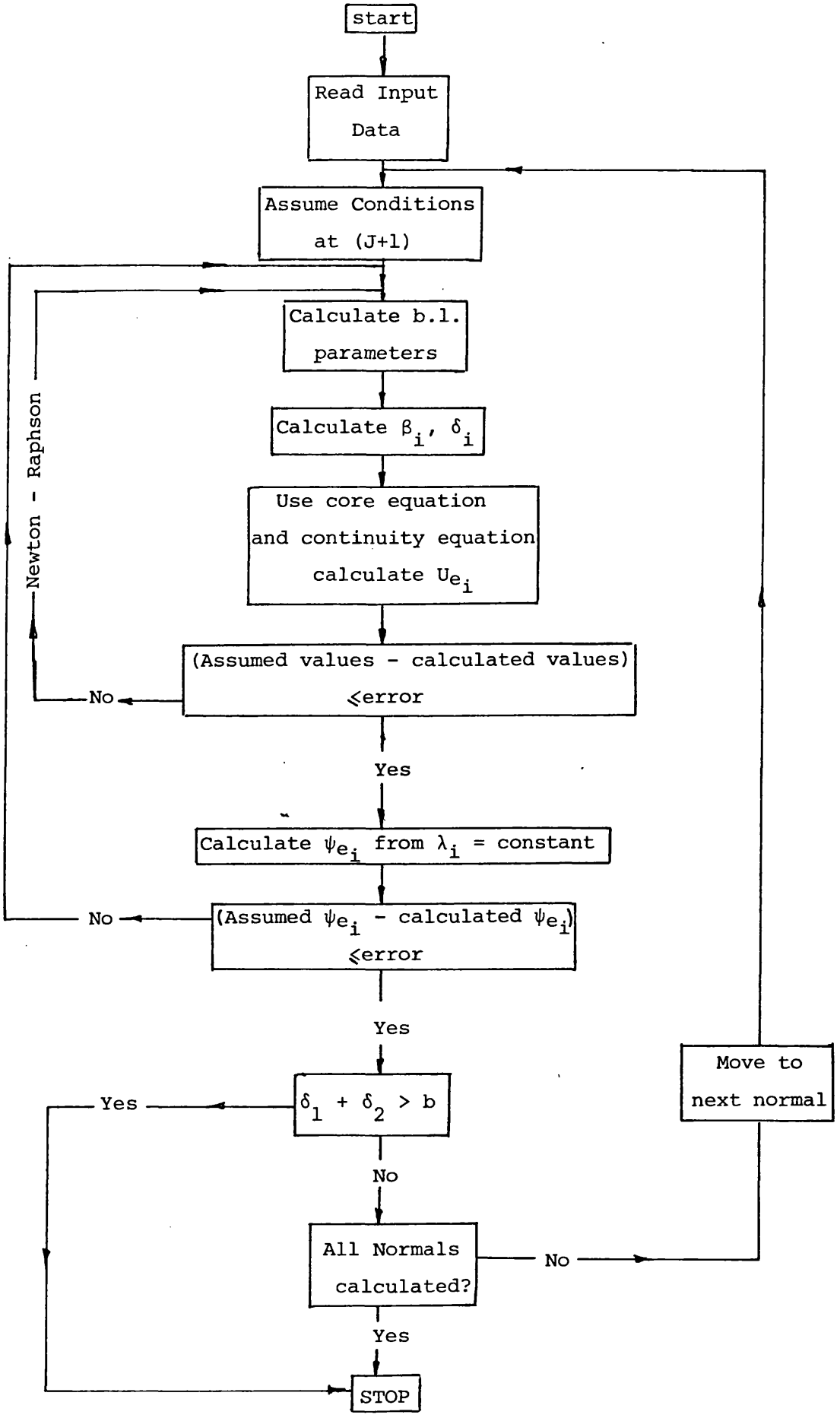

FIG. 2.15 FLOW CHART OF THE BOUNDARY LAYER COMPUTER PROGRAM

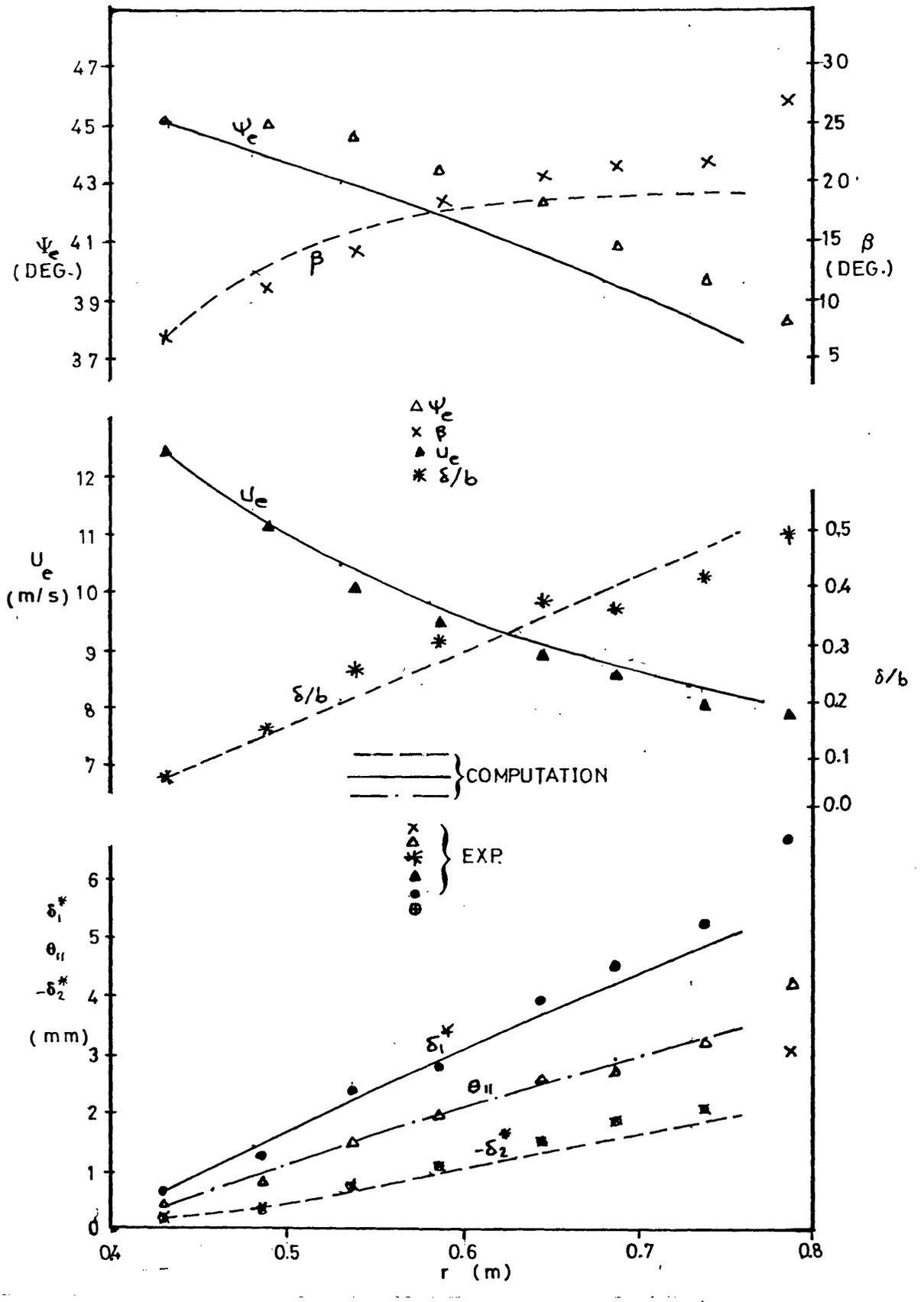

FIG. 2.16 COMPARISON BETWEEN BOUNDARY LAYER CALCULATION AND GARDOW A-45.2 RADIAL DIFFUSER (REF.49)

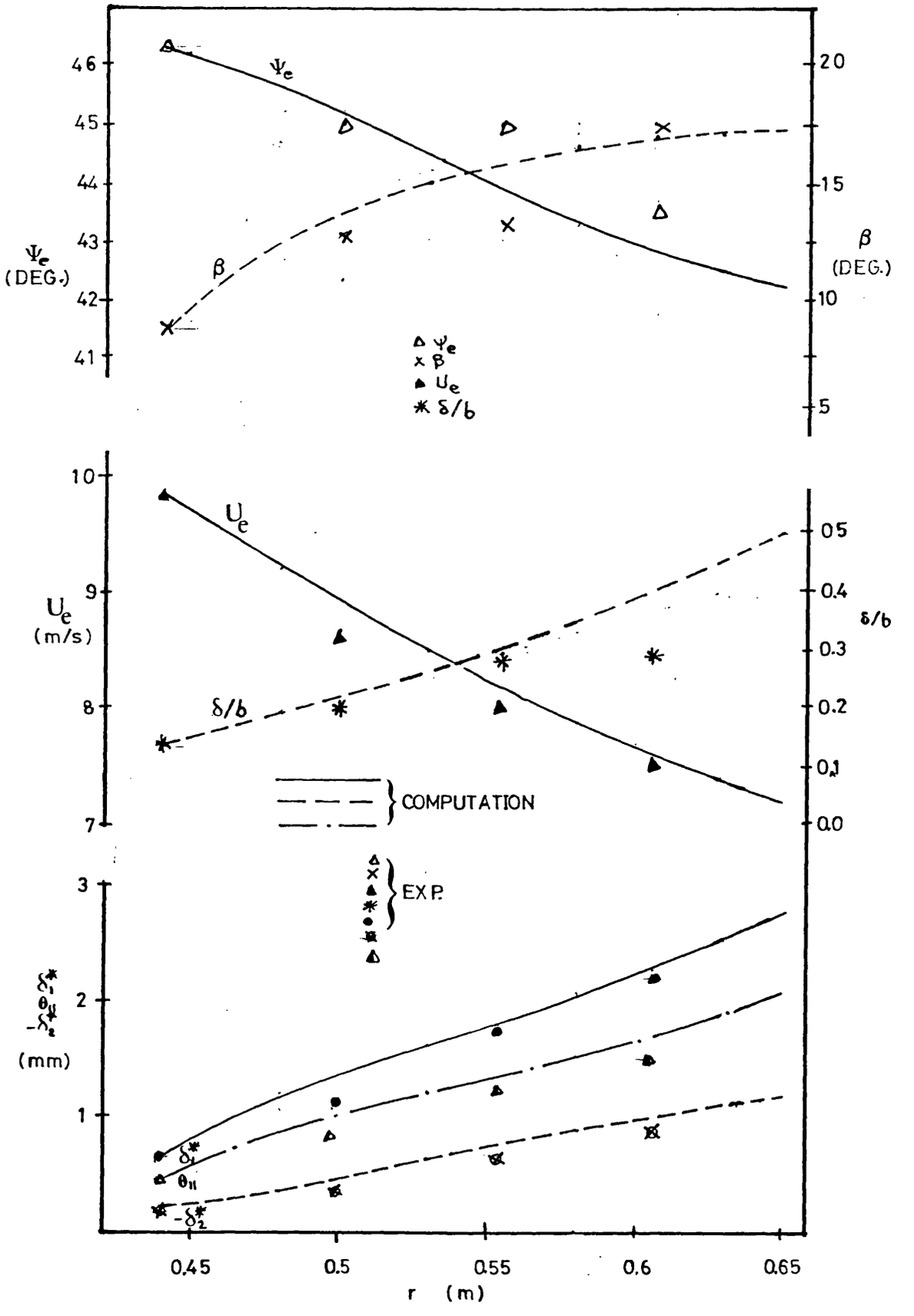

FIG. 2.17 COMPARISON BETWEEN BOUNDARY LAYER CALCULATION AND JANSEN 47° RADIAL DIFFUSER (REF.93)

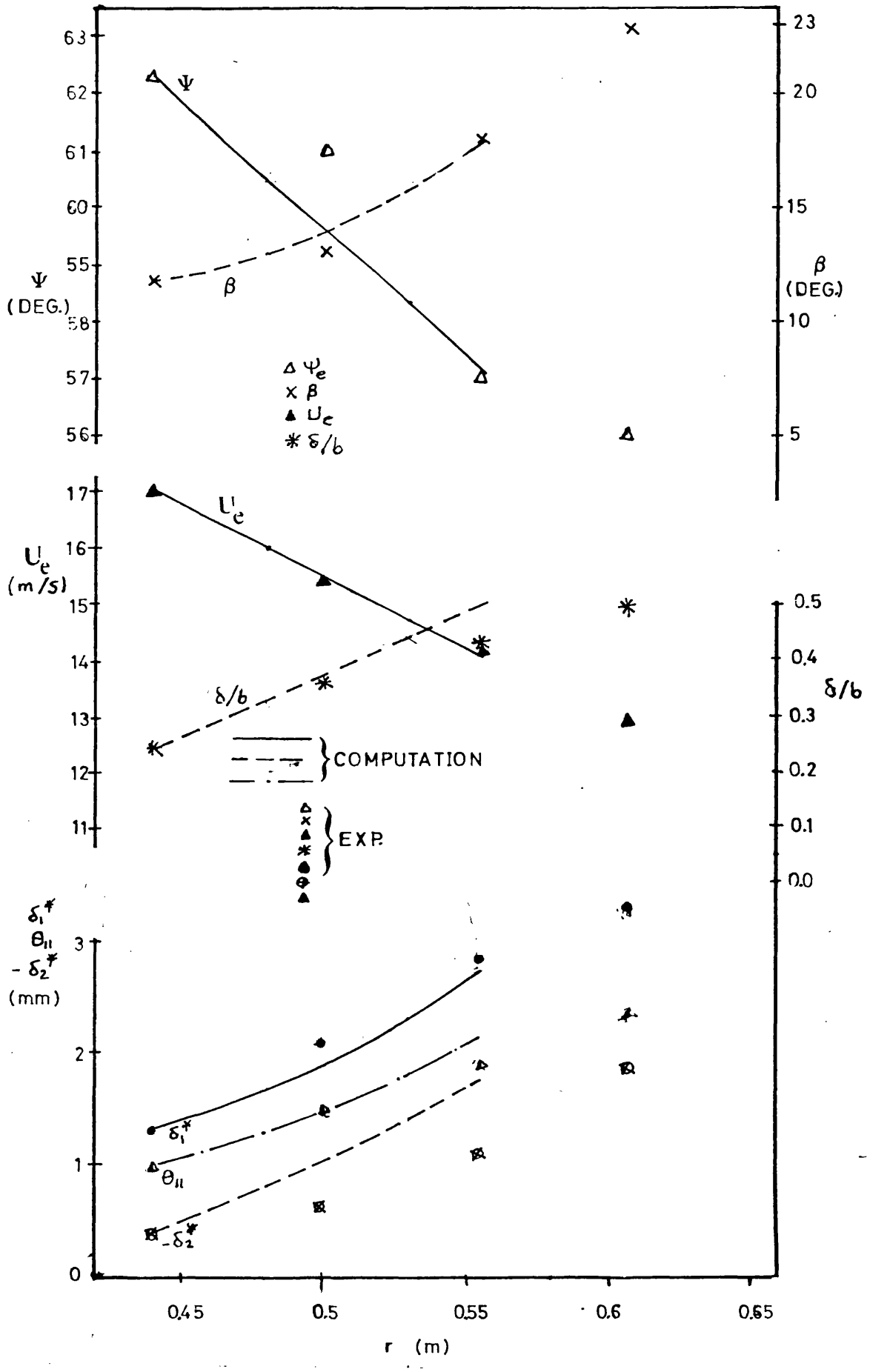

FIG. 2.18 COMPARISON BETWEEN BOUNDARY LAYER CALCULATION AND JANSEN 67° RADIAL DIFFUSER (REF.93)

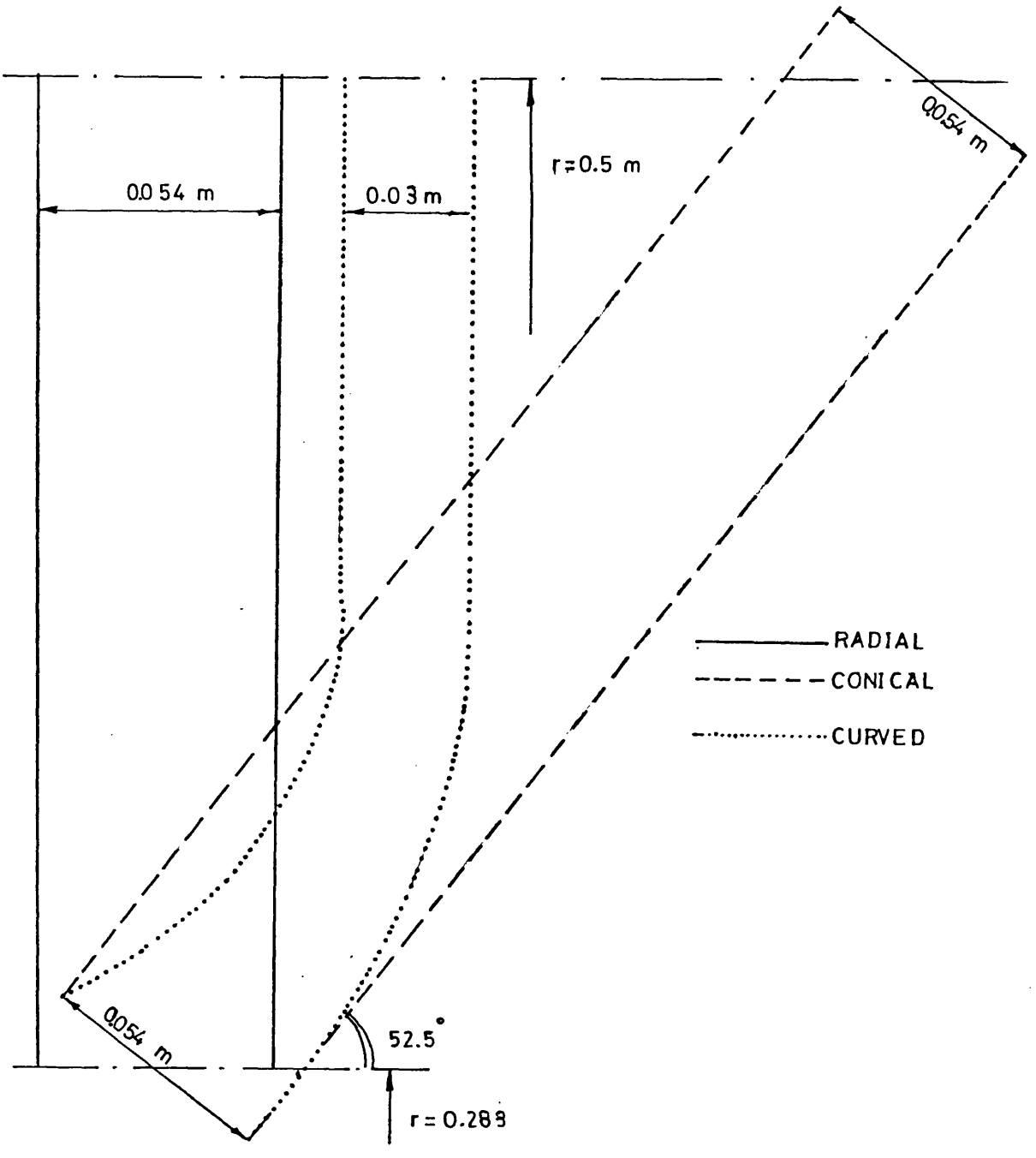

FIG. 2.19 RADIAL, CONICAL AND CURVED DIFFUSER GEOMETRIES USED IN THEORETICAL COMPARISON

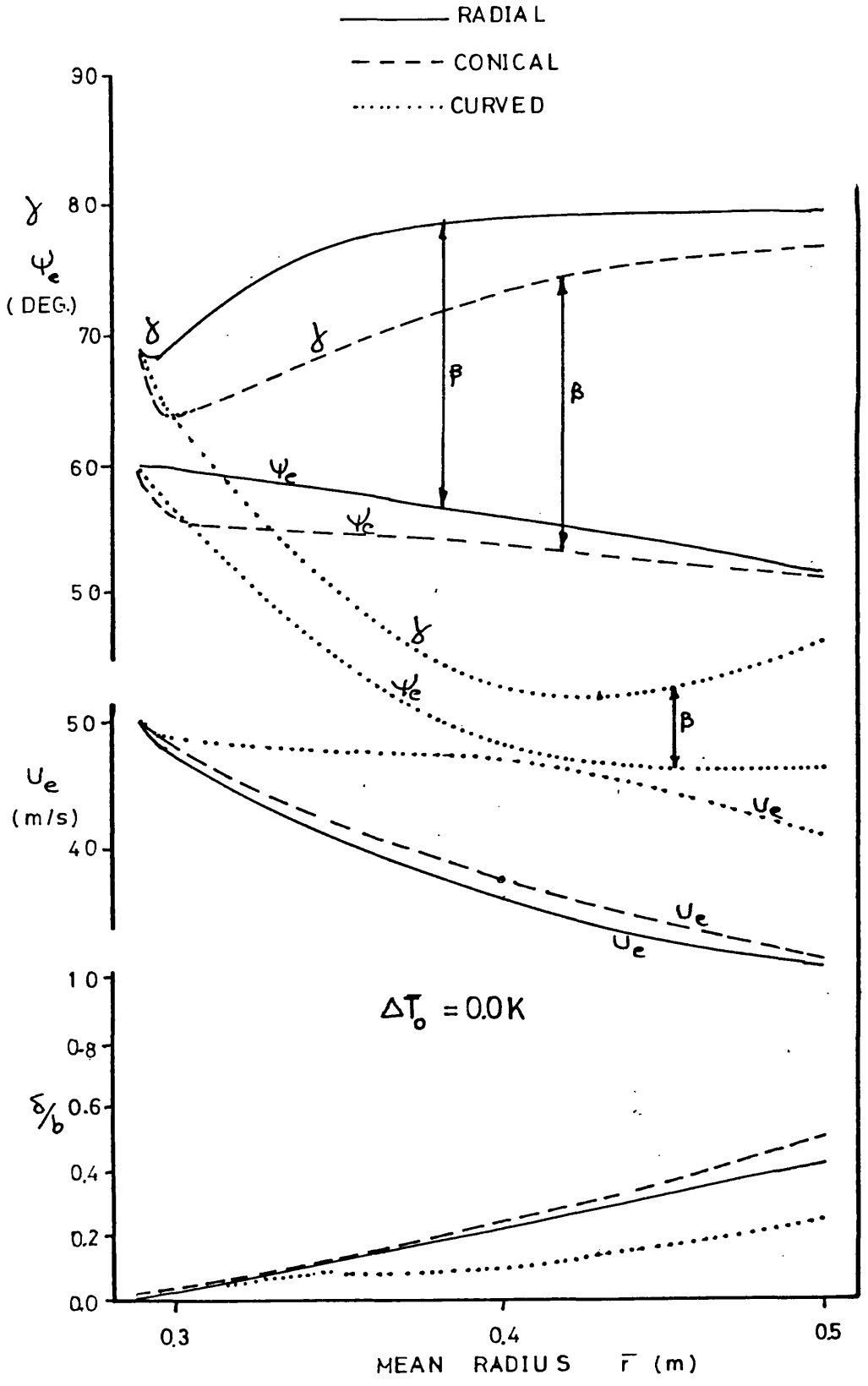

FIG. 2.20 DEVELOPMENT OF HUB BOUNDARY LAYERS FOR UNIFORM INLET CONDITIONS

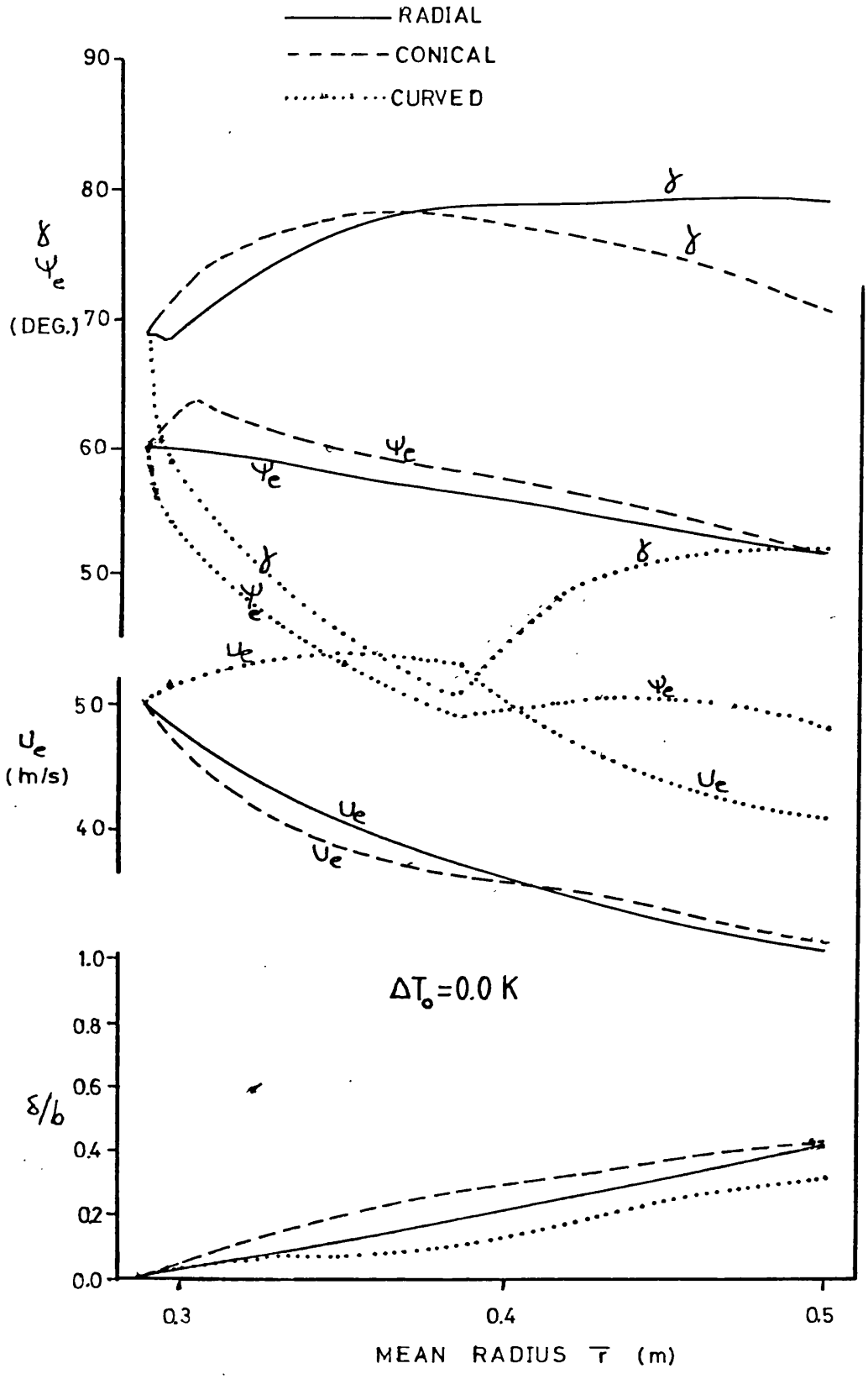

FIG. 2.21 DEVELOPMENT OF SHROUD BOUNDARY LAYERS FOR UNIFORM INLET CONDITIONS

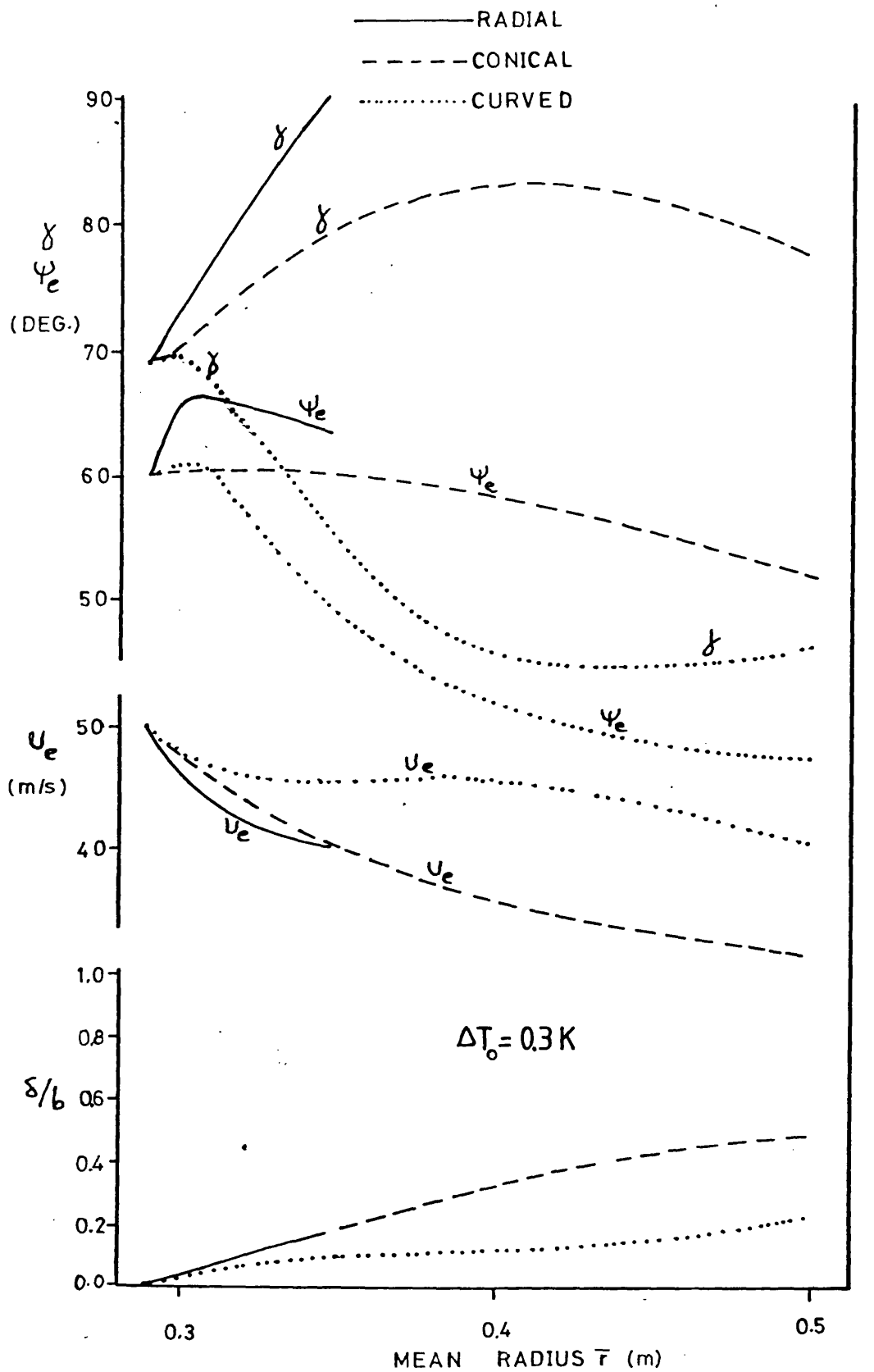

FIG. 2.22 DEVELOPMENT OF HUB BOUNDARY LAYERS FOR UNIFORM VELOCITY WITH TOTAL ENTHALPY GRADIENT AT INLET

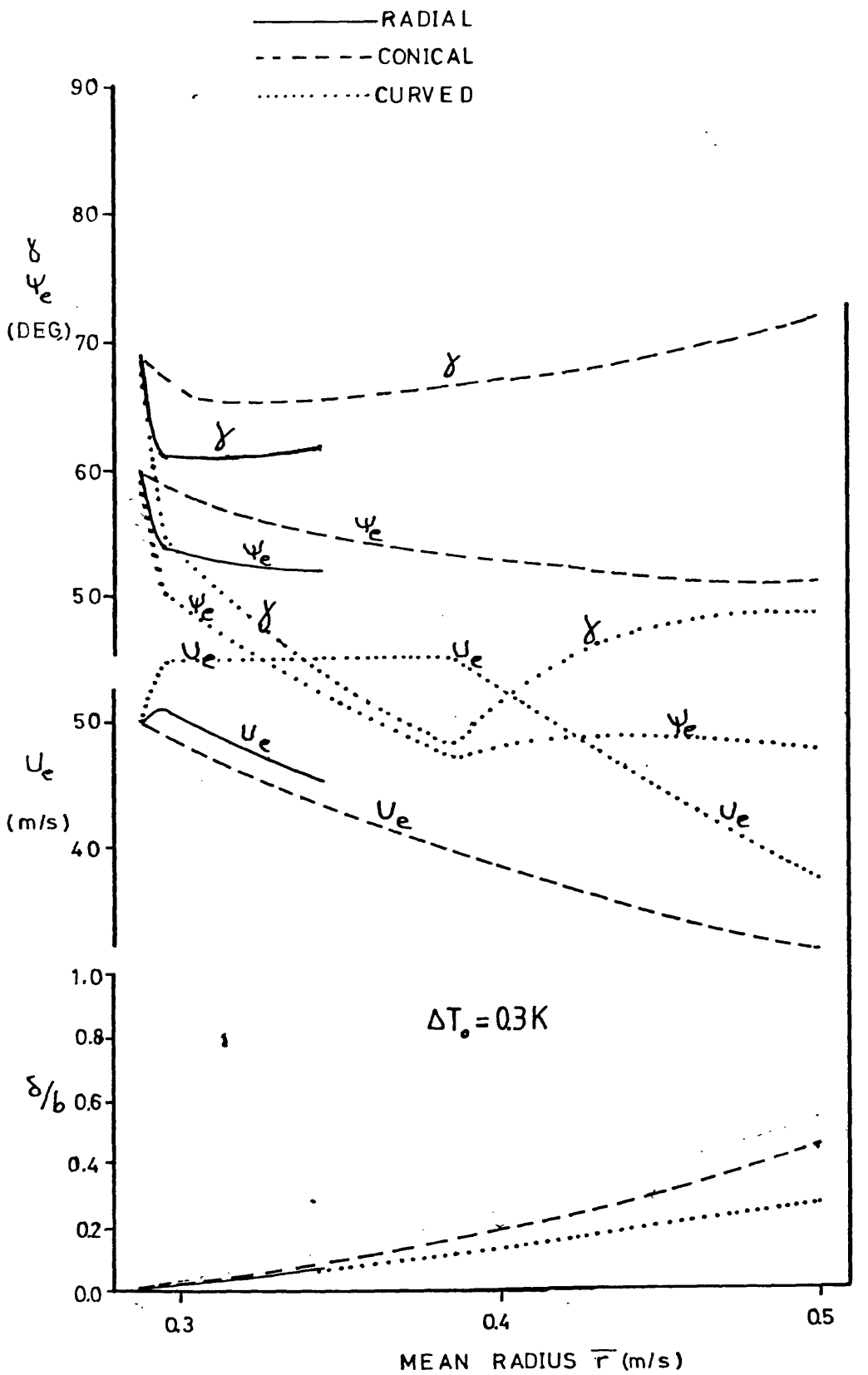

FIG. 2.23 DEVELOPMENT OF SHROUD BOUNDARY LAYERS FOR UNIFORM VELOCITY WITH TOTAL ENTHALPY GRADIENT AT INLET

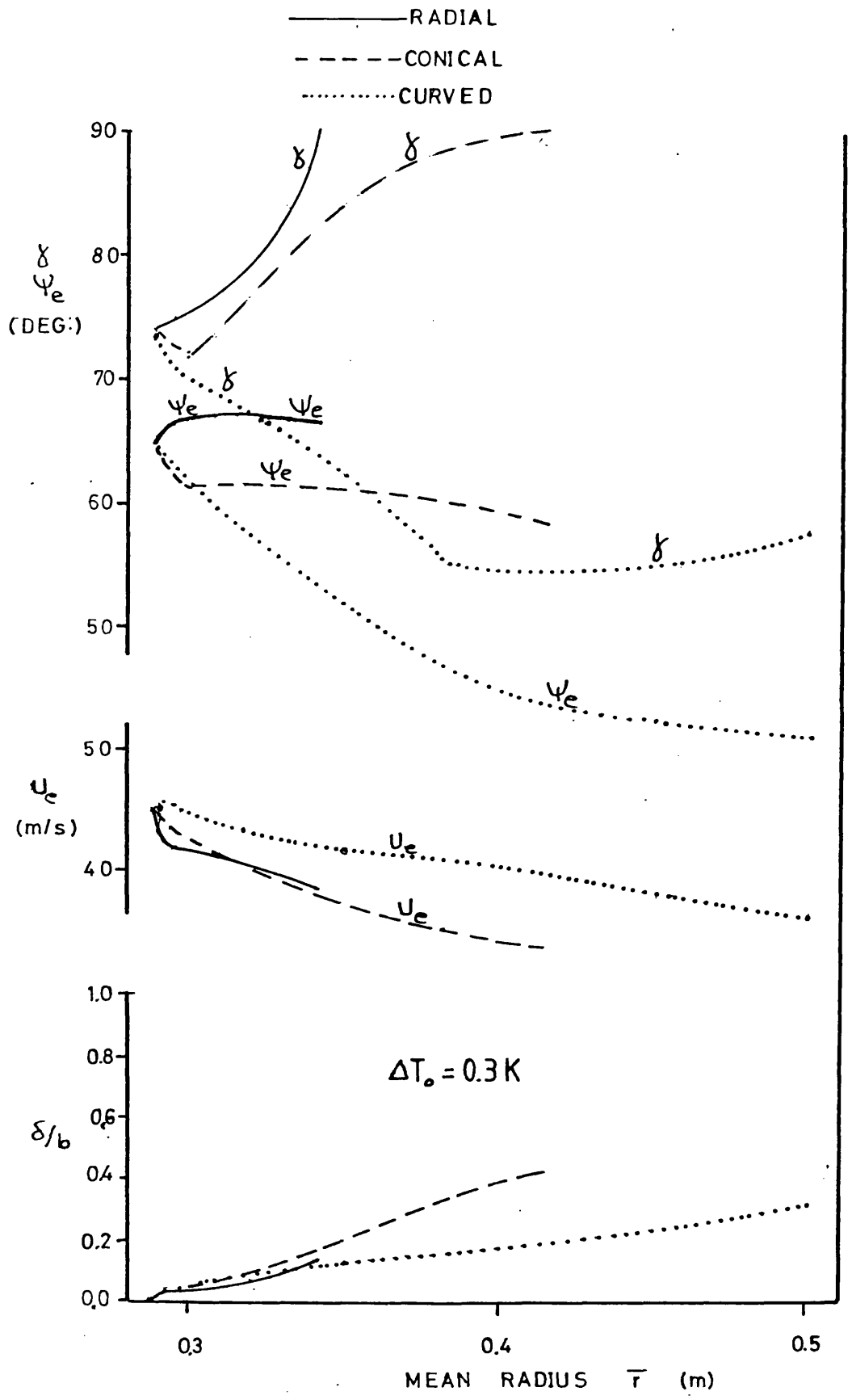

FIG. 2.24 DEVELOPMENT OF HUB BOUNDARY LAYERS FOR NON-UNIFORM INLET CONDITIONS

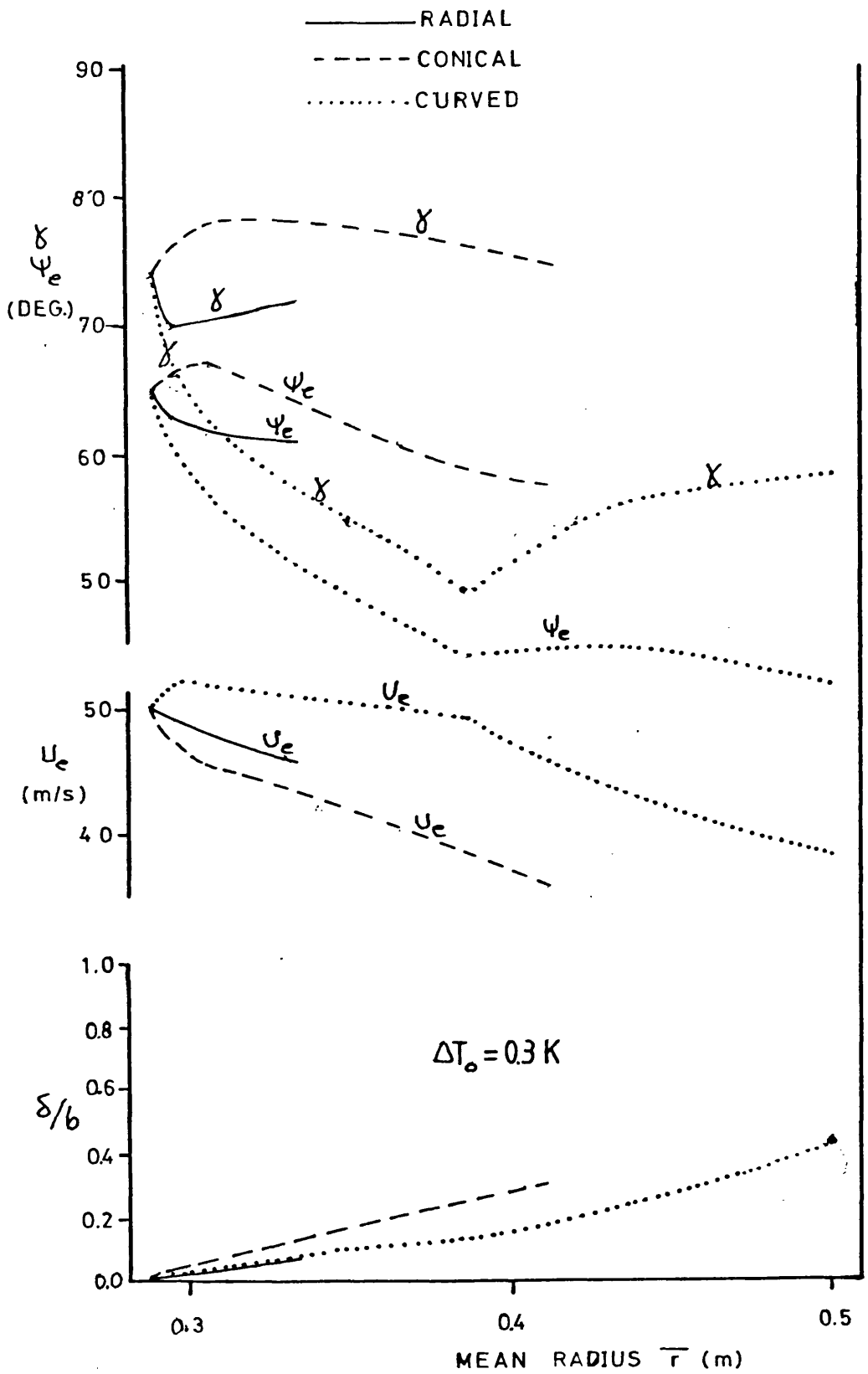

FIG. 2.25 DEVELOPMENT OF SHROUD BOUNDARY LAYERS FOR NON-UNIFORM INLET CONDITIONS

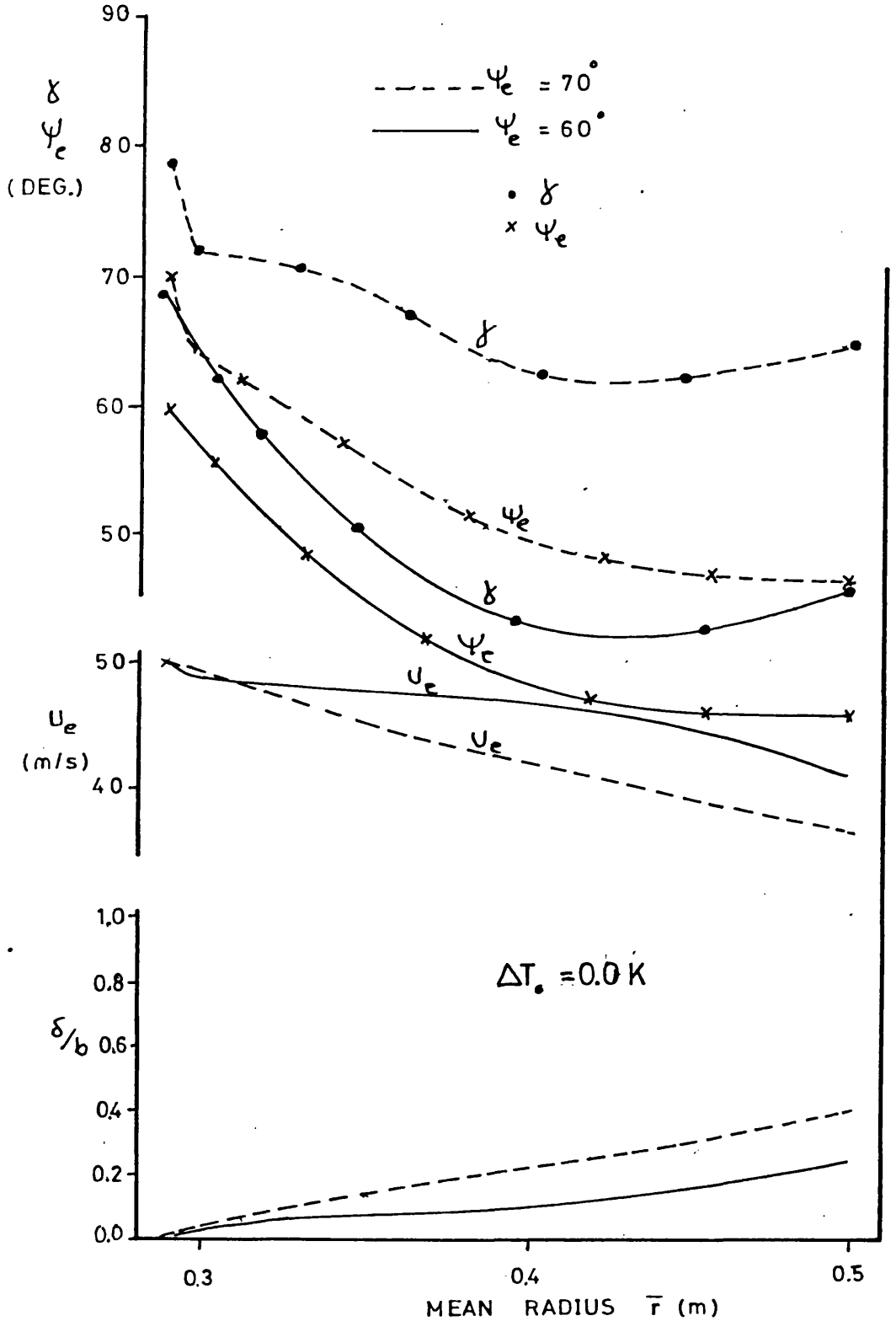

FIG. 2.26 EFFECT OF INLET SWIRL ANGLE ON CURVED DIFFUSER HUB BOUNDARY LAYER DEVELOPMENT

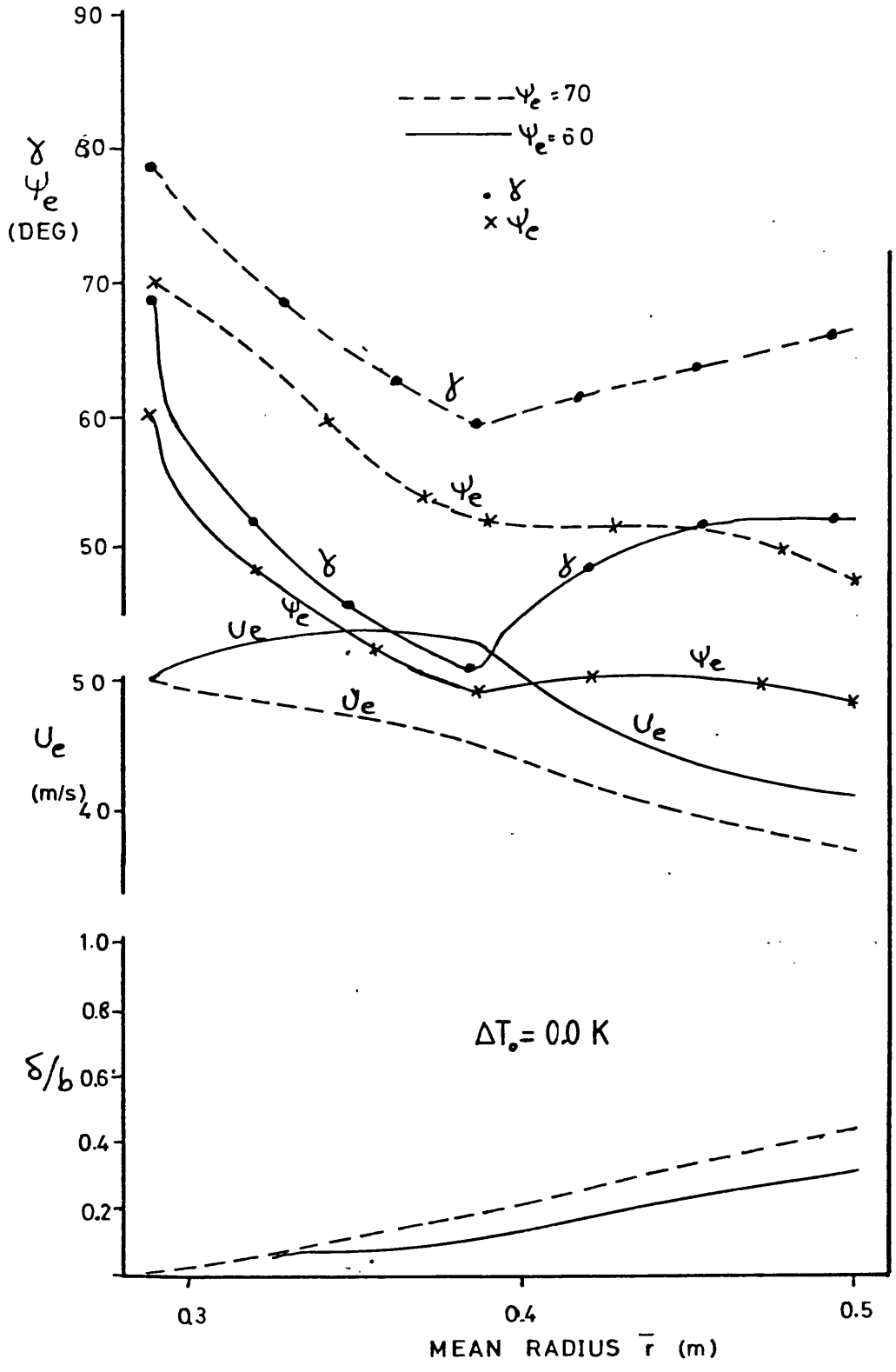

FIG. 2.27 EFFECT OF INLET SWIRL ANGLE ON CURVED DIFFUSER SHROUD BOUNDARY LAYER DEVELOPMENT

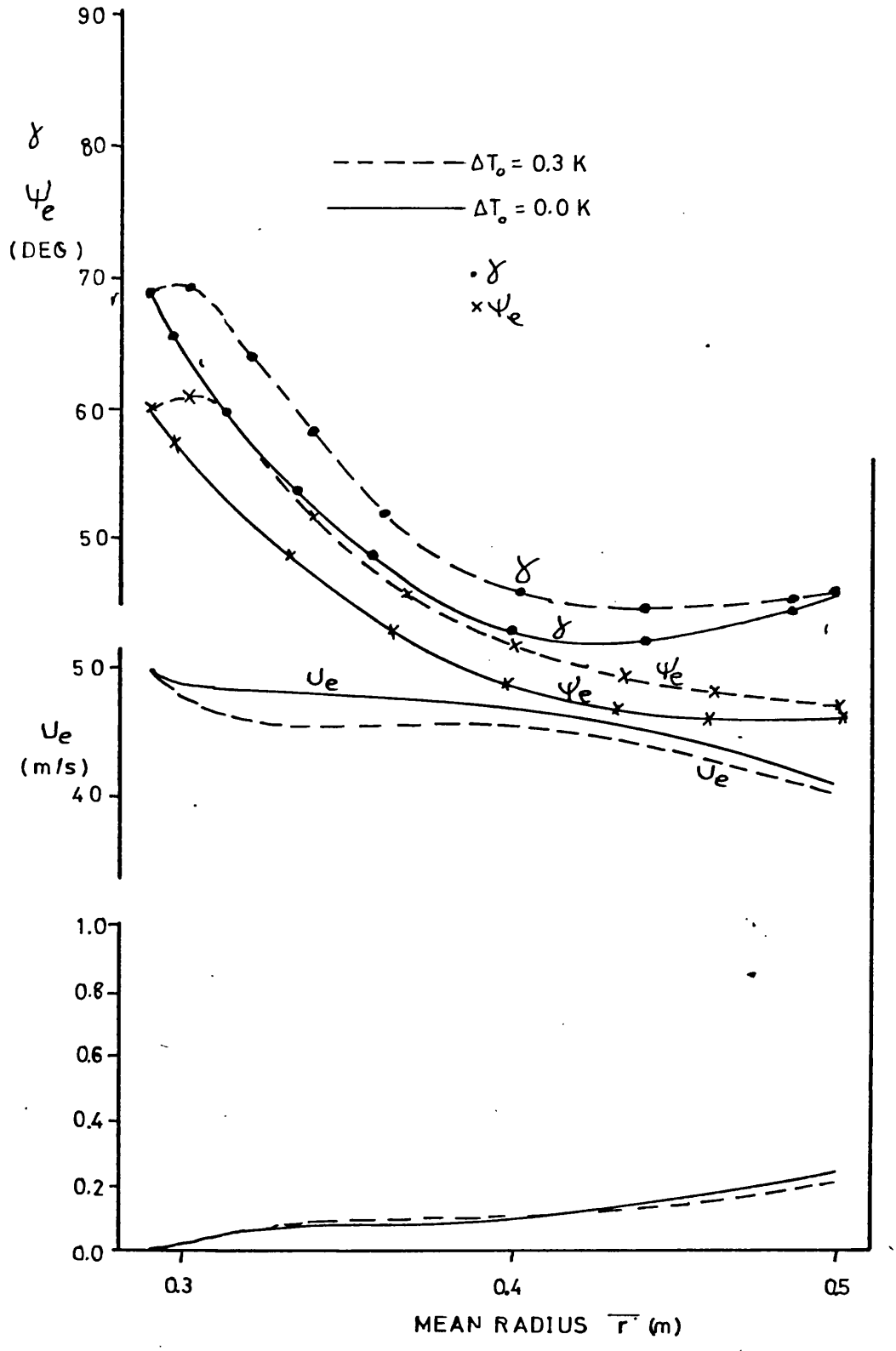

FIG. 2.28 EFFECT OF ENTHALPY GRADIENT ON CURVED DIFFUSER HUB BOUNDARY LAYER DEVELOPMENT

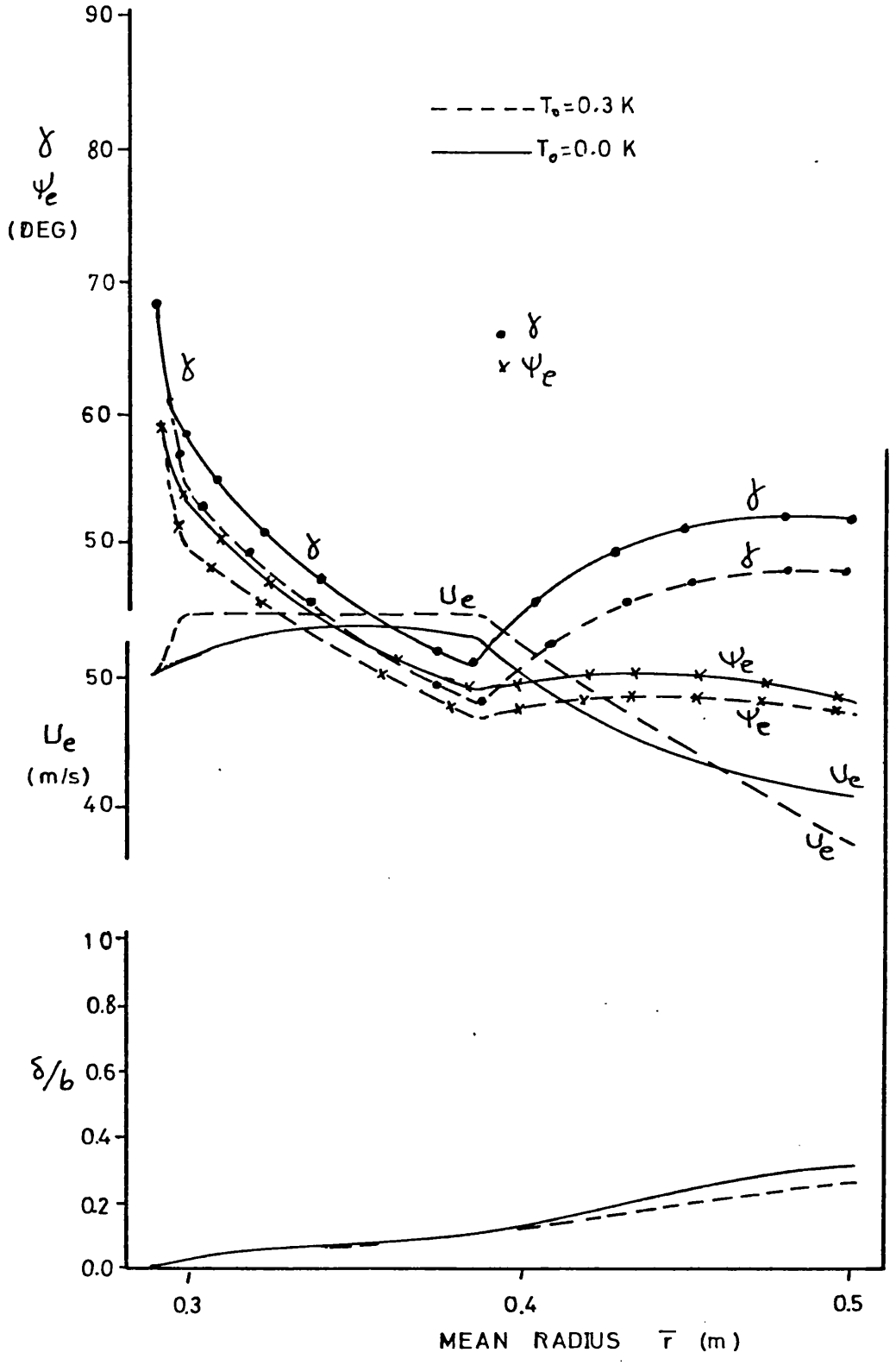

FIG. 2.29 EFFECT OF ENTHALPY GRADIENT ON CURVED DIFFUSER SHROUD BOUNDARY LAYER DEVELOPMENT

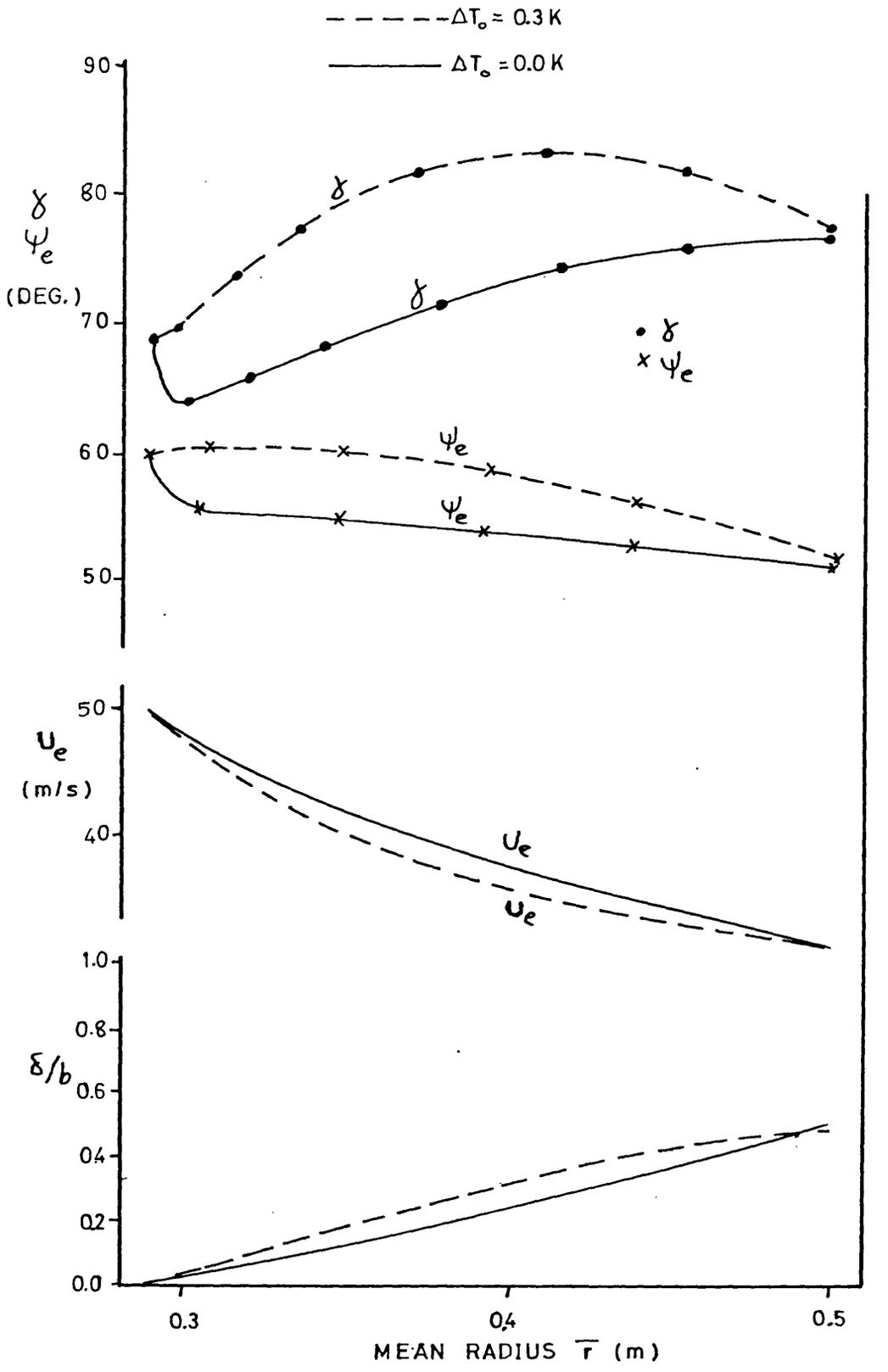

FIG. 2.30 EFFECT OF ENTHALPY GRADIENT ON CONICAL DIFFUSER HUB BOUNDARY LAYER DEVELOPMENT

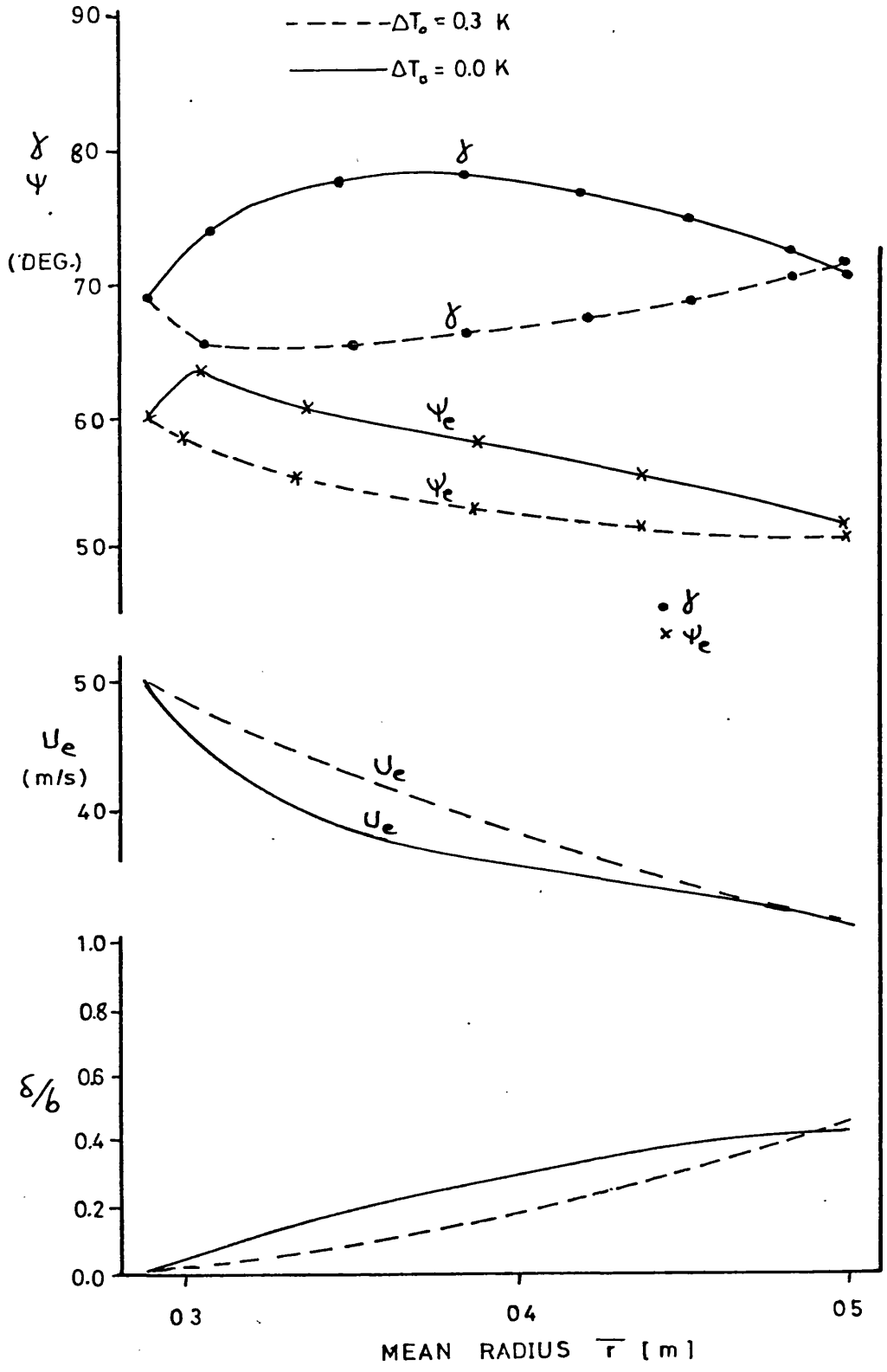

FIG. 2.31 EFFECT OF ENTHALPY GRADIENT ON CONICAL DIFFUSER SHROUD BOUNDARY LAYER DEVELOPMENT

CHAPTER 3 : TEST RIG AND INSTRUMENTATION

3.1 Description of the Rig

The general layout of the experimental set up is shown in fig. 3.1 with the curved diffuser installed. A two stage axial fan was used to draw air from the atmosphere through a 0.4826 m (19 inch) dia. pipe. Downstream of the fan the ducting contained a 50 mm flow straightening honeycomb. The pipe diameter was then contracted to 0.381 m (15 inch) leading to a rotating screen assembly which gave the flow a swirling component. The air then passed freely through an annular diffuser.

The fans were powered by a 1.49 kW motor running at rotational speed of 2900 rev/min. The design mass flow rate of the fans was 2 kg/s with a pressure rise of approximately 110 mm of water gauge. Either of the stages could be used separately.

Two diffusers with a curved and pure conical profile were tested. The curved diffuser consisted of two parts (see fig. 3.2), a curved converging part having non-parallel hub and shroud profiles which turned the flow into a radial section having two parallel walls. The pure conical diffuser, fig. 3.3 had straight parallel walls and a cone angle of 105 degrees. The overall dimensions of the conical diffuser were similar to those of the curved one as shown in the figures.

Two conical rotating screens were used in order to ensure a uniform velocity profile. Jansen (46) showed that the use of a single screen created a distorted through flow velocity component. The screens which have a radius of approximately 300 mm, were belt driven by an electric motor giving a rotational speed of 2620 rev/min. Earlier investigations on the rig by Barbotin (22) showed that the meridional velocity profile at inlet to the diffuser had a very high peak near the shroud with a corresponding reduction in flow angle. The same phenomenon was encountered by James (47) using a similar rig configuration for a radial vaneless diffuser. This was attributed to the passage of a substantial part of the flow through the clearance

between the rotating screen and the stationary shroud rather than through the rotating screen. To eliminate this, an annular ring was inserted between the rotating screen and stationary surface as shown in figs. 3.2 and 3.3. This substantially reduced the flow around the rotating screen and consequently reduced the inlet flow distortion.

3.2 Instrumentation

The frame work of the experimental programme was aimed at achieving the following objectives :-

1) to obtain a detailed measurement of the mean flow properties in curved and conical diffuser passages with a steady flow at inlet.
2) to investigate the effect of the jet-wake flow pattern at the inlet of both diffusers.

The measurements for the first objective was made by time averaging probes.

In order to simulate the flow pattern issuing from an impeller, for the second objective, the rotating screen was divided into 24 equal parts, and by partially blocking every other part, a distribution of regions of high and low velocities was obtained, this gave a resemblence of a 12 blade impeller.

The wake regions issuing from the rotating screen were initially obtained by partially blocking parts of the screen with a fine mesh. This, however, only produced a small difference in velocity level. The fine mesh parts were therefore replaced by parts of a steel plate of 0.126 mm thickness, which completely blocked segments of the rotating screen, thereby giving a large difference in velocity level. Fig. 3.4 illustrates the rotating screen configuration for the simulation of the jet-wake flow and the corresponding velocity pattern results from its use.

It was proposed to use a hot-wire anemometry system in conjunction with

pressure transducers at the diffuser wall to measure and calculate the mass average properties of the flow for the jet-wake flow. A delay in the purchasing process of the hot-wire system and the time limitation of the experimental programme forced the use of the time averaging probes in this case also. Senoo and Ishida (64) pointed out that a use of a time averaging probe rather than a mass averaging one will over-estimate the average total pressure. However, the use of the time averaging probes can still give a good overall map of the flow properties. The error in estimating the average total pressure will be higher where the jet-wake pattern is distinct, i.e. at inlet.

3.2.1 Description of the probes

The use of pressure probes was selected for their simplicity of manufacture, durability and ease of application. General requirements for a pressure probe are : small size to cause minimum disturbance in the flow field, rapid pressure response, calibration which is not affected by flow conditions, and all simultaneous measurements to be made as near as possible to one point.

Since a detailed study of the three dimensional flow characteristics was required, the choice of a three-hole cobra headed probe offered a simple, convenient and robust tool for the measurement of total and static pressure, and flow direction.

The probe consisted of a central tube to which were attached two side tubes with forward ends chamfered at 45 degrees. Brayer and Pankhurst (94) reported that with this apex angle the probe is insensitive to change of pitch angle within the range of ± 12 degrees, hence they recommended it for general use.

Each probe was fixed to a traversing gear which was bolted to the diffuser wall. The traverse gear (fig. 3.5) enabled the probe to rotate about its vertical axis and to be traversed across the diffuser passage. Three probes with different head lengths were used to measure the flow parameters at three different locations simultaneously,

at inlet, midway and outlet of each diffuser. Detailed drawings of the three probes are given in figs. 3.6a, 3.6b and 3.6c for the inlet, middle, and outlet probe respectively. The inlet probe had a short head so that measurement could be made as near as possible to the inlet section without conflicting with the rotating screen.

Wall static pressure tappings were evenly distributed along a radial line on both the hub and shroud. Fig. 3.7 and 3.8 give the locations of the wall tappings and the three traversing stations for the curved and conical diffuser respectively.

A water manometer bank inclined at 30 degrees with the horizontal was used for all probe and wall tapping pressure measurements. The same manometer was used for both calibration and experimental investigations.

3.2.2 Calibration of the probes

Principles of calibration

In steady, three dimensional flow, four independent parameters - measured with reference to a certain direction - are needed to completely define the flow at a point. These parameters are : the total pressure P_t, the static pressure P_s, the angle of pitch and the yaw angle. If, however, a direct measure of these parameters is not possible, one can substitute them by four quantities which have a known relation with the four parameters. The relationship between the measured quantities and flow parameters must be established by calibration.

In the case of a three-hole probe an assumption of a known angle of pitch is made. The remaining quantities to be measured are the angle between a fixed reference position and the null position, when the side tubes have the same readings and the reading of the pressures in the side and central tubes at that position.

It is assumed that

$P_2 = P_3 = P_{2.3}$ = Pressure reading of the side tubes at the null position

P_1 = Pressure reading of the central tube at null position

ψ'' = angle between null position and a fixed reference position.

The central tube reading P_1 will represent the total pressure in the case of an ideal probe. For this ideal probe the static pressure will be represented by

$$P_s = P_{2.3} + K(P_1 - P_{2.3}) \qquad 3.1$$

Due to non-symmetry of the side tubing, the reading of the central tube at the null position will not necessarily give the true value of total pressure P_t. In that case three calibration factors rather than one are needed where

$$q = \tfrac{1}{2} \rho C^2 = K1 \, (P_1 - P_{2.3}) \qquad 3.2$$

$$P_s = P_{2.3} + K2 \, (P_1 - P_{2.3}) \qquad 3.3$$

$$P_t = P_1 + K3 \, (P_1 - P_{2.3}) \qquad 3.4$$

and since

$$P_t = P_s + \tfrac{1}{2} \rho C^2 \qquad 3.5$$

$$\therefore \quad K1 + K2 = 1 + K3 \qquad 3.6$$

It can be seen from equation 3.6 that it is necessary to evaluate two coefficients only.

The probe was calibrated with the aid of a standard pitot-static tube which was known to give accurate values for the static and total pressures for the range of velocities and pressures expected. By

observing corresponding values of P_1 and $P_{2.3}$, values of K1, K2 and K3 were established from the above relations.

Due to manufacturing tolerances and the mounting of the probe in the traversing mechanism, the side tubes could not be considered to be perfectly symmetrical about the known reference surface, consequently the flow angle could not be directly measured. In order to correct for this lack of symmetry, measurements were made in a fluid stream of known direction with the probe inserted from opposite sides. If the probes were symmetrical the angle measurement would be identical irrespective of which side of the jet it was inserted; any difference due to lack of symmetry represents the correction to be applied. Fig. 3.9a and 3.9b illustrate the procedure for correcting the error in flow angle measurements. The corresponding flow angles for the two steps are ψ_1' and ψ_2' as observed from a fixed reference position. $\Delta\psi_1$ and $\Delta\psi_2$ represent the error in estimating the flow angle ψ.

From fig. 3.9a and 3.9b

$$\psi = \psi_1' + \Delta\psi_1 = \psi_2' - \Delta\psi_2 \qquad 3.7$$

$$\psi_2' - \psi_1' = \Delta\psi_2 + \Delta\psi_1 \qquad 3.8$$

also $$\Delta\psi_1 = \Delta\psi_2 = \psi_c \qquad 3.9$$

where ψ_c = correction angle for flow angle ψ

$$\psi_2' - \psi_1' = 2\psi_c \qquad 3.10$$

$$\psi_c = \frac{\psi_2' - \psi_1'}{2} \qquad 3.11$$

By measuring ψ_2' and ψ_1' as shown in fig. 3.9 the correction angle was calculated from equation 3.11

hence $\psi = \psi_1' + \psi_c = \psi_2' - \psi_c$

where ψ is the true flow angle.

Calibration procedure and results

Fig. 3.10 shows the arrangement of the experimental apparatus to service as a calibration rig for the pressure probes. A convergent pipe having a cone angle of 26 degrees was used to gradually reduce the inlet pipe diameter from 0.4826m to 0.1016m. This reduced diameter gave a maximum velocity of approximately 80 m/s, a limit expected in the experimental diffusers. The pipe connecting the rotating screen assembly with the outlet from the fan was removed and a throttle valve was fitted downstream of the fan. The throttle valve was used to control the mass flow rate, hence, varying the air velocity in the inlet pipe. The inlet pipe was used as the calibration section with its open end fitted with a honeycomb flow straightener. An NPL standard pitot-static tube was used for the calibration of the probes. Two different fixing positions for the pitot tube and the probes were prepared to ensure that the tip of both the pitot tube and the probe would lie at the same point. Four equally spaced wall pressure tappings were provided in the calibration section. The pressure tappings served to check that the difference in scale effect between the pitot tube and the probes was negligible. They also showed that the static pressure at the calibration section was equal to that registered by the pitot tube.

The pitot tube was first introduced into the calibration section at a particular throttle valve setting. The head of the tube was horizontal and facing the incoming air at the centre of the pipe. Readings of the pressure were recorded and the pitot tube was then withdrawn. The pressure probe was introduced from the other side of the pipe, and traversed to the same point, then yawed to the null position and readings of the centre and side tubes were observed. The procedure was repeated with different throttle valve settings for a velocity range between 3 m/s and 80 m/s. The same steps were carried out for each of the three pressure probes.

The result of the probe calibrations are shown in figs. 3.11, 3.12 and 3.13 for the inlet, midway and outlet probe respectively. A repeat of the calibration procedure before, during and after completion of the experimental work showed that the maximum deviation for the calibration

factors were about 6%. A check was also made upon the effect of the diameter of the calibration pipe on the calibration factors. The 0.1016 m diameter pipe was replaced by an 0.1702 m diameter one and calibration was repeated. Also calibrations were performed with a low speed open wind tunnel where the velocity of air ranged from approximately 1 m/s to 22 m/s and the static pressure was atmospheric. In all conditions values evaluated for the calibration factors were consistent.

The evaluation of the correction angle ψ_c was performed using air issuing from an 0.065 m diameter wind tunnel.

Values of ψ_c for the three probes were

for the inlet probe	ψ_c =	0.7 degrees
for the midway probe	ψ_c =	0.4 degrees
for the outlet probe	ψ_c =	0.5 degrees

3.2.3 Accuracy

Using the traverse gear shown in fig. 3.5 the maximum accuracy attained in flow angle was 0.4 degrees and in distance between diffuser wall was 0.025 mm (0.001"). The maximum accuracy in reading pressure from probes and wall tappings was 0.5 mm of water.

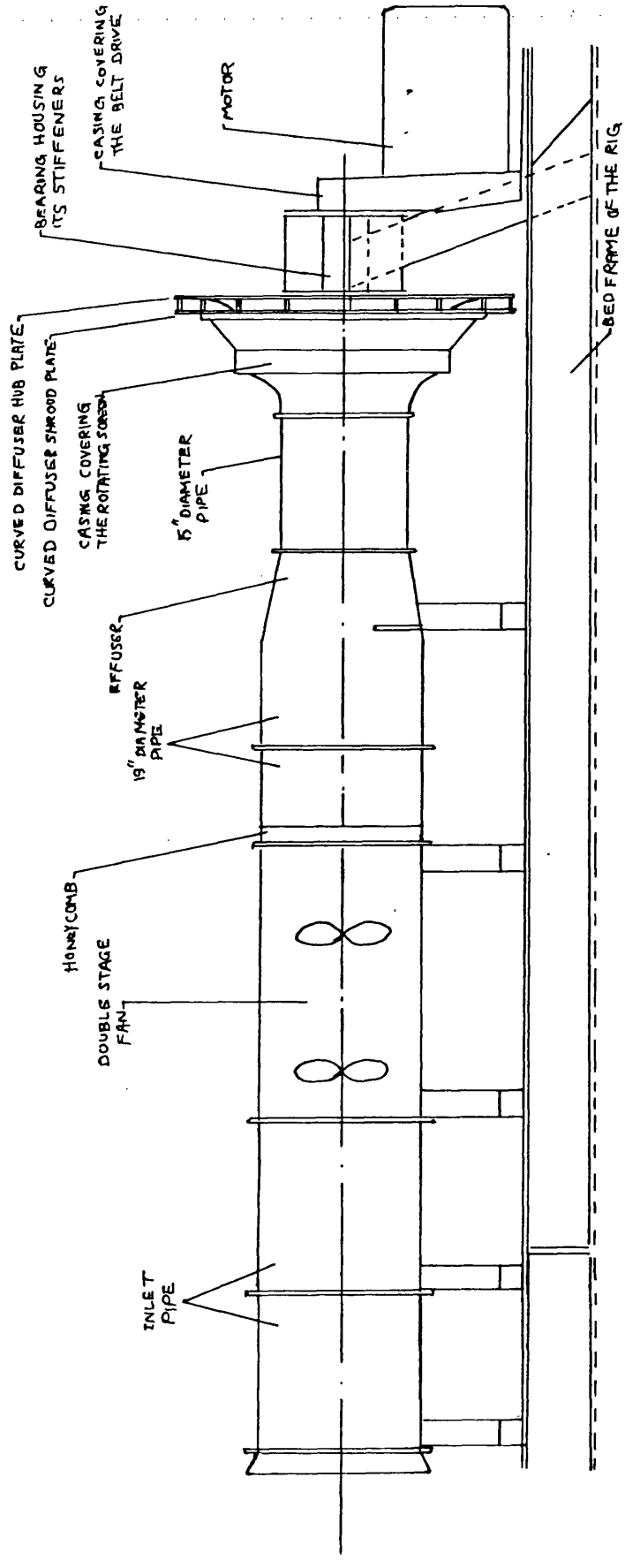

FIG. 3.1 GENERAL LAYOUT OF THE TEST RIG

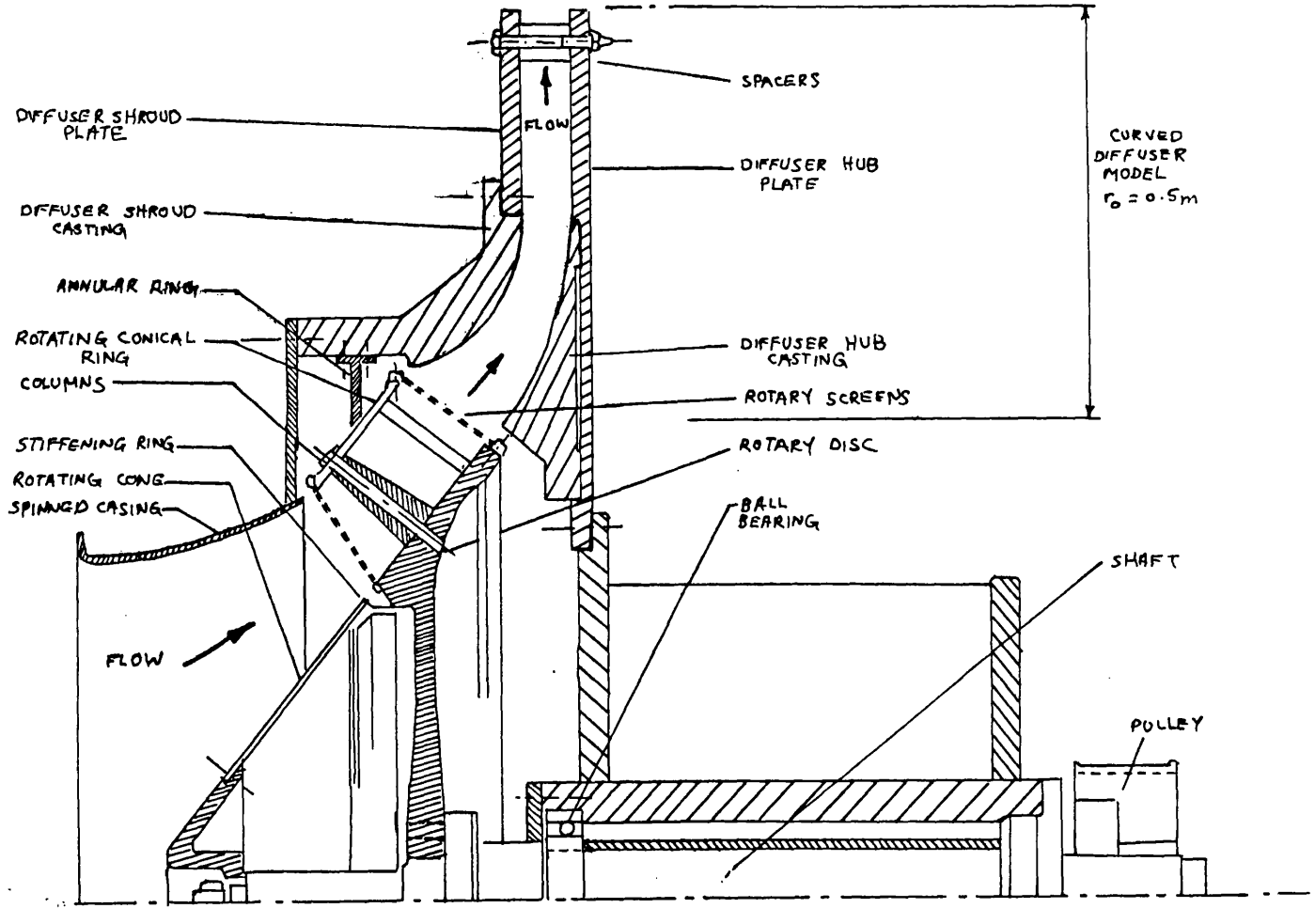

FIG. 3.2 ROTATING ASSEMBLY AND CURVED DIFFUSER MODEL

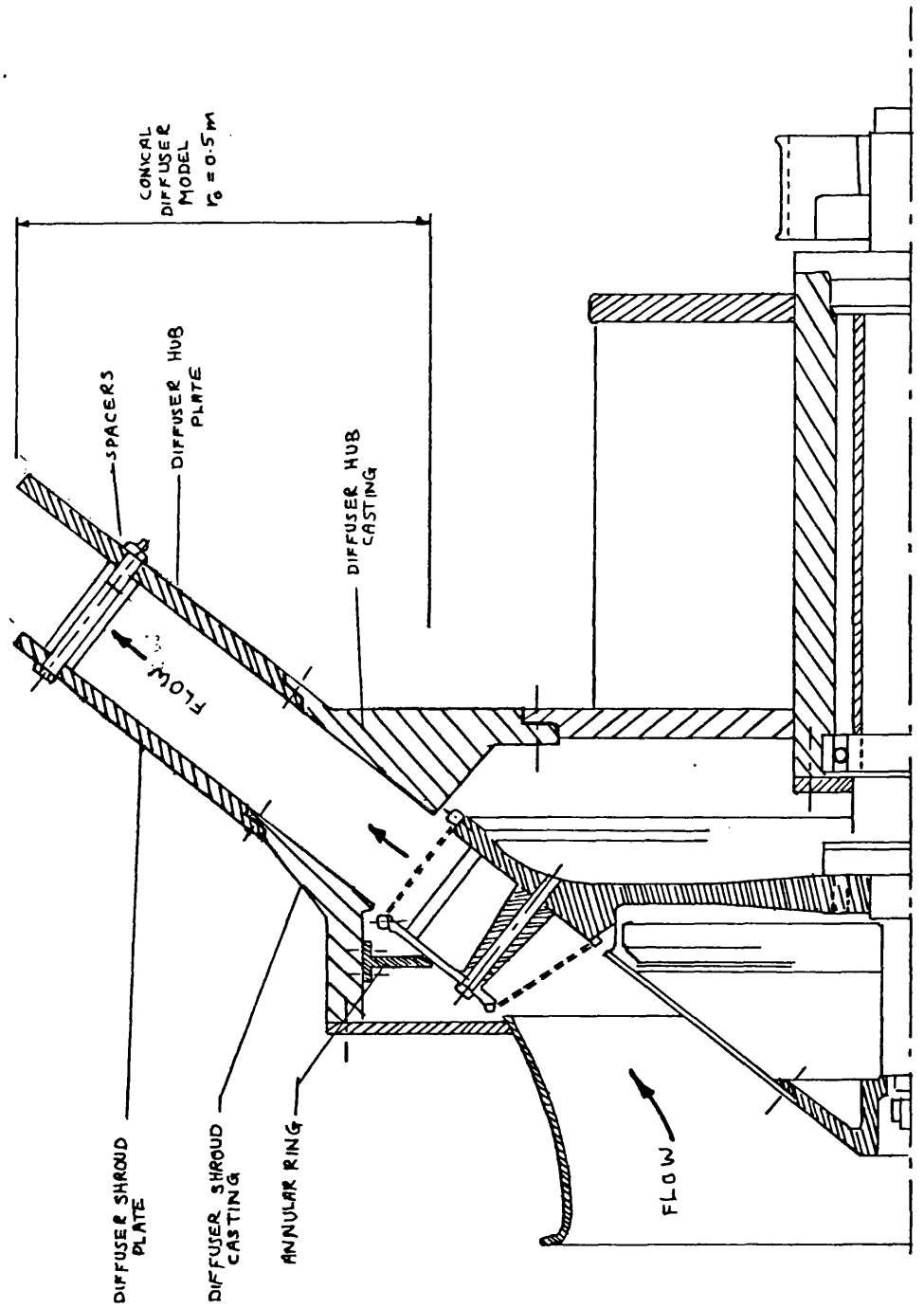

FIG. 3.3 ROTATING ASSEMBLY AND CONICAL DIFFUSER MODEL

HOT-WIRE ANEMOMETER TRACES OF THE JET-WAKE FLOW

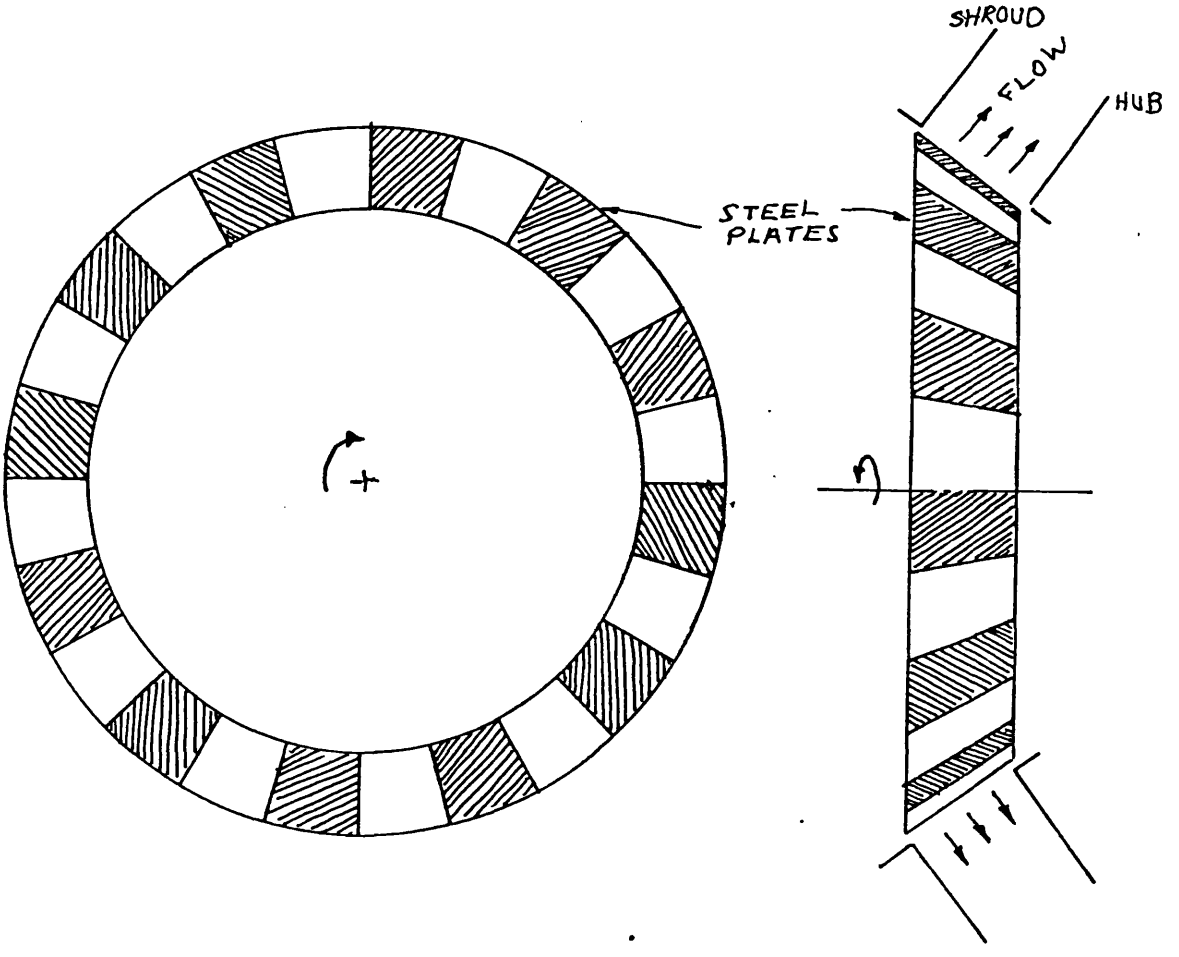

FIG. 3.4 ROTATING SCREEN ARRANGEMENT FOR JET-WAKE FLOW AND CORRESPONDING VELOCITY PATTERN

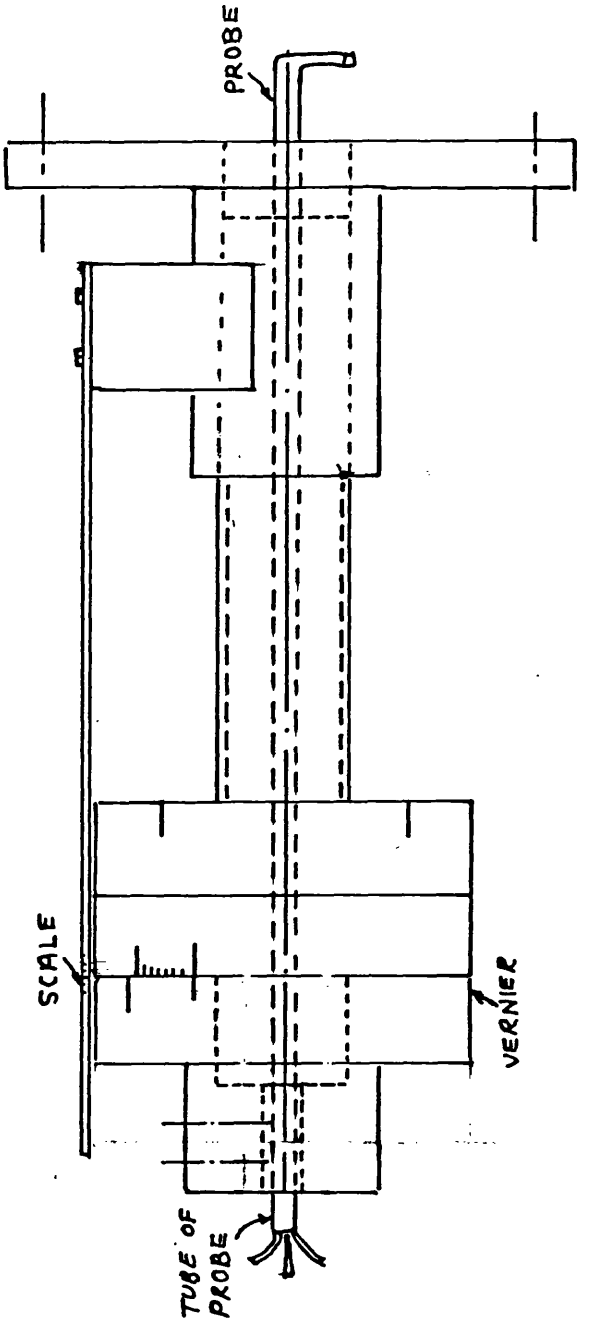

FIG. 3.5 TRAVERSING GEAR

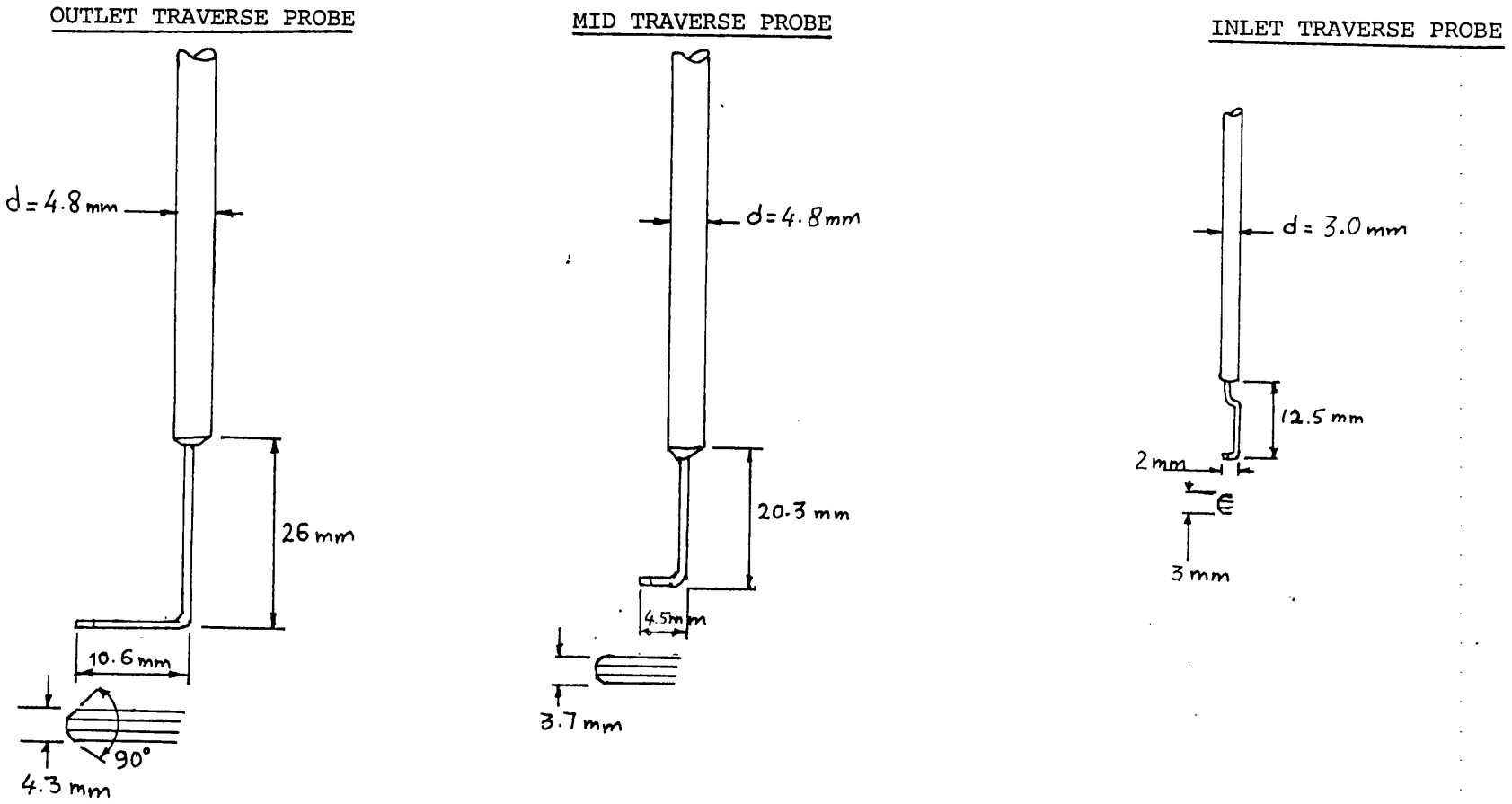

FIG. 3.6 THREE HOLES COPRA PRESSURE PROBES USED IN MEASUREMENTS

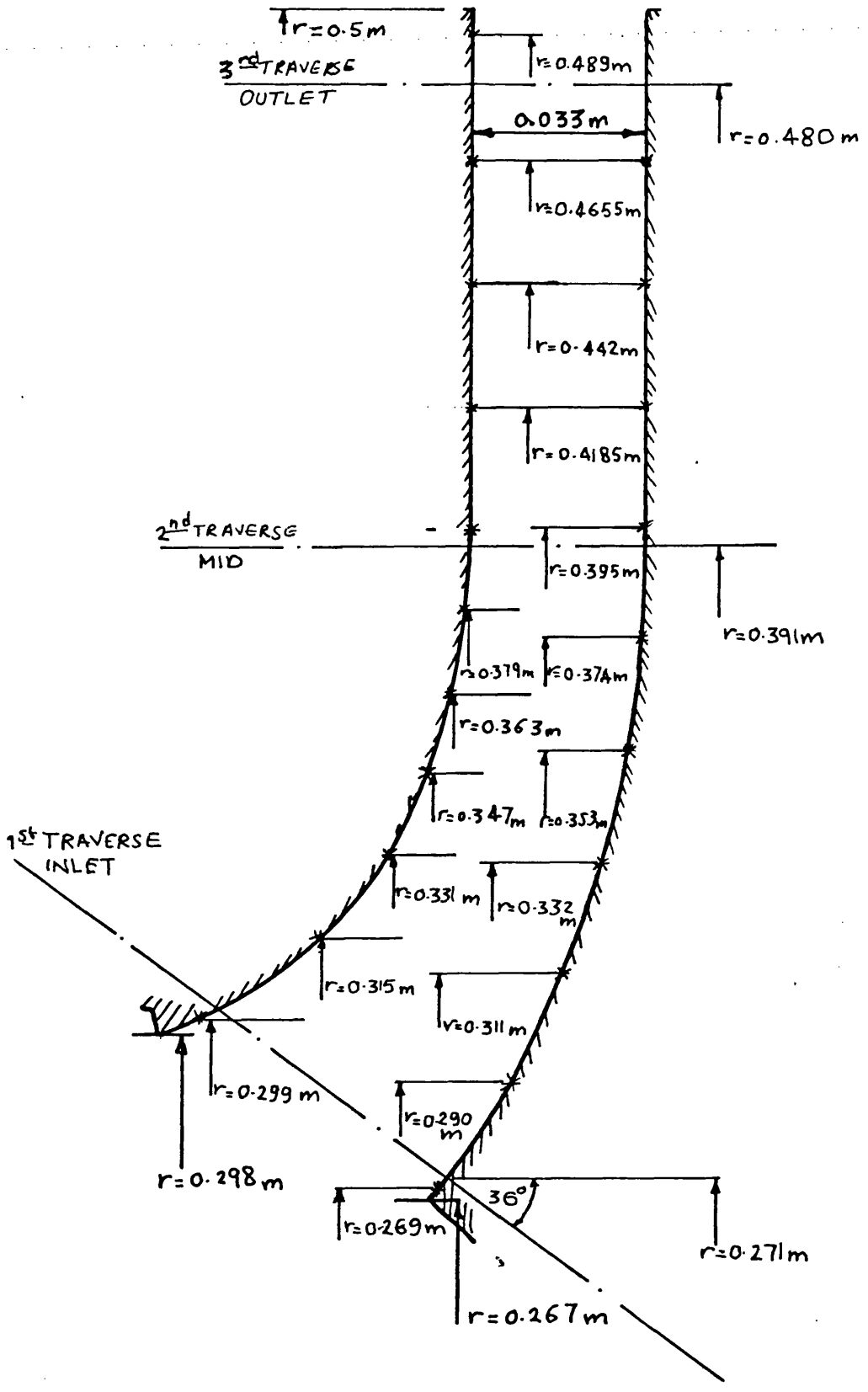

FIG. 3.7 PROBE TRAVERSE AND STATIC PRESSURE STATIONS OF THE CURVED DIFFUSER

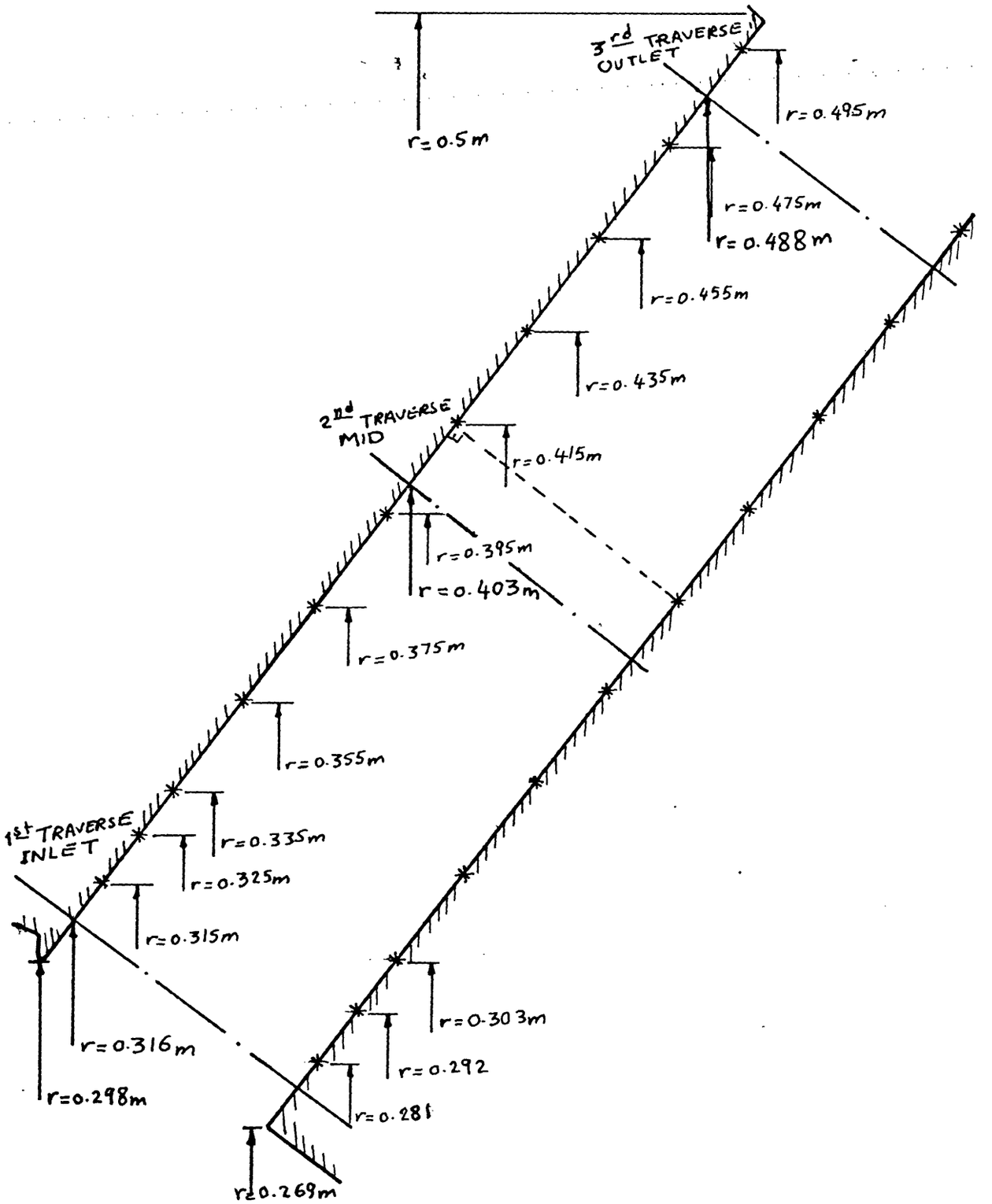

FIG. 3.8 PROBES TRAVERSE AND STATIC PRESSURE STATIONS OF THE CONICAL DIFFUSER

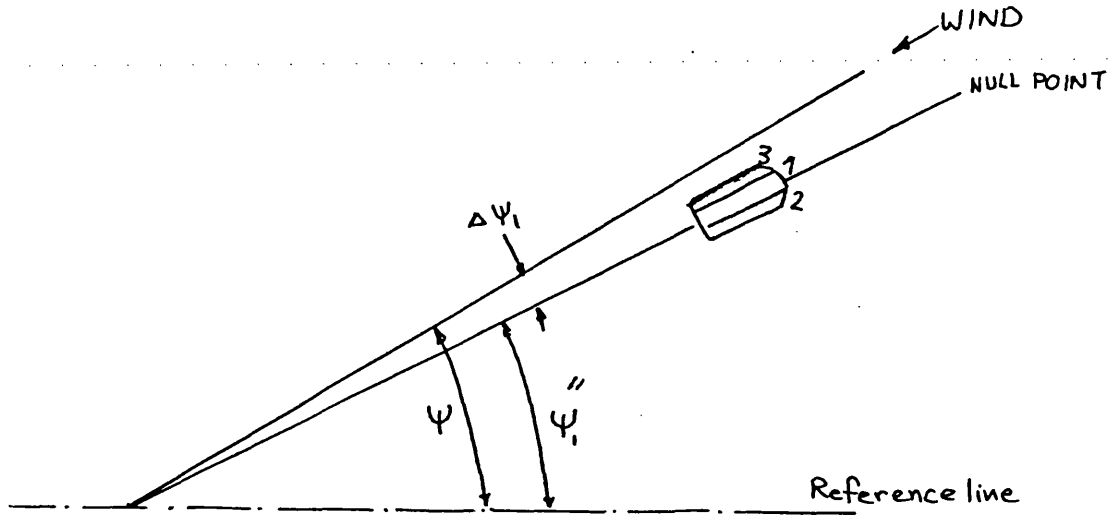

FIG. 3.9a FIRST STEP OF THE CALIBRATION

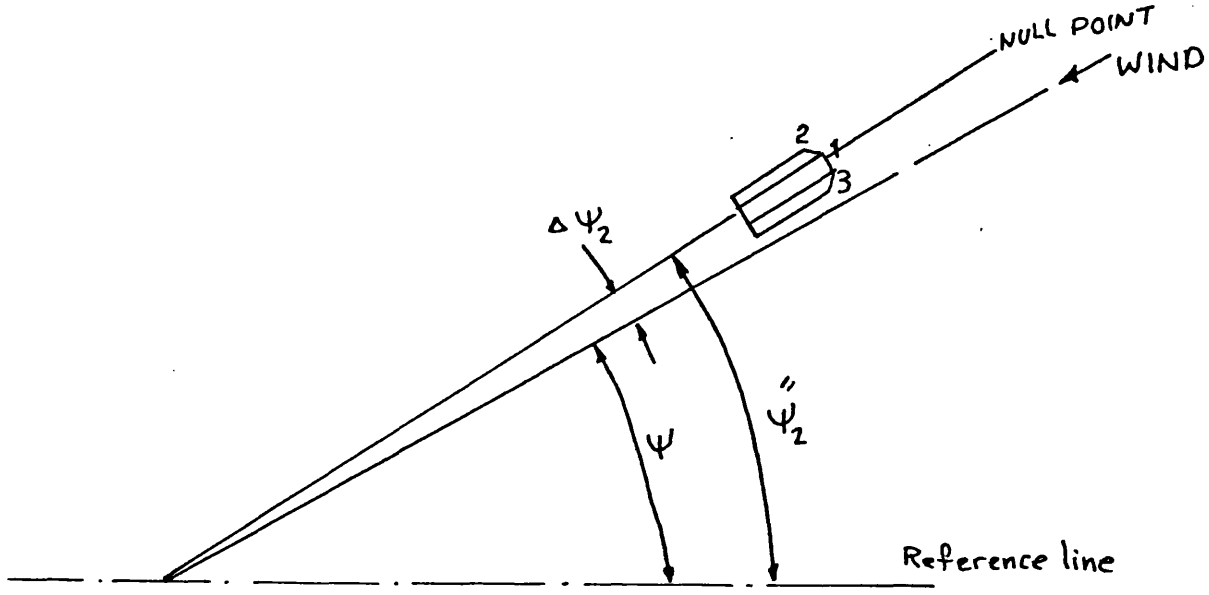

FIG. 3.9b SECOND STEP OF THE CALIBRATION

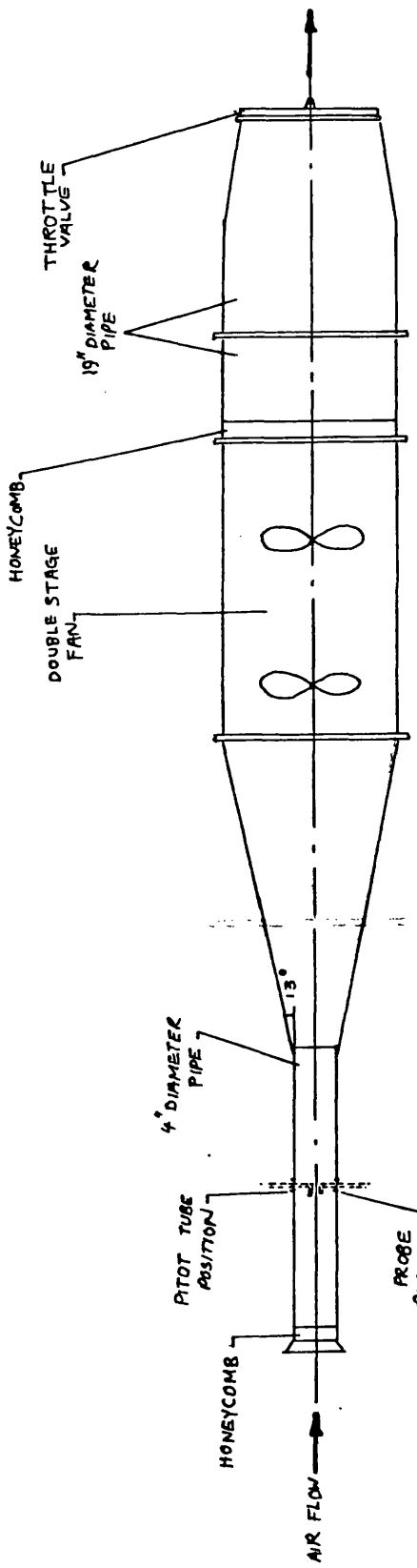

FIG. 3.10 ARRANGEMENT OF THE TEST RIG FOR PROBES CALIBRATION

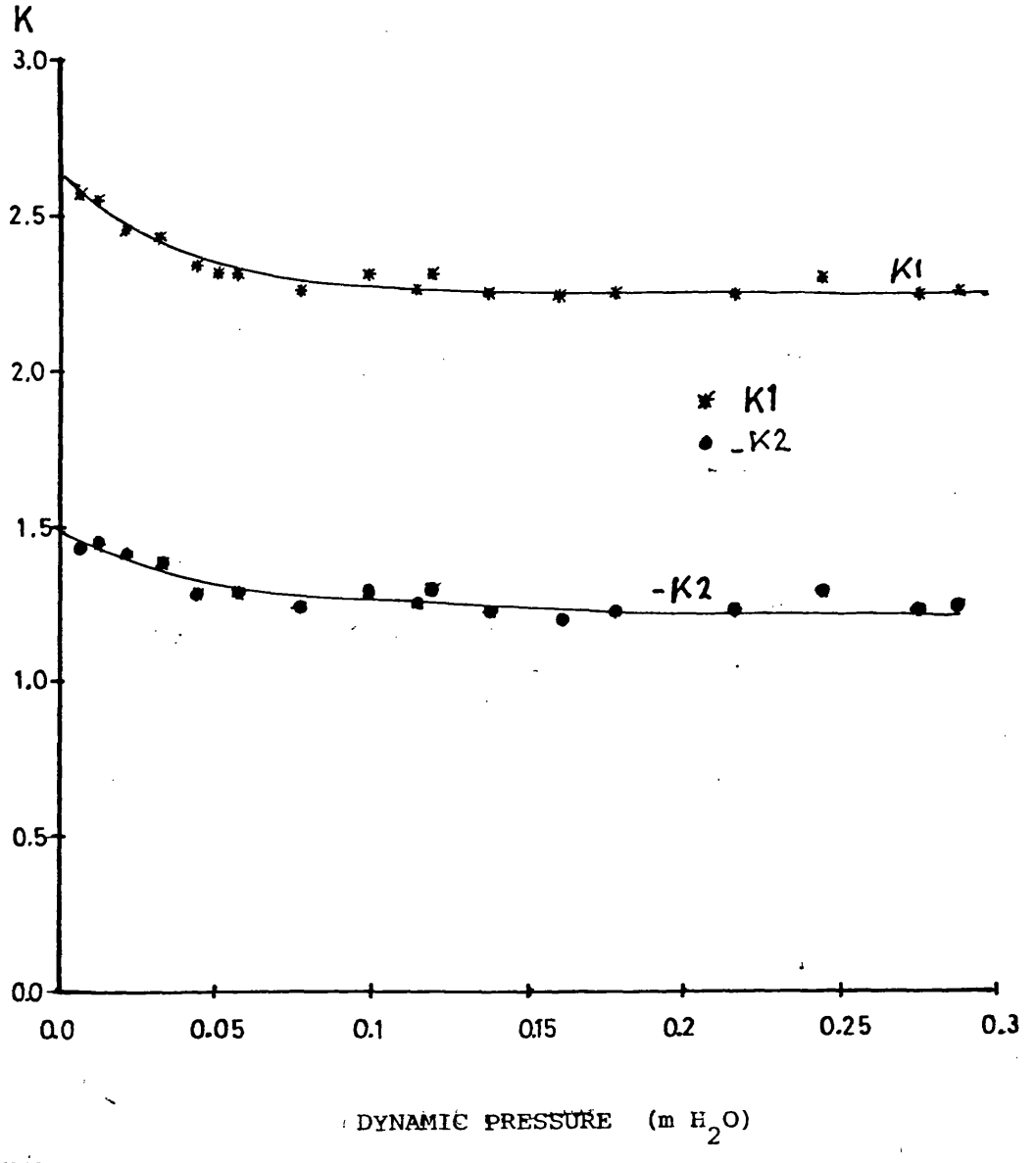

FIG. 3.11 CALIBRATION CURVES FOR THE INLET TRAVERSE PROBE

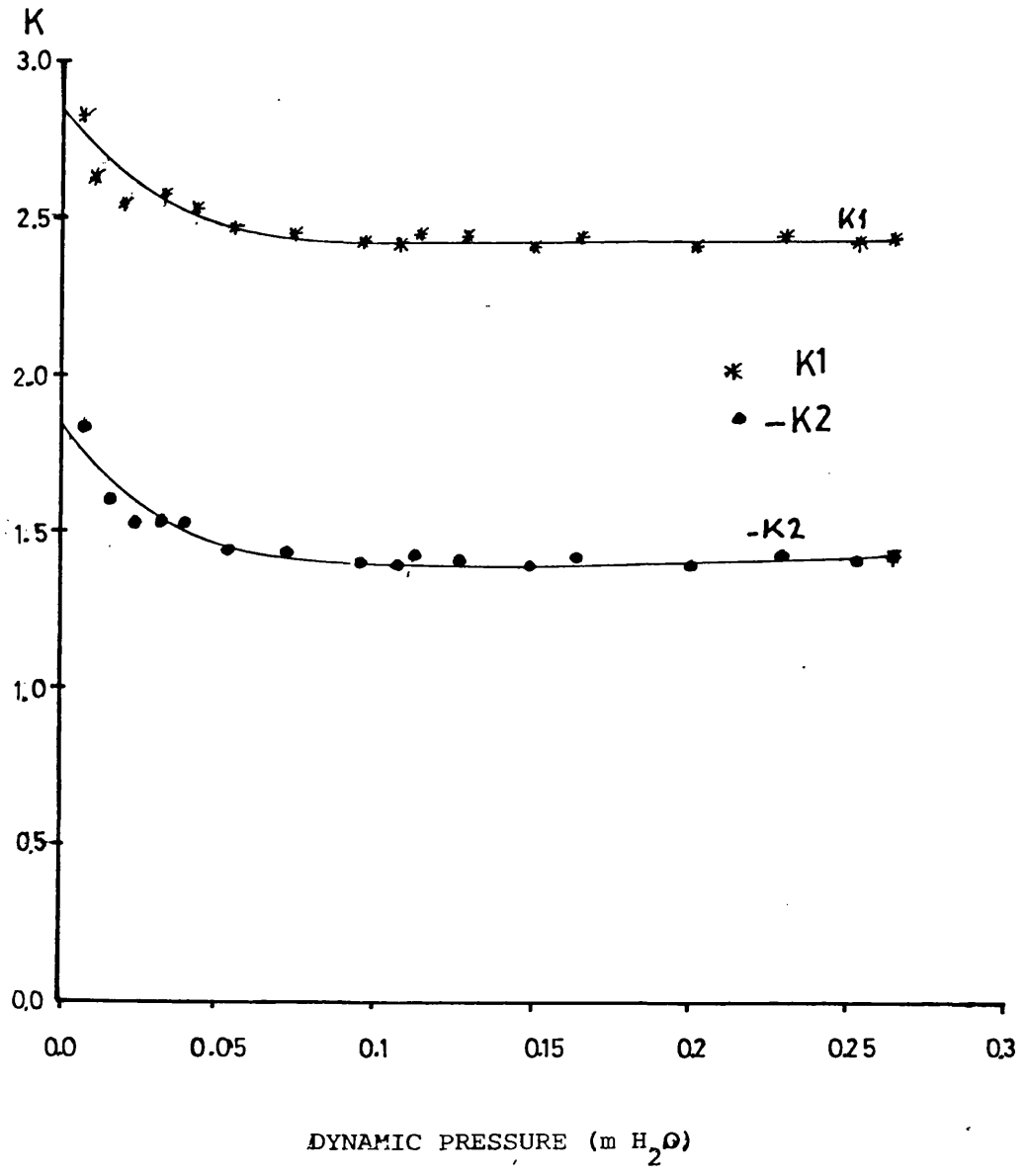

FIG. 3.12 CALIBRATION CURVES FOR THE MIDDLE TRAVERSE PROBE

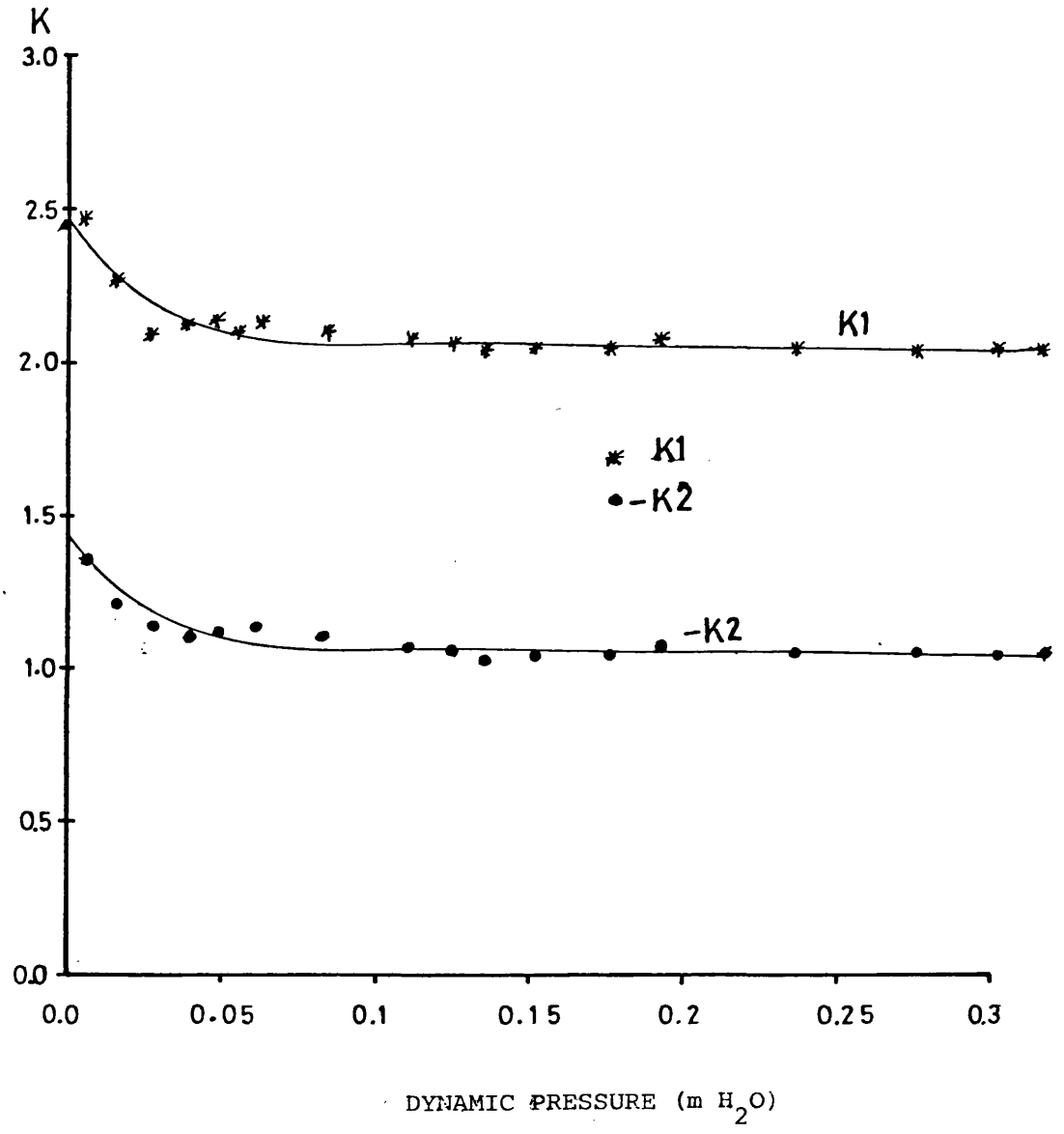

FIG. 3.13 CALIBRATION CURVES FOR THE OUTLET TRAVERSE PROBE

CHAPTER 4 : PRESENTATION AND DISCUSSION OF EXPERIMENTAL RESULTS

4.1 Introduction

The objective of the experimental programme was :

1) To study the performance and flow regimes of curved and conical diffusers under steady inlet conditions by varying the mass flow rate and inlet flow angle.

2) To study the influence of jet-wake type flow patterns on the performance and flow regimes of the same diffusers under varying inlet conditions of mass flow rate and inlet flow angle.

3) To compare the stability and performance of both diffusers under the above mentioned conditions.

The test rig facility offered the possibility of varying the mass flow rate and inlet flow angle by operating one or two fans together with the rotating screen, hence it was possible to obtain three different mass flow rates and inlet flow angles. Since the case in which one fan and the rotating screen are operating represents an intermediate condition between the rotating screen operating alone and with two fans, it has been omitted from the description of the results and will be referred to only when needed. Table 4.1 gives details of each test condition. Test series A refers to the curved diffuser while test series B refers to the conical diffuser. S refers to the steady flow tests and J refers to the jet-wake flow tests. Hence AS1 is a curved diffuser test with steady flow having high mass flow rate, BJ3 is a conical diffuser test with jet-wake flow having low mass flow rate.

In each test performed the flow properties were recorded by traversing the width of the diffuser passage at three stations inlet, middle and outlet by means of pressure probes. The mass flow rate was calculated from integrated inlet meridional velocity profiles and are presented in table 4.1. Diffuser performance was also calculated from integrated velocity and pressure profiles. All profiles obtained for the different flow patterns for both diffusers

were analysed to evaluate pressure recovery and flow distortion parameters using the analysis presented in Appendix D.

Table 4.2 presents at each of the three traverse stations the values of kinetic energy flux coefficient α and coefficient of separation as defined by equations D.9 and D.22 respectively.

Various performance coefficients are presented in table 4.3. Each parameter was calculated using the equations in Appendix D which are also referred to in the table. Figure 4.1 represents the plot of equation D.3. which calculates the ideal pressure recovery for uniform flow for both conical and curved diffuser. The ideal pressure recovery is seen to remain constant for all values of mean inlet flow angles in the case of a conical diffuser, while for the curved diffuser C_{p_i}, as calculated from equation D.3 increases progressively with increasing mean inlet flow angle $\bar{\psi}_1'$.

4.2 Steady Inlet Flow Test Series AS and BS

4.2.1 Curved diffuser test series AS

Figures 4.2a to 4.4 show the flow pattern for test AS1 where both fans and the rotating screen were running. The inlet conditions show a non-distorted flow pattern with almost linear distribution of velocity in the core, with an inlet flow angle of about 68 degrees. The uniformity of the flow was reflected in a low value of coefficient of kinetic energy flux at inlet as shown in table 4.2.

The tangential velocity component of inlet, fig. 4.2b shows a linear increase from hub to shroud as does the absolute velocity and total pressure (figs. 4.3a and 4.4a respectively). This is to be expected from a rotor which increases in radius from hub to shroud. The inlet static pressure, fig. 4.4b, also increases slightly from hub to shroud. This pressure gradient is necessary to balance the centrifugal force created by the swirl as expressed in equation A.21, Appendix A. This is also apparent from the wall tapping traces fig. 4.5. The wall pressure tapping at inlet showed a lower value than that recorded by the

pressure probes as seen from fig. 4.4b. This was attributed to the wall effect upon the probe response, however, if a straight line is connected between the two wall pressure tappings as in figure 4.4b, the same pressure gradient as that recorded by the probe is obtained but with pressure values lower than those given by the probe traverse.

The development of the flow parameters through the diffuser passage showed a non-separated pattern on either wall. The static pressure trace is almost uniform at mid and outlet stations, fig. 4.4b. This is expected from a radial geometry as expressed by equation A.21.

Fig. 4.4b and the wall pressure tapping traces figure 4.5 showed that most of the diffusion process takes place in the curved part of the diffuser. The diffuser performance parameters listed in table 4.3 indicated that the pressure recovery coefficient calculated from the wall pressure tappings is higher than that calculated from the traverse results due to the difference in level of inlet static pressure indicated by the wall tappings and pressure probe.

4.2.1.1 The effect of reducing the mass flow rate Test AS3

The mass flow rate was reduced by running the rotating screen with one fan, then alone. The case in which one fan was running represented an intermediate change, hence test AS3 where the rotating screen only was running will be considered.

Fig. 4.6 compares the meridional velocity profiles for tests AS1 and AS3 at the three satations. The inlet profiles were similar in general features with a difference only in magnitude. The mid and outlet profiles showed that the effect of the reduction of mass flow rate was to produce lower velocities on the hub with the flow at the onset of separation at outlet. This effect of mass flow reduction corresponds with that shown theoretically by the inviscid analysis in part 2.3.1, where it was proved that an increase in mean meridional velocity will have a favourable effect upon separation. Fig. 4.7 compares the flow angle for tests AS1 and AS3 at the three stations. From this it can be seen that as separation is approached the flow angle increases towards 90 degrees.

The tangential and total velocity showed general similarity between the two tests as did the total and static pressure traces. The coefficient of kinetic energy flux α, table 4.2 showed similar distortion at inlet while at outlet it indicated a slight decrease in the flow distortion with increase in mass flow rate.

A comparison between wall pressure tappings of test AS1 and AS3 in fig. 4.8 shows that while the hub pressure was not significantly affected by the reduction in mass flow rate, the shroud wall pressure in the curved part did not show an initial reduction in pressure as that in test AS1. The pressure recovery coefficient as expected from the wall pressure traces was not significantly affected by the reduction in mass flow rate, see table 4.3. The loss coefficient indicated a continuous increase with mass flow rate decrease. Computed pressure recovery showed generally good agreement with the measured ones especially at the low mass flow rate. The diffuser effectiveness showed higher values with higher mass flow rate due to the decrease in C_{p_i} with the decrease in inlet flow angle as explained in fig. 4.1.

4.2.2 Conical diffuser test series BS

Figs. 4.9 to 4.11 show the flow pattern for test BS1 where both fans and the rotating screen were running. The inlet conditions show a non-distorted flow pattern with a linear distribution of properties. Flow distortion at inlet was low as indicated from the kinetic energy flux coefficient α, table 4.2. The inlet static pressure, fig. 4.11b showed the same trend as that in test AS1 with a slight increase from hub to shroud.

The development of the flow inside the diffuser shows a 3-dimensional separation on the hub which occupied 20% of the diffuser width at mid traverse and 15% at outlet traverse. The total pressure profile showed a marked change between inlet and outlet with a distinctive drop in total pressure on the hub side indicating high losses associated with the separation.

The wall static pressure fig. 4.12, showed a steady rise between inlet

and outlet with the shroud pressure drop in the middle due to the effect of flow separation which reduced the flow area causing an acceleration of the flow. The wall pressures at inlet again differed from those obtained from the probe traverse.

A comparison of the wall static pressure development in the conical and curved diffusers tests BS1 and AS1, is also included in fig. 4.12. For the curved diffuser test it can be seen that the hub wall pressure exceeded that on the shroud through most of the diffuser whilst the opposite was the case with the conical diffuser. The overall pressure rise through the curved diffuser was in excess of that in the conical diffuser. This is reflected in the relative magnitudes of the pressure recovery coefficients given in table 4.3. The effectiveness of the curved diffuser is also well in excess of that given by the conical diffuser.

The higher level of losses and lower values of pressure recovery in the case of the conical diffuser can be attributed to the existence of separation. Fig. 4.13 compares the flow development represented by the meridional velocity profiles at the three traversing stations of the curved and conical diffusers. Together with fig. 4.14 which compares the flow angles, they show quite clearly that while the inlet flow conditions were almost identical, the flow in the conical diffuser exhibited a large reversed flow on the hub. Comparison between the total pressure traces of the two diffusers figs. 4.4a and 4.11a illustrates the large pressure loss between inlet and mid position of the conical diffuser.

Separation associated with the geometry was discussed in section 2.3.1 where the favourable effect of positive wall curvature and contraction upon separation was demonstrated by the inviscid flow analysis. However, the effect of curvature on the boundary layer development was investigated in references (95), (96) and (97); these reports showed that a concave surface, as that of the hub in case of curved diffuser, increases mixing and hence improved momentum transfer and delays separation while for a flow developing against a convex wall, as in the conical diffuser hub for a swirling flow, mixing is hindered and flow is much more prone to separation.

4.2.2.1 The effect of reducing the mass flow rate test BS3

By reducing the mass flow rate, the region of reversed flow at the mid traverse station was increased to 40% of the diffuser width, whilst that at outlet was reduced to 10% of the diffuser passage. This is illustrated by the comparative plots of the meridional velocity distribution in fig. 4.15. The reduction in magnitude of the reversed flow region at discharge is due to the separation bubble moving further into the diffuser with the point of re-attachment moving closer to the discharge radius, as illustrated in fig. 4.16. The comparison of the flow angle fig. 4.17 also illustrates the extent of the reversed flow zones. The shroud flow angle which decreases through the diffuser at the high flow rate, test BS1, shows a significant increase between the mid station and discharge when the flow rate is reduced, test BS3. This is indicative of an approaching separation on the shroud side and shows a tendency for the separation to switch from the hub to the shroud.

Flow distortion as expressed by the kinetic energy flux coefficient indicated a reduction in flow distortion at discharge as the mass flow was reduced due to the reduced separation zone. The overall performance of the diffuser has deteriorated as the mass flow rate has been reduced. This is apparent from the recovery and loss coefficients given in table 4.3. The pressure development through the diffuser fig. 4.18, shows similar behaviour at both flow rates with the shroud static pressure falling more rapidly in the inlet region at the low flow rate due to separation on the hub.

4.3 Jet-wake Flow Test Series AJ and BJ

To simulate the real flow issuing from a centrifugal impeller, the rotating screen was prepared as shown in fig. 3.4. The same traversing probes were used for this study of unsteady inlet flow, hence errors of over-estimation of total pressure can be expected, see Senoo and Ishida (64).

4.3.1 Curved diffuser test series AJ

Figs. 4.19 to 4.21 represent the flow development through the curved diffuser for the case of a jet-wake flow, The inlet conditions are distinguished by the existence of an area of high constant total pressure near the shroud as seen from fig. 4.21a. The same feature was apparent in the tangential and total velocity profiles fig. 4.19b and 4.20a. This high total pressure part is attributed to the existence of unmixed jet-wake pattern which caused the traversing probe at inlet to over-predict total pressure values as mentioned in reference (64). The inlet conditions were also characterised by the existence of a belt of high meridional velocity near the shroud. The inlet flow angle was approximately 76 degrees and of the same order of magnitude as test AS3, see fig. 4.20b.

The development of the flow through the diffuser showed that while at inlet the meridional velocity profile fig. 4.19a showed a tendency towards separation on the hub at outlet the profile rotated with a tendency towards separation on the shroud surface. This rotation was also apparent from the total pressure profiles fig. 4.21a. A large drop in total pressure between inlet and mid traverse position shows a high indicated loss level.

The wall static pressures fig. 4.22 and the static pressure profile, fig. 4.21b, showed that the pressure gradient changed sign between inlet and mid traverse position, a feature which was apparent in all the curved diffuser tests. Comparing the wall pressures of test AJ1 with those of test AS1, fig. 4.22, it can be seen that they show the same general behaviour but with a lower pressure level through the curved part in the case of the jet-wake flow pattern.

Table 4.3 shows that the computed pressure recovery is much less in test AJ1 than in test AS1. This is due to the large indicated loss which is possibly over estimated due to an over-estimation of total pressures at inlet in the jet-wake flow. However, the measured pressure recovery coefficient showed almost similar values while the wall pressure based pressure recovery coefficient showed about 10%

reduction in the case of the jet-wake flow. Effectiveness also dropped for the jet-wake flow due to the higher mean inlet flow angle which led to an increase in the ideal pressure recovery coefficient (see fig. 4.1).

Figs. 4.23 and 4.24 compares the meridional velocity and flow angle development for the unsteady and steady flow tests AJ1 and AS1. The differences between the inlet flow conditions are clearly indicated. As the flow develops through the diffuser the flow patterns become similar at the mid traverse station. At discharge, however, the unsteady flow test shows a substantial reduction in velocity on the shroud surface indicating a tendency to separation on the opposite wall to that for the steady flow test. This difference is attributed to the total pressure gradient at the mid traverse station, see fig. 4.25. The behaviour of the flow between the mid traverse station and discharge qualitatively follows equation 2.24.

The flow distortion represented by the kinetic energy coefficient was high at inlet in test AJ1 than that of test AS1 (see table 4.2), while at outlet the jet-wake flow test showed less distortion than that of the steady flow test. This is attributed to the fact that the distortion of the outlet flow represented by the difference between maximum and minimum values were higher in test AS1 than in test AJ1.

4.3.1.1 The effect of reducing the mass flow rate test AJ3

Figs. 4.26 to 4.28 compare test AJ1 with maximum possible mass flow rate to test AJ3 in which mass flow rate was reduced. As observed from fig. 4.26 the inlet profiles were generally similar with a difference only in levels. However, the inlet meridional velocity profile showed that by reducing the mass flow rate the belt of high velocity moved closer to the shroud. Test AJ2, which is intermediate between AJ1 and AJ3, also showed this trend with the peak velocity lying between that of test AJ1 and test AJ3. This phenomenon of a peak meridional velocity which shifts towards the shroud as the mass flow rate was decreased could be due to

(i) An error caused by the nature of the probes which have a much slower response than the frequency of the jet-wake pattern. The jet region may have dominated the response of the probes and that domination was more distinctive where minimum mixing of the jet and wake occurred. Fig. 4.29 presents hot-wire anemometer traces of the flow in the diffuser during test AJ3. From these it can be seen that the mixing of the jet-wake at inlet is more complete near hub than near shroud. Also mixing of the jet-wake was almost completed at the mid traverse. If the constant high total pressure regions at inlet fig. 4.28 belong to non-mixed jet-wake flow, it can be seen how the jet domination moved towards shroud by mass flow reduction, which coincides with the peak meridional velocity shift fig. 4.26.

(ii) A genuine phenomenon which was the result of possible stall due to boundary layer separation on the shroud side shortly after inlet because of the convex curvature downstream of the measuring station. The streamlines upstream adjust to smooth paths allowing this narrowing of the streamtubes to build up early resulting in a high meridional velocity. As mass flow rate was decreased, the flow angle was increased causing the convex curvature for a swirling fluid particle to decrease, adding to that the reduction in local Reynolds number by reduction in mass flow rate, the centrifugal force acting up on the fluid particles near the shroud was reduced. As a result of that the stall region diminishes, resulting in a shift of the position of maximum meridional velocity towards the shroud. Similar behaviour to this was reported by Marris (98) for the flow of water in curved channel. Fig. 4.30a shows the meridional velocity profiles at inlet for different mass flow rates tests AJ1, AJ2 and AJ3 while fig. 4.30b shows velocity profiles of Marris (98).

To decide the full nature of this phenomenon, detailed measurements of flow along the curved part of the diffuser at several traverse stations are needed. The instrumentation then has to be of the

mass averaging type, such as a hot-wire anemometry system, to eliminate any possible error due to the response of the time averaging probes used in this investigation.

Flow development through the diffuser in test AJ3 differs from that of test AJ1. An initial separation of the hub appeared on the shroud side at discharge, see fig. 4.26 and 4.27. The meridional velocity and total pressure profiles at the mid traverse station fig. 2.26 and 2.28 showed complete rotation of the profiles when the mass flow rate was reduced. Fig. 4.31 compares the wall static pressure development for tests AJ1 and AJ3. While these are identical at both inlet and discharge, the shroud pressure in test AJ1 shows a distinctive decrease in the curved part. This reduction in shroud pressure was usually associated with an increase in mass flow rate in both the steady and jet-wake tests, but was most distinctive in the jet-wake tests (see fig. 4.22).

Flow distortion, expressed by the kinetic energy coefficient α (table 4.2) for test AJ3 was slightly higher than that of AJ1 at inlet and outlet due to the existence of separation. The computed pressure recovery coefficients showed a slight deterioration as the mass flow rate was reduced (see table 4.3). The effectiveness also decreased with the mass flow rate much because C_{p_i} increased due to the increase in inlet flow angle (see fig. 4.1).

4.3.2 Conical diffuser test series BJ

Various velocity, flow angle, pressure profiles for test BJ1, where the two fans in addition to the rotating screen were operating, are presented in figs. 4.32 to 4.34. The inlet conditions show a highly distorted flow with total pressure, tangential and absolute velocity having a broad peak near the shroud. This is attributed, as was the case in test AJ1, to the non-mixed jet-wake flow. The development of the flow showed a large area of reversed flow at the mid traverse station which occupied about 40% of the diffuser width. At discharge the reversed flow zone occupied approximately 15% of the passage see fig. 4.33b. The static pressure traces, fig. 4.34b, showed

an area of constant pressure which occupied most of the diffuser width at mid and outlet positions. The total pressure profiles also have a constant magnitude from the hub surface through 55% of the passage, see fig. 4.34.

The wall static pressures, fig. 4.35, showed, as in previous tests, the shroud pressure first decreasing and then increasing while hub surface pressure increased steadily through the diffuser. The coefficient of kinetic energy indicated that the distortion was highest at the mid position due to the large separation (see table 4.2), this is also indicated by the coefficient of separation K_s. The outlet distortion for test BS1 was higher than that for test BJ1, this is due to the difference between the maximum and minimum velocities at outlet which was less in test BJ1 than in the steady flow test BS1. Comparison between the performance parameters of test BJ1 and BS1 reveals a reduction in pressure recovery with the application of the jet-wake flow, see the measured and wall pressure based coefficients, table 4.3. Comparison of the wall static pressures between tests BJ1 and BS1 is also included in fig. 4.35. This shows similar trend although shroud pressure in test BJ1 decreased steadily through the first half of the diffuser while it stayed almost constant in test BS1.

Figs. 4.36 to 4.38 compare meridional velocity, flow angle and total pressure profiles of the steady flow test BS1 and the jet-wake flow test BJ1. The inlet conditions reveal large differences in uniformity as seen from the meridional velocity profiles, fig. 4.36 and the total pressure profiles, fig. 4.38. The flow angle and meridional velocity at the mid traverse station showed a large reversed flow zone for the jet-wake flow. At discharge, however, the reversed flow zones were of equal magnitude. The main differences between the two tests was in the total pressure distortion which was quite large at inlet but was reduced at outlet. This again may have been partially due to probe error in the unsteady flow field at inlet.

To distinguish between the effect of inlet distortion and variation in mass flow rate on flow development, test BJ1 was compared with the steady flow test BS3 which had approximately the same mass flow rate. Fig. 4.39 compares the meridional velocity profiles of these tests. While the inlet profile was uniform in test BS3 and distorted in test BJ1, the mid and outlet traverse traces showed almost identical results. This demonstrates that the main parameter controlling the magnitude of the separation, or reversed flow zone was the variation in flow rate and not the introduction of unsteady flow. This was not the case with the curved diffuser where the unsteady flow had the effect of switching the separation zone from the hub to the shroud, this is illustrated by the meridional velocity profiles of tests AJ1 and AS3 fig. 4.40.

The geometrical effect of using a curved rather than a conical diffuser is illustrated by the comparison of the unsteady flow tests AJ1 and BJ1 in fig. 4.41, 4.42 and 4.43. Whilst the inlet conditions are broadly similar, the extensive reversed flow zone developed in the conical diffuser is clearly seen. In contrast no reverse flow occurred in the curved diffuser.

Comparising performance parameters in table 4.3 shows clearly that the conical diffuser performance calculated by all expressions is considerably less than that of the curved diffuser.

4.3.2.1 The effect of reducing the mass flow rate test BJ3

By stopping one fan, test BJ2 showed comparable behaviour to that of BJ1, further reduction of the mass flow rate by operating the rotating screen only (test BJ3) led to strong low frequency pulsations. These pulsations at approximately 10 hz had a frequency much lower than that of the rotating jet-wake pattern which was 580 Hz. A single wall static pressure transducer was used to measure these pulsations, fig. 4.44. The pulsating flow was confined to the diffuser itself, there was no evidence of pulsations at inlet to the system. It is probable, that a form of rotating stall, similar to that reported by Jansen (65) was occurring. However, to measure this in detail it would be necessary to employ at least two transducers and only one was available.

The flow behaviour through the diffuser during this test is compared to the high mass flow rate test BJ1 in figs. 4.45 to 4.47. A major difference in inlet conditions lies in the existence of separation on the hub for test BJ3 at inlet, this is shown by the meridional velocity and flow angle traces fig. 4.45 and 4.46. Generally, for the rest of the passage the two tests showed similar features with separation occurring on the hub. Total pressure profile becomes uniform more quickly in the case of test BJ3 and the outlet conditions indicated less distorted flow which was reflected in the values of the kinetic energy coefficient α, table 4.2, where they were less for test BJ3 than for test BJ1.

The wall static pressure traces, presented in fig. 4.48, indicate a more gradual increase of static pressure along the shroud. The performance parameters showed approximately similar pressure recovery values with only a slight increase with increasing mass flow rate. The computed pressure recovery showed extremely low values due to the high level of total pressure at inlet which led to large computed losses and hence low computed pressure recovery.

4.3.2.2 The effect of mass flow rate on pulsating flow

To further investigate the cause of the pulsating flow and its relation with the mass flow rate, the steel plates generating the wakes were removed and the rig restored to its configuration as for test series BS. The inlet to the diffuser rig was then gradually throttled to reduce the flow rate, on doing so, the same pulsating flow began to develop. The throttle was then increased until a mean inlet flow angle equal to that of test BJ3 was obtained, at this condition the pulsating flow was well established. A comparison between flow behaviour under this reduced mass flow rate condition, test BS4 (see table 4.1) and test BJ3 are given in figs. 4.49 and 4.50. The inlet traverse results indicated similar profiles to those of the jet-wake test BJ3 although slightly more uniform. The seame feature of flow separation on the hub at inlet was observed in test BS4 as in test BJ3. The development of the flow profiles through the diffuser also followed a similar pattern to those in the jet-wake tests. The wall static pressure transducer traces in test BS4 show similar patterns to those obtained for test BJ3 fig. 4.44. Further reduction of the

mass flow rate by increasing the inlet throttle did not affect the pulsation frequency and magnitude as is apparent from fig. 4.51 where the minimum possible mass flow rate was obtained.

These results again demonstrate that the mass flow rate through the conical diffuser is more significant than the jet-wake flow distortion at inlet. Once the flow rate has been reduced to that which gives rise to strong pulsations, further flow reduction had no measurable effect.

Finally, from all jet-wake flow tests, it is concluded that the curved diffuser gave much more stable operation than the conical diffuser. The curved diffuser also gave better pressure recovery than the conical diffuser with similar inlet conditions.

Test Code	Diffuser Type	Inlet Flow Type	Test Rig Condition	Mass Flow Rate kg/s
AS1	Curved	Steady	Screen + 2 fans	2.15
AS2	Curved	"	Screen + 1 fan	1.88
AS3	Curved	"	Screen only	1.60
BS1	Conical	"	Screen + 2 fans	2.24
BS2	Conical	"	Screen + 1 fan	1.95
BS3	Conical	"	Screen only	1.63
BS4	Conical	"	Screen only, inlet throttle	1.27
AJ1	Curved	Jet-wake	Screen + 2 fans	1.77
AJ2	Curved	"	Screen + 1 fan	1.58
AJ3	Curved	"	Screen only	1.25
BJ1	Conical	"	Screen + 2 fans	1.68
BJ2	Conical	"	Screen + 1 fan	1.43
BJ3	Conical	"	Screen only	1.11

TABLE 4.1 Test Conditions used for both the Curved and the Conical Diffusers

Test Code	Coefficient of K.E.α	Coefficient of separation K_s	Diffuser Type	Inlet Flow Type
	1.014	1.00		
AS1	1.063	1.00	Curved	Steady
	1.092	1.00		
	1.009	1.00		
AS2	1.082	1.00	Curved	Steady
	1.121	1.00		
	1.008	1.00		
AS3	1.131	1.00	Curved	Steady
	1.119	1.00		
	1.005	1.00		
BS1	1.189	1.035	Conical	Steady
	1.378	1.013		
	1.004	1.00		
BS2	1.204	1.078	Conical	Steady
	1.329	1.042		
	1.001	1.00		
BS3	1.213	1.253	Conical	Steady
	1.097	1.016		
	1.005	1.031		
BS4	1.053	1.071	Conical	Steady
	1.108	1.002		
	1.033	1.00		
AJ1	1.041	1.00	Curved	Jet-wake
	1.026	1.00		

TABLE 4.2 Flow Distortion Parameters for the Three Successive Traverse Stations across the Curved and the Conical Diffusers

CONT'D

TABLE 4.2 cont'd

	1.029	1.00		
AJ2	1.035	1.00	Curved	Jet-wake
	1.035	1.00		
	1.019	1.003		
AJ3	1.028	1.00	Curved	Jet-wake
	1.050	1.0003		
	1.039	1.00		
BJ1	1.369	1.202	Conical	Jet-wake
	1.157	1.025		
	1.031	1.00		
BJ2	1.284	1.416	Conical	Jet-wake
	1.049	1.001		
	1.021	1.008		
BJ3	1.081	1.309	Conical	Jet-wake
	1.059	1.002		

Test Code	Diffuser Type	Inlet Flow Type	Inlet Mean Flow Angle Degrees Eq. D.8	C_{p_i} Uniform Flow Eq. D.2	$C_{p_{in}}$ Non uniform Flow Eq. D.16	Coefficient of Losses Eq. D.14	C_p Computed Eq. D.15	C_{p_m} measured Eq. D.20	Effectiveness $\xi = \frac{C_{p_m}}{C_{pi}}$	C_{p_w} wall Eq. D.21
AS1	Curved	Steady	69.0	0.549	0.535	0.083	0.451	0.425	0.773	0.591
AS2	"	"	71.6	0.570	0.544	0.103	0.441	0.428	0.752	0.617
AS3	"	"	75.1	0.593	0.566	0.143	0.423	0.433	0.729	0.581
BS1	Conical	"	67.8	0.622	0.559	0.178	0.382	0.364	0.585	0.505
BS2	"	"	71.6	0.622	0.550	0.248	0.301	0.323	0.519	0.476
BS3	"	"	75.2	0.622	0.579	0.254	0.325	0.327	0.525	0.493
BS4	"	"	78.2	0.622	0.546	0.437	0.110	0.331	0.532	0.486
AJ1	Curved	Jet-wake	76.1	0.599	0.579	0.309	0.271	0.423	0.706	0.532
AJ2	"	"	77.2	0.605	0.560	0.308	0.253	0.415	0.686	0.537
AJ3	"	"	79.5	0.616	0.550	0.302	0.249	0.428	0.694	0.545
BJ1	Conical	"	76.3	0.622	0.523	0.418	0.110	0.333	0.536	0.393
BJ2	"	"	77.9	0.622	0.543	0.397	0.140	0.355	0.571	0.439
BJ3	"	"	80.2	0.622	0.505	0.498	0.010	0.319	0.514	0.419

TABLE 4.3 CURVED AND CONICAL DIFFUSERS PERFORMANCE PARAMETERS

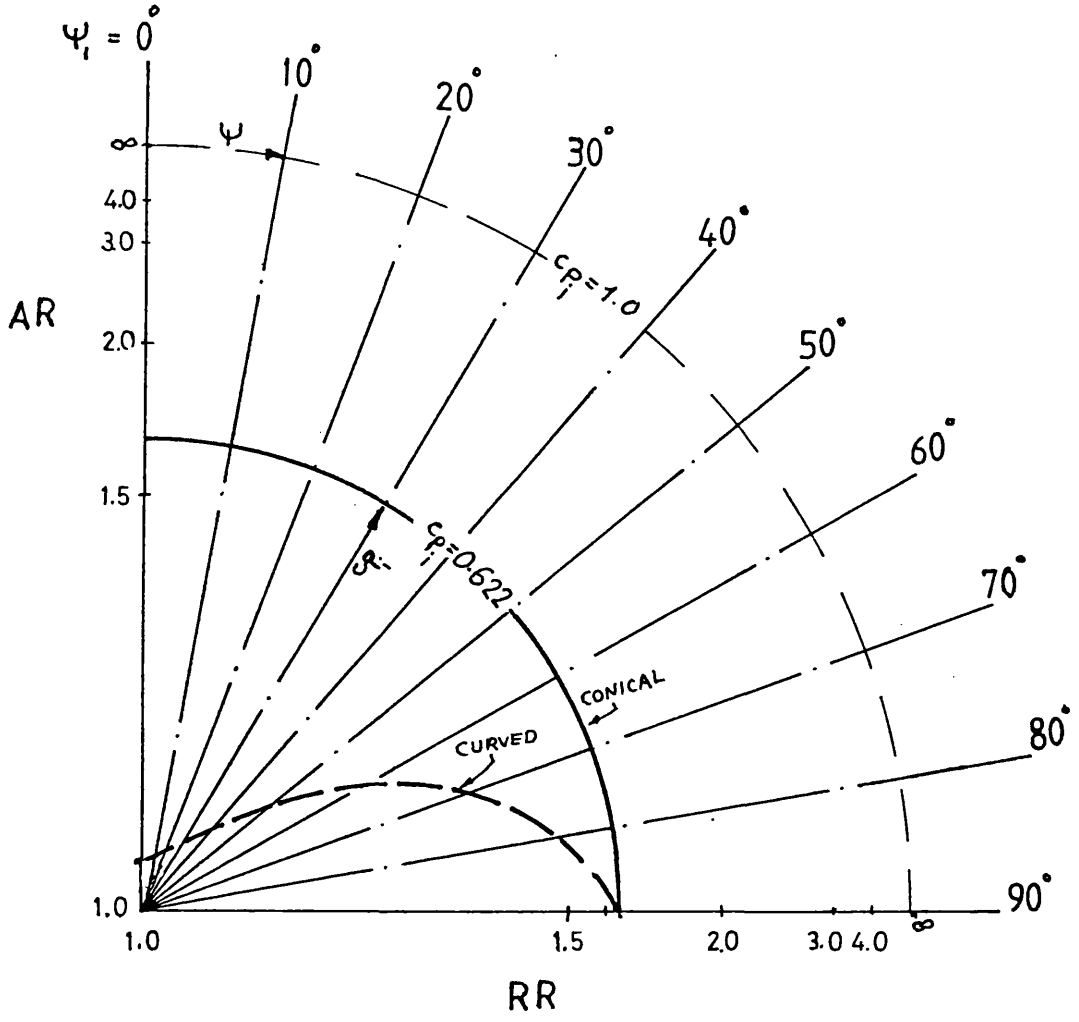

FIG. 4.1 VARIATION OF C_{p_i} FOR CONICAL AND CURVED DIFFUSER WITH INLET FLOW ANGLE

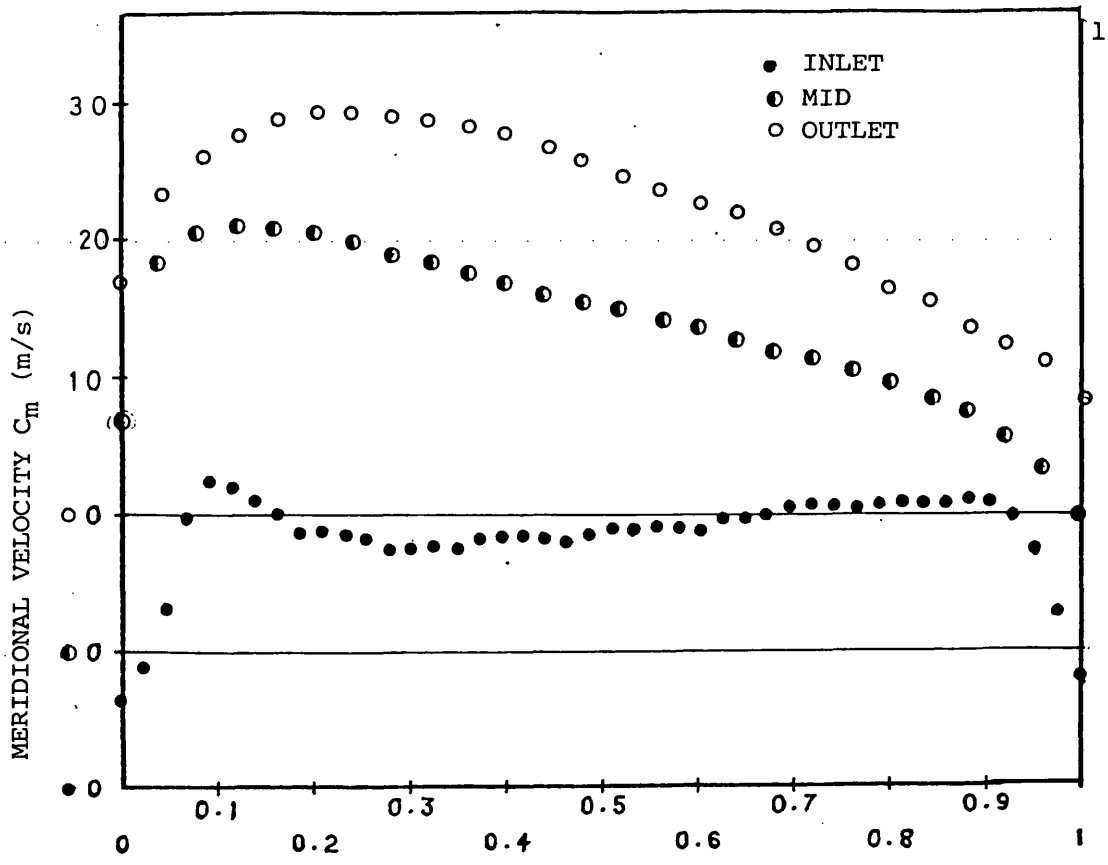

FIG.4.2a MERIDIONAL VELOCITY DISTRIBUTION
TEST AS1

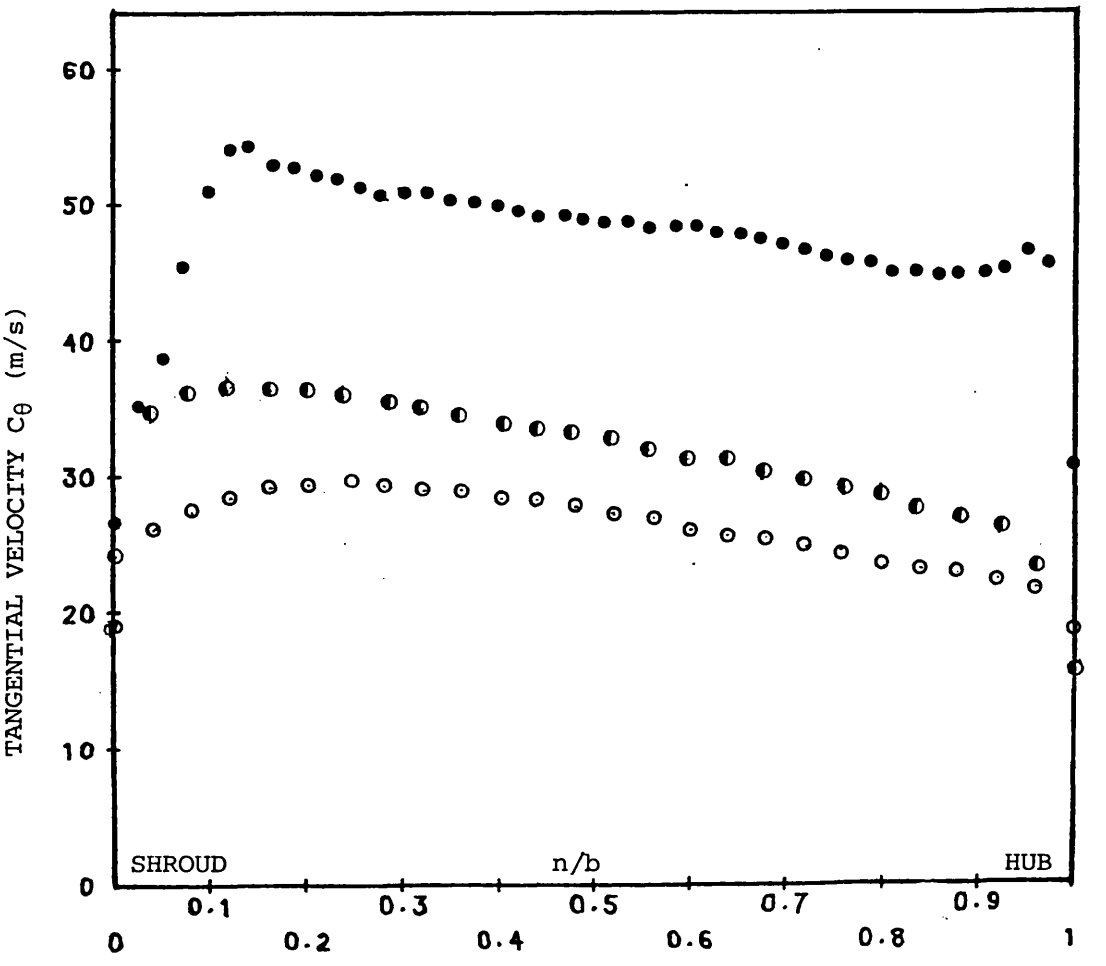

FIG. 4.2b TANGENTIAL VELOCITY DISTRIBUTION
TEST AS1

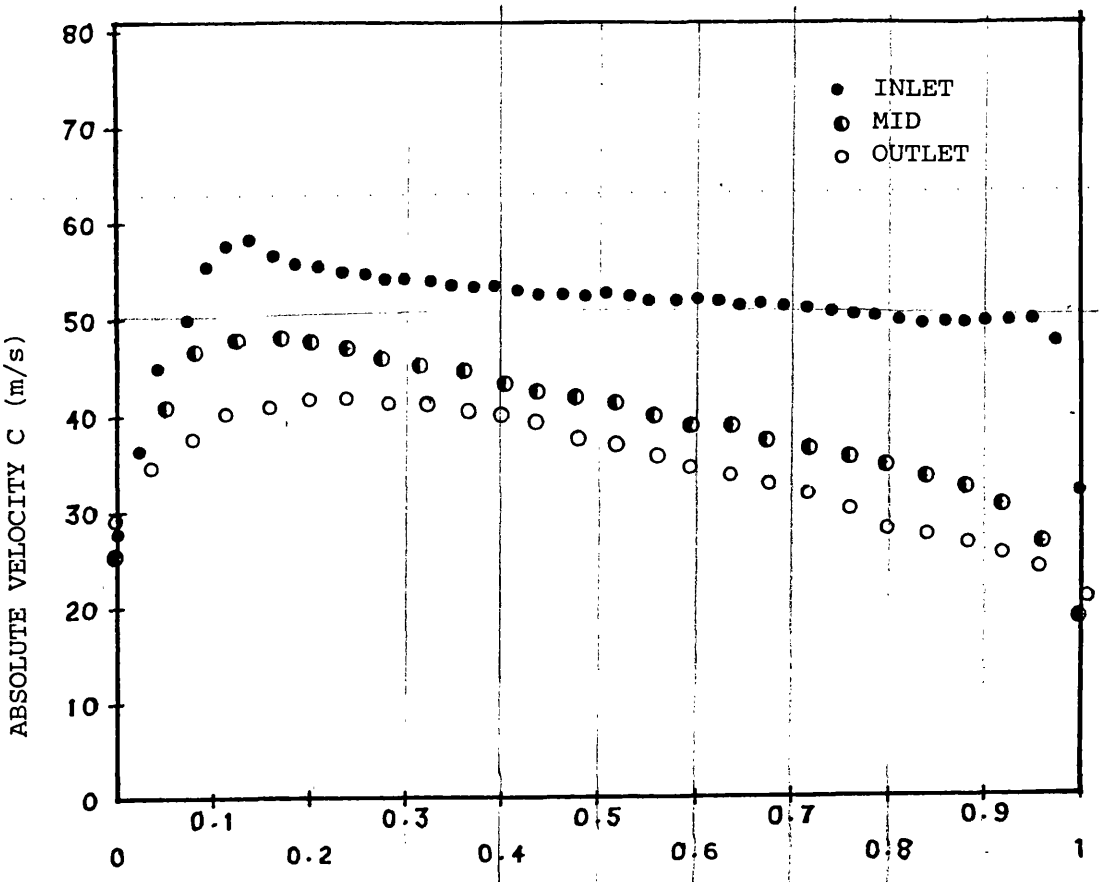

FIG. 4.3a ABSOLUTE VELOCITY DISTRIBUTION TEST AS1

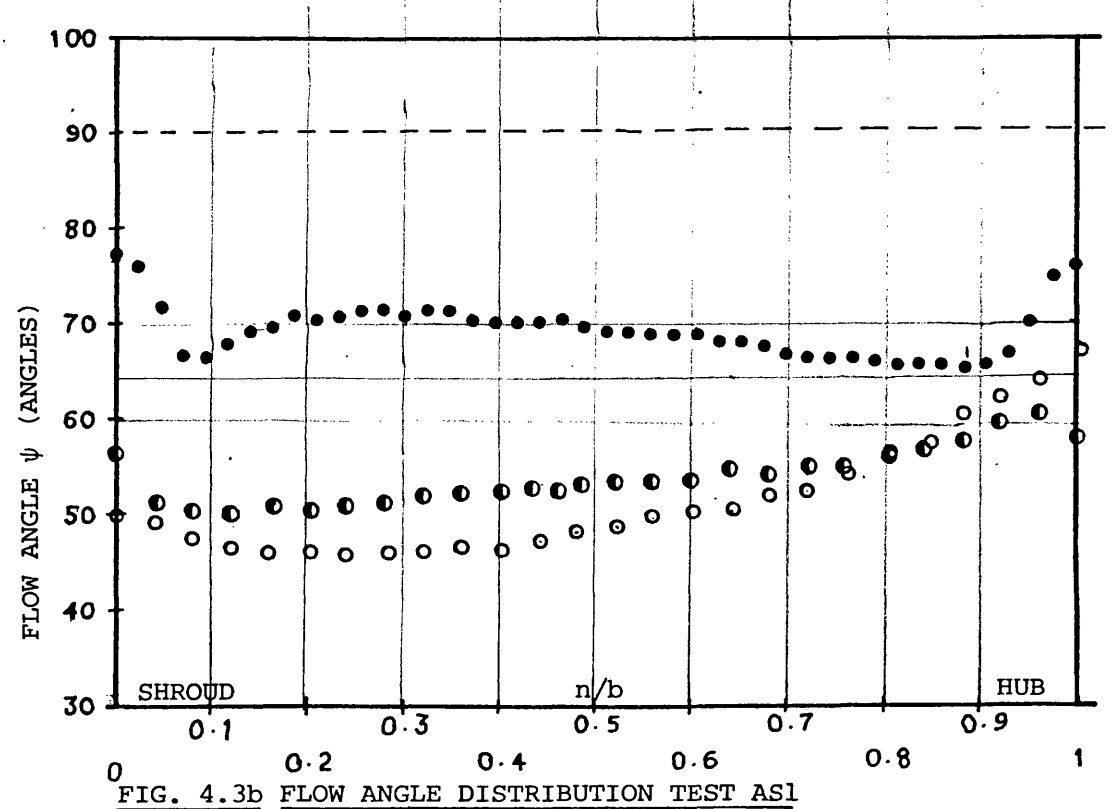

FIG. 4.3b FLOW ANGLE DISTRIBUTION TEST AS1

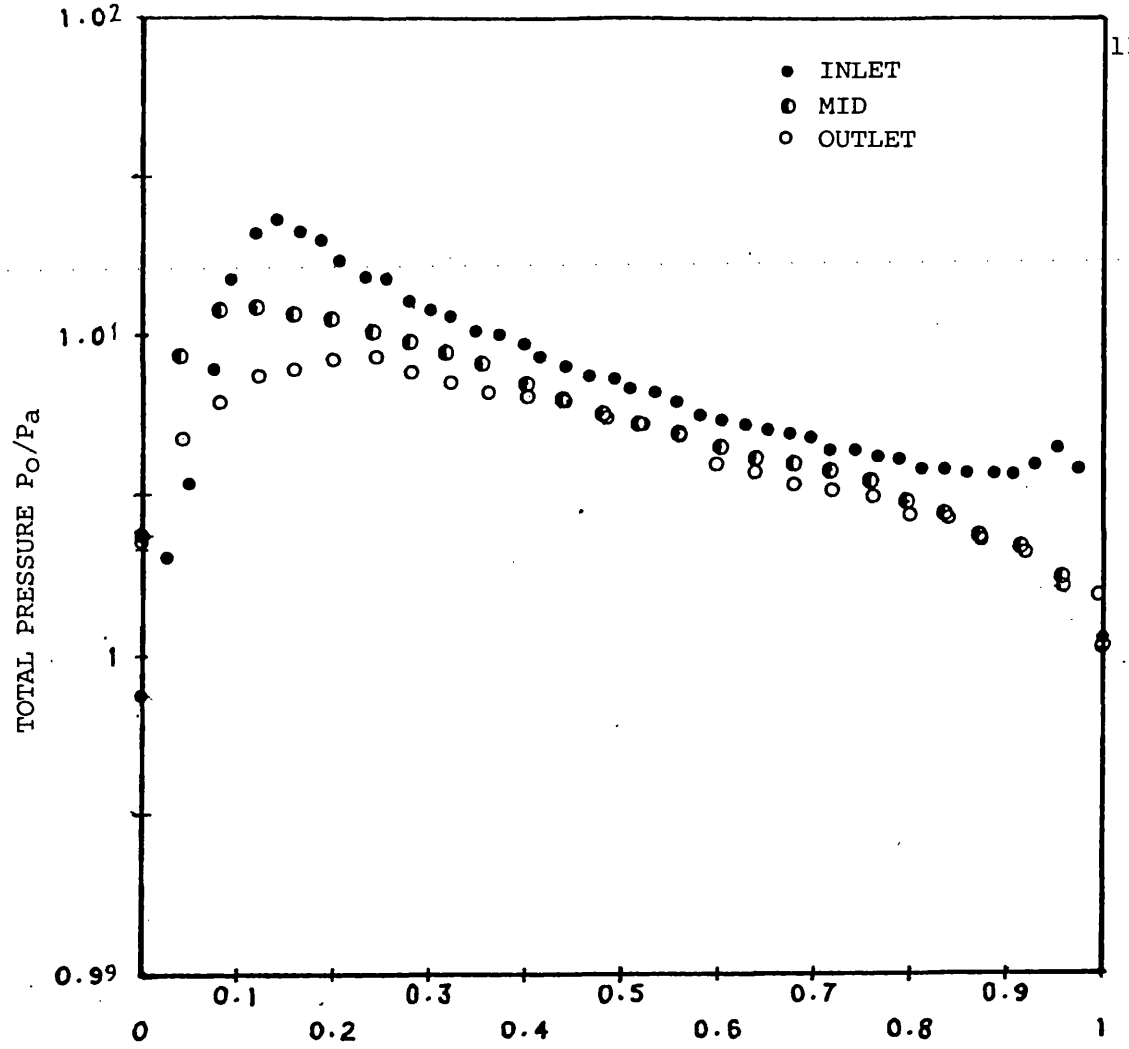

FIG.4.4a TOTAL PRESSURE DISTRIBUTION TEST AS1

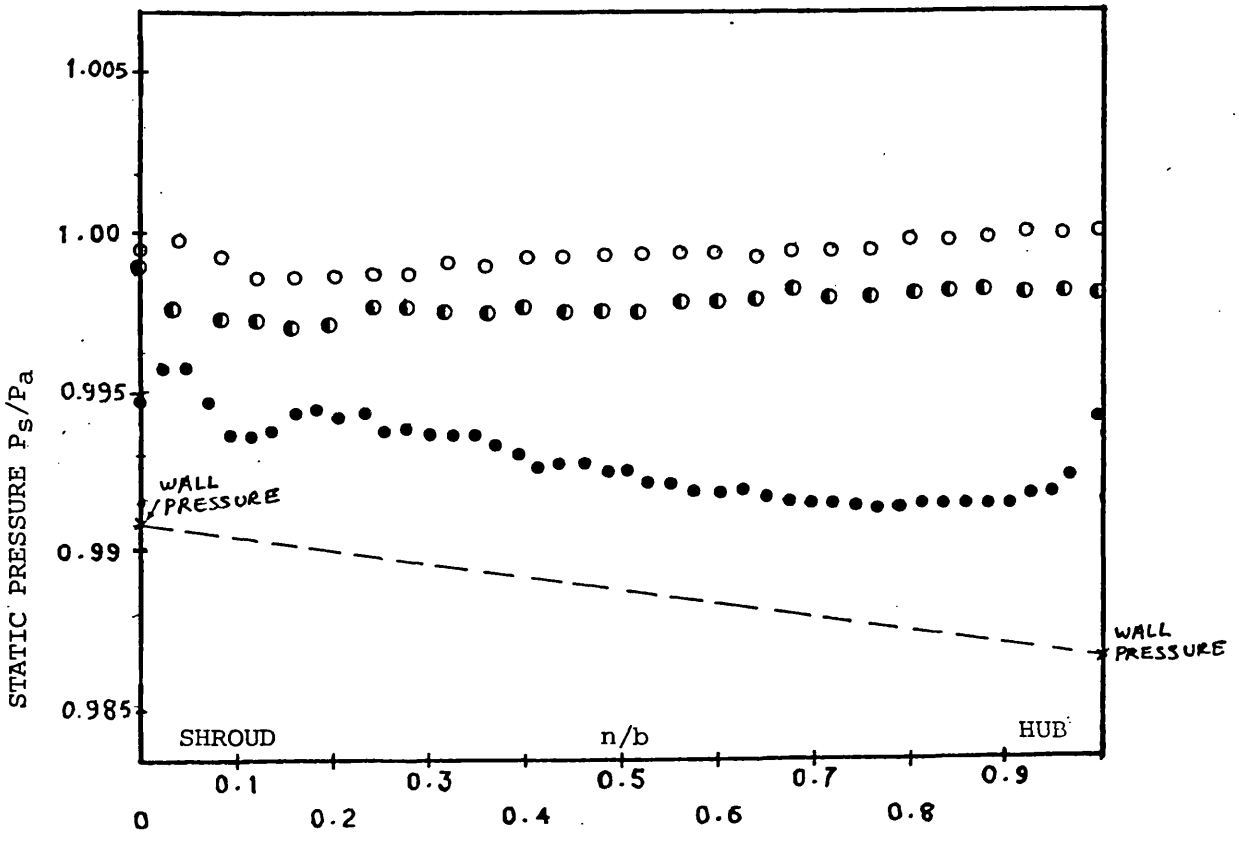

FIG.4.4b STATIC PRESSURE DISTRIBUTION TEST AS1

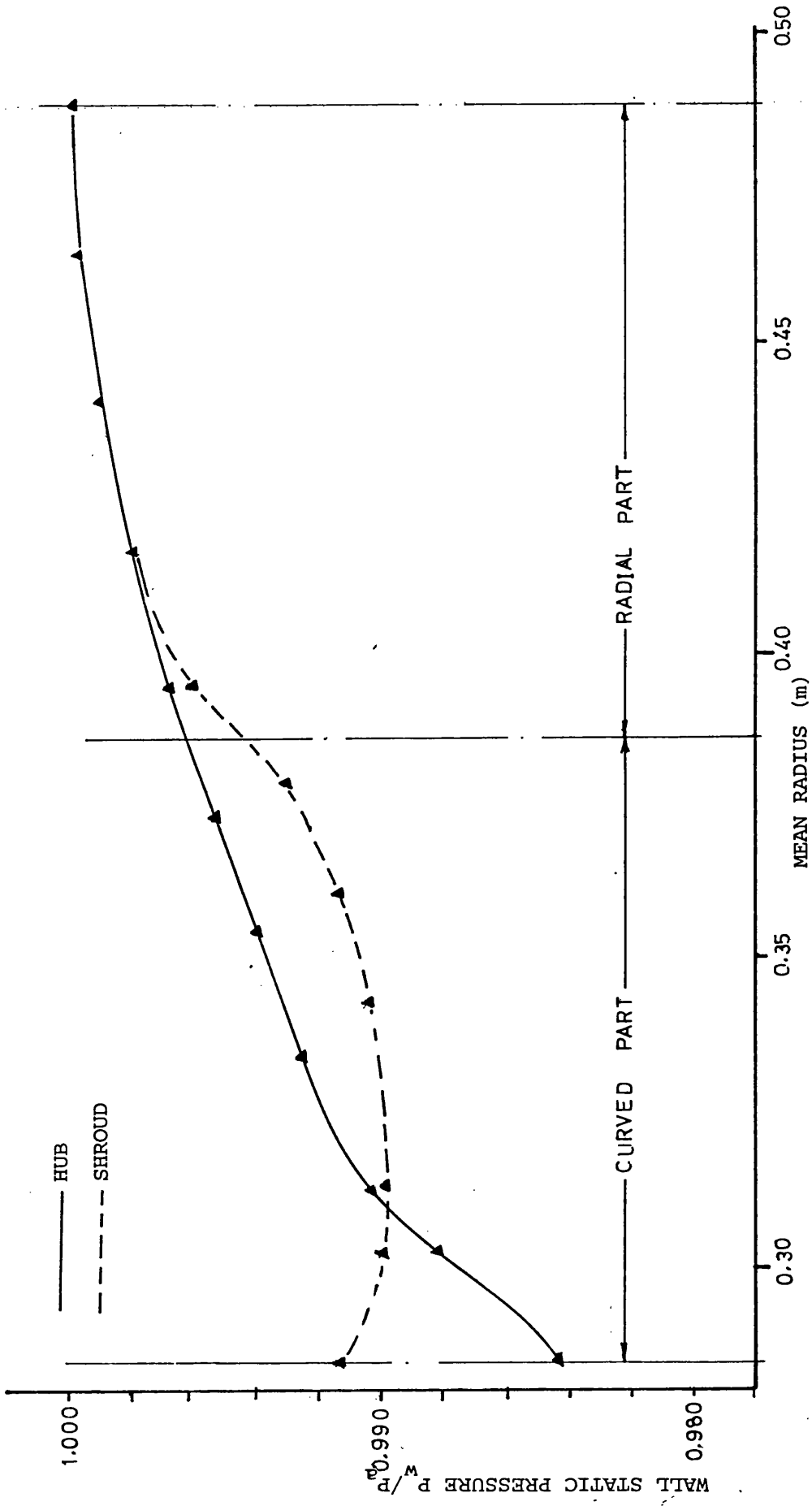

FIG. 4.5 WALL STATIC PRESSURE DISTRIBUTION, TEST AS1

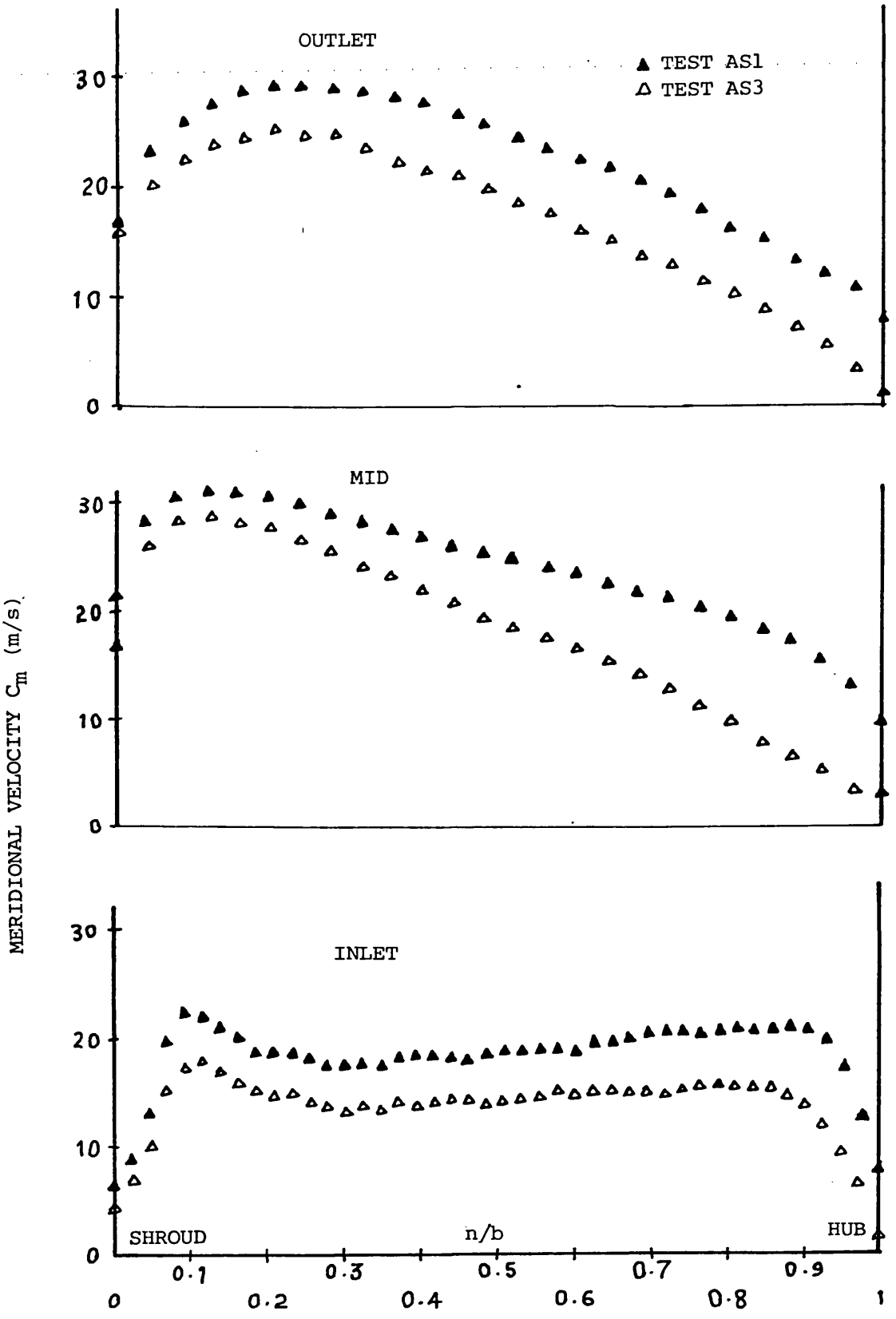

FIG.4.6 EFFECT OF MASS FLOW RATE ON MERIDIONAL VELOCITY DISTRIBUTION TESTS AS1, AS3

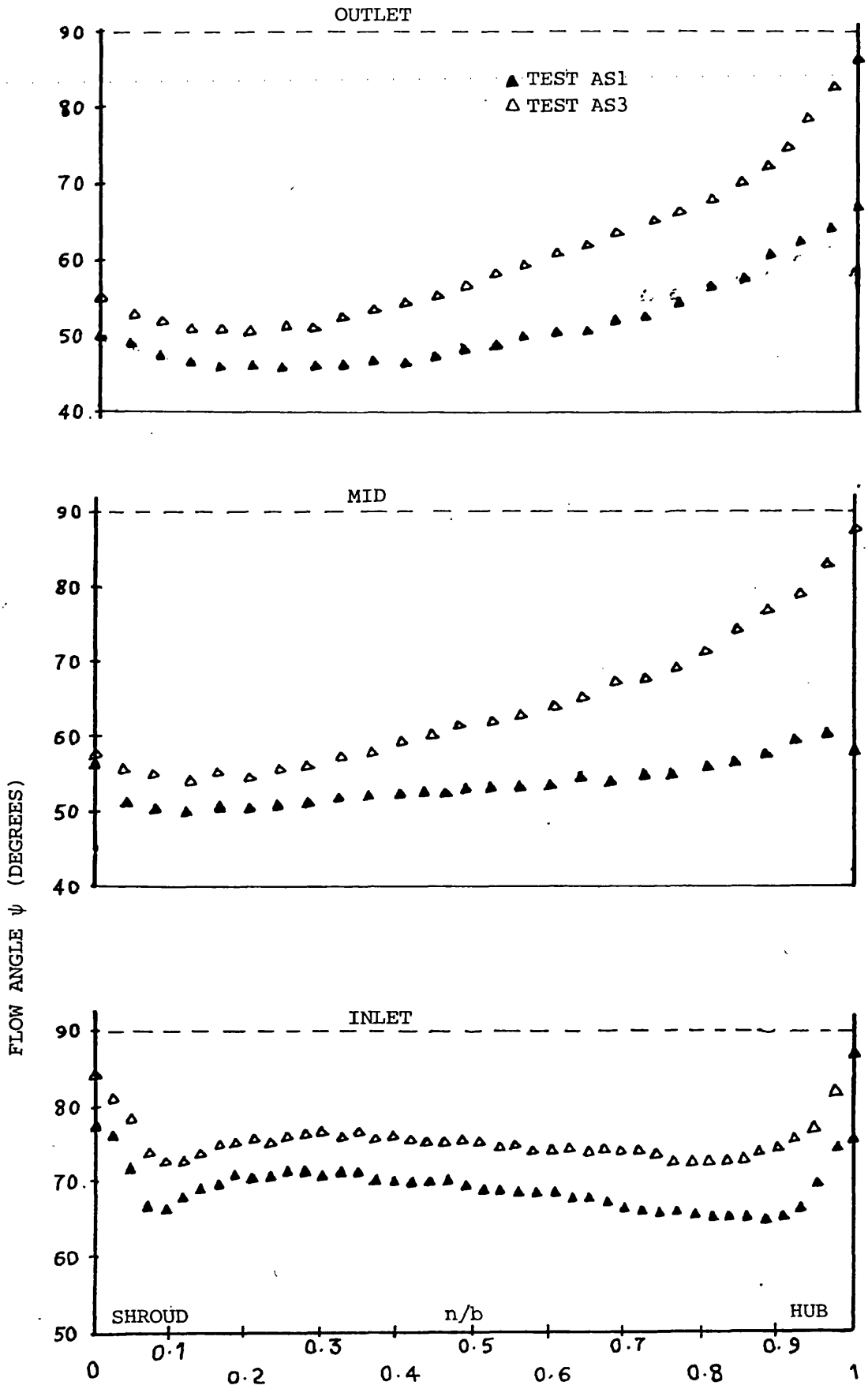

FIG. 4.7 EFFECT OF MASS FLOW RATE ON FLOW ANGLE DISTRIBUTION TESTS AS1, AS3

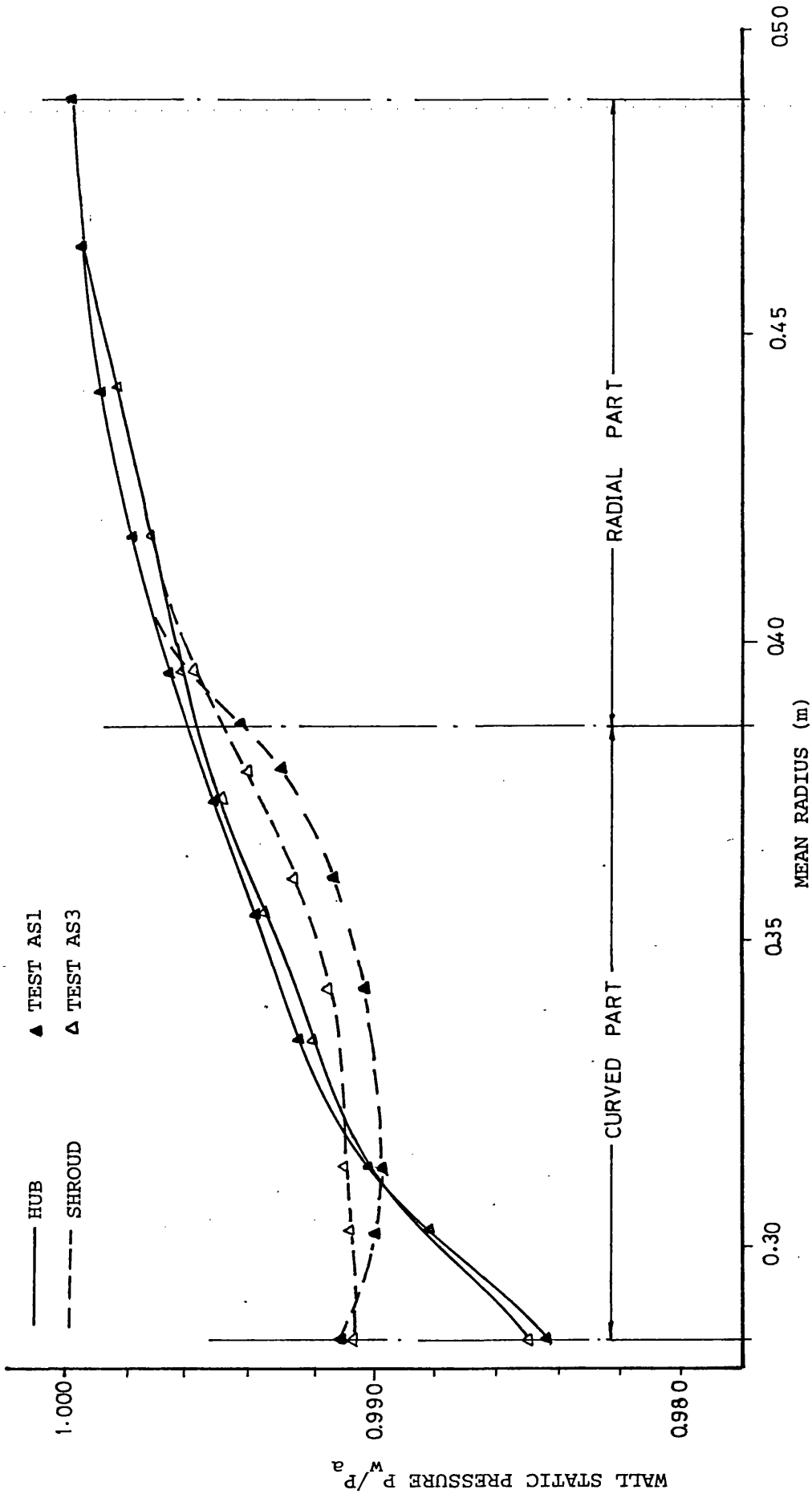

FIG. 4.8 EFFECT OF MASS FLOW RATE ON WALL STATIC PRESSURE DISTRIBUTIONS, TESTS AS1, AS3

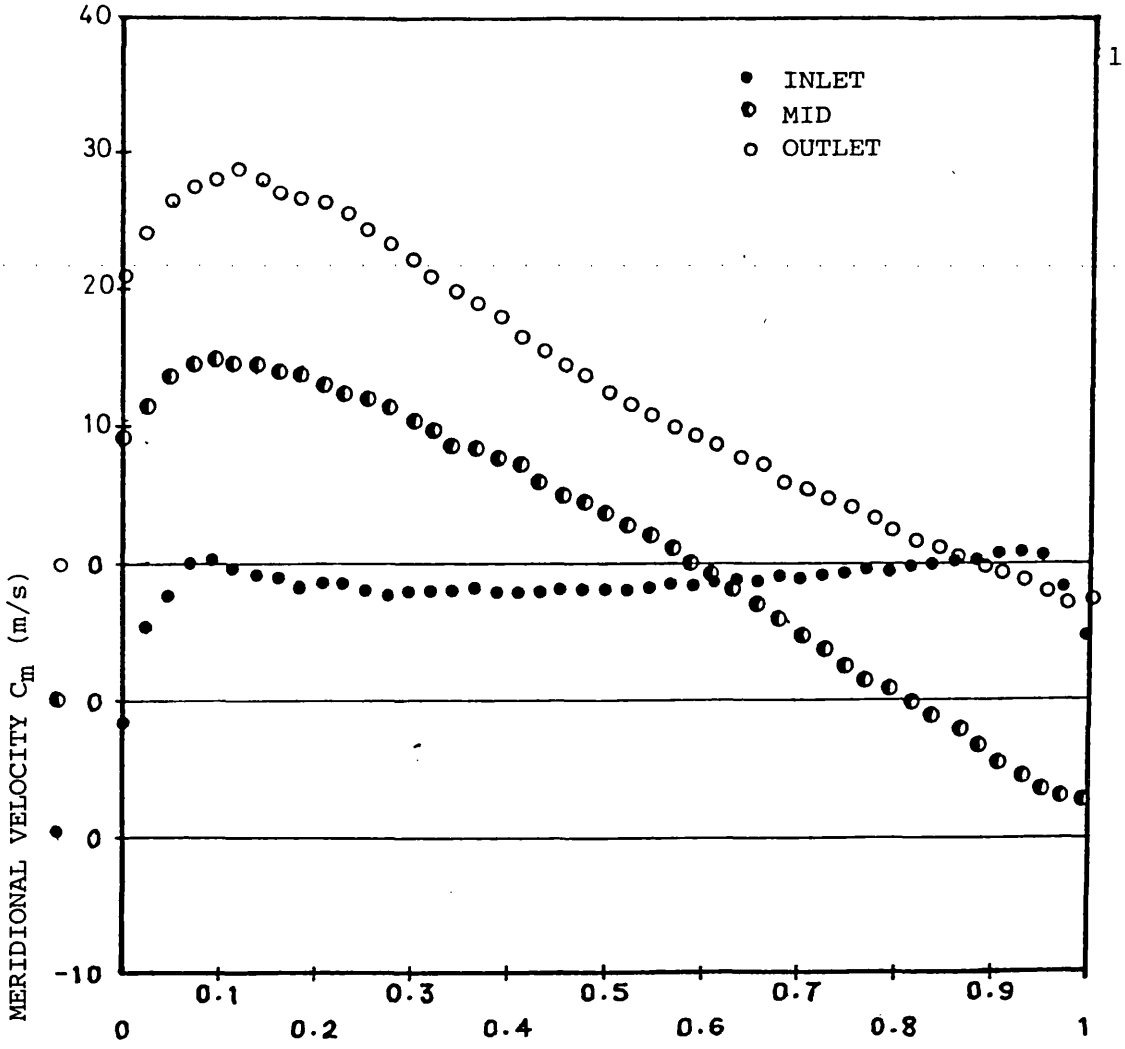

FIG. 4.9a MERIDIONAL VELOCITY DISTRIBUTION TEST BS1

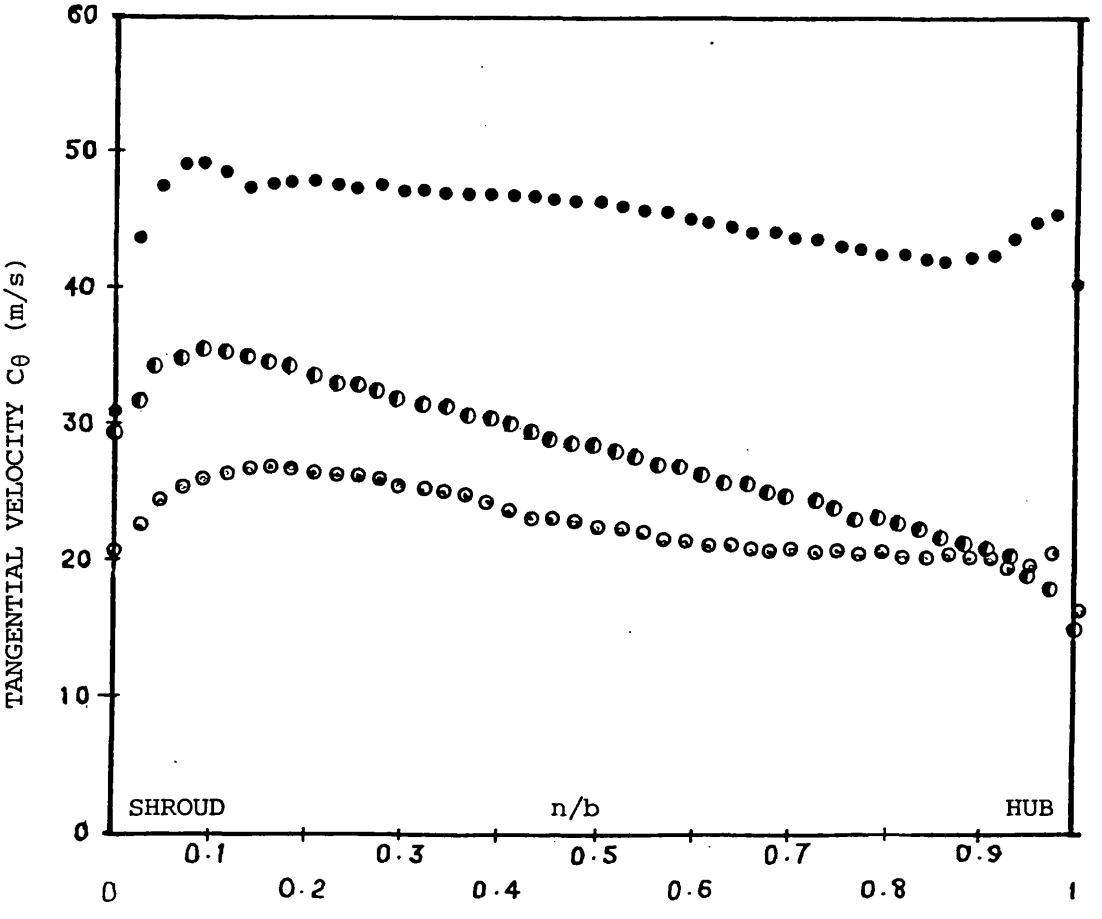

FIG. 4.9b TANGENTIAL VELOCITY DISTRIBUTION TEST BS1

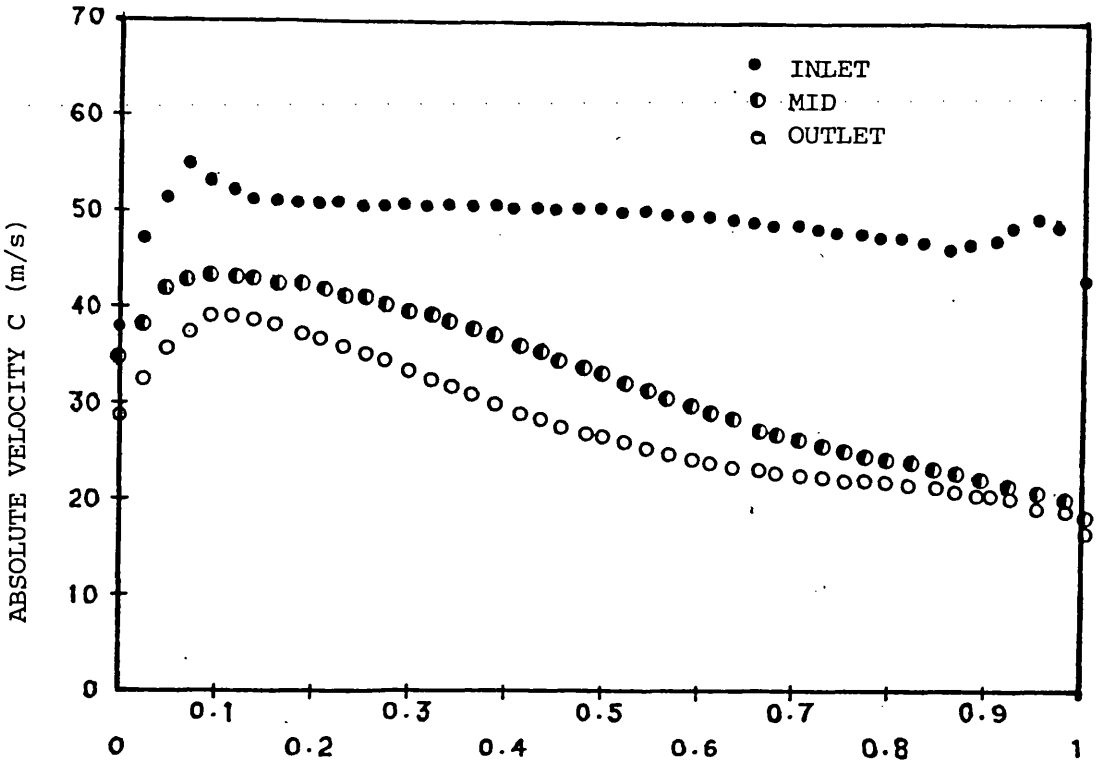

FIG.10a ABSOLUTE VELOCITY DISTRIBUTION TEST BS1

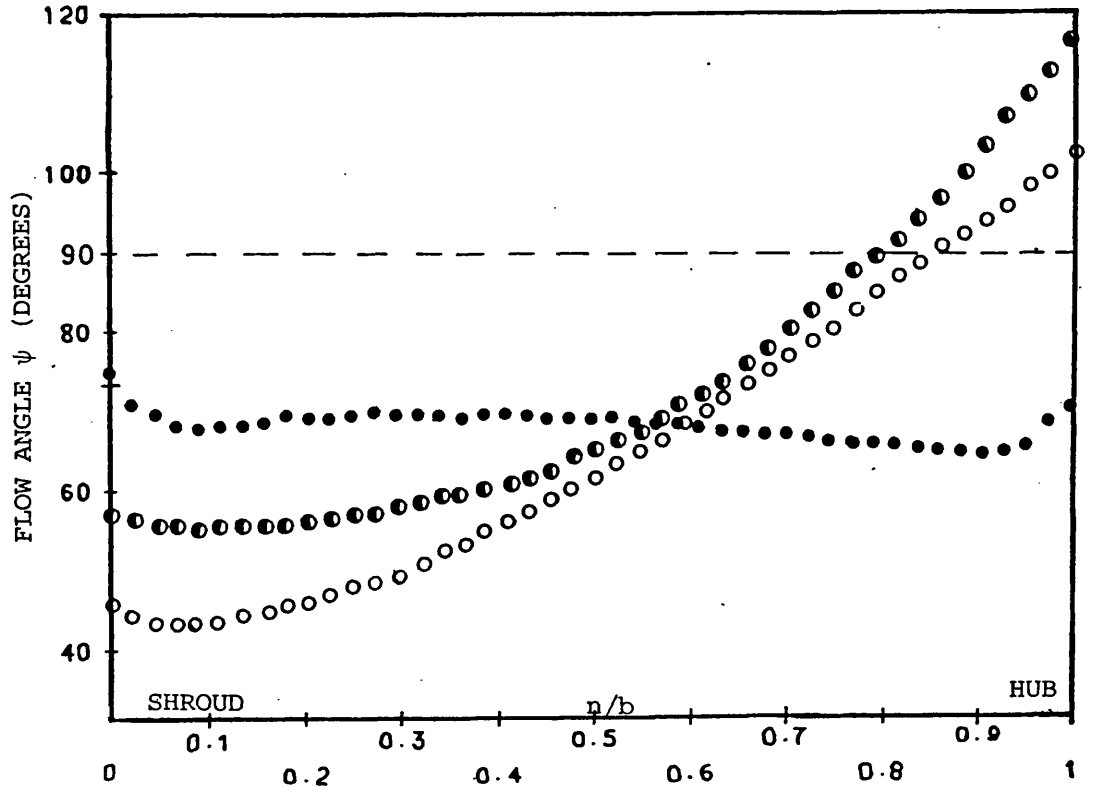

FIG. 4.10b FLOW ANGLE DISTRIBUTION TEST BS1

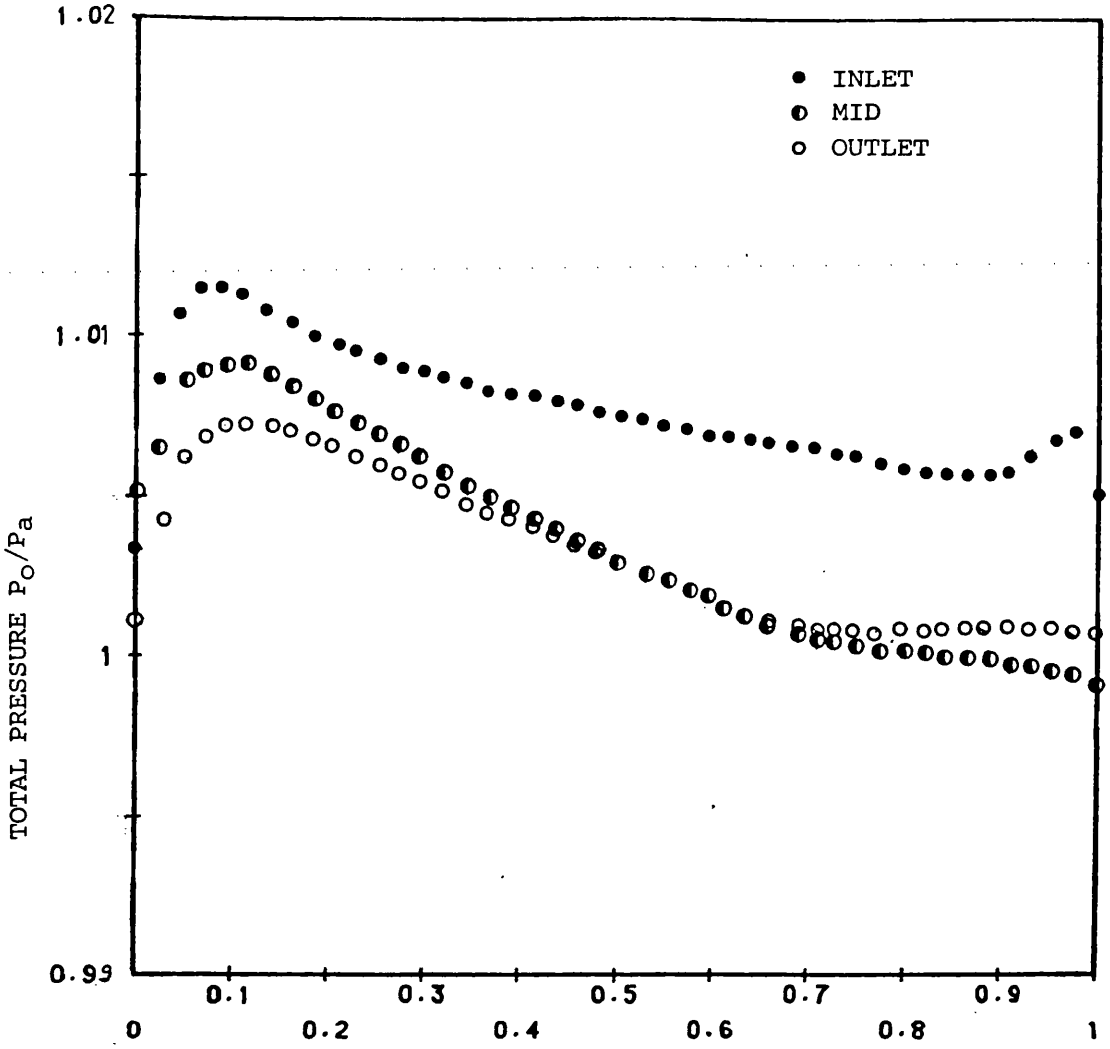

FIG. 4.11a TOTAL PRESSURE DISTRIBUTION TEST BS1

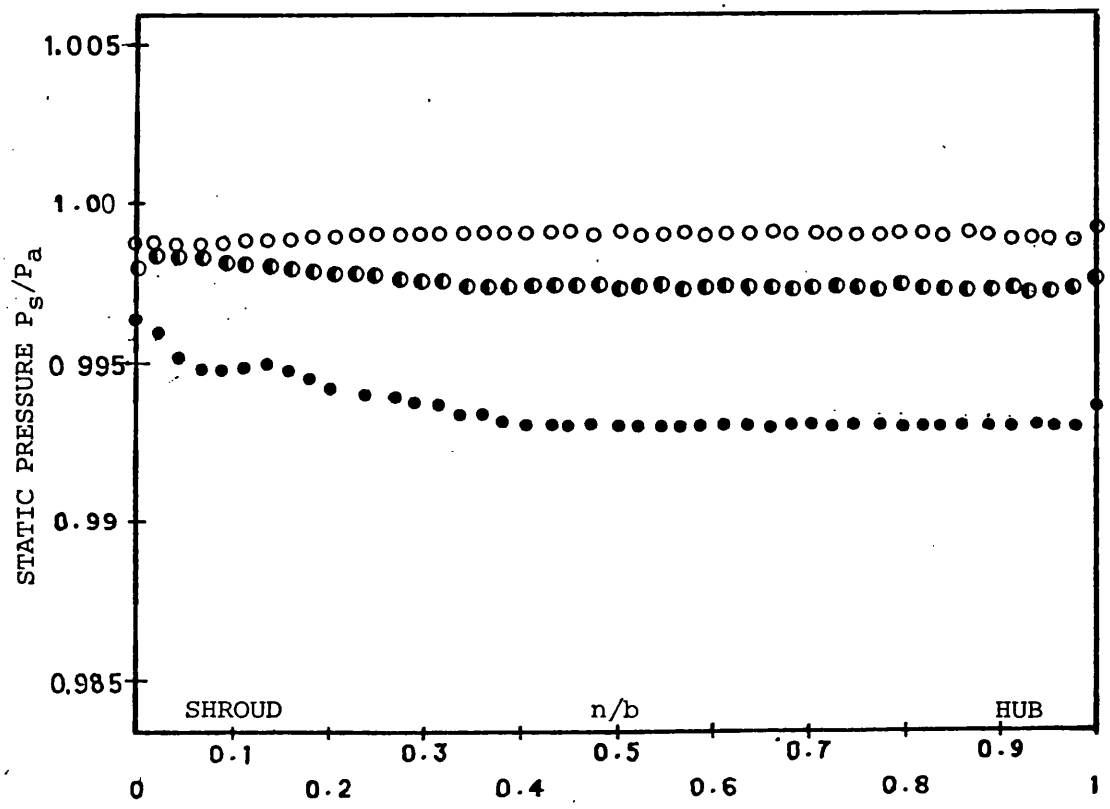

FIG. 4.11b STATIC PRESSURE DISTRIBUTION TESTS AS1, BS1

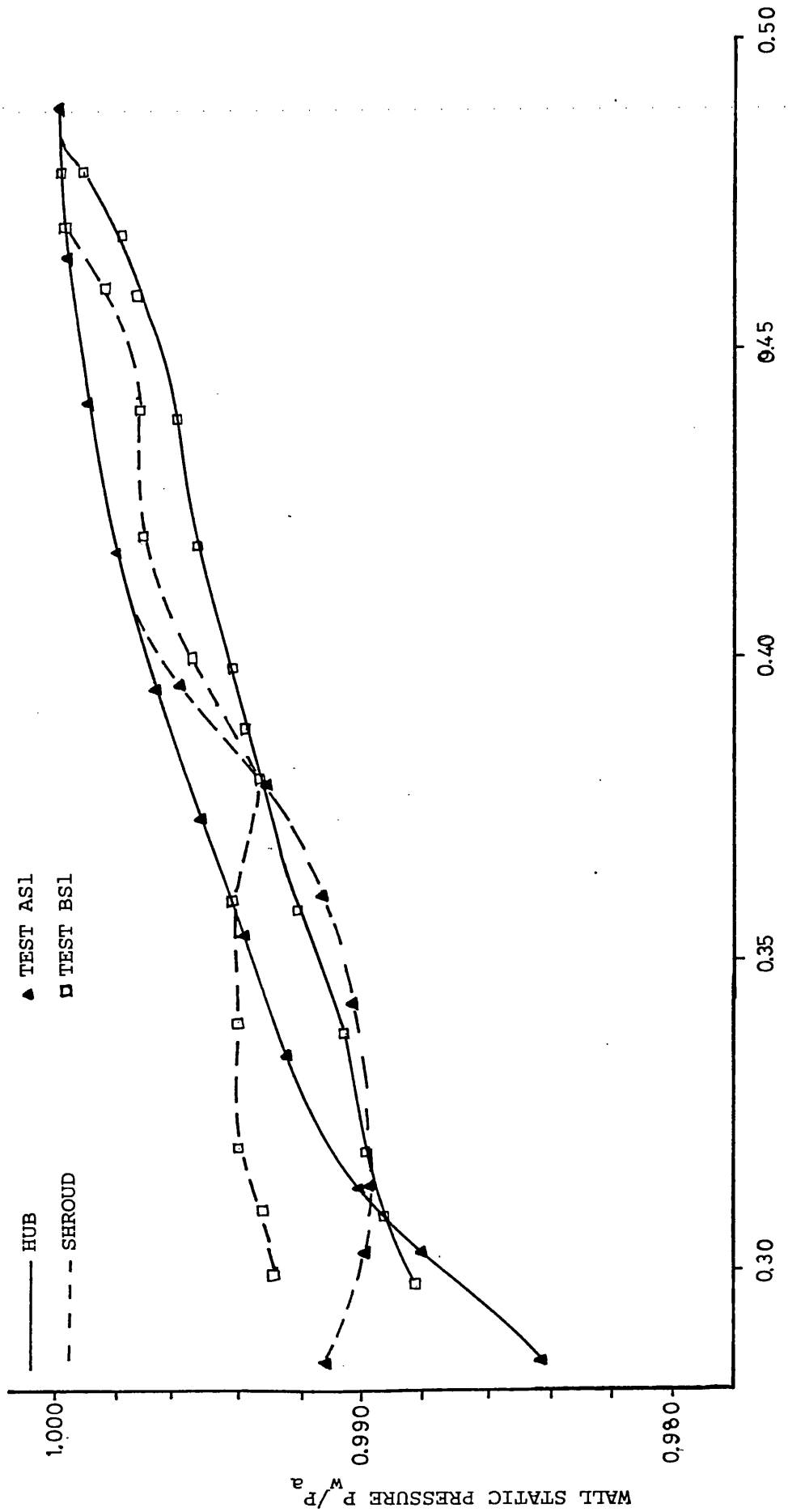

FIG. 4.12 COMPARISON OF WALL STATIC PRESSURE DISTRIBUTION IN THE CURVED AND THE CONICAL DIFFUSERS, TESTS AS1, BS1.

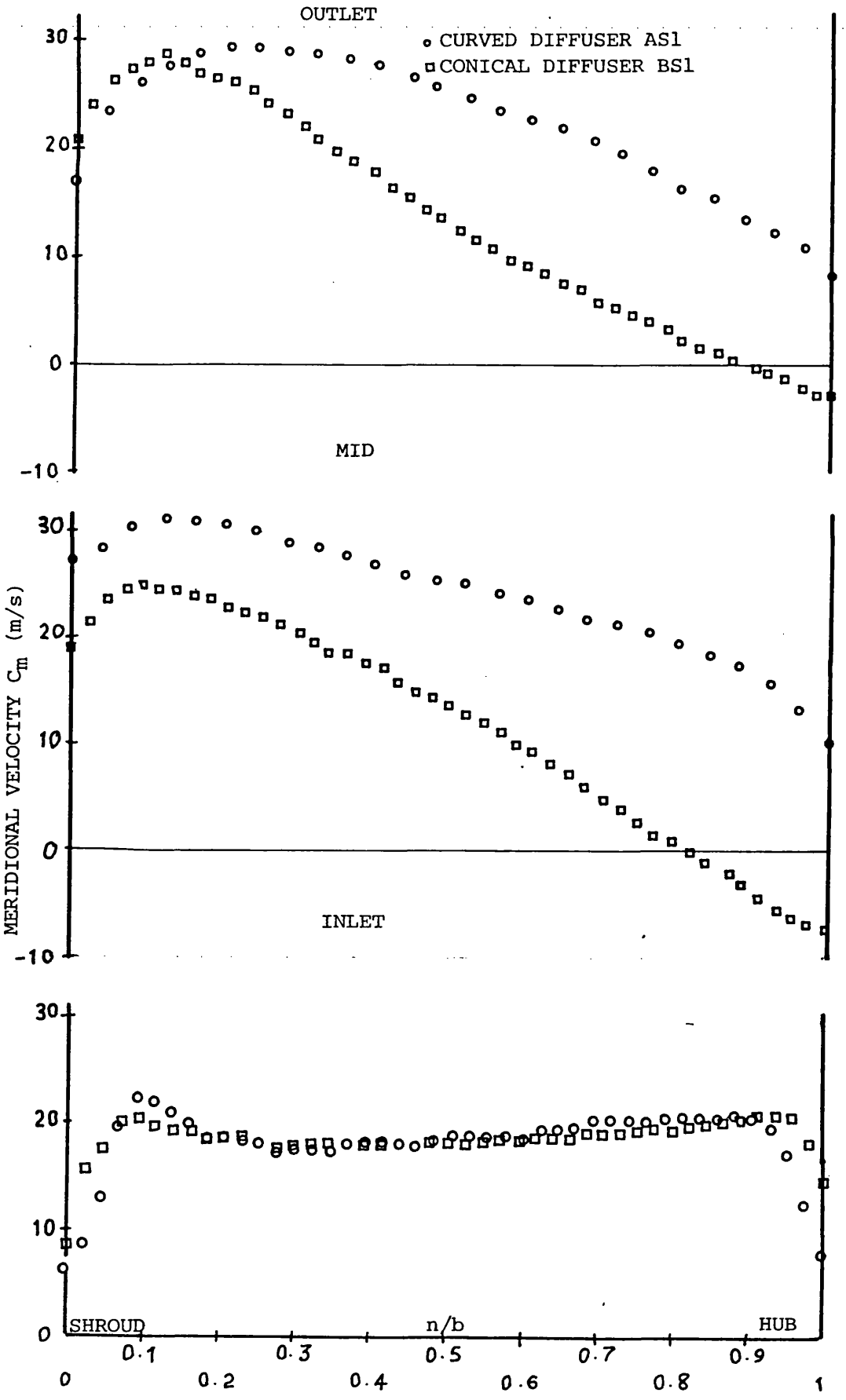

FIG. 4.13 COMPARISON OF MERIDIONAL VELOCITY DISTRIBUTION IN CURVED AND CONICAL DIFFUSERS, TESTS AS1 BS1

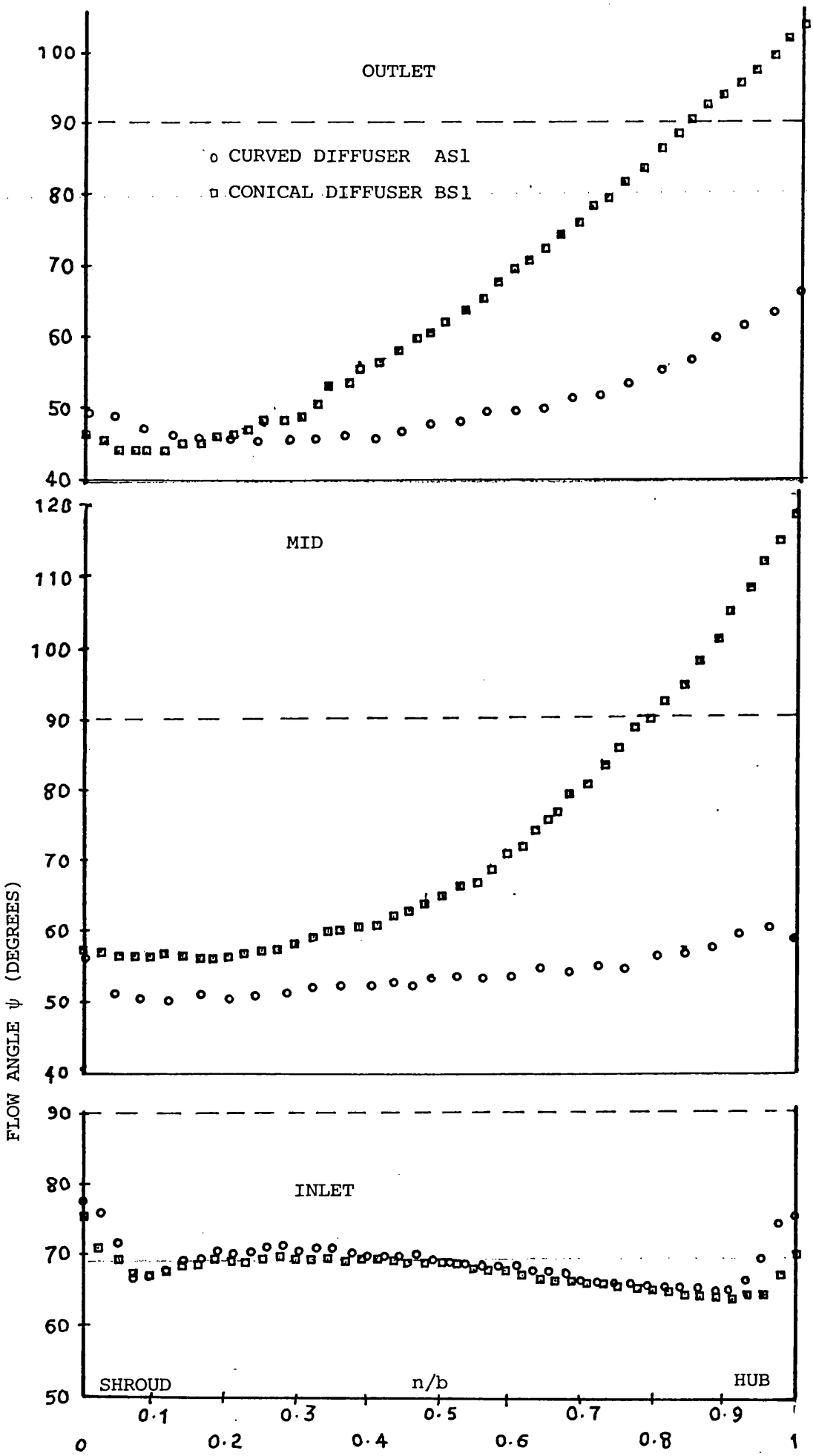

FIG. 4.14 COMPARISON OF FLOW ANGLE DISTRIBUTION IN CURVED AND CONICAL DIFFUSERS TESTS AS1, BS1

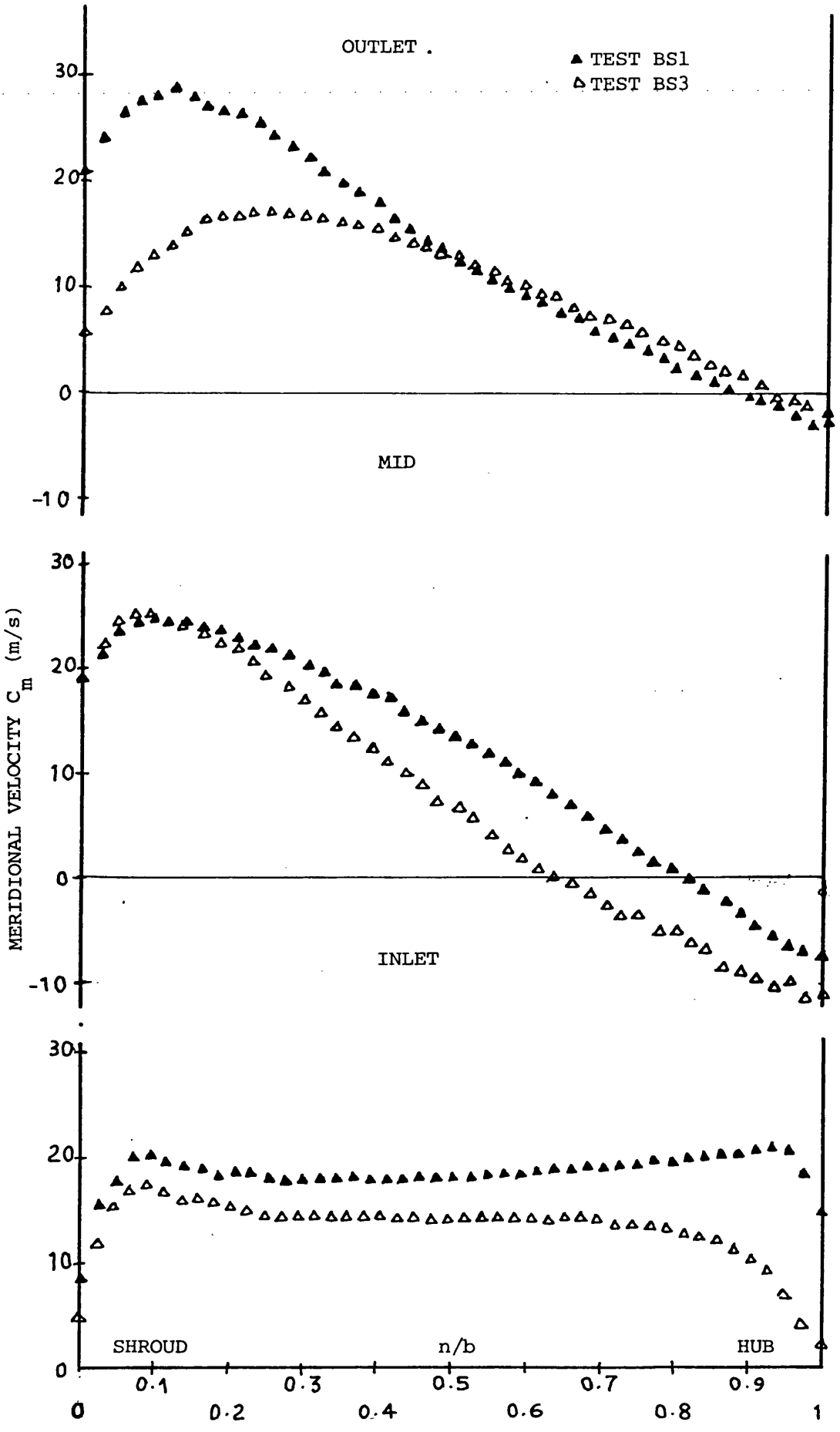

FIG.4.15 EFFECT OF MASS FLOW-RATE ON MERIDIONAL VELOCITY DISTRIBUTION TESTS BS1, BS3

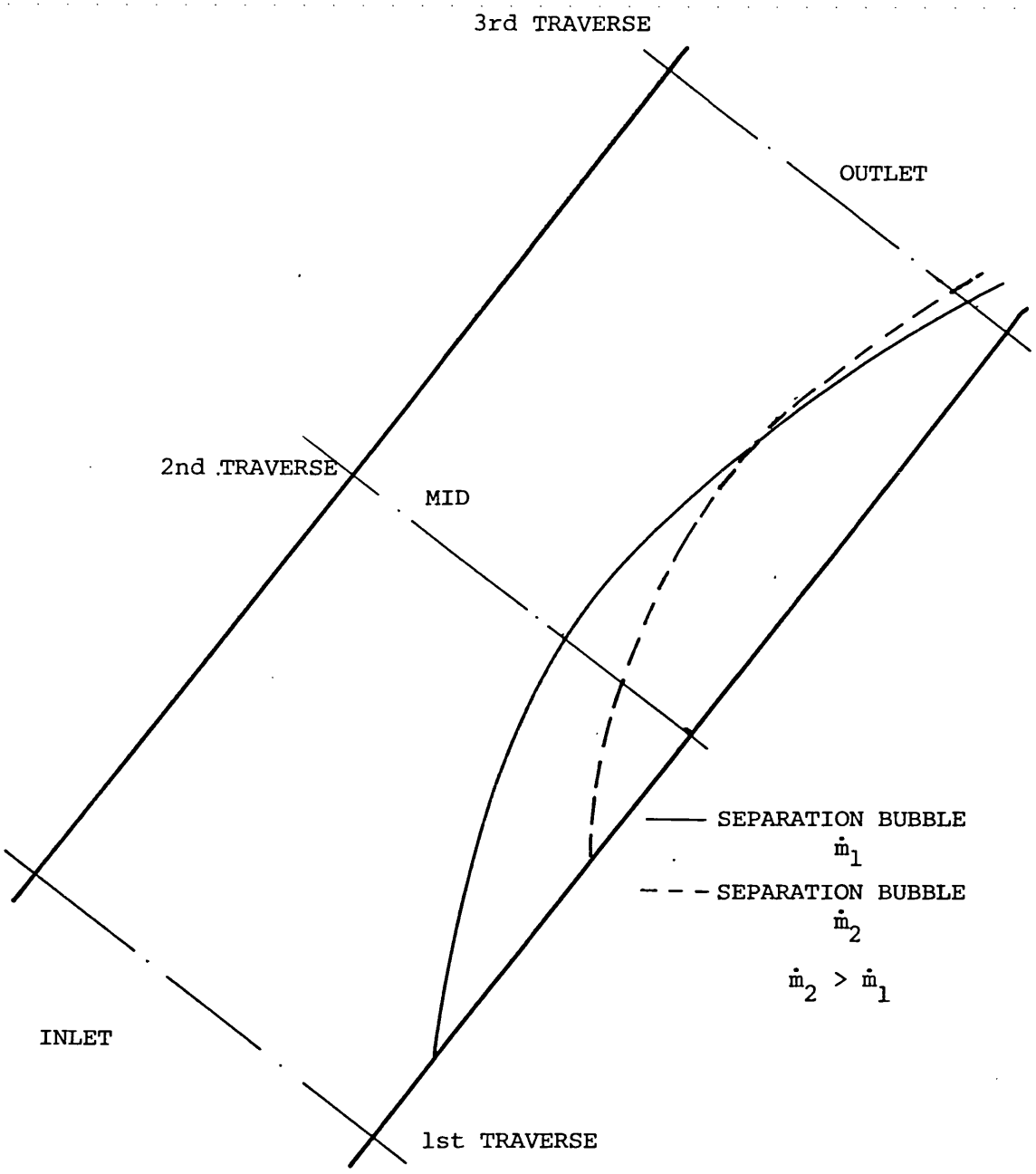

FIG. 4.16 ILLUSTRATIVE DIAGRAM OF THE EFFECT OF MASS FLOW RATE REDUCTION ON SEPARATION BUBBLE

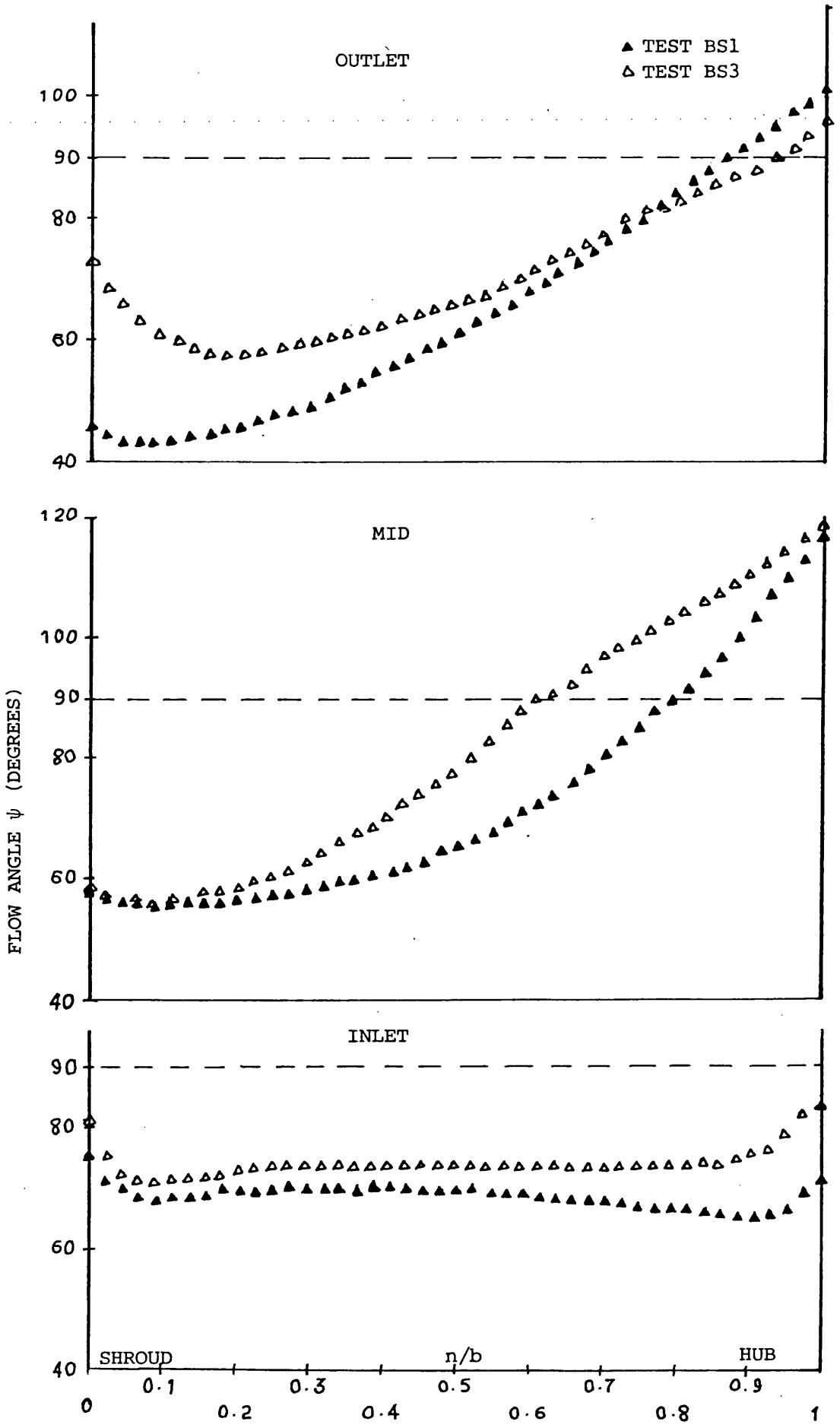

FIG. 4.17 EFFECT OF MASS FLOW RATE ON FLOW ANGLE DISTRIBUTION TESTS BS1, BS3

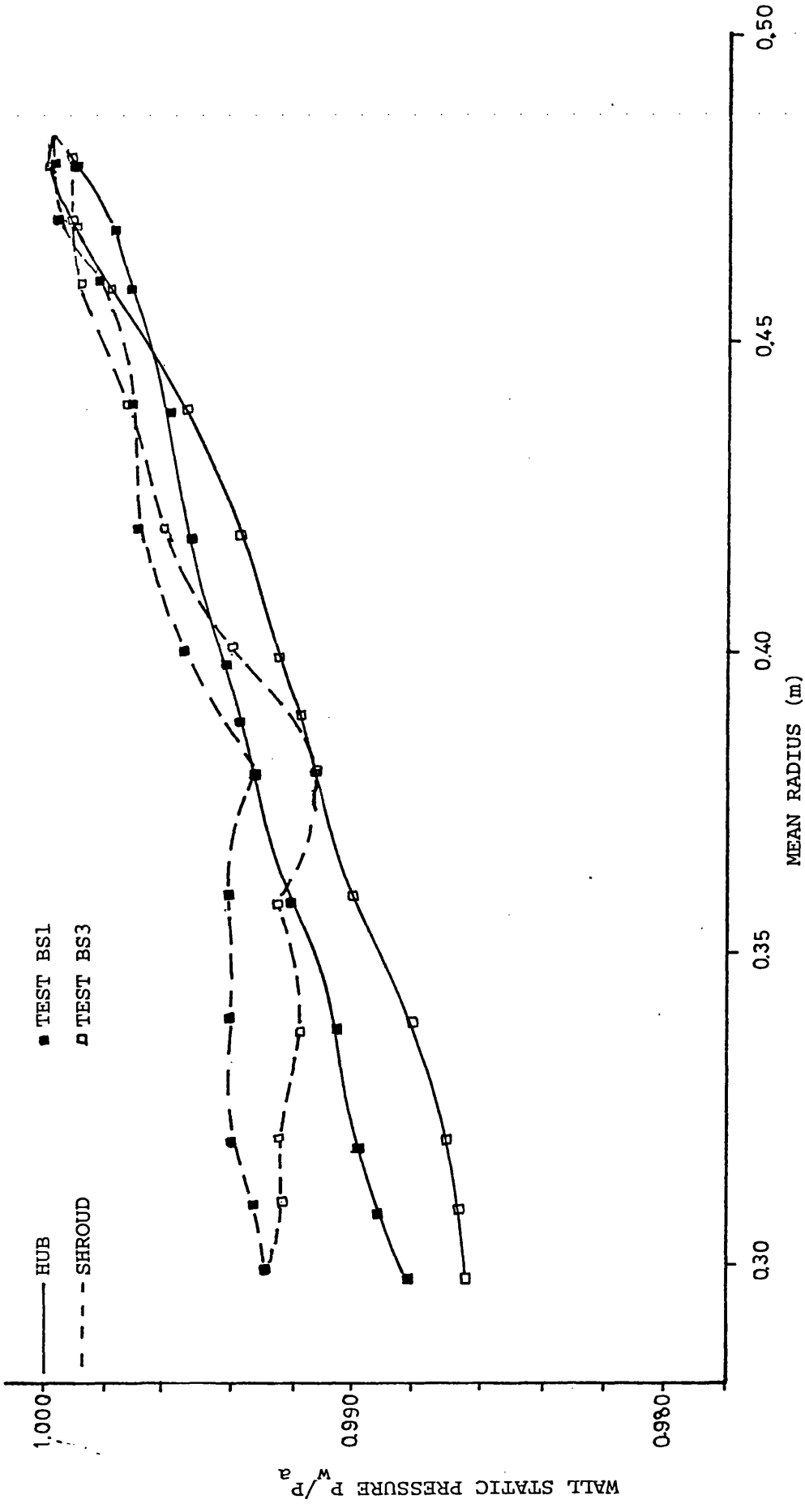

FIG. 4.18 EFFECT OF MASS FLOW RATE ON WALL STATIC PRESSURE DISTRIBUTION, TESTS BS1, BS3

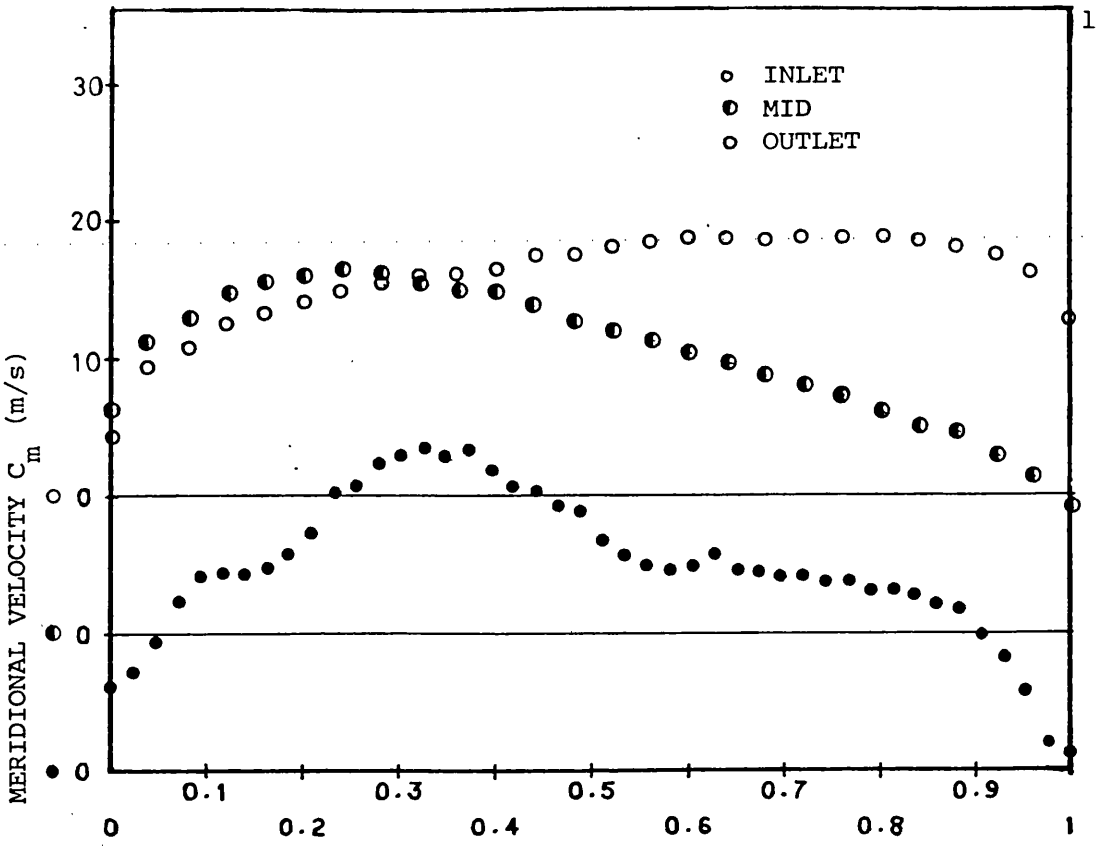

FIG.4.19a MERIDIONAL VELOCITY DISTRIBUTION
TEST AJ1

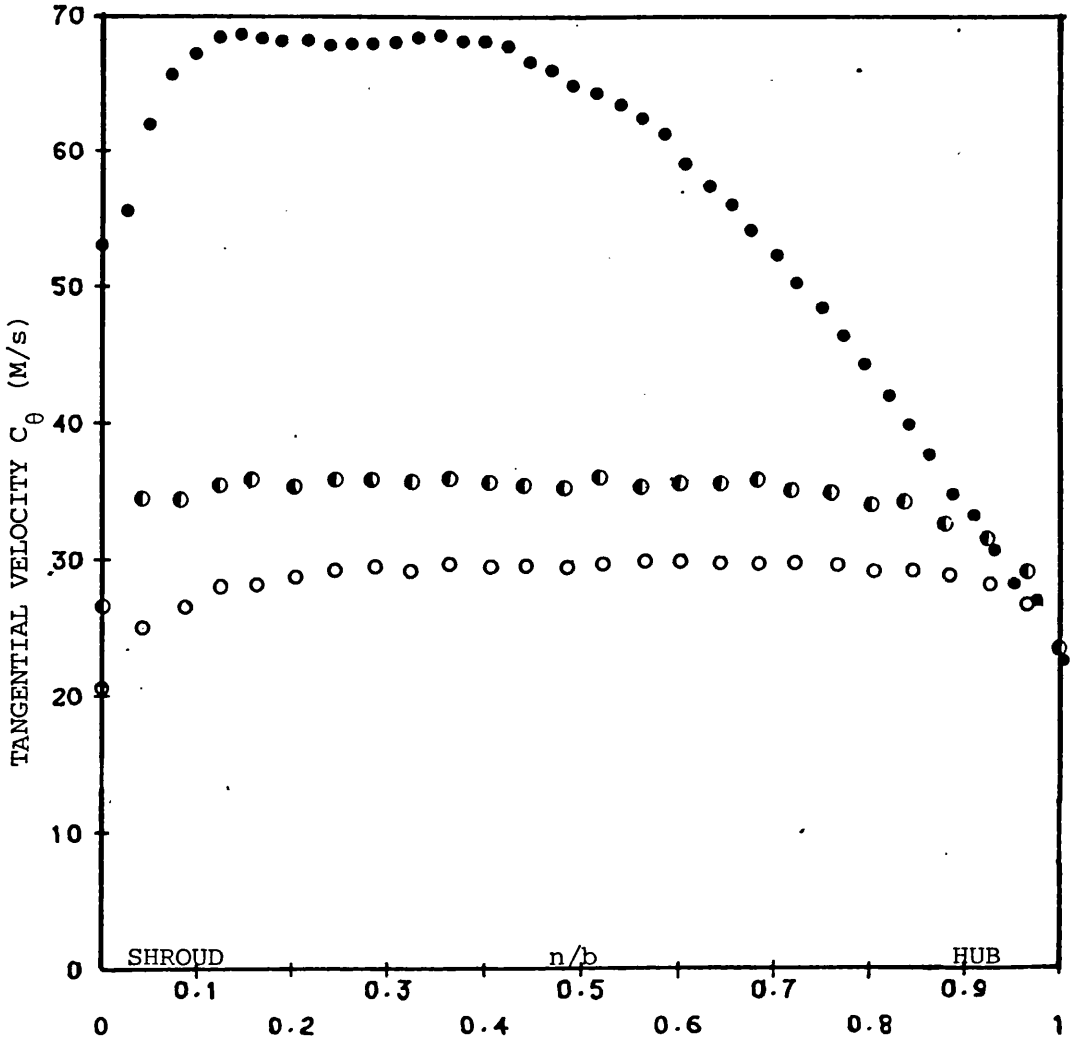

FIG.4.19b TANGENTIAL VELOCITY DISTRIBUTION
TEST AJ1

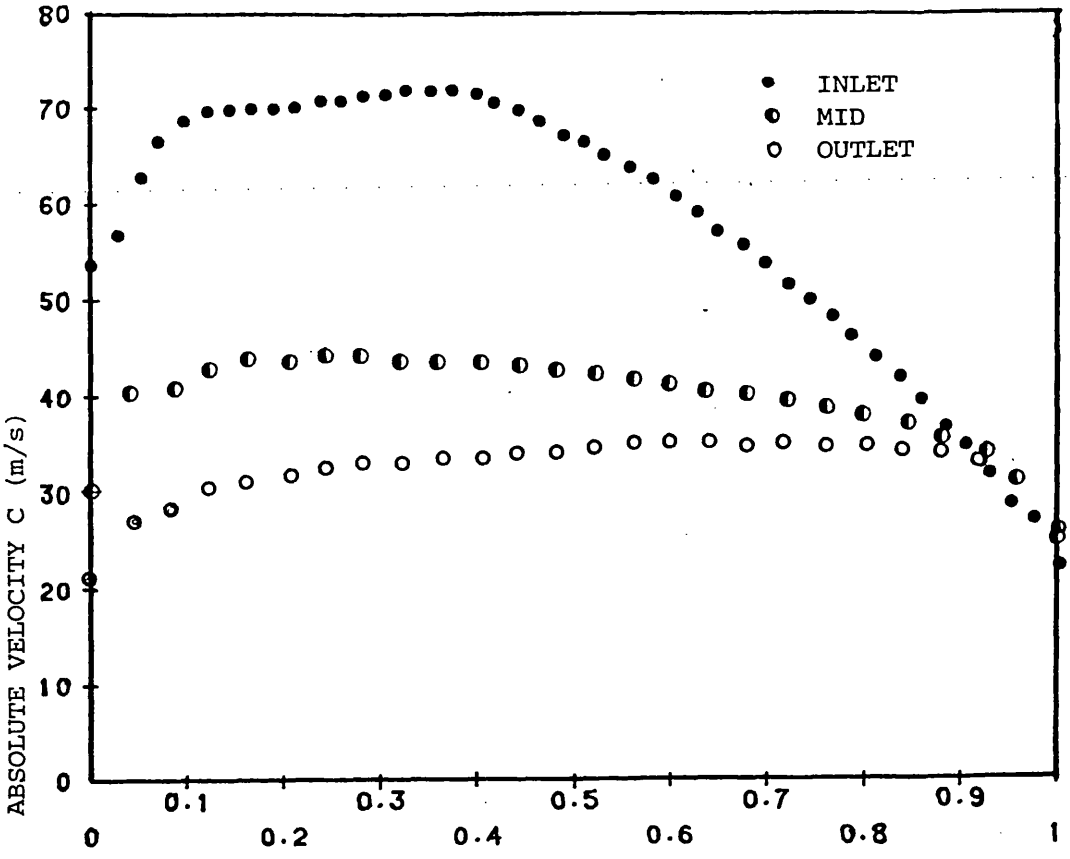

FIG. 4.20a ABSOLUTE VELOCITY DISTRIBUTION TEST AJ1

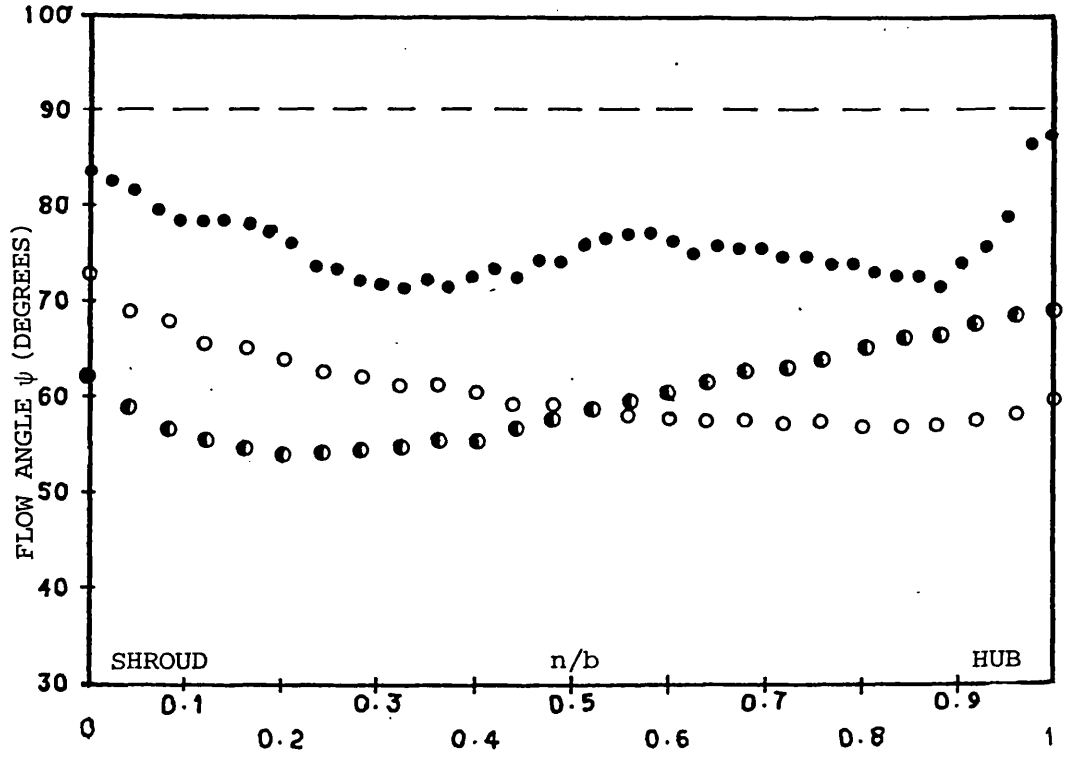

FIG.4.20b FLOW ANGLE DISTRIBUTION TEST AJ1

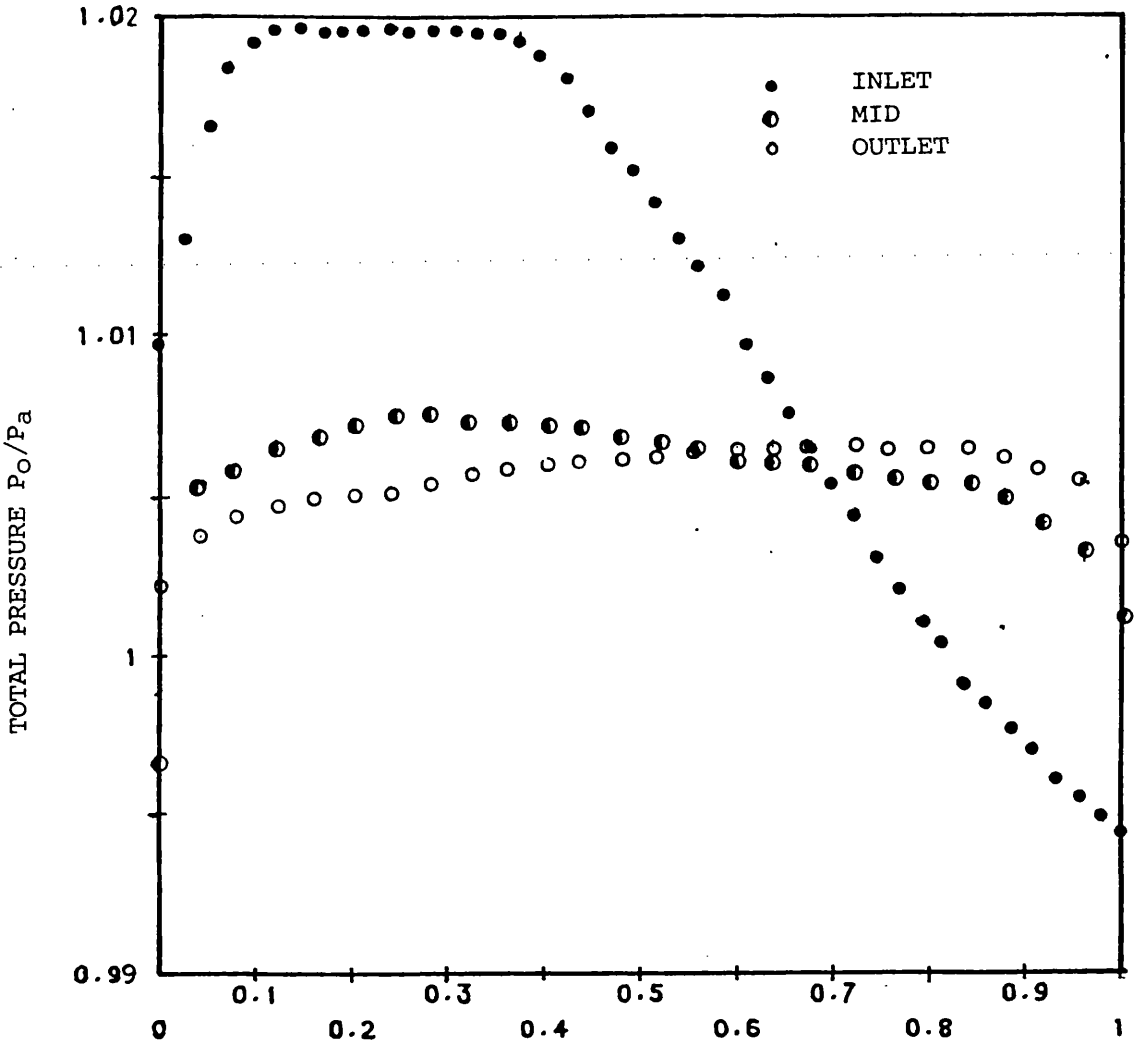

FIG.4.21a TOTAL PRESSURE DISTRIBUTION TEST AJ1

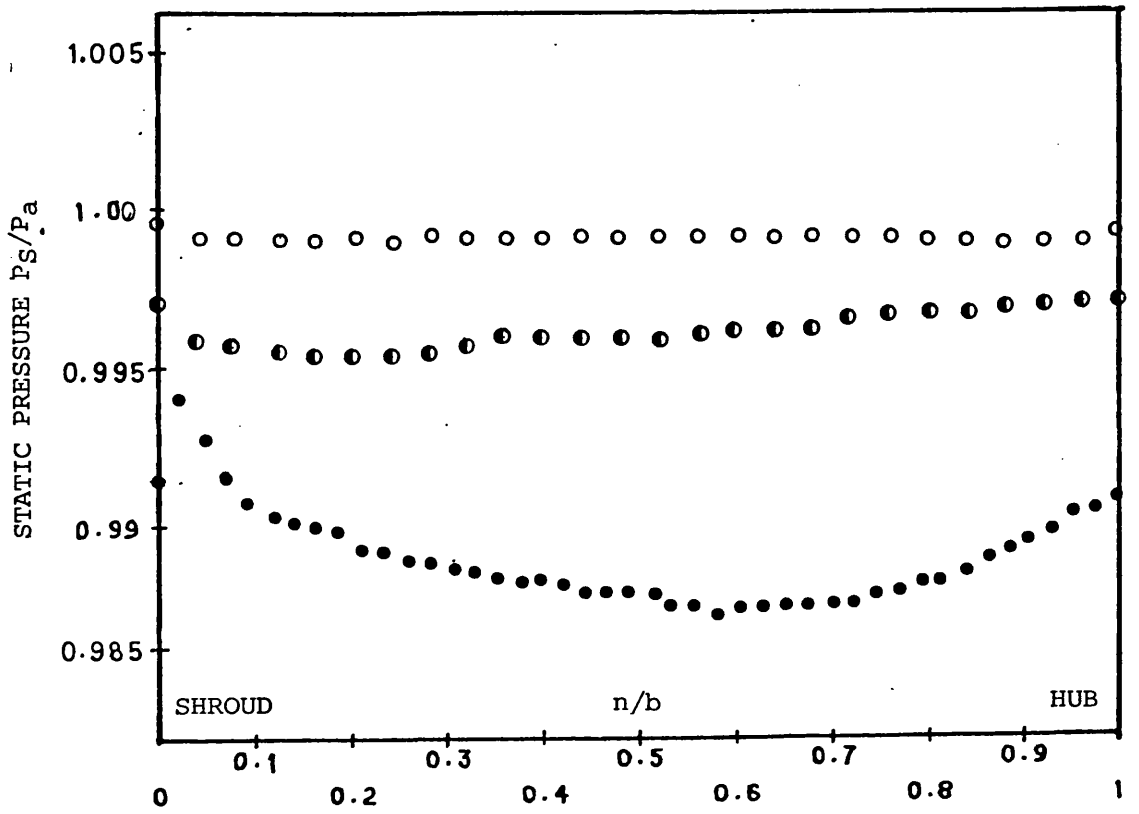

FIG. 4.21b STATIC PRESSURE DISTRIBUTION TEST AJ1

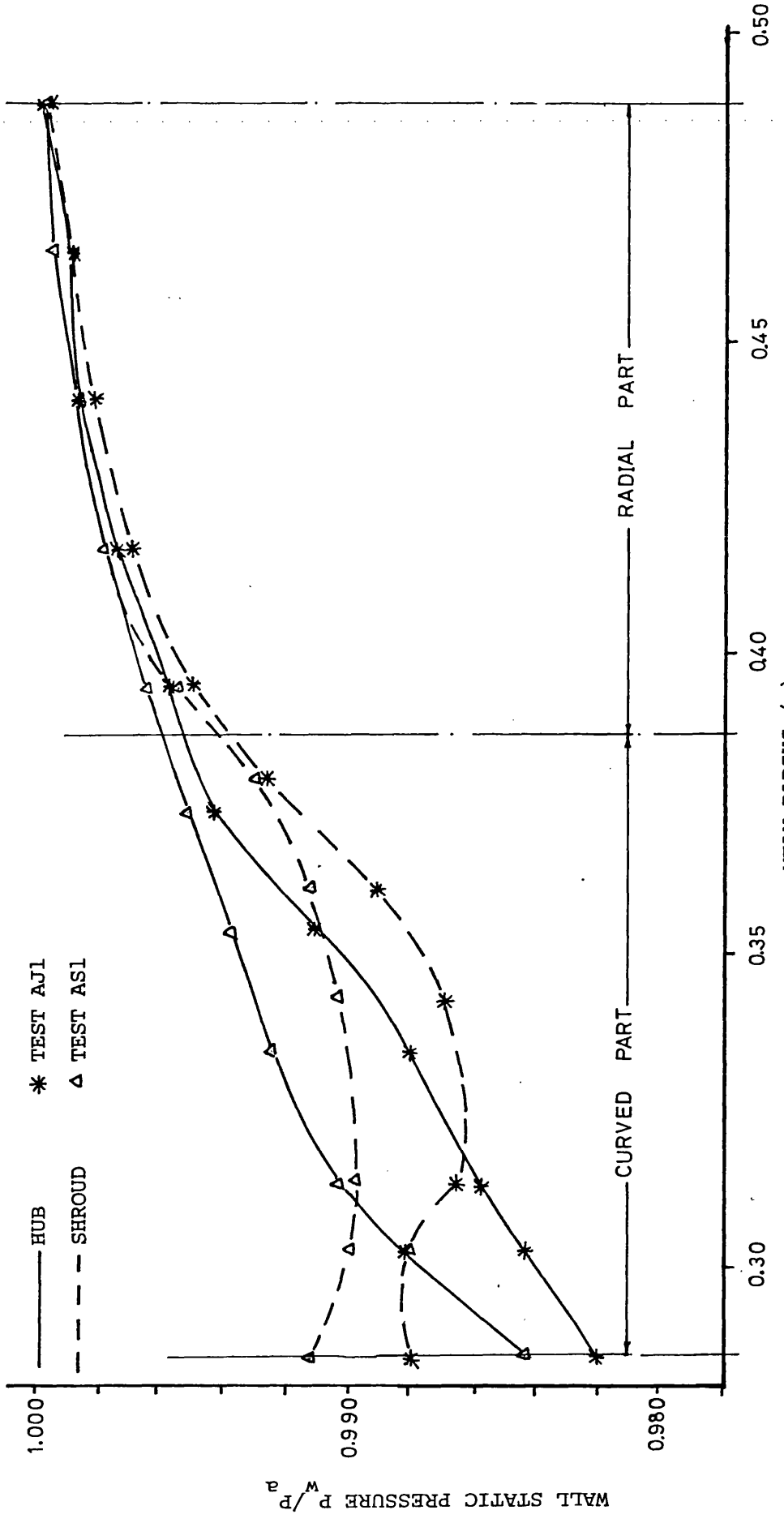

FIG. 4.22 EFFECT OF JET-WAKE FLOW ON WALL STATIC PRESSURE DISTRIBUTION, TESTS AJ1, AS1

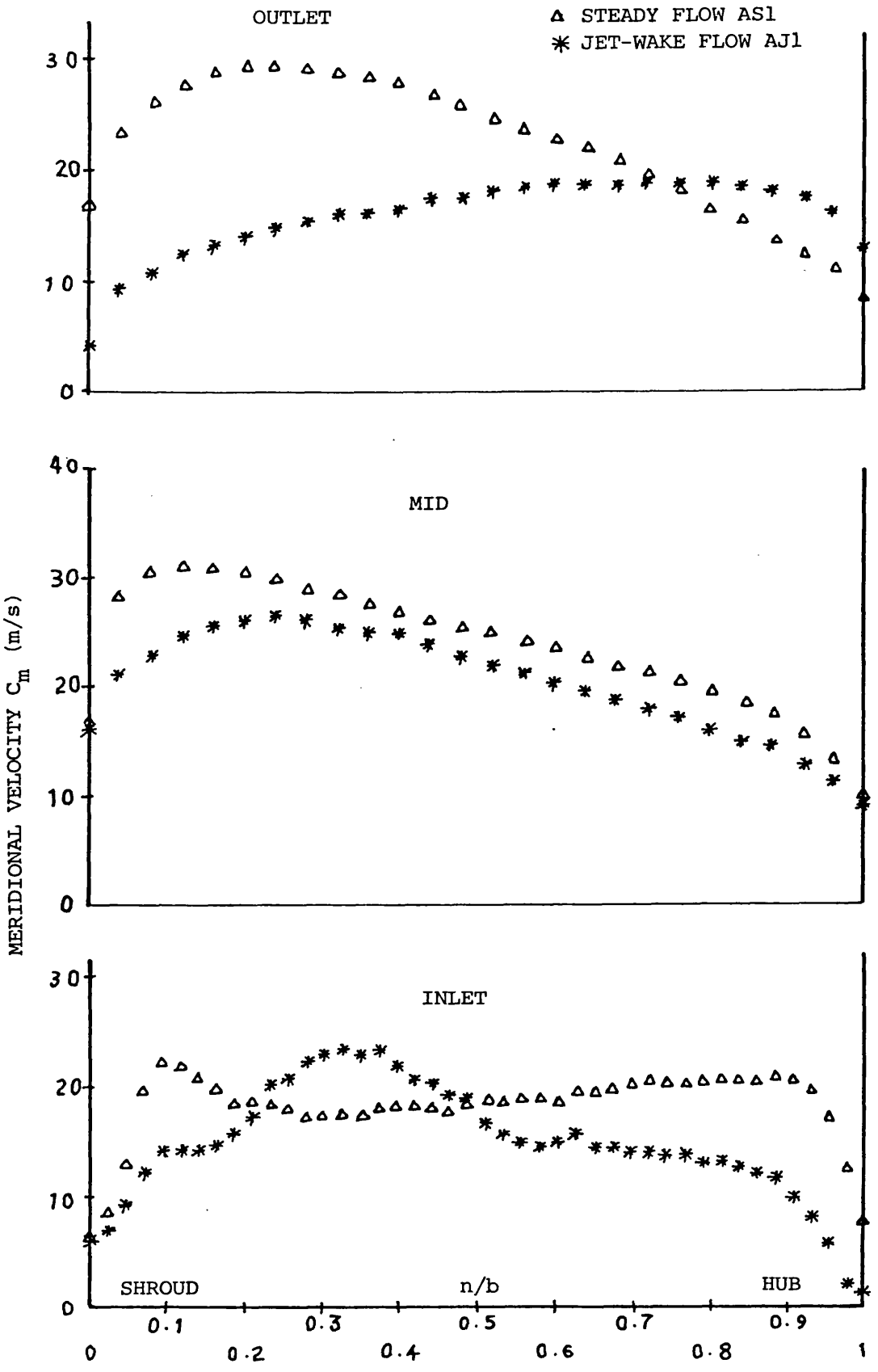

FIG. 4.23 EFFECT OF JET-WAKE FLOW ON MERIDIONAL VELOCITY DISTRIBUTION IN THE CURVED DIFFUSER TESTS AS1, AJ1

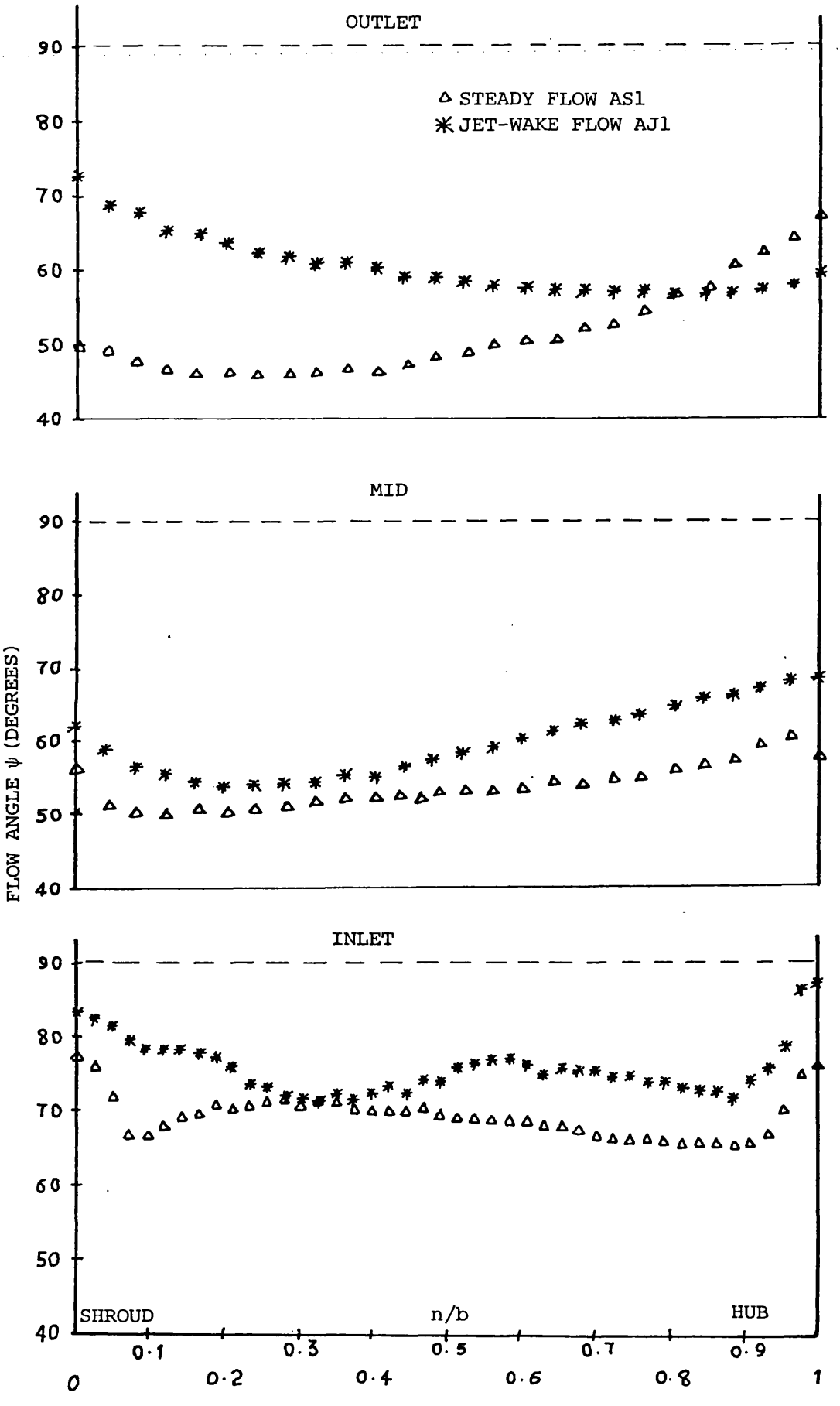

FIG.4.24 EFFECT OF JET-WAKE FLOW ON FLOW ANGLE DISTRIBUTION IN THE CURVED DIFFUSER TESTS AS1,AJ1

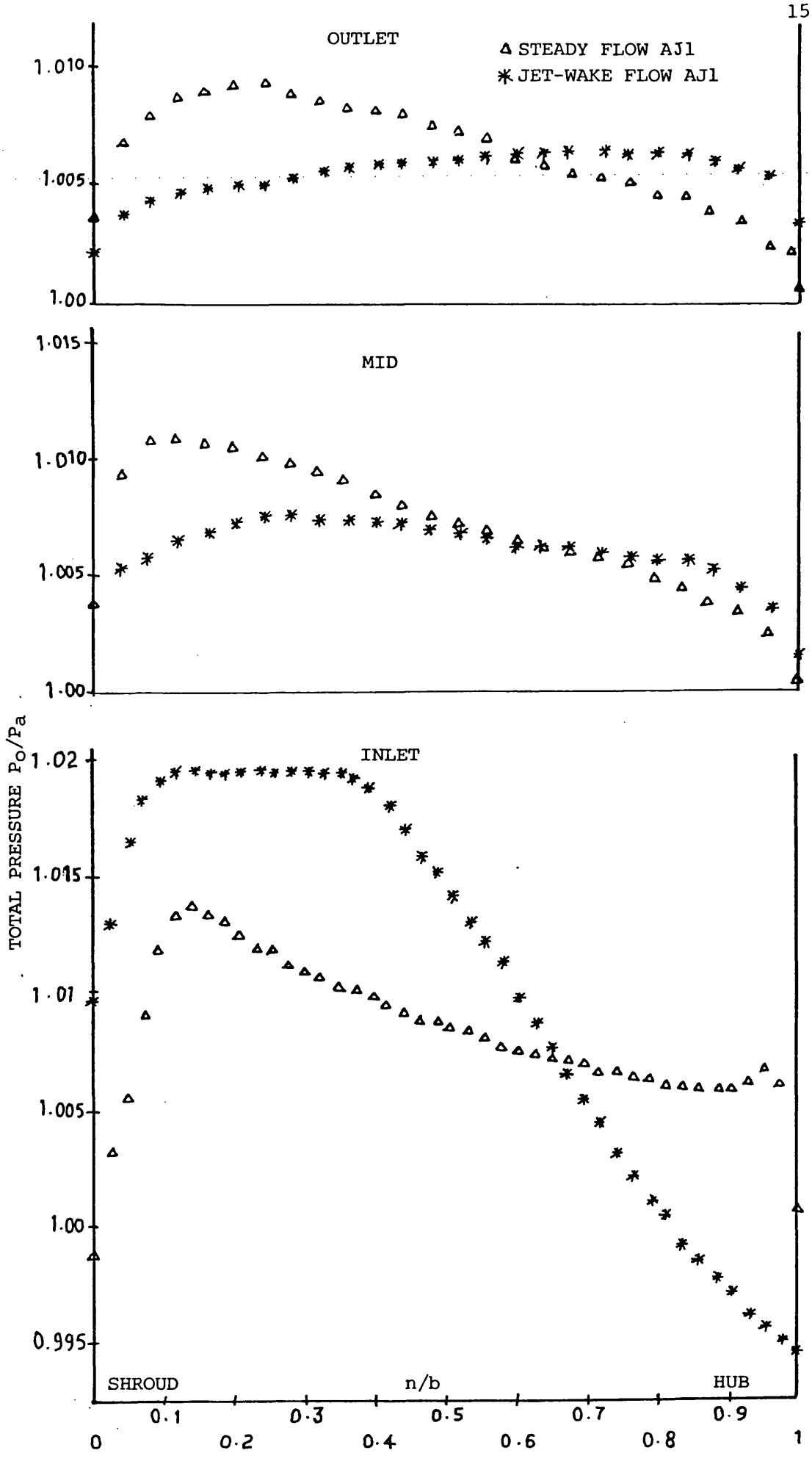

FIG.4.25 EFFECT OF JET-WAKE FLOW ON TOTAL PRESSURE DISTRIBUTION IN THE CURVED DIFFUSER TESTS AS1,AJ1

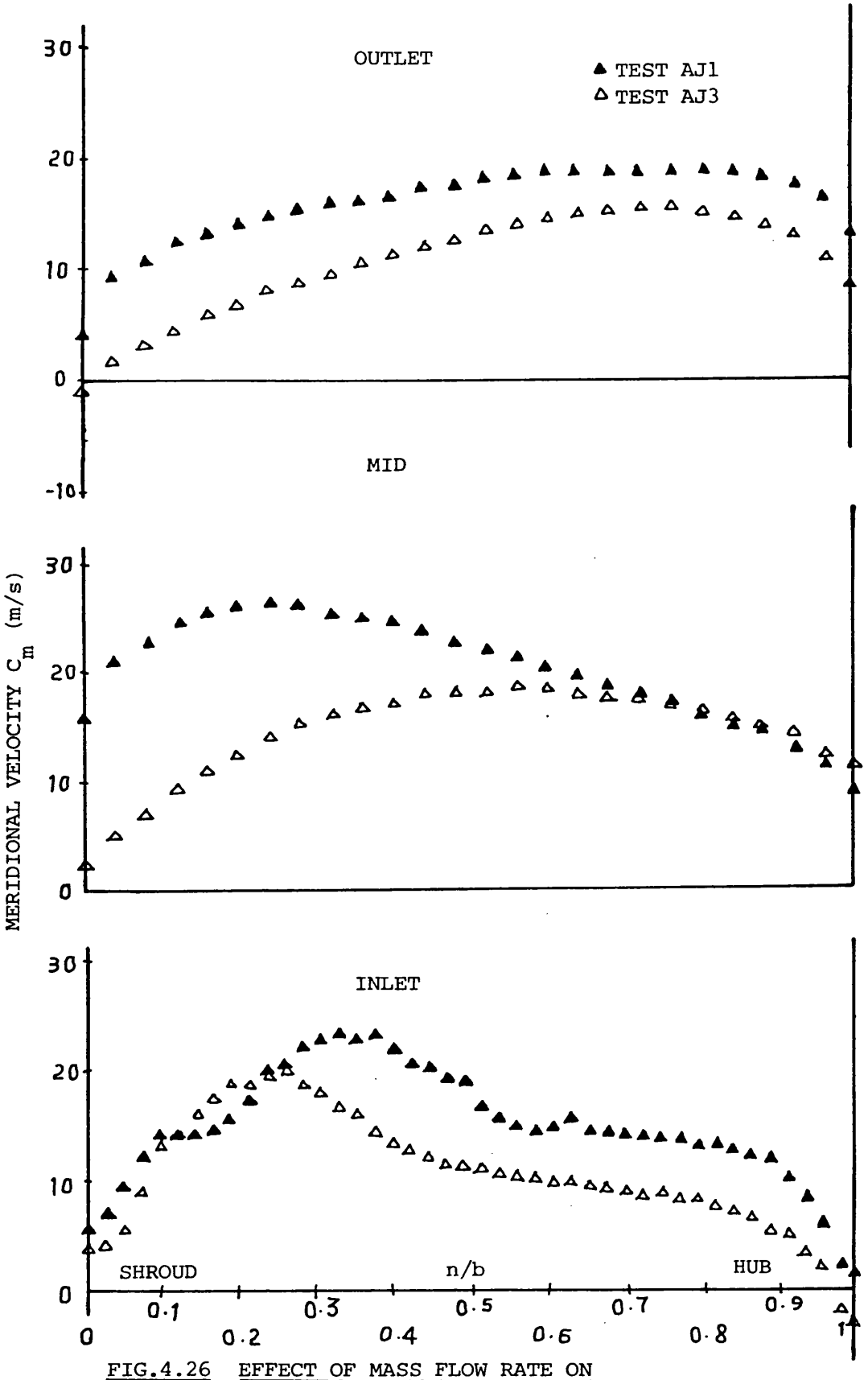

FIG.4.26 EFFECT OF MASS FLOW RATE ON MERIDIONAL VELOCITY DISTRIBUTION TESTS AJ1, AJ3

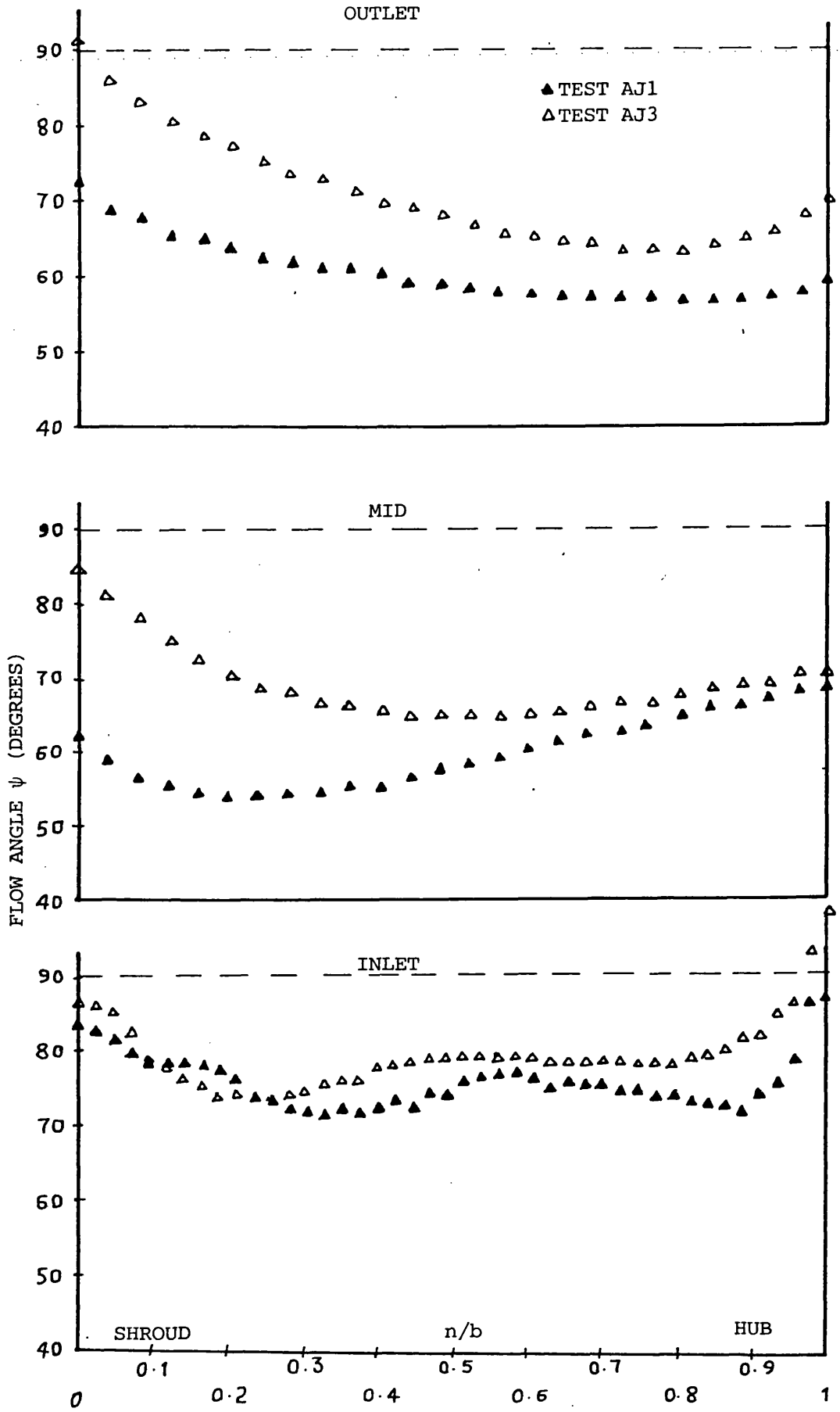

FIG.4.27 EFFECT OF MASS FLOW RATE ON FLOW ANGLE DISTRIBUTION TESTS AJ1, AJ3

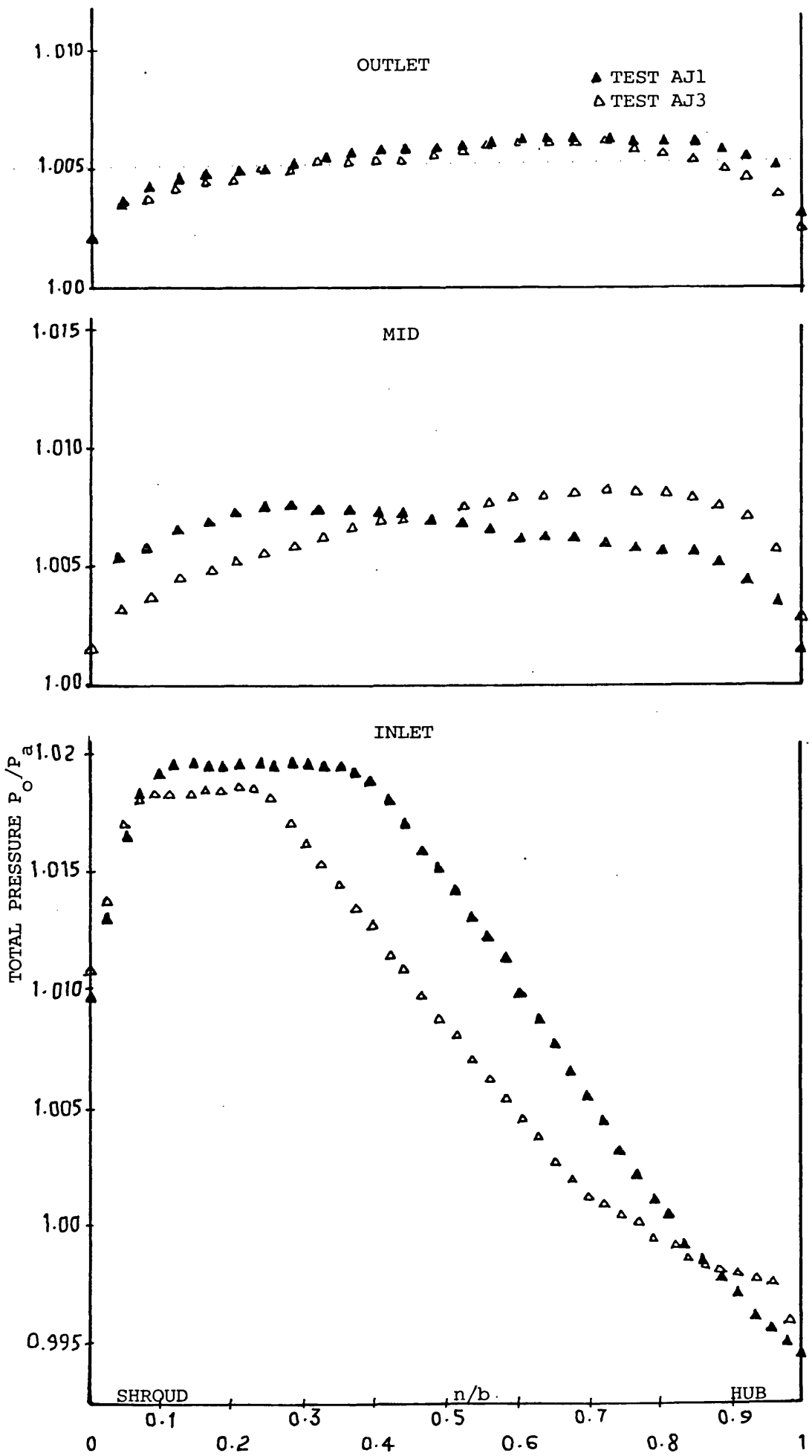

FIG.4.28 EFFECT OF MASS FLOW RATE ON TOTAL PRESSURE DISTRIBUTION TESTS AJ1, AJ3

INLET - CENTRE

INLET - NEAR HUB

INLET - NEAR SHROUD

MID - CENTRE

OUTLET - CENTRE

FIG. 4.29 HOT-WIRE ANEMOMETER TRACES OF JET-WAKE PATTERN AT DIFFERENT LOCATIONS

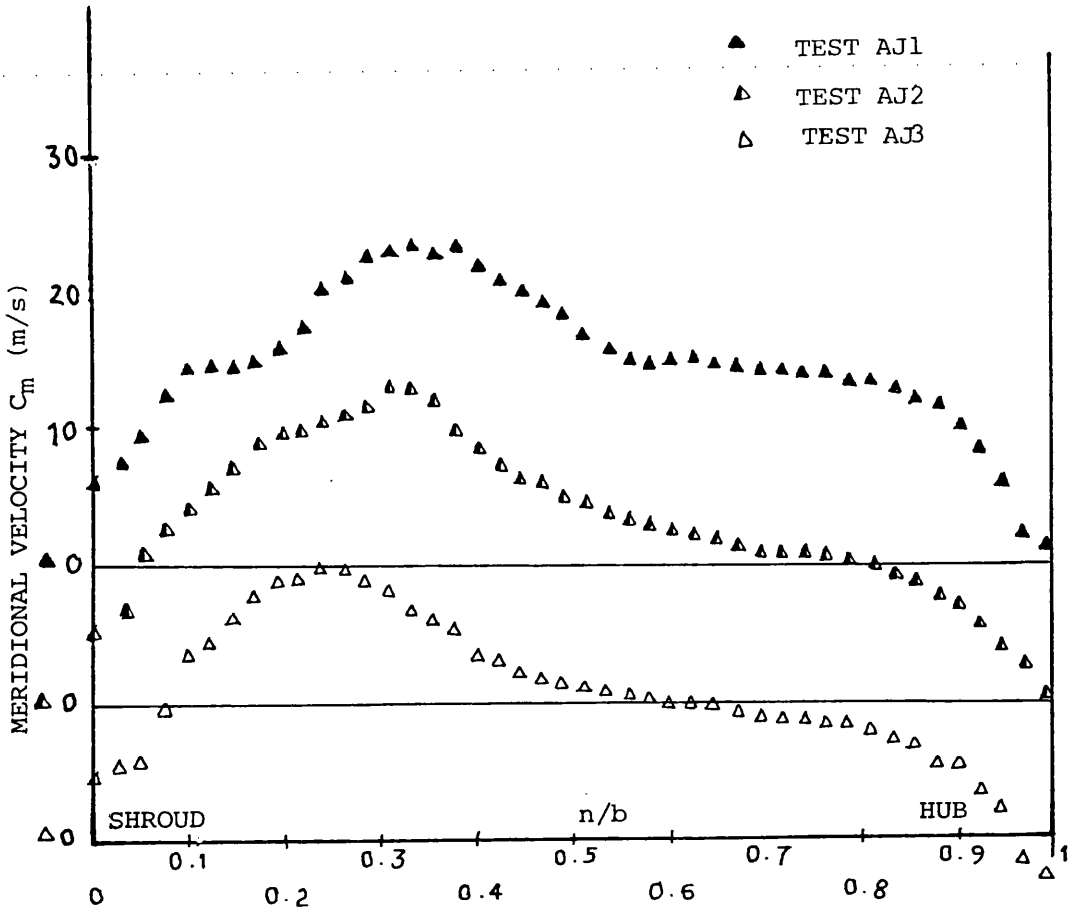

FIG. 4.30a EFFECT OF MASS FLOW RATE ON MERIDIONAL VELOCITY DISTRIBUTION, TESTS AJ1, AJ2, AJ3

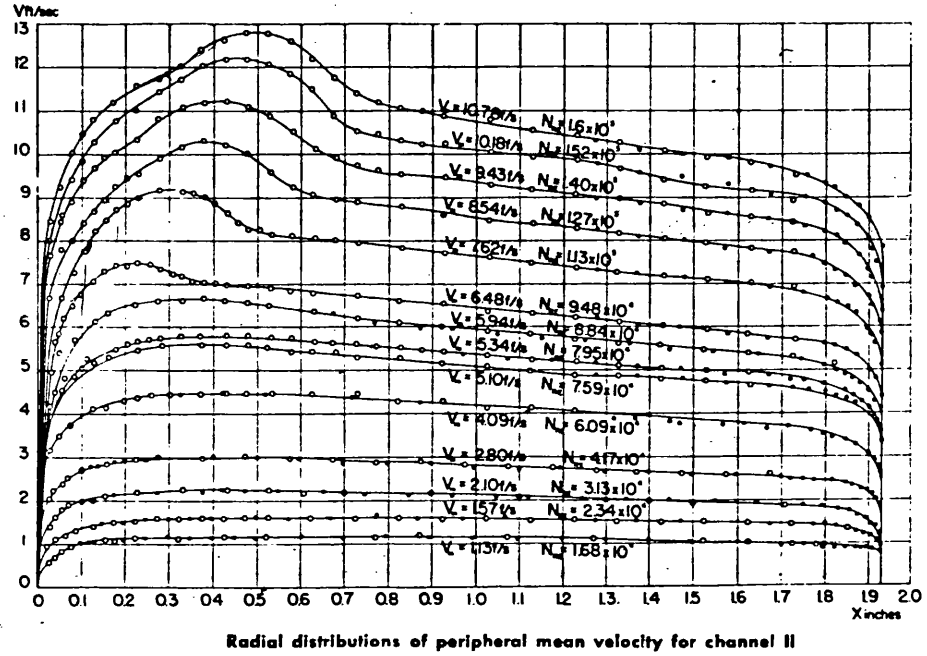

FIG. 4.30b VELOCITY DISTRIBUTIONS IN CURVED CHANNEL (FROM REF.98)

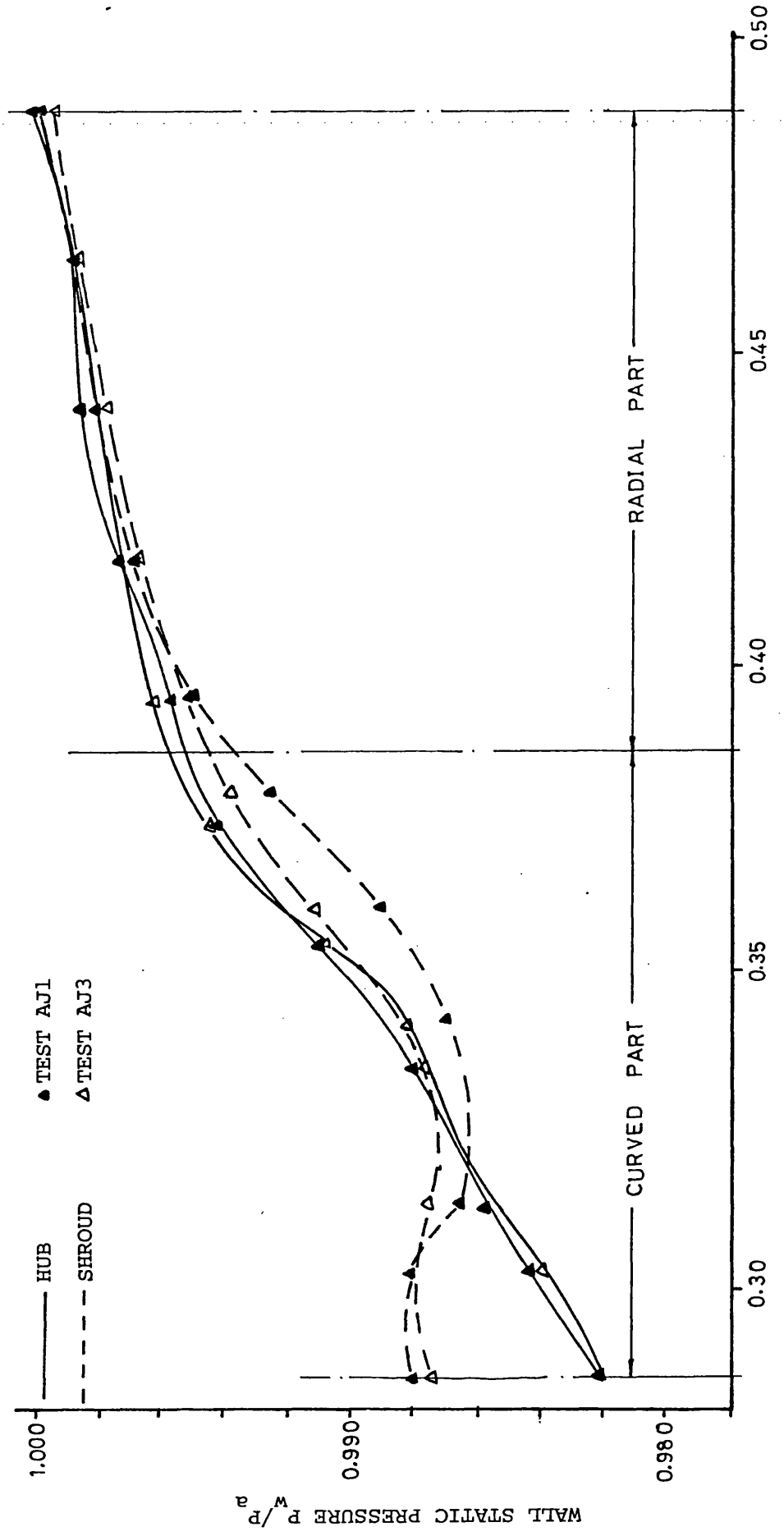

FIG. 4.31 EFFECT OF MASS FLOW RATE ON WALL STATIC PRESSURE DISTRIBUTION, TESTS AJ1, AJ3

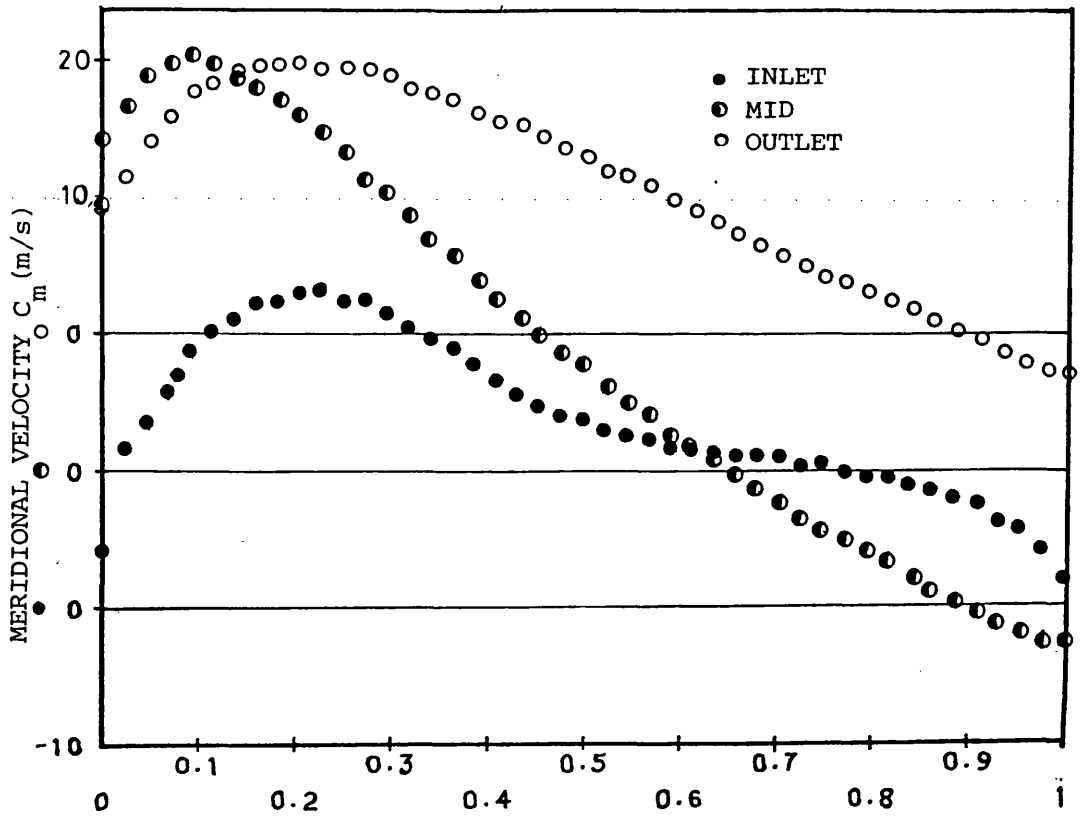

FIG.4.32a MERIDIONAL VELOCITY DISTRIBUTION TEST BJ1

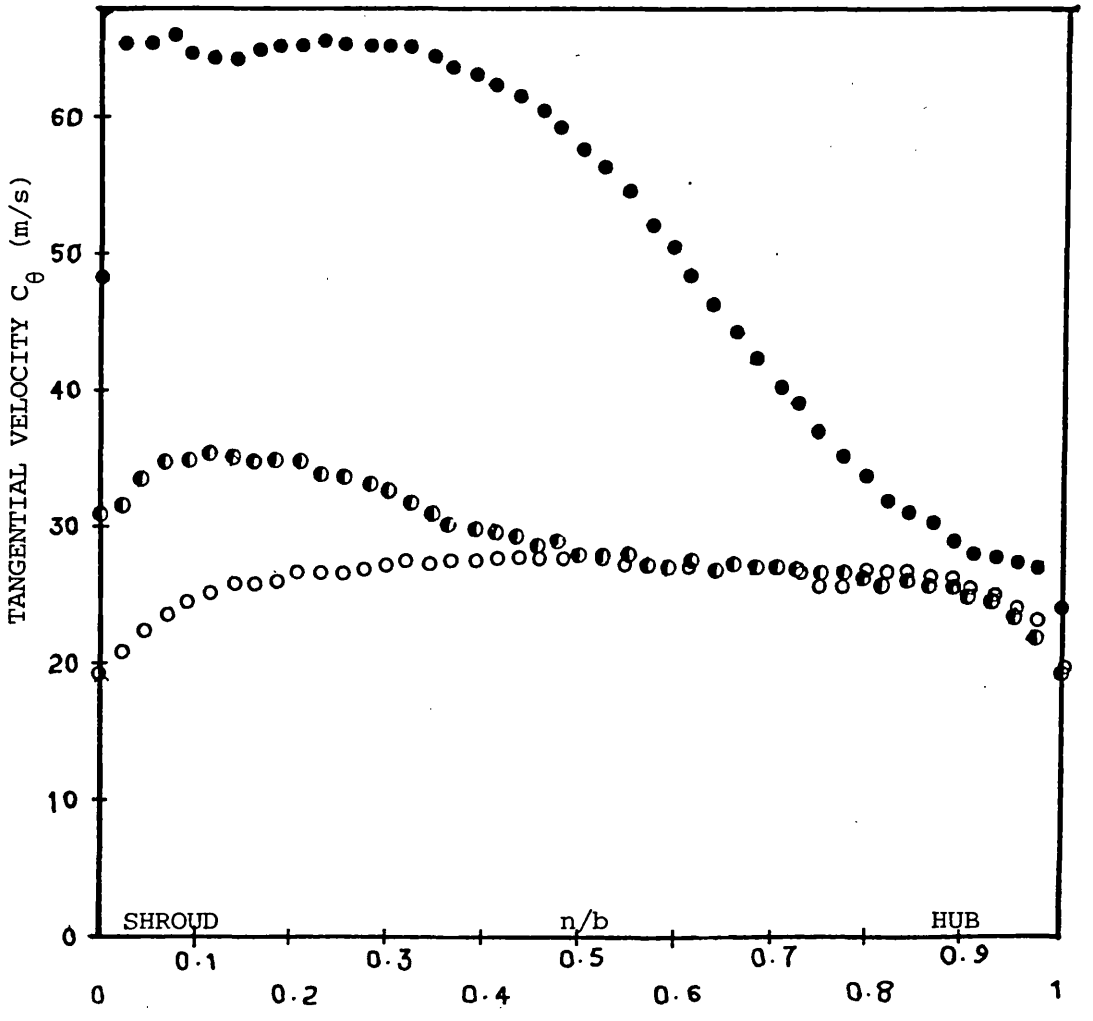

FIG. 4.32b TANGENTIAL VELOCITY DISTRIBUTION TEST BJ1

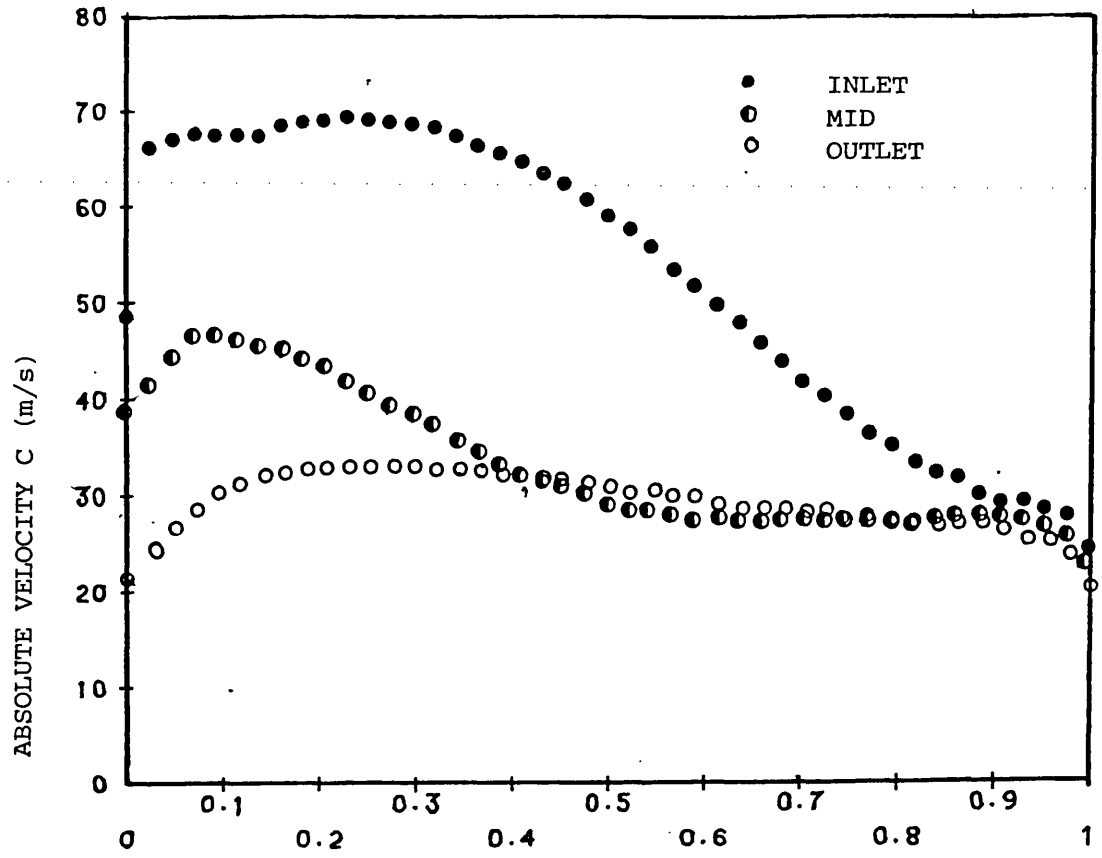

FIG.4.33a ABSOLUTE VELOCITY DISTRIBUTION TEST BJ1

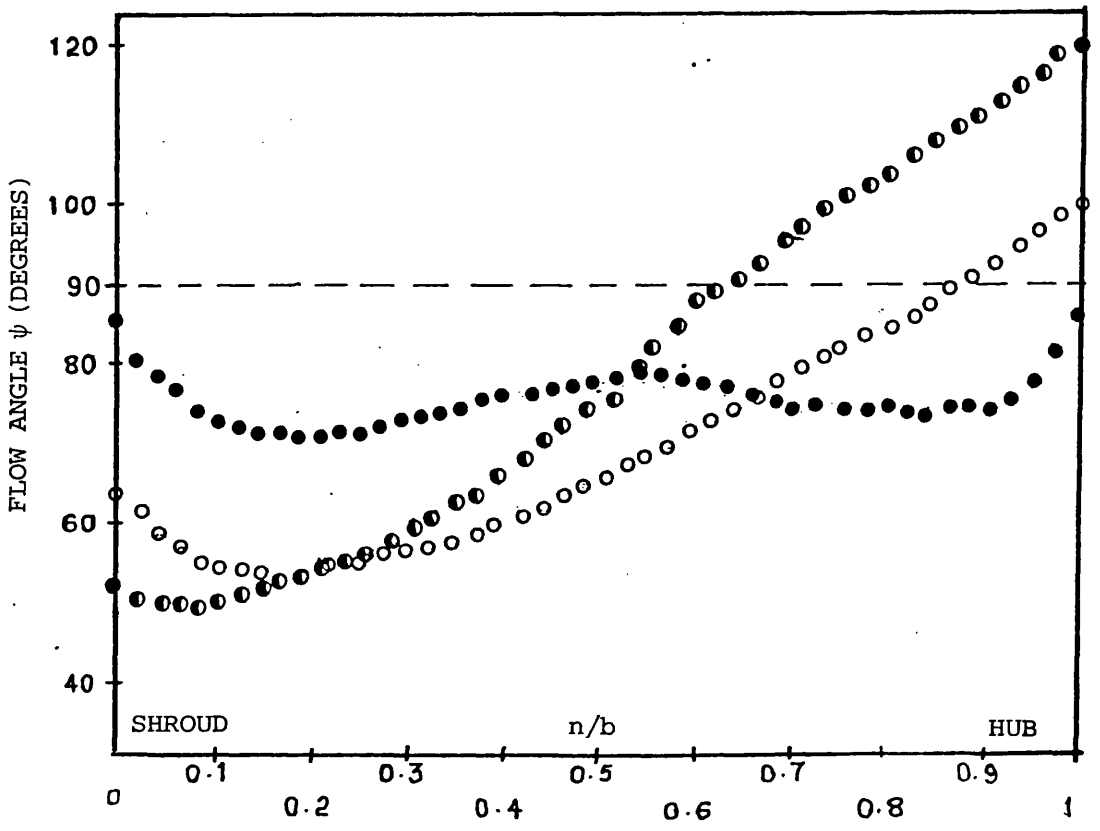

FIG.4.33b FLOW ANGLE DISTRIBUTION TEST BJ1

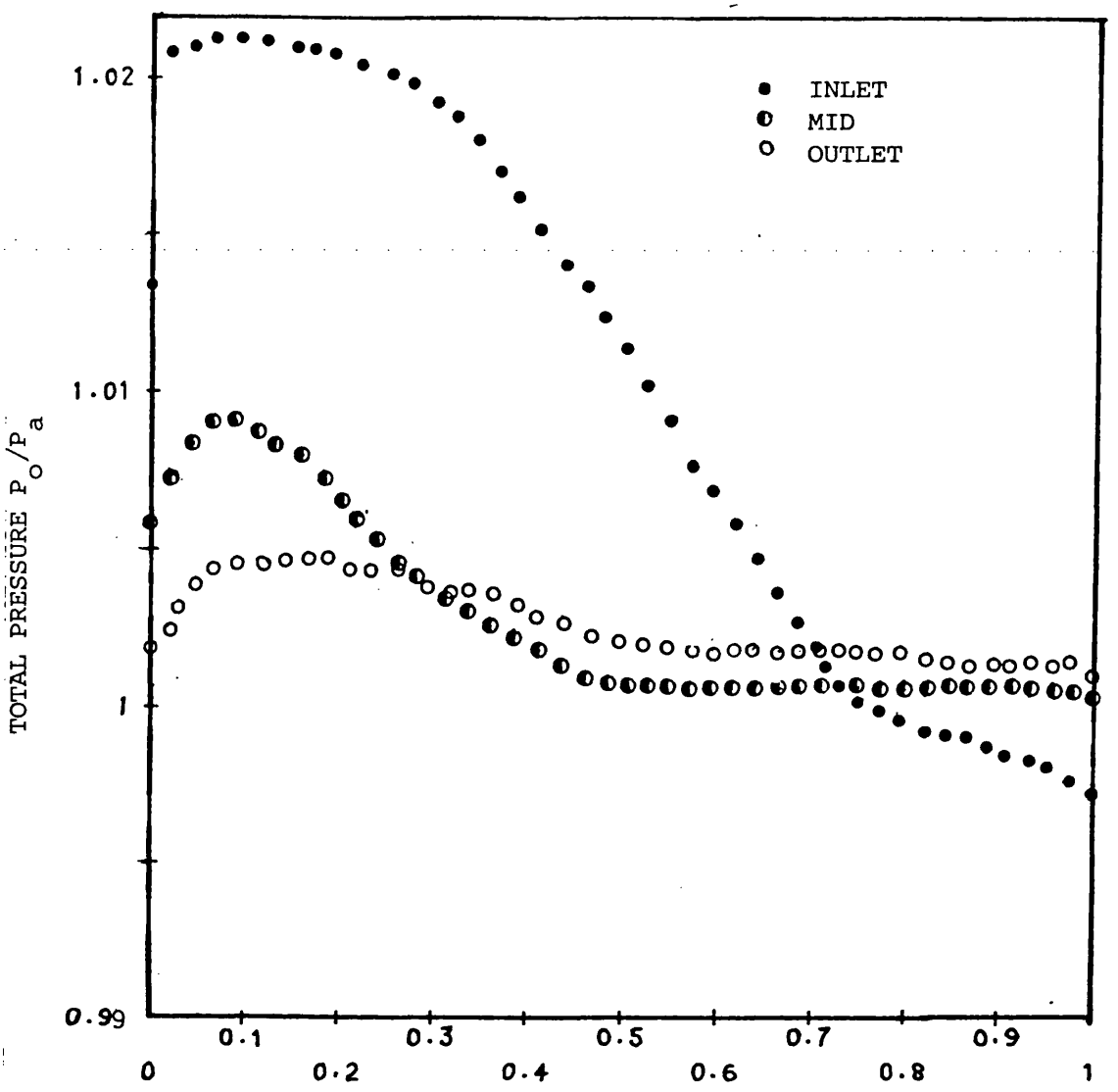

FIG.4.34a TOTAL PRESSURE DISTRIBUTION TEST BJ1

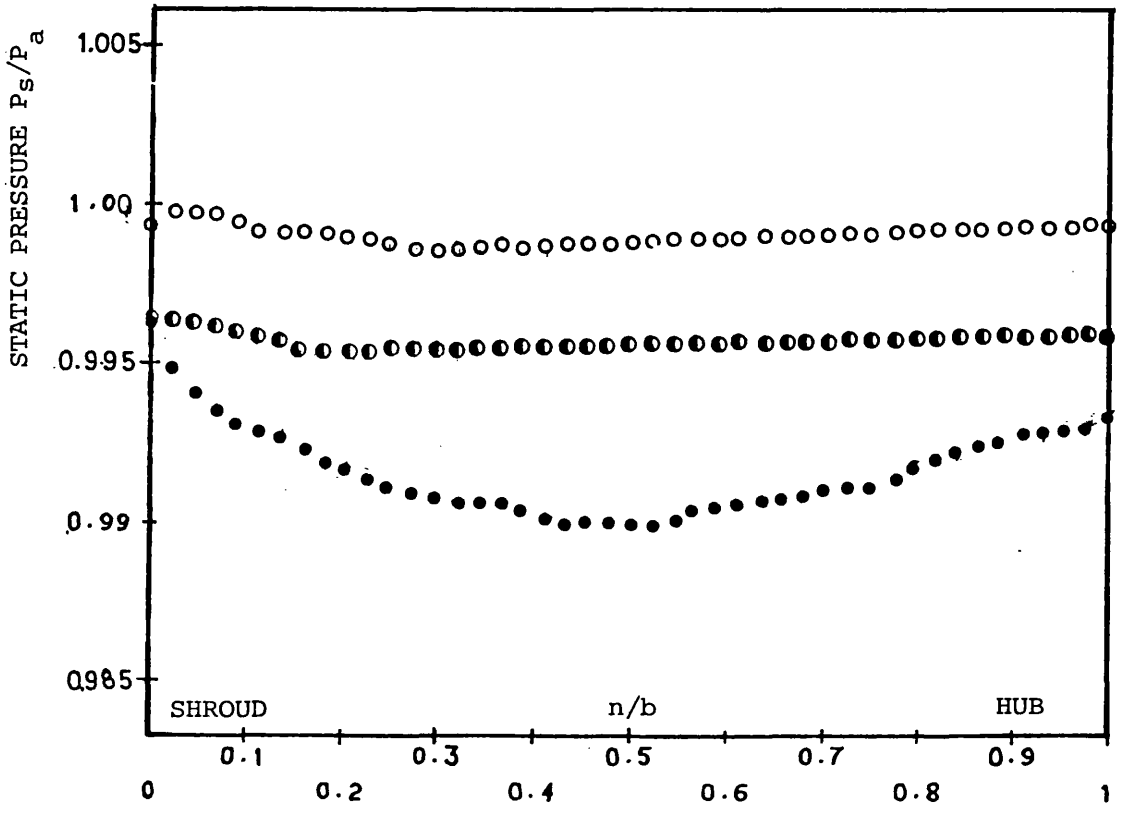

FIG. 4.34b STATIC PRESSURE DISTRIBUTION TEST BJ1

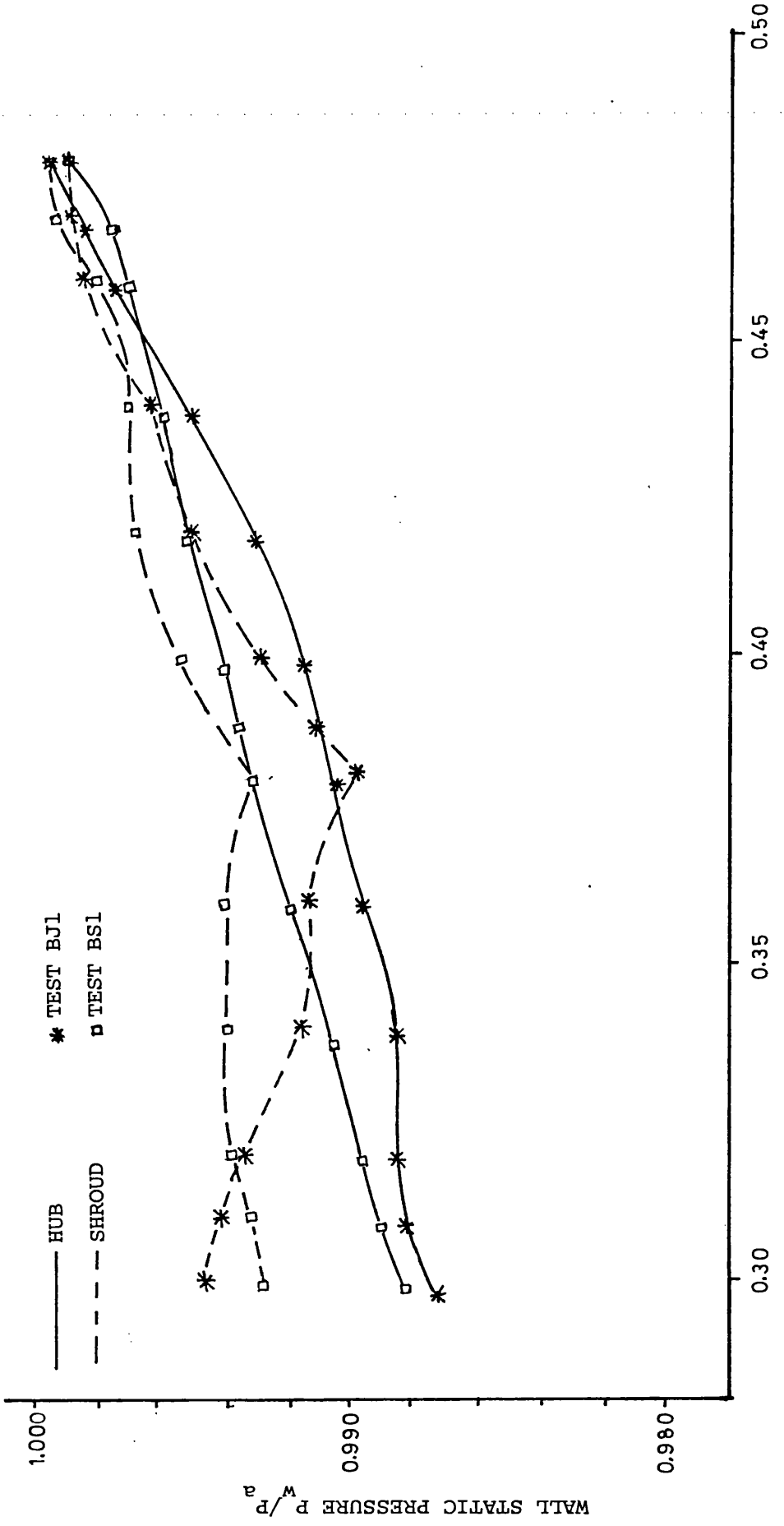

FIG. 4.35 EFFECT OF JET-WAKE FLOW ON WALL STATIC PRESSURE DISTRIBUTION, TESTS BJ1, BS1

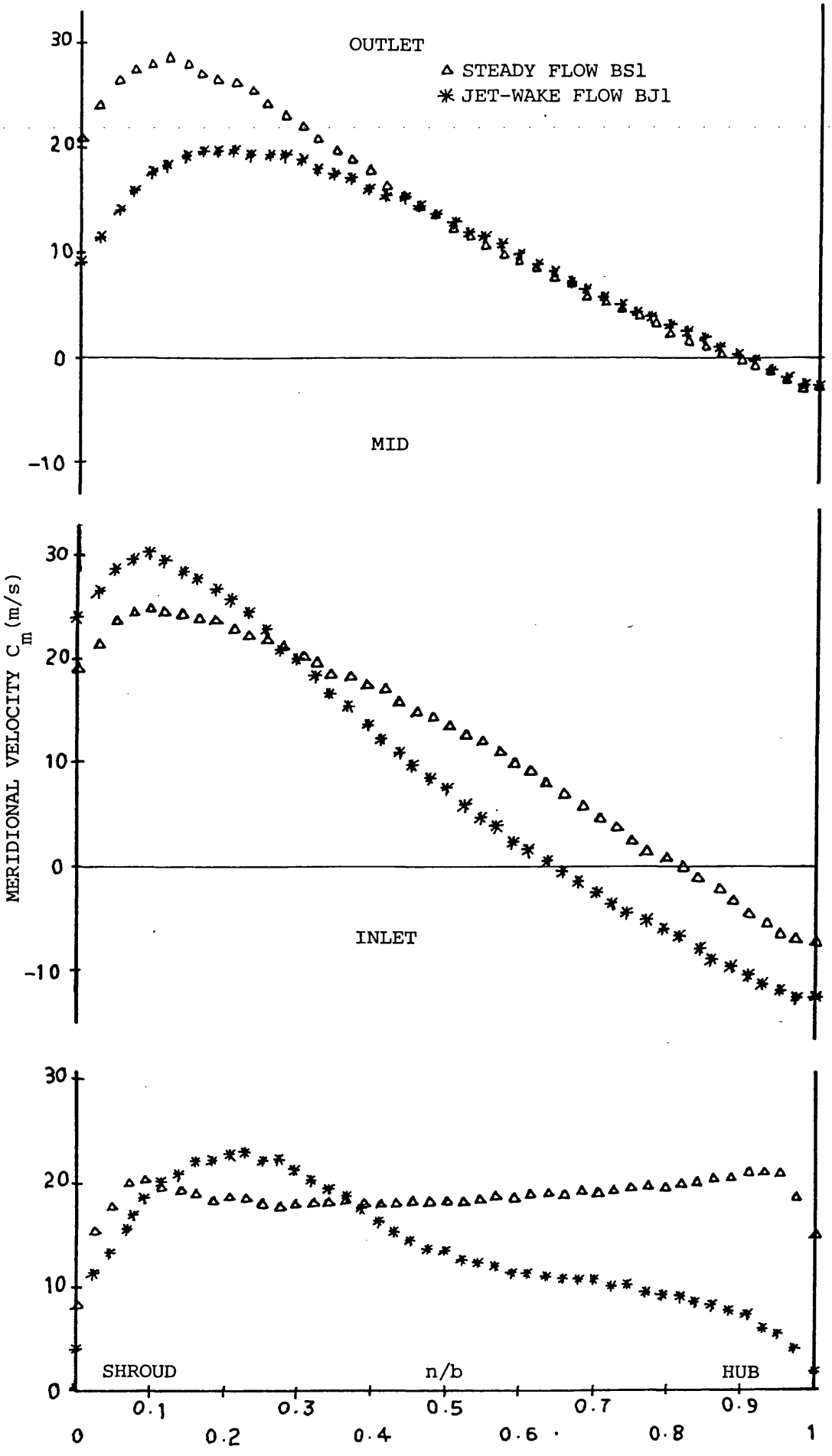

FIG.4.36 EFFECT OF JET-WAKE FLOW ON MERIDIONAL VELOCITY DISTRIBUTION IN THE CONICAL DIFFUSER TESTS BS1, BJ1

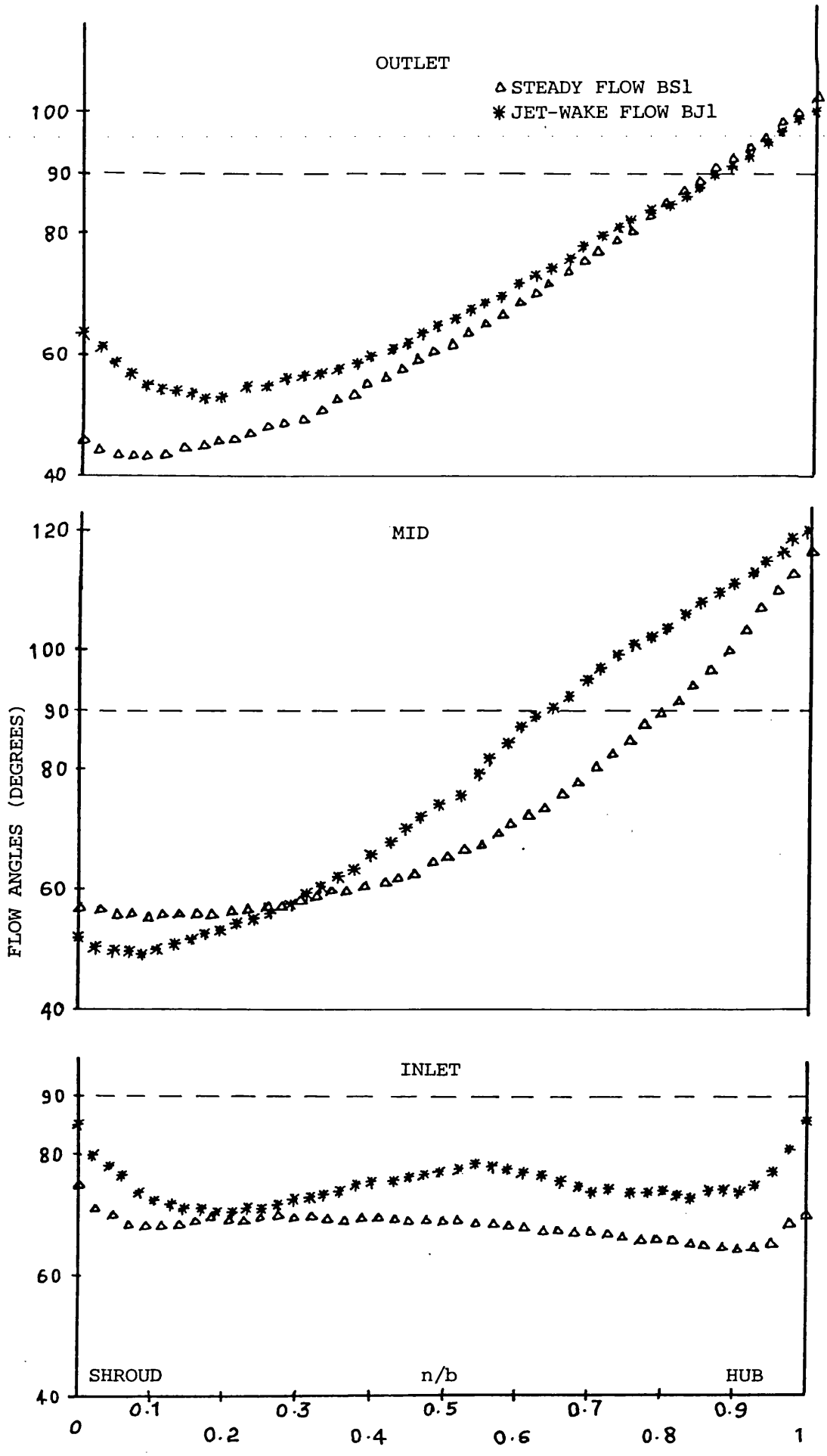

FIG.4.37 EFFECT OF JET-WAKE FLOW ON FLOW ANGLE DISTRIBUTION IN THE CONICAL DIFFUSER TESTS BS1,BJ1

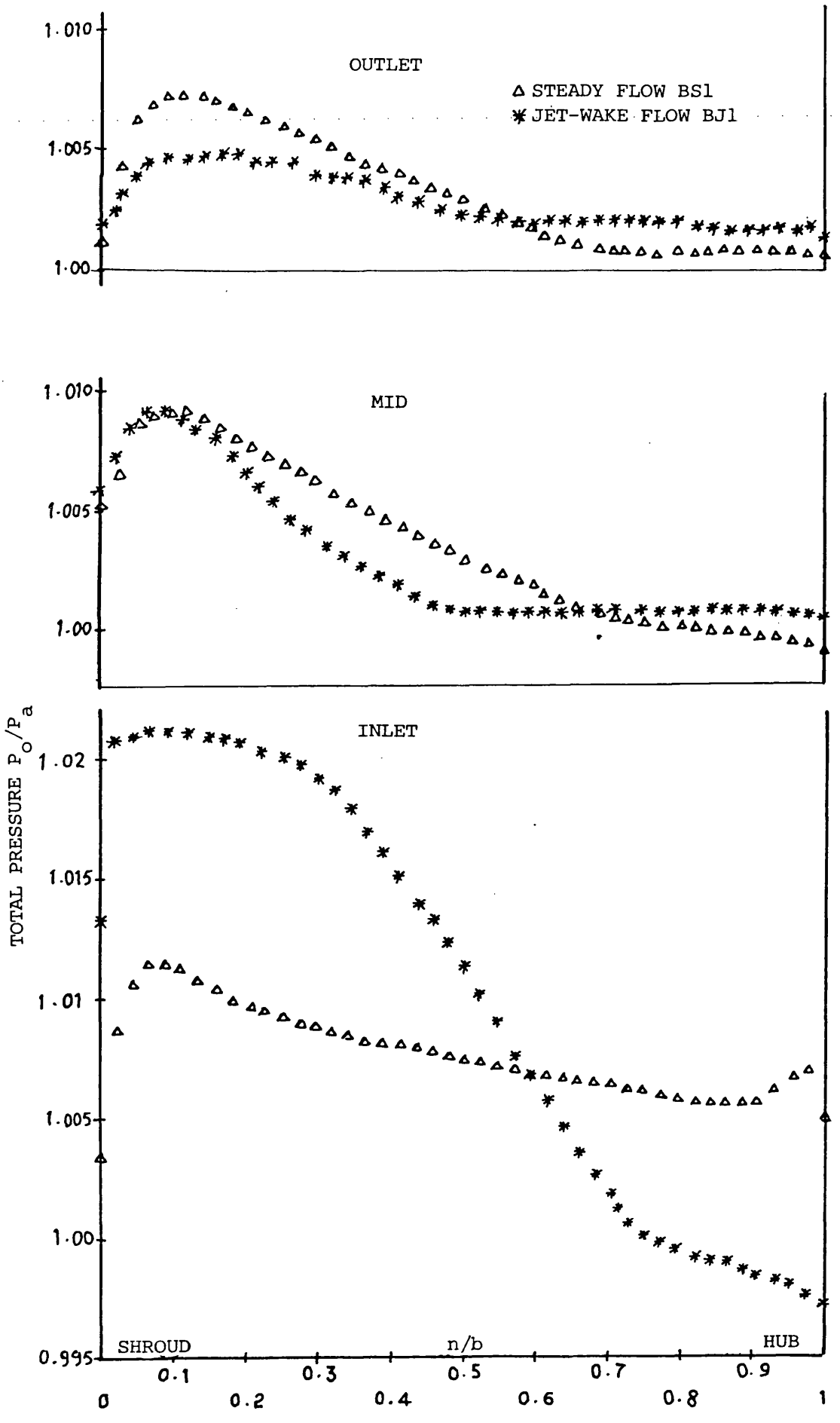

FIG. 4.38 EFFECT OF JET-WAKE FLOW ON TOTAL PRESSURE DISTRIBUTION IN THE CONICAL DIFFUSER TESTS BS1, BJ1

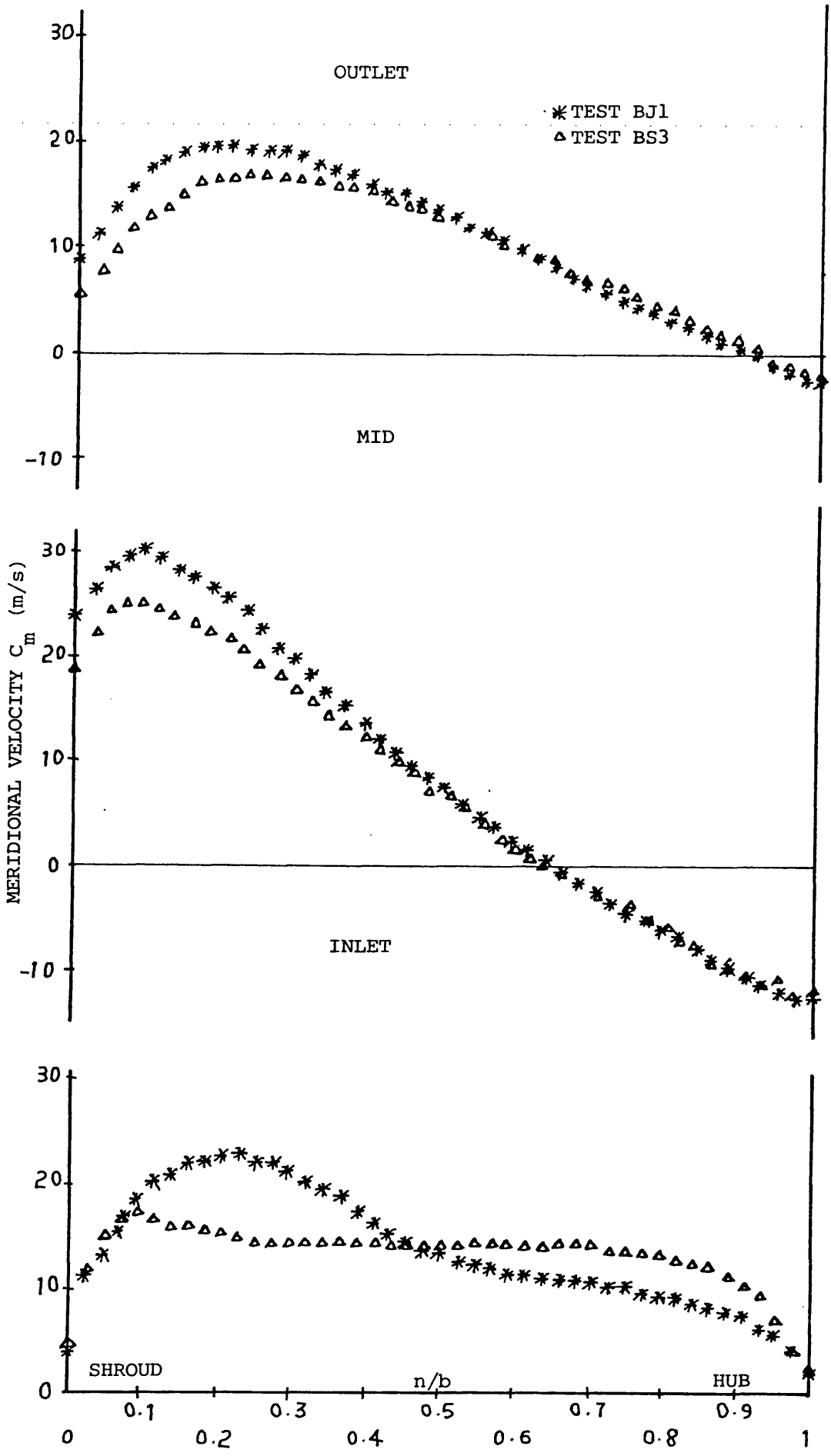

FIG.4.39 MERIDIONAL VELOCITY DISTRIBUTION IN THE CONICAL DIFFUSER, COMPARISON BETWEEN TEST BJ1 and BS3

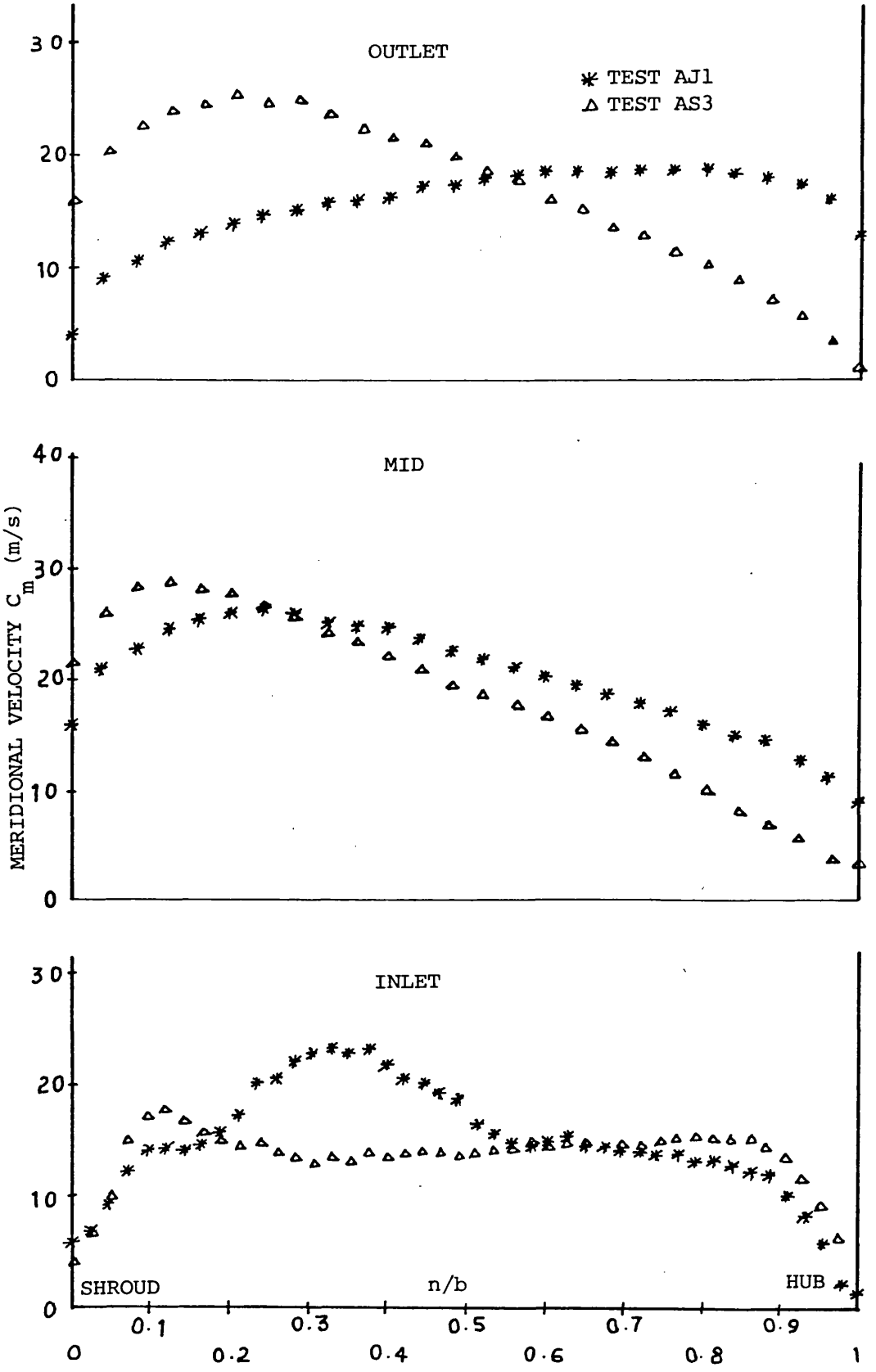

FIG.4.40 MERIDIONAL VELOCITY DISTRIBUTION IN THE CURVED DIFFUSER, COMPARISON BETWEEN TEST AJ1 and AS3

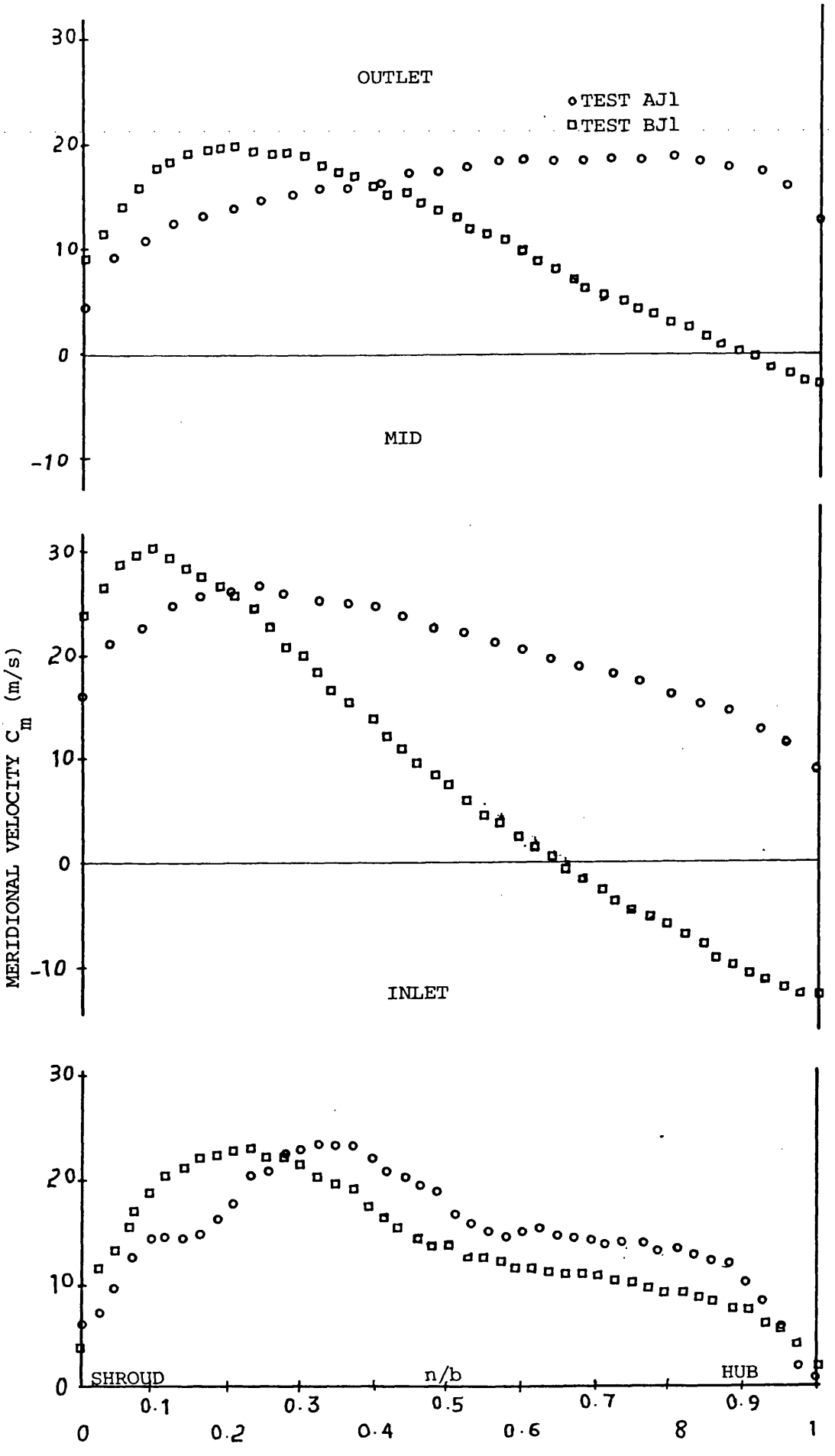

FIG.4.41 COMPARISON OF MERIDIONAL VELOCITY DISTRIBUTION IN CURVED AND CONICAL DIFFUSERS TESTS AJ1, BJ1

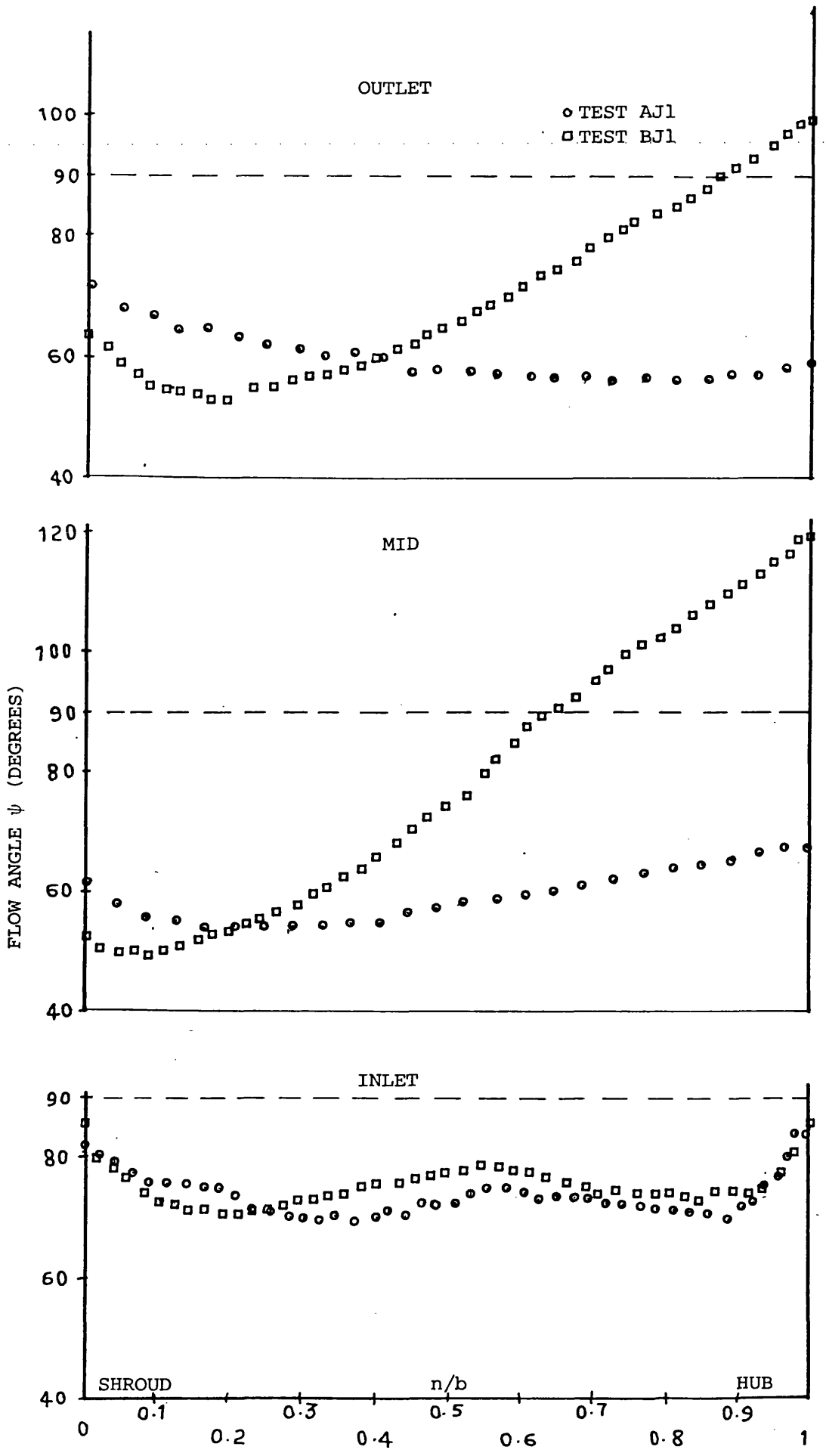

FIG.4.42 COMPARISON OF FLOW ANGLE DISTRIBUTION IN CURVED AND CONICAL DIFFUSERS TESTS AJ1,BJ1

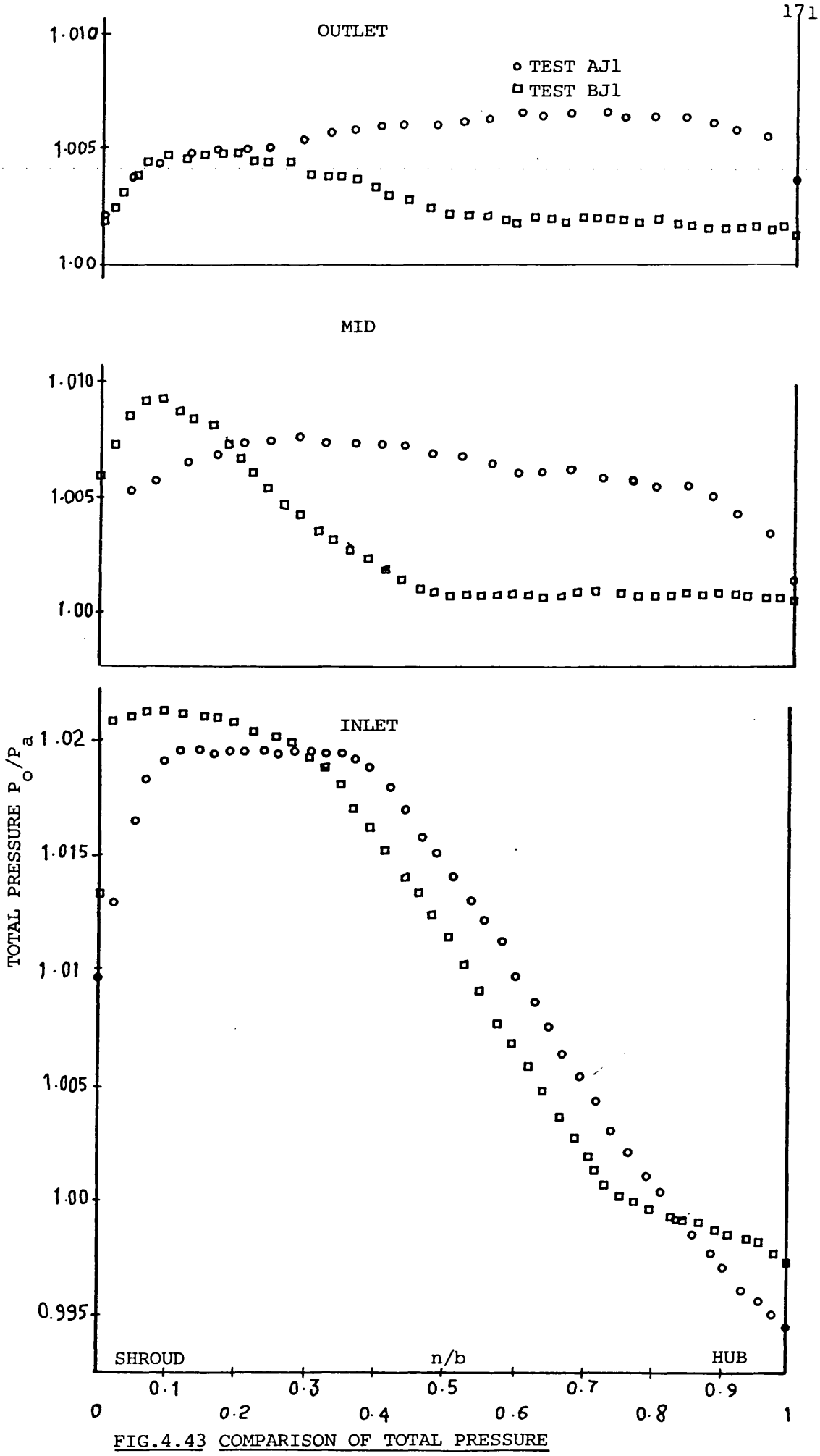

FIG.4.43 COMPARISON OF TOTAL PRESSURE DISTRIBUTION IN CURVED AND CONICAL DIFFUSERS TESTS AJ1, BJ1

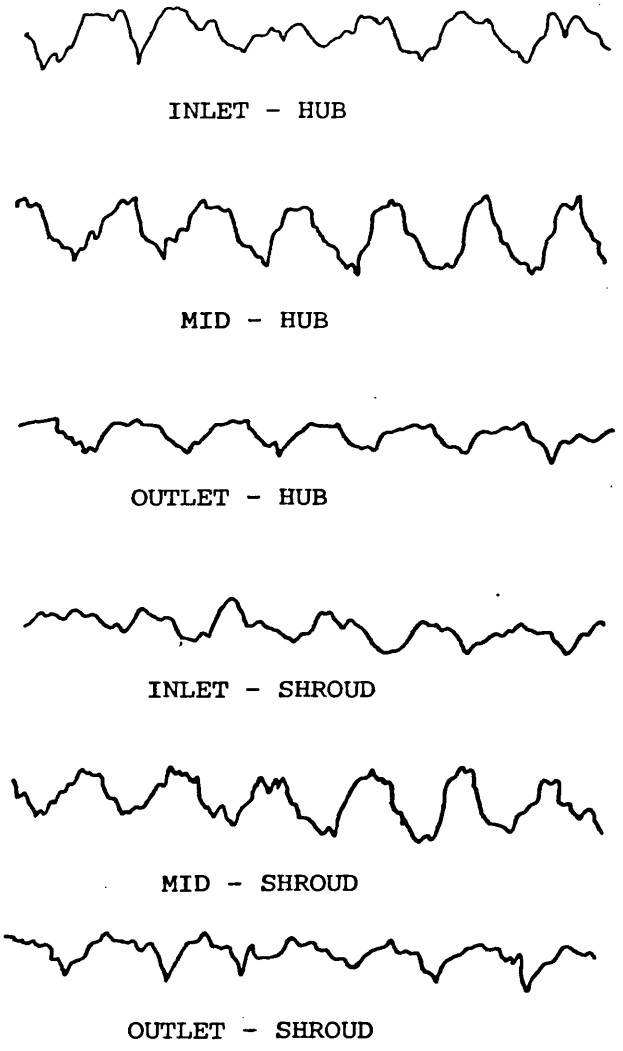

FIG. 4.44 PRESSURE TRANSDUCER TRACES OF PULSATING FLOW AT DIFFERENT LOCATIONS, TEST BJ3

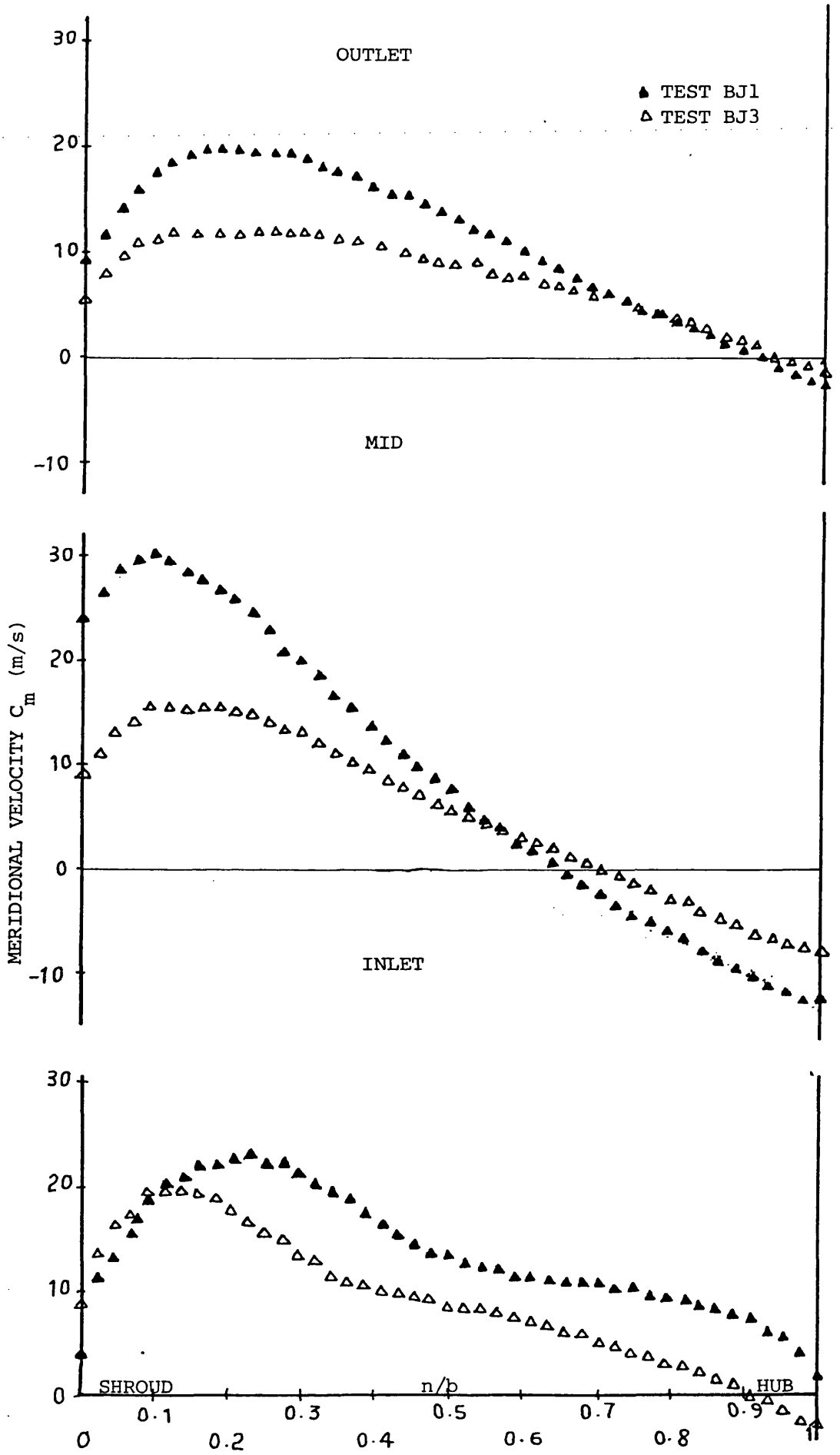

FIG.4.45 EFFECT OF MASS FLOW RATE ON MERIDIONAL VELOCITY DISTRIBUTION TESTS BJ1,BJ3

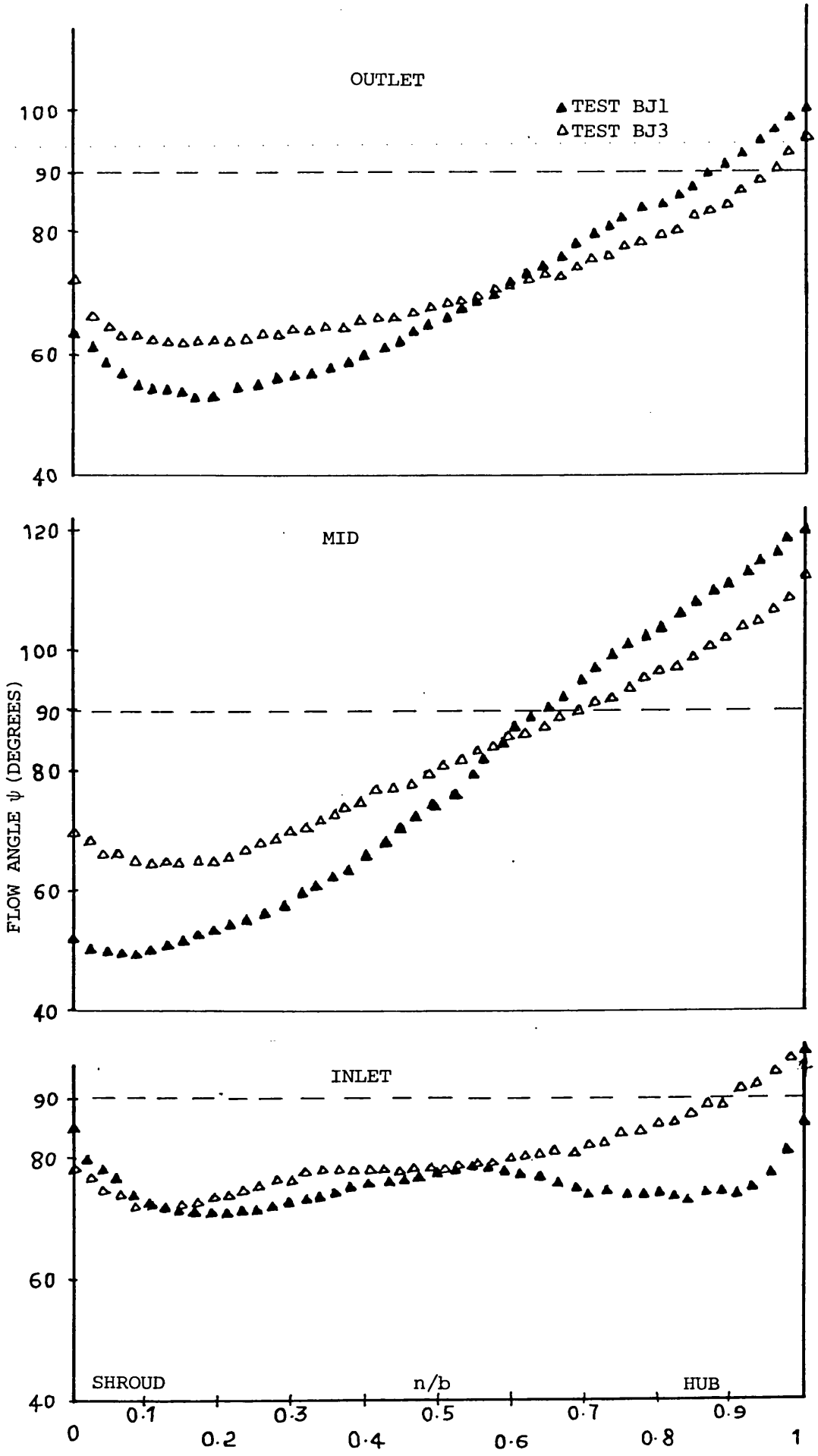

FIG.4.46 EFFECT OF MASS FLOW RATE ON FLOW ANGLE DISTRIBUTION TESTS BJ1, BJ3

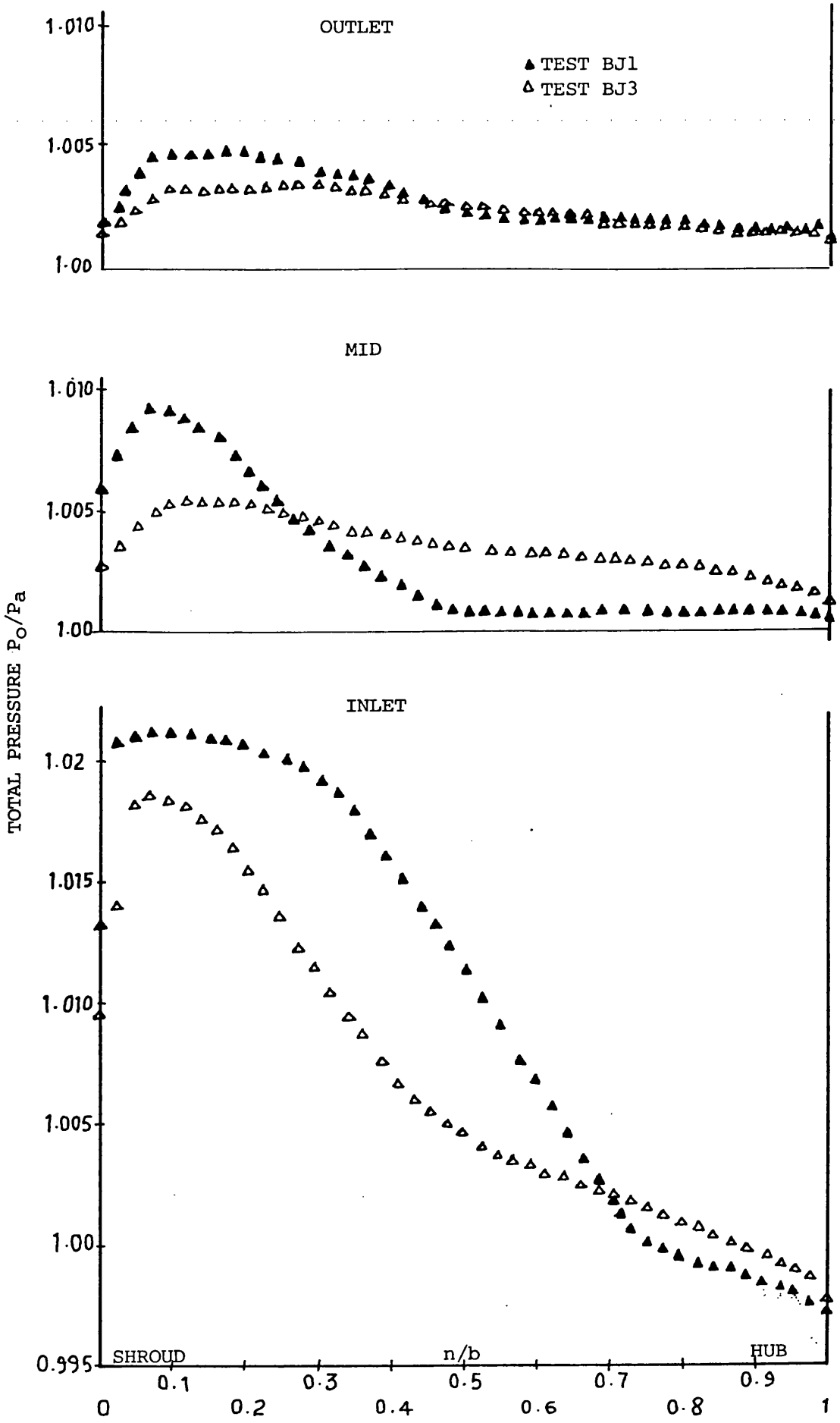

FIG.4.47 EFFECT OF MASS FLOWRATE ON TOTAL PRESSURE DISTRIBUTION TESTS BJ1, BJ3

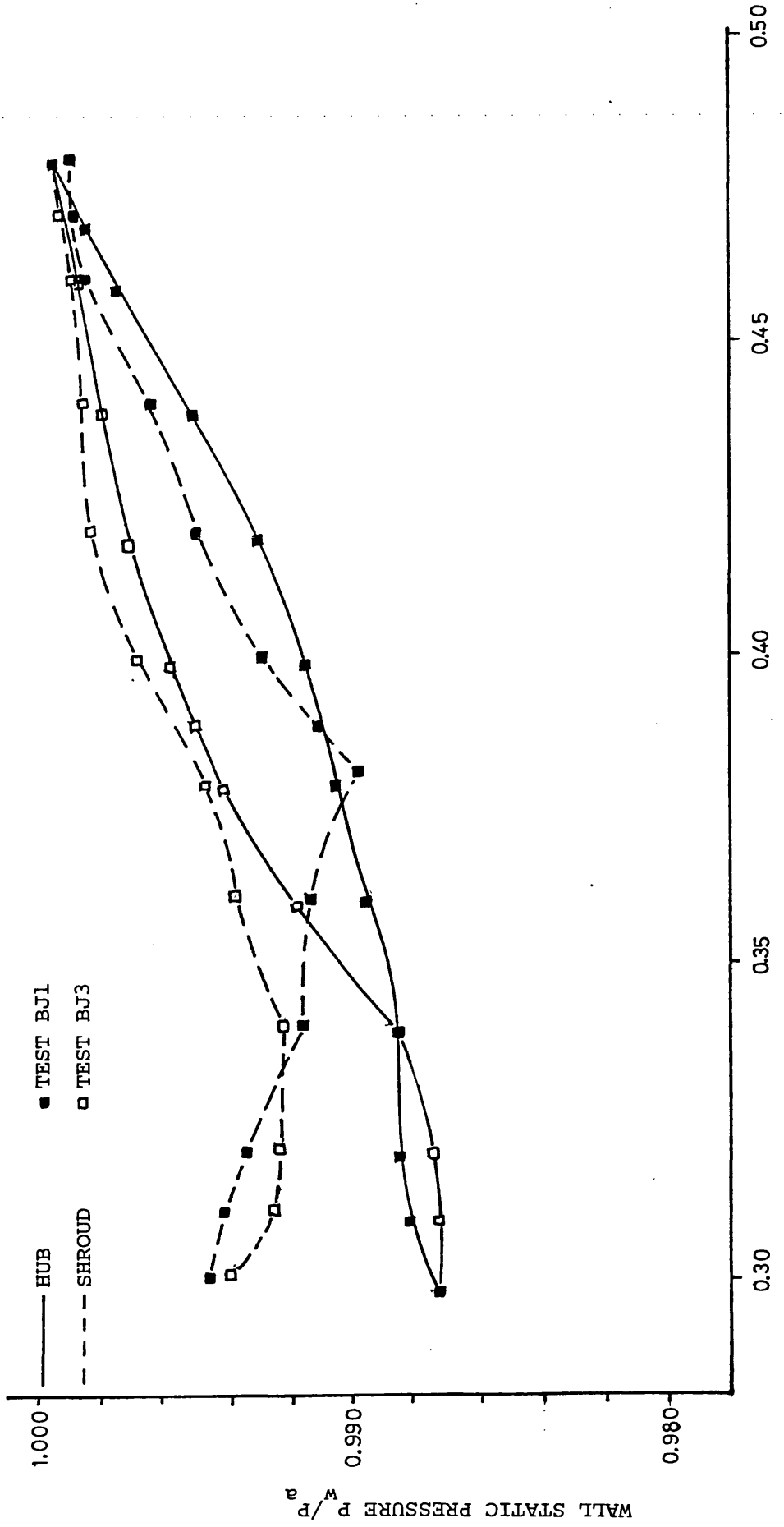

FIG. 4.48 EFFECT OF MASS FLOW RATE ON WALL STATIC PRESSURE DISTRIBUTION, TESTS BJ1, BJ3

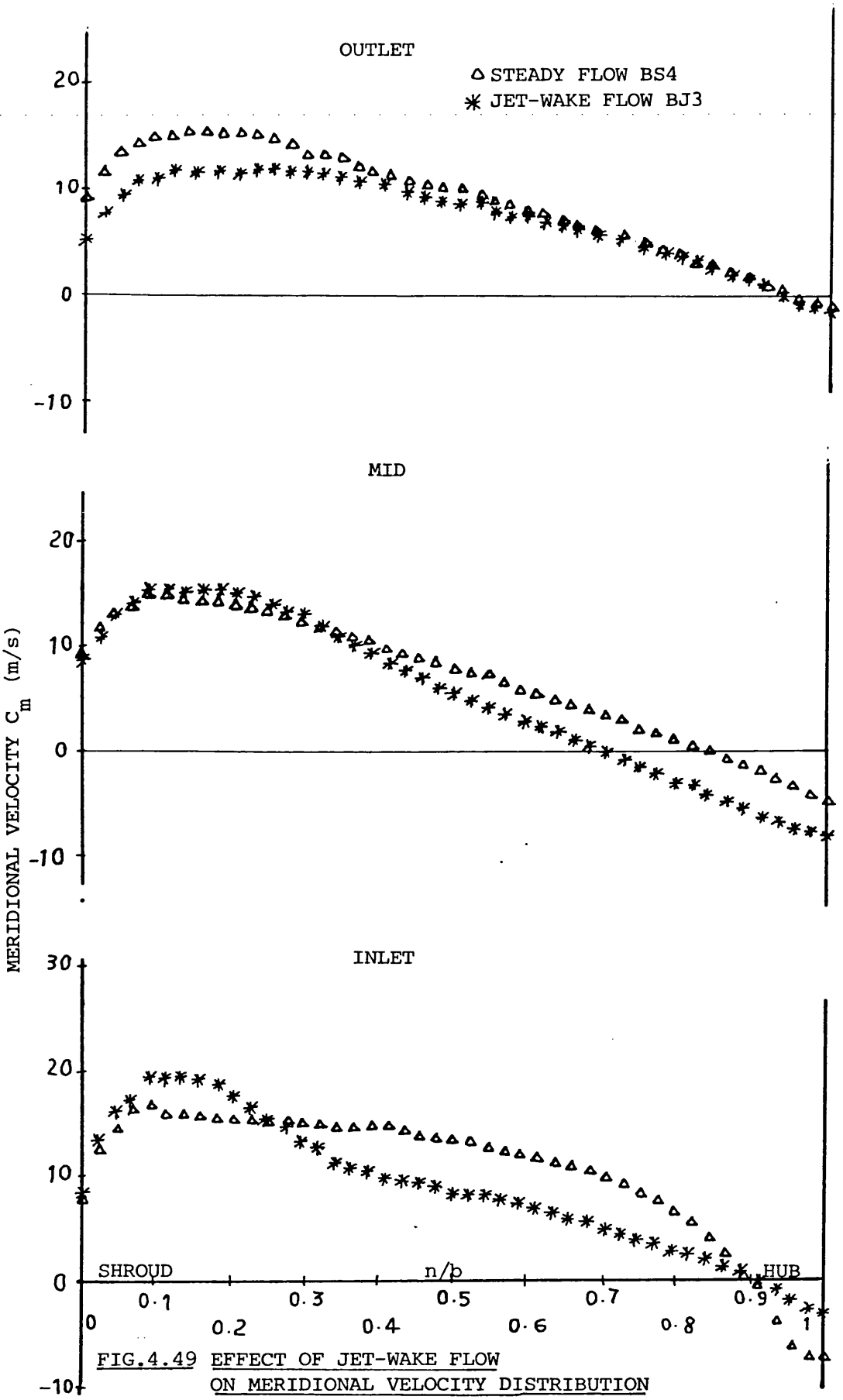

FIG.4.49 EFFECT OF JET-WAKE FLOW ON MERIDIONAL VELOCITY DISTRIBUTION IN THE CONICAL DIFFUSER AT LOW MASS FLOW RATE TESTS BS4,BJ3

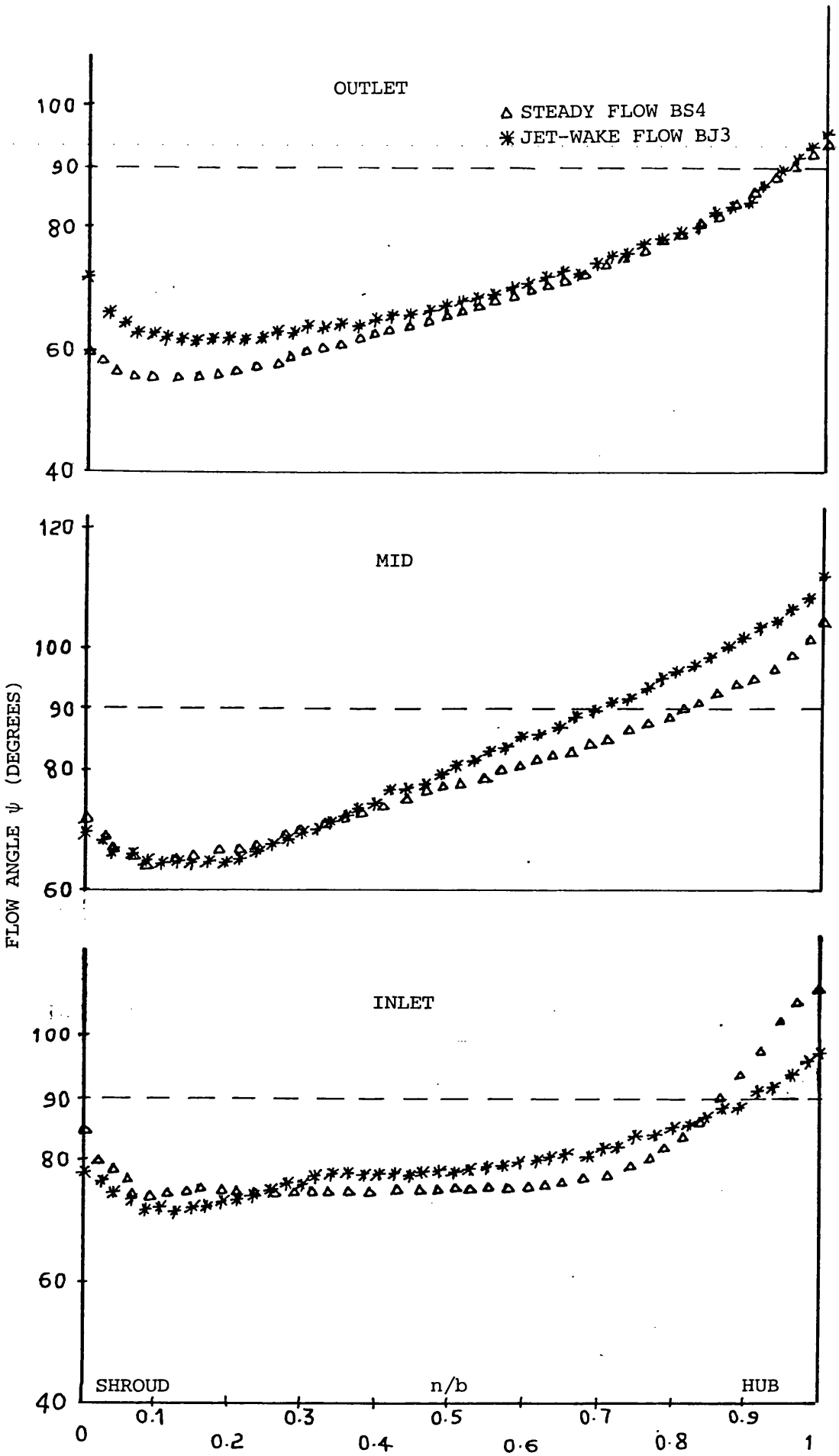

FIG.4.50 EFFECT OF JET-WAKE FLOW ON FLOW ANGLE DISTRIBUTION IN THE CONICAL DIFFUSER AT LOW MASS FLOW RATE TESTS BS4,BJ3

INLET - HUB

MID - HUB

OUTLET - HUB

INLET - SHROUD

MID - SHROUD

OUTLET - SHROUD

FIG. 4.51 PRESSURE TRANSDUCER TRACES OF PULSATING FLOW AT MINIMUM POSSIBLE MASS FLOW RATE

CHAPTER 5 : COMPARISON BETWEEN EXPERIMENTAL AND THEORETICAL RESULTS

5.1 Introduction

The flow profiles obtained experimentally and presented in the previous chapter were used to test the validity of the direct inviscid solution and the interactive boundary layer-inviscid core computation method presented in Chapter 2. The inlet conditions assumed in both theoretical methods we approximated from the experimental results.

5.2 Comparison with the Direct Inviscid Solution

In order to use the inlet conditions obtained experimentally in the direct solution, the total enthalpy and meridional and tangential components of velocity were approximated by linear distributions. The total enthalpy gradient was calculated from the total and static pressure profiles assuming the flow to be isentropic and incompressible.

The resultant enthalpy profile was then approximated by a linear distribution. Table 5.1 gives details of the linearized inlet conditions used in the direct solution.

5.2.1 Steady flow tests AS and BS

Figures 5.1 and 5.2 represent meridional velocity and flow angle profiles obtained experimentally for the curved diffuser tests AS1 and AS3. Superimposed on these profiles are the linearized inlet conditions and the predicted downstream behaviour from the direct inviscid solution.

The gradient of meridional velocity profile is well predicted and the flow angle distributions show good agreement with the experimental results. The predicted meridional velocities on the hub side at mid traverse were higher than the experimental values due to two factors : (i) the linearized inlet conditions gave slightly higher mass flow rates than those obtained experimentally, this tends to decrease flow distortion as discussed in section 2.3.1

(ii) The calculation was carried out using equation 2.23 of the straight wall diffuser since the mid and outlet traverses lie in the radial part of the diffuser, yet the mid traverse lies at the beginning of the radial part, hence the streamlines at that position would still be curved causing more distortion to the experimentally measured values. This was discussed in section 2.3.1 where it was shown that the direct effect of a positive streamlines curvature is to distort the meridional velocity profile leading to reduced velocities on the wall. At outlet the correct behaviour was predicted with the tendency to separation on the hub being shown.

Figures 5.3 and 5.4 compare the conical diffuser test results BS1 and BS3 with the direct solution. The separation at mid traverse was well predicted with the meridional velocity and flow angle profiles showing remarkable agreement with the measured results. At outlet, however, the direct solution indicates an increase in the extent of separation whilst the experimental results showed a trend towards re-attachment. This continuous increase in predicted distortion with radius was explained, in section 2.3.1 where it was shown that a distortion caused by an energy gradient will increase continuously with radius. The experimental results at outlet showed a rotation of the total pressure profiles (see fig. 4.11a). This cannot be predicted by the inviscid solution as it assumes that the total pressure remains constant along a streamline.

In general it has been shown that the direct solution can predict the flow behaviour quite well up to the point of separation for steady inlet flow conditions for both the curved and conical diffusers.

5.2.2 Jet-wake flow tests AJ and BJ

For the curved diffuser reasonable agreement of meridional velocity was only obtained for the low mass flow rate test AJ3 on the hub side and at the mid traverse station, see fig. 5.5. The flow angles predicted correctly only in the centre of the passage at mid traverse (see fig. 5.6).

The predicted conditions at discharge show no correspondence with those measured, reverse flow being predicted on the hub rather than the shroud surface. The poor predictions in this case are considered to be due to:

(i) the early separation in the curved part of the diffuser; it has already been shown that the inviscid procedure is not satisfactory after separation has occurred.

(ii) the possible over-estimate of the total enthalpy gradient due to the inaccuracy of the total pressure probes in the unsteady jet-wake flow field.

The predictions were, therefore, repeated using as the initial conditions the measured parameters at the mid traverse station. From fig. 5.7 it can be seen that the discharge conditions are more closely predicted with the reverse flow correctly shown to be on the shroud surface.

The conical diffuser results, figs. 5.8 and 5.9, showed reverse flow on the hub surface and this was correctly predicted. However, the overall correspondence between theory and experiment is poor, the accuracy of the predictions becoming increasingly poor with early separation. For test BJ3 reverse flow is shown at inlet and the predicted results at the other traverse stations are poor. With increased flow rate, test BJ1, reverse flow is not indicated at inlet and the predicted profiles at the mid traverse station are satisfactory.

It can be concluded that if there is no shift in energy gradient between inlet and the considered section, the direct inviscid solution will predict quite well both the flow behaviour and point of separation. The direct solution is however unsatisfactory after the occurrence of separation due to the change in energy distribution in the flow.

5.3 Boundary Layer Prediction

The inlet profiles obtained experimentally were again used as an input data to the theoretical procedure. In both cases of curved and conical diffusers, the jet-wake tests AJ and BJ were excluded as the

theoretical analysis indicated an immediate flow separation after inlet due to the high total enthalpy gradient, high flow angle and high skew angles at inlet.

For the steady flow tests, the procedure predicted that the boundary layer filled the curved diffuser passage shortly after the mid traversing position, beyond which the computational technique is not valid. Comparison between the experimental and predicted profiles of absolute velocity and flow angle at the mid traverse position are given in figs. 5.10 and 5.11 for test AS1 and AS3 respectively. Good agreement is demonstrated for test AS1 with a high mass flow rate, while fair agreement is obtained in the case of a low mass flow rate, test AS3, where the hub surface flow and skew angles were underestimated. This is attributed to the limitation of the boundary layer equations where the effect of wall curvature was neglected, and to the limitation of using constant value shape factors together with a fixed cross flow velocity profile. Some or all of the previous factors contributed in the poor hub prediction, however, the general flow behaviour was reasonably well predicted.

The development of various boundary layer and core flow parameters through the curved diffuser for test AS1 is shown in fig. 5.12. The procedure predicted high rate of growth of the hub boundary layer with it occupying about 80% of the passage width at the final calculation positions. To confirm this prediction a detailed turbulence level measurement would have to be carried out. However, So and Mellor (95), Yeh (96) and Meroney (97) reported that the effect of a concave curvature, as that of the hub, is to increase turbulence and to thicken the boundary layer, while a convex curvature will have the opposite effect. Any curvature, however, affects the solution via the inviscid core calculation only.

For the case of steady inlet flow with the conical diffuser test BS1 and BS3 separation was predicted on the hub shortly after inlet. To investigate the flow behaviour in this case the inlet conditions were modified by reducing the inlet flow angle to 60 degrees and the total enthalpy difference to 0.5 K in order to obtain flow without separation

throughout the passage. Fig. 5.13 represents the development of the flow parameters in this case. It is clear that the hub flow angle γ increases rapidly to values near separation within a short distance from the inlet. This result therefore indicates the ability of the procedure to successfully predict the flow trends in the conical diffuser.

Test Code	Total Δ To Enthalpy Difference K	λ_{shroud}	λ_{hub}	Traverse position
AS1	1.0	16.8	11.5	inlet
AS3	1.0	17.3	12.7	"
BS1	0.9	16.0	11.3	"
BS3	0.9	17.6	12.4	"
AJ1	2.0	25.8	5.9	"
AJ3	2.0	24.3	7.5	"
BJ1	2.2	25.0	6.9	"
BJ3	2.0	18.9	8.0	"
AJ1	-0.4	14.1	14.5	mid
AJ3	-0.7	13.7	16.4	"

TABLE 5.1 Linearized Conditions used in Direct Inviscid Flow Solution

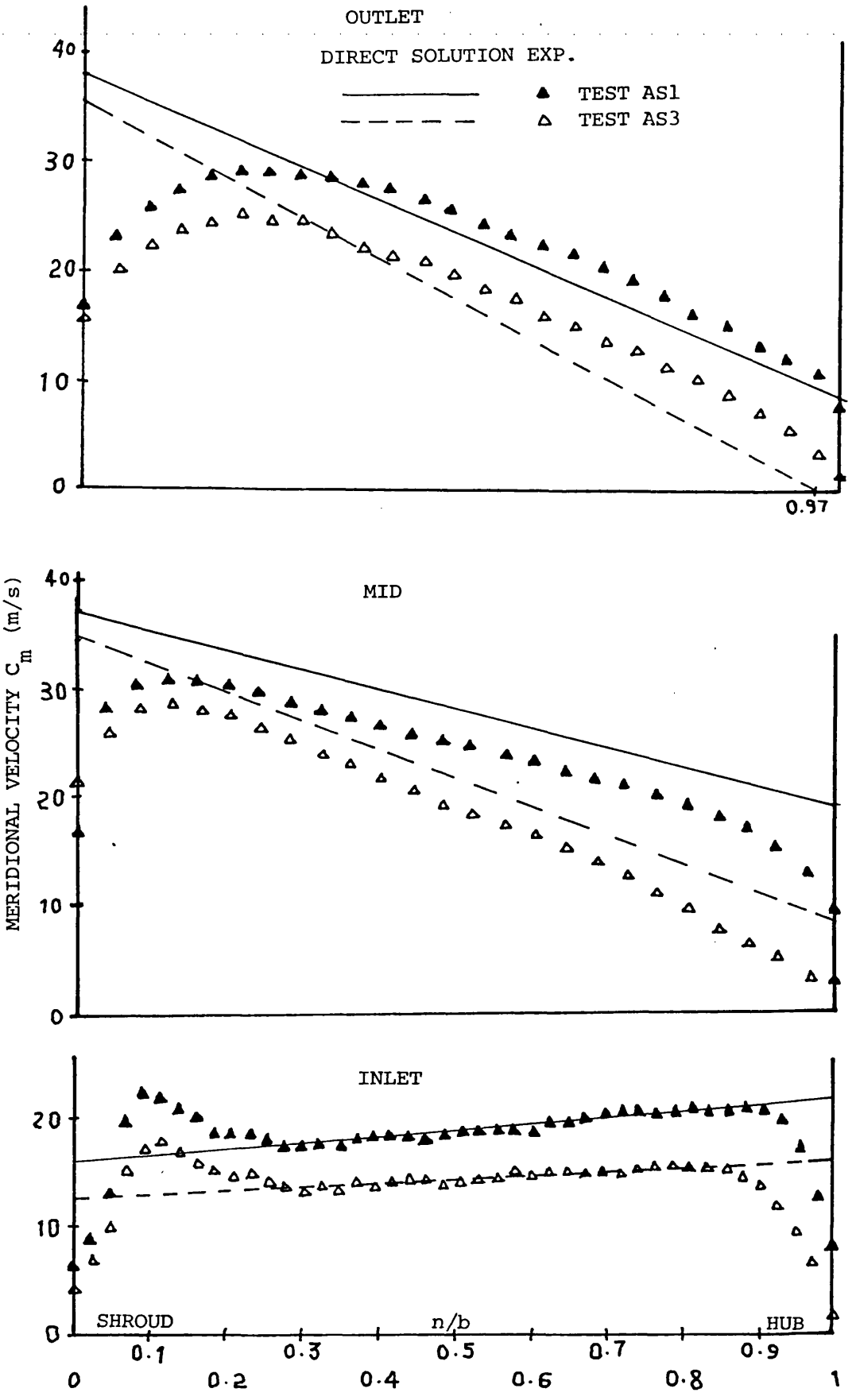

FIG.5.1 COMPARISON BETWEEN DIRECT INVISCID SOLUTION AND EXPERIMENTAL MERIDIONAL VELOCITY DISTRIBUTION TESTS AS1,AS3

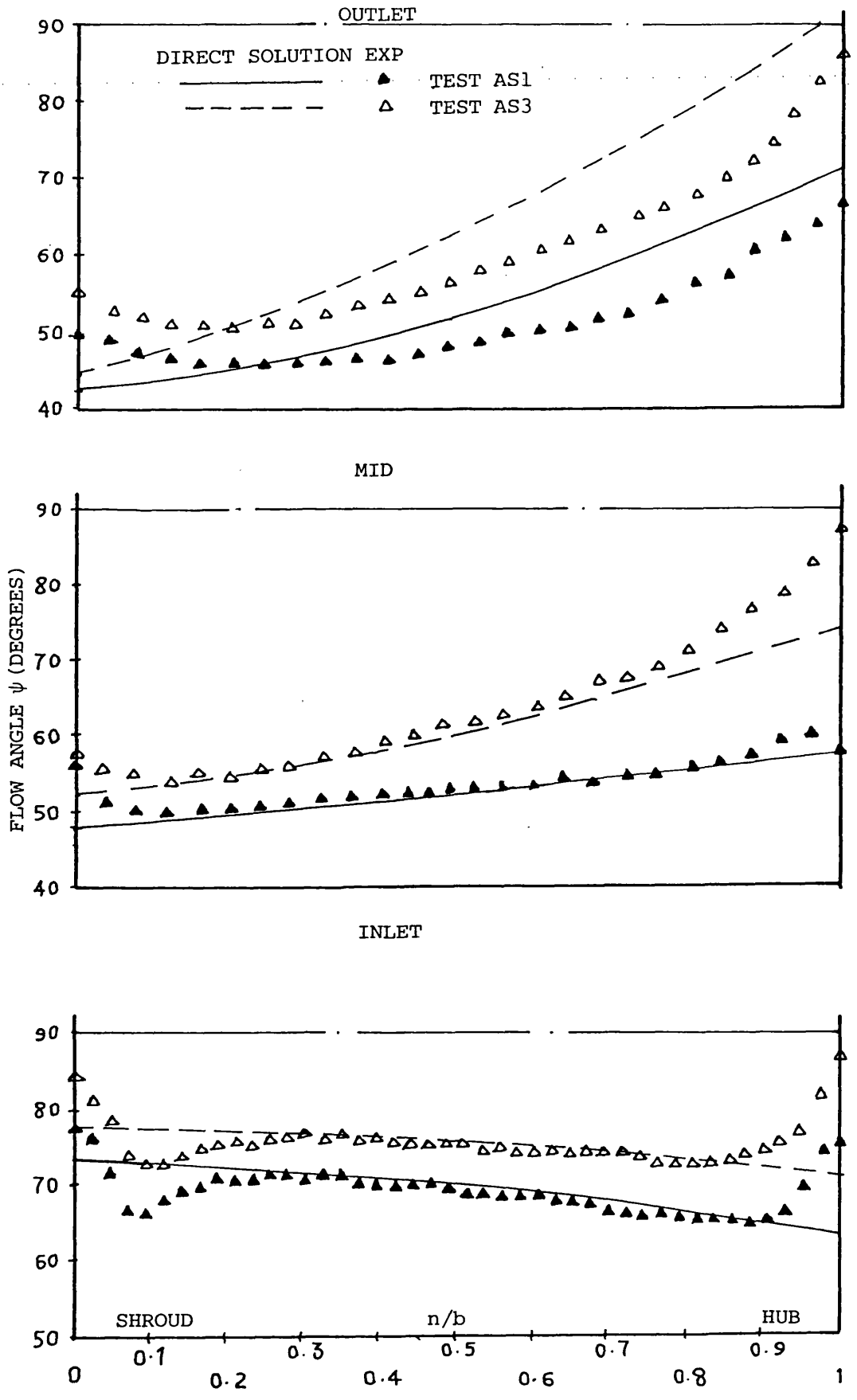

FIG.5.2 COMPARISON BETWEEN DIRECT INVISCID SOLUTION AND EXPERIMENTAL FLOW ANGLE DISTRIBUTION TESTS AS1, AS3

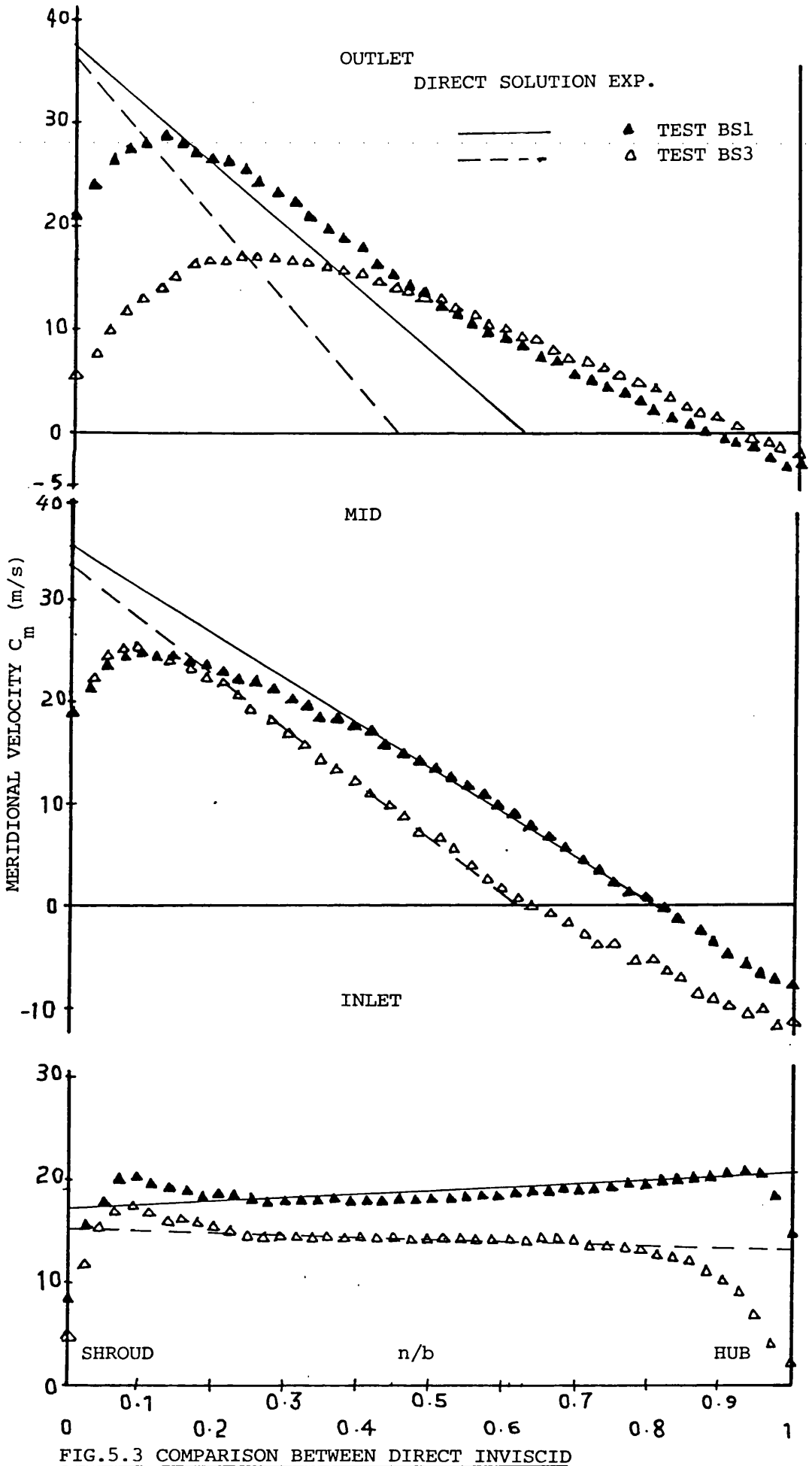

FIG.5.3 COMPARISON BETWEEN DIRECT INVISCID SOLUTION AND EXPERIMENTAL MERIDIONAL VELOCITY DISTRIBUTION TESTS BS1,BS3

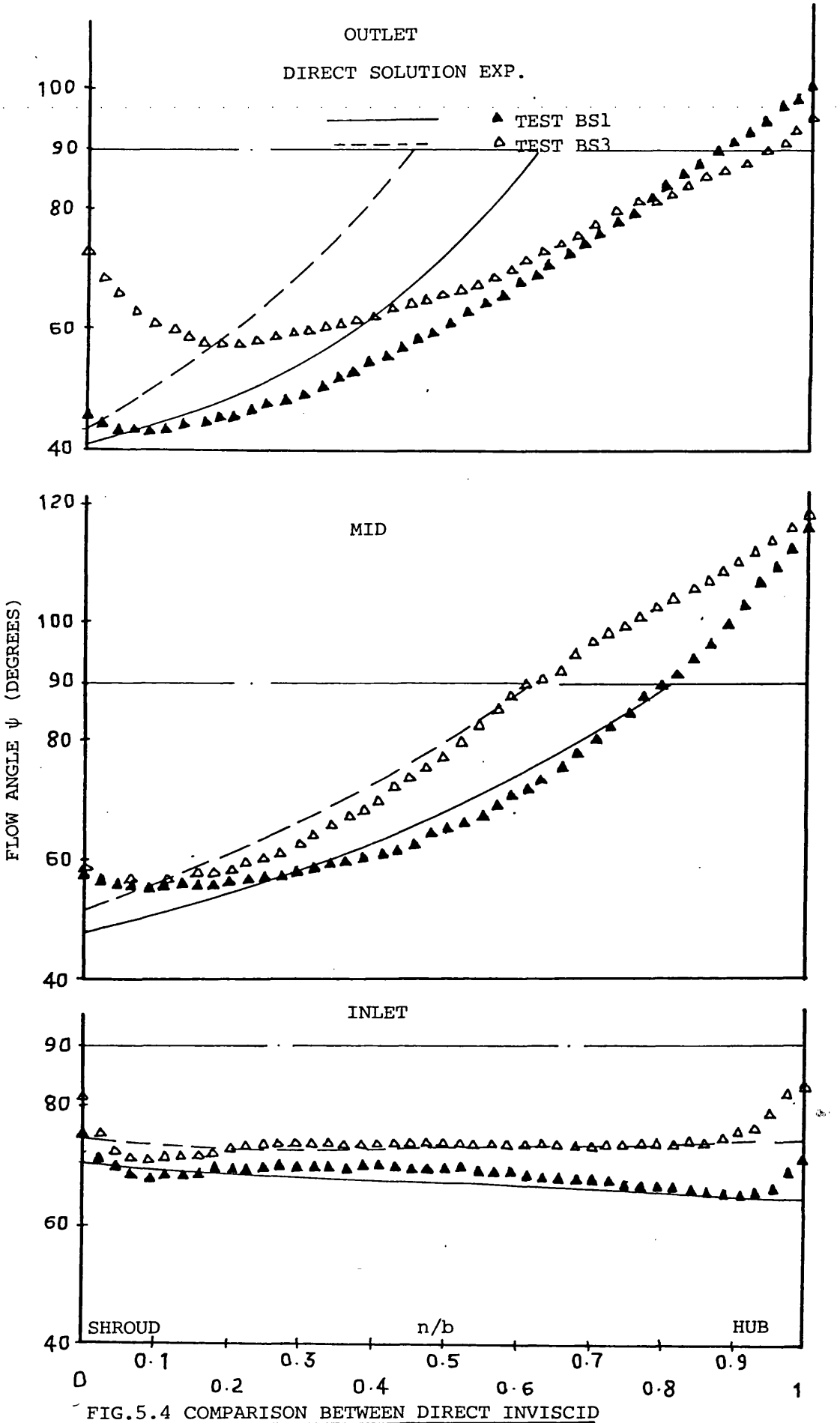

FIG.5.4 COMPARISON BETWEEN DIRECT INVISCID SOLUTION AND EXPERIMENTAL FLOW ANGLE DISTRIBUTION TESTS BS1, BS3

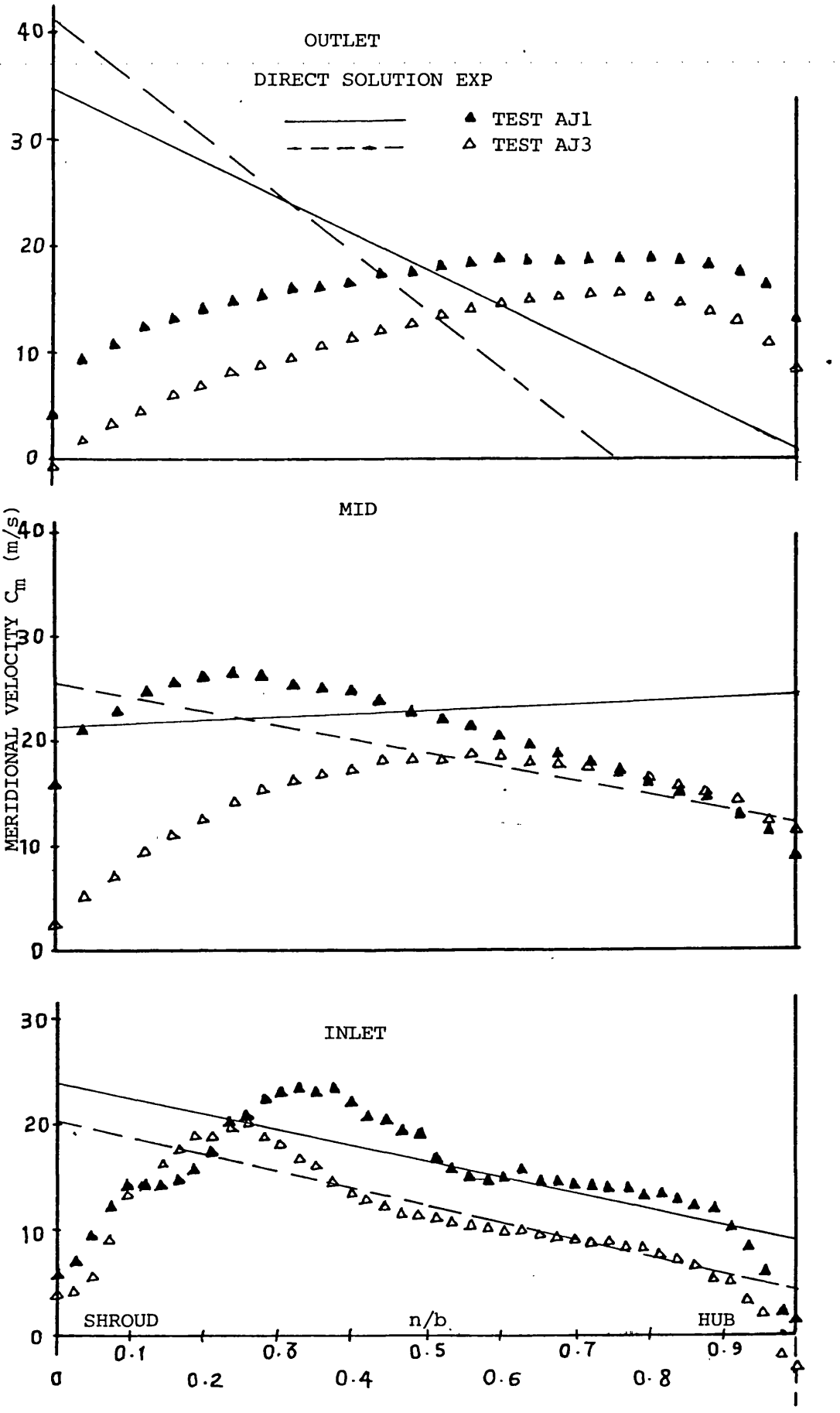

FIG.5.5 COMPARISON BETWEEN DIRECT INVISCID SOLUTION AND EXPERIMENTAL MERIDIONAL VELOCITY DISTRIBUTION TESTS AJ1,AJ3

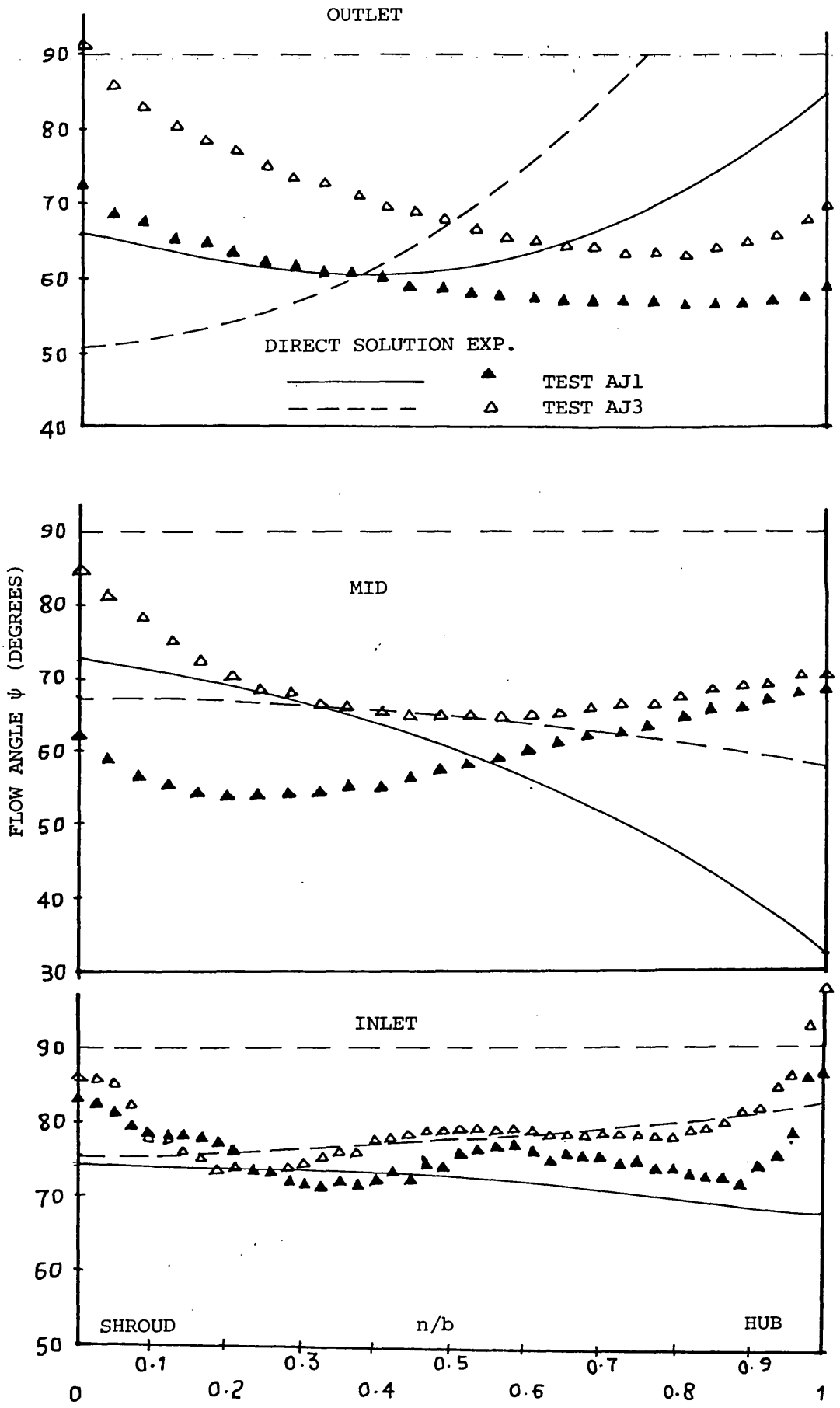

FIG.5.6 COMPARISON BETWEEN DIRECT INVISCID SOLUTION AND EXPERIMENTAL FLOW ANGLE DISTRIBUTION TESTS AJ1, AJ3

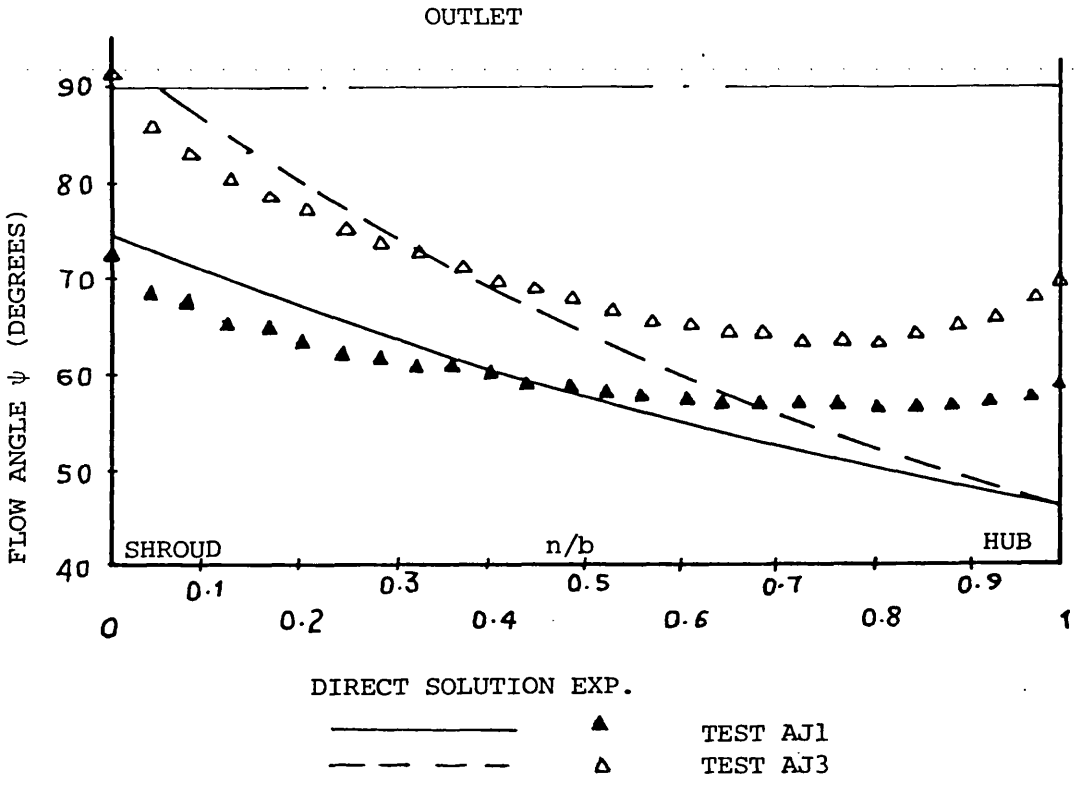

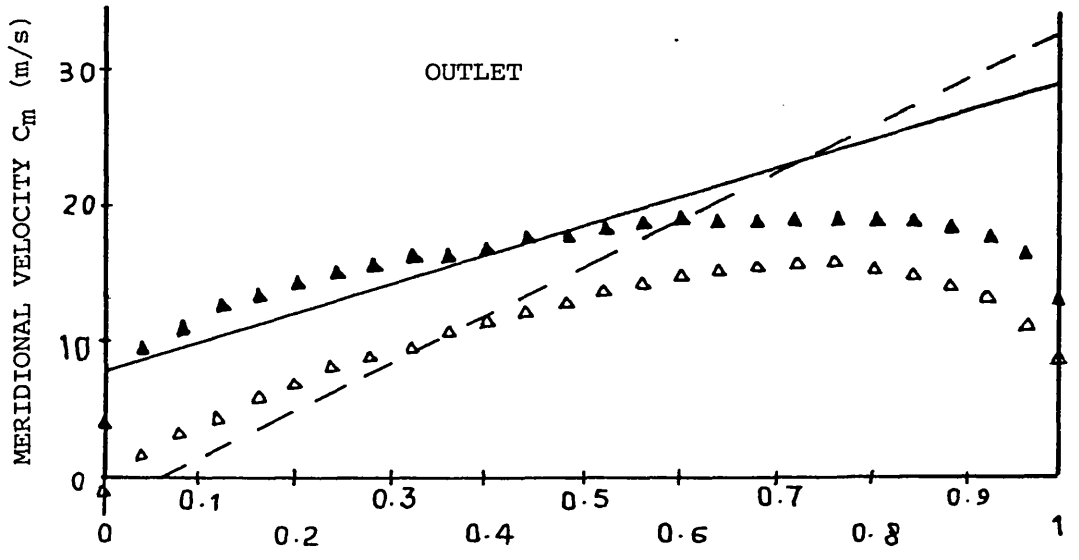

FIG.5.7 DIRECT INVISCID SOLUTION WITH MID MEASUREMENTS AS INITIAL CONDITIONS TESTS AJ1,AJ3

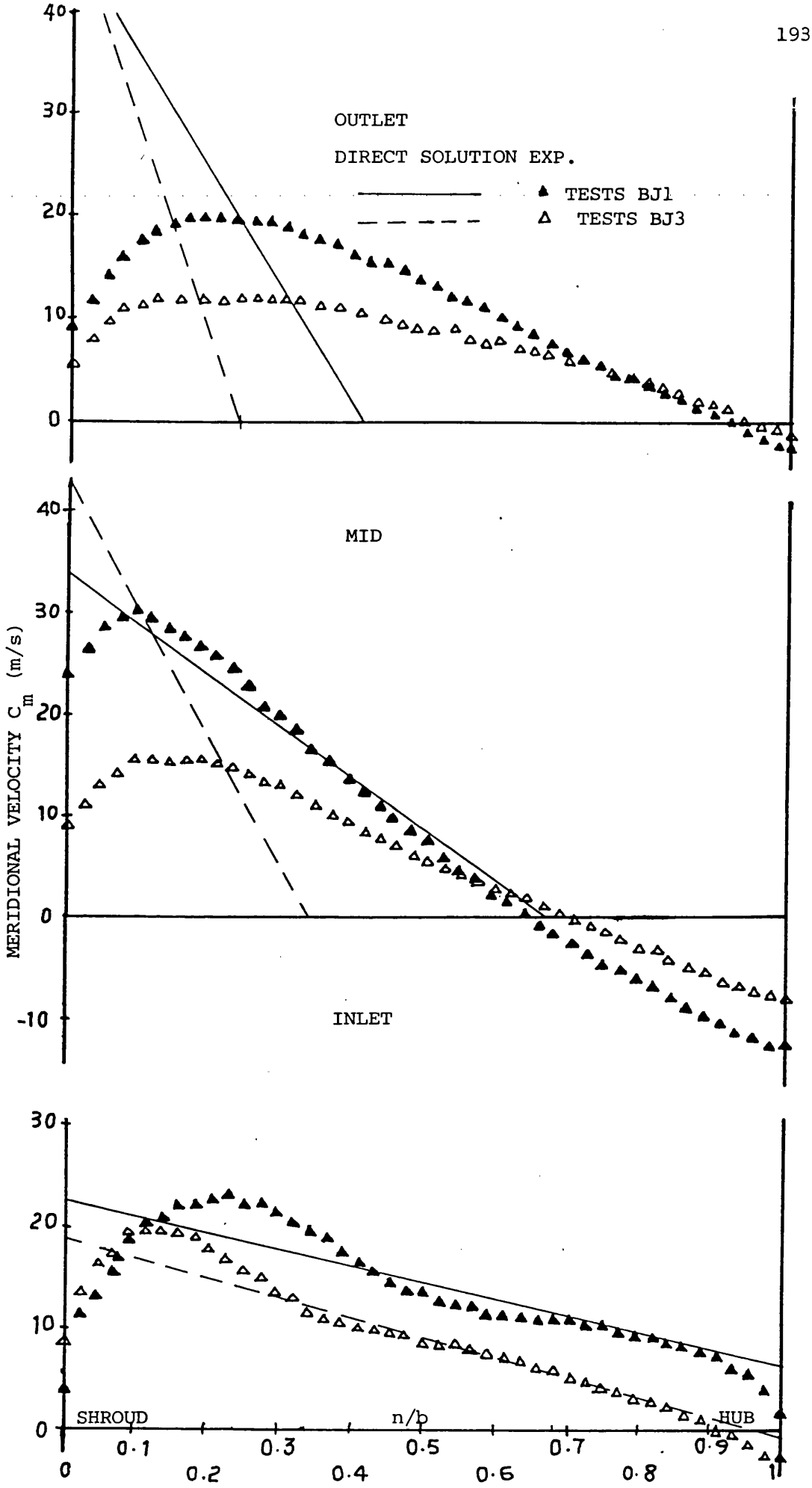

FIG.5.8 COMPARISON BETWEEN DIRECT INVISCID SOLUTION AND EXPERIMENTAL MERIDIONAL VELOCITY DISTRIBUTION TESTS BJ1,BJ3

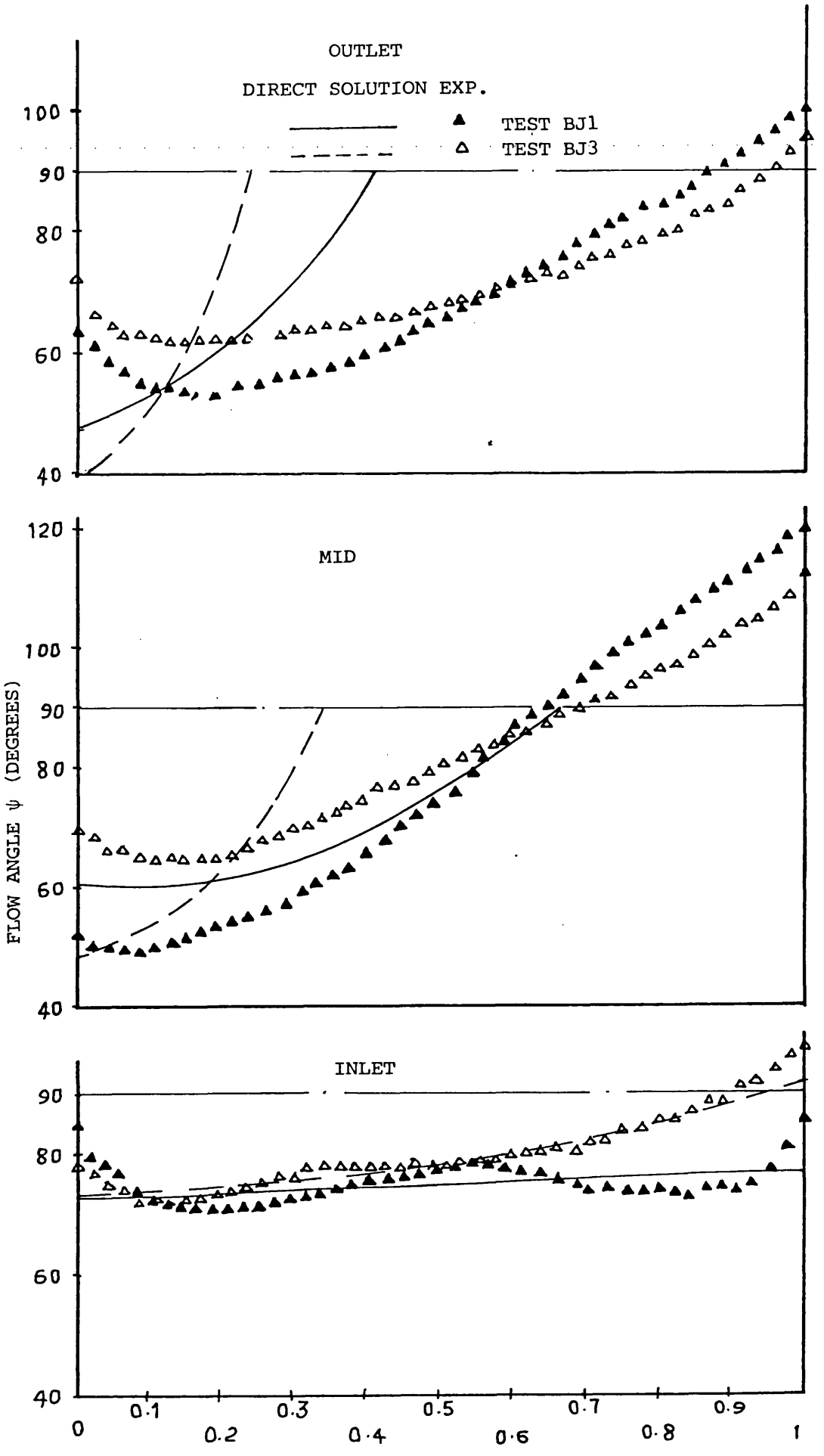

FIG.5.9 COMPARISON BETWEEN DIRECT INVISCID SOLUTION AND EXPERIMENTAL FLOW ANGLE DISTRIBUTION TESTS BJ1,BJ3

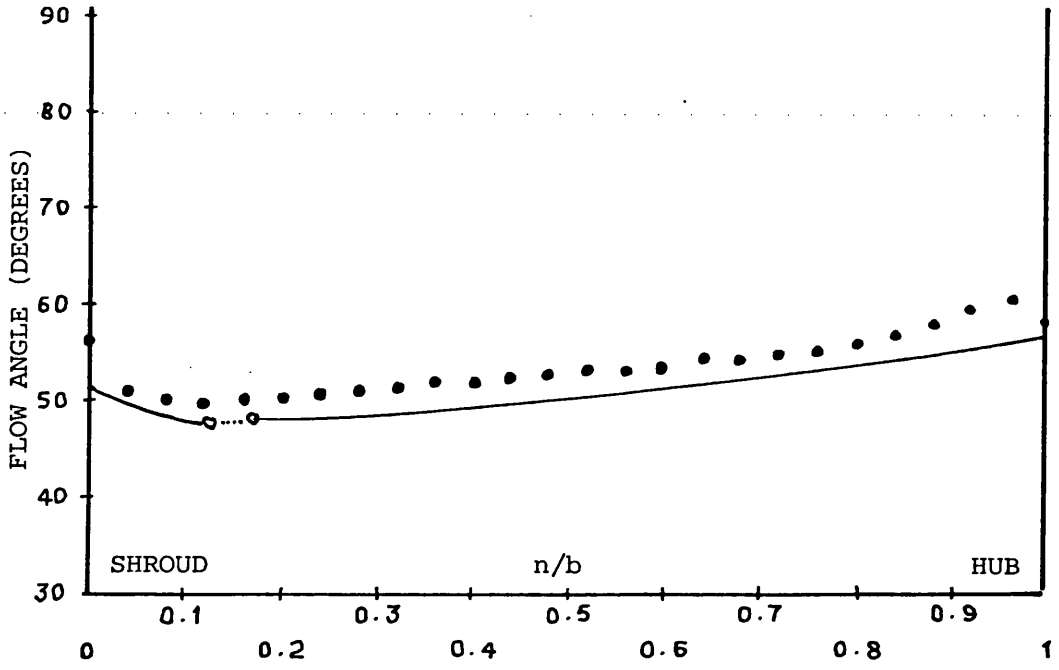

a. FLOW ANGLE DISTRIBUTION

B.L. CALCULATION

EXPERIMENTAL

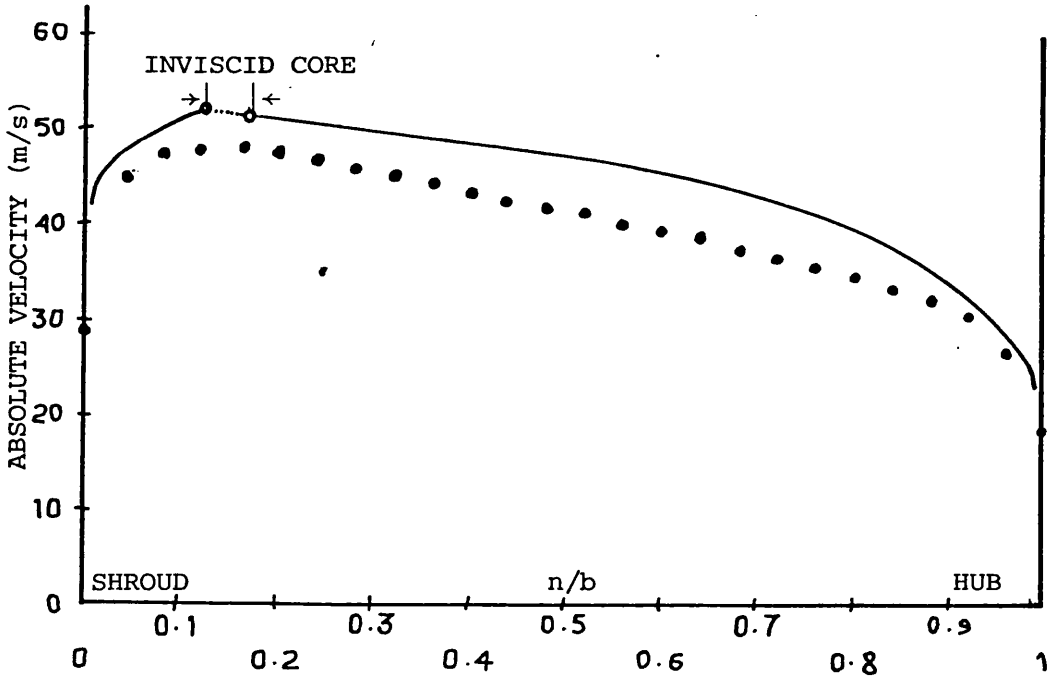

b. ABSOLUTE VELOCITY DISTRIBUTION

FIG. 5.10 BOUNDARY LAYER PREDICTION OF TEST AS1 AT MID TRAVERSE

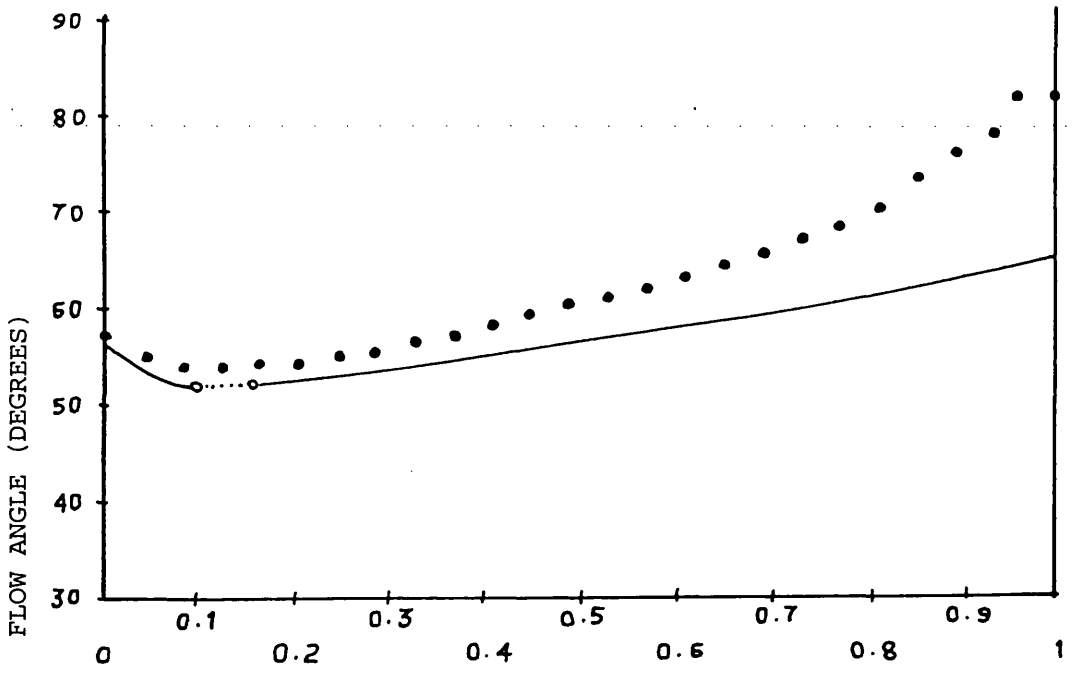

a. FLOW ANGLE DISTRIBUTION

B.L. CALCULATION

EXPERIMENTAL

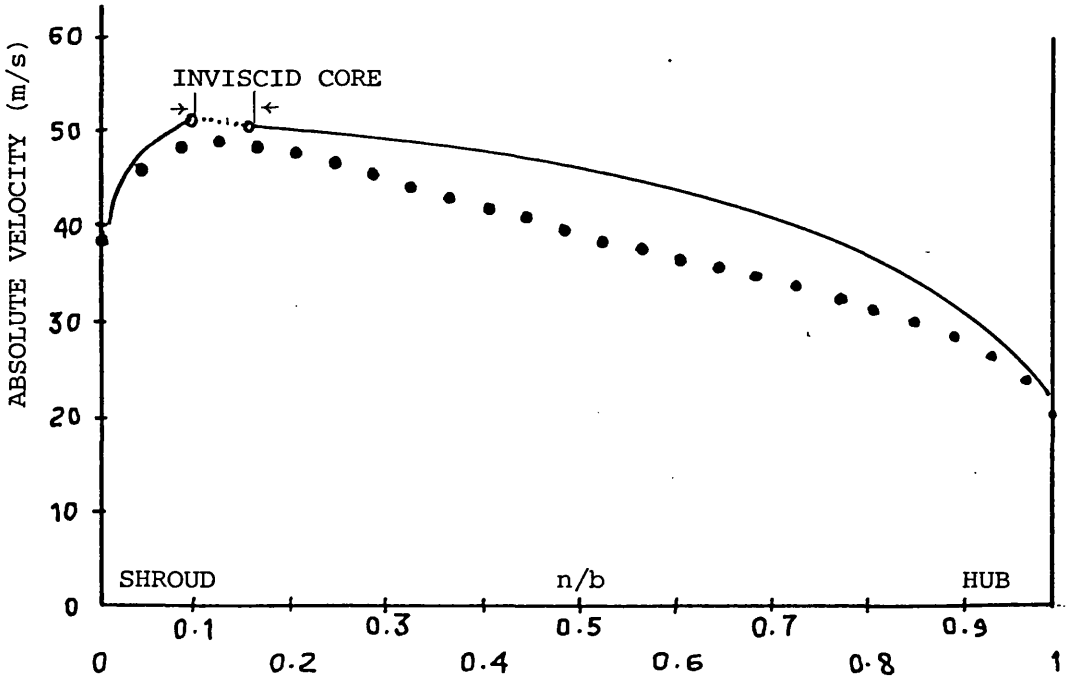

b. ABSOLUTE VELOCITY DISTRIBUTION

FIG.5.11 BOUNDARY LAYER PREDICTION OF TEST AS3 AT MID TRAVERSE

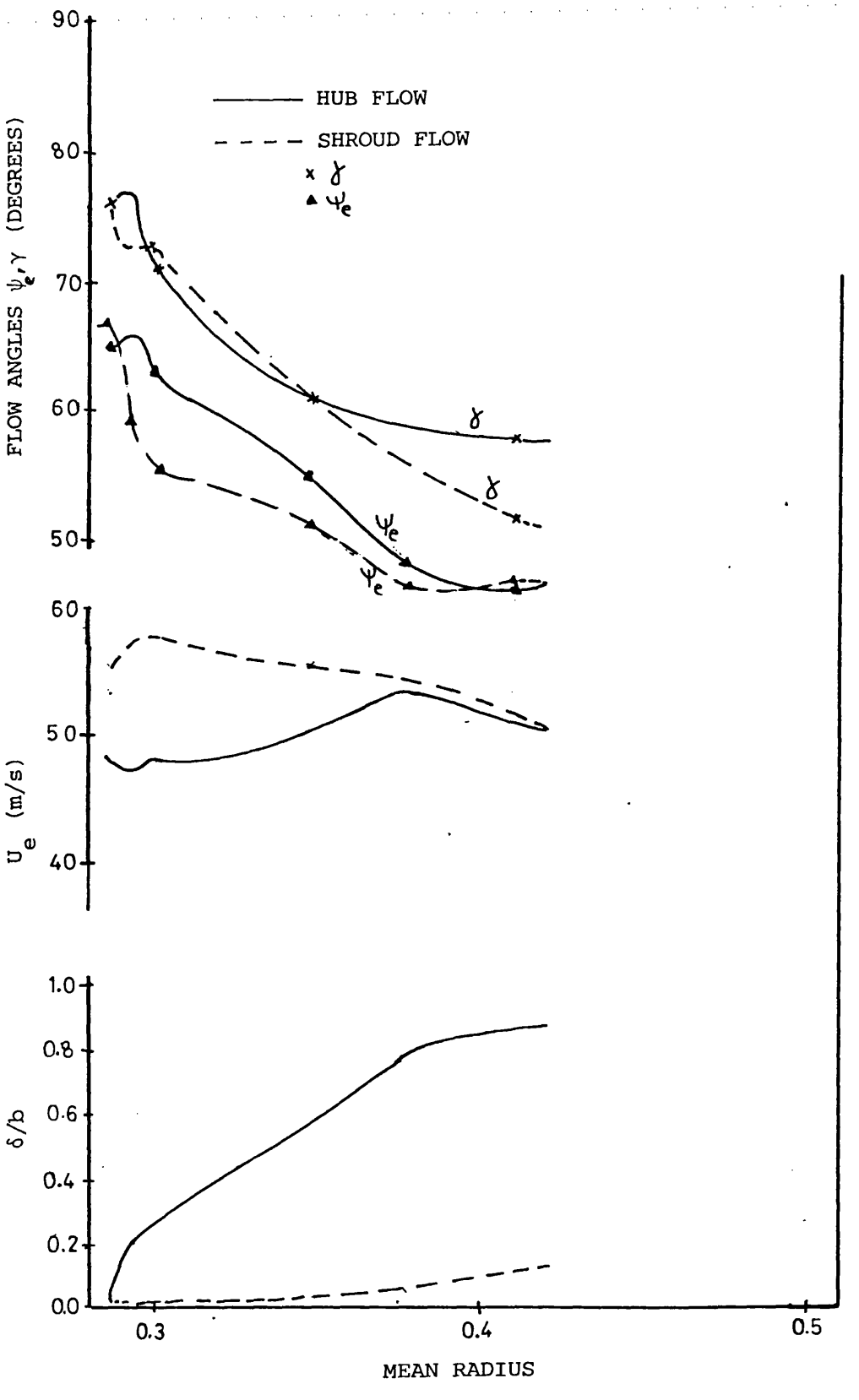

FIG. 5.12 BOUNDARY LAYER DEVELOPMENT IN CURVED DIFFUSER

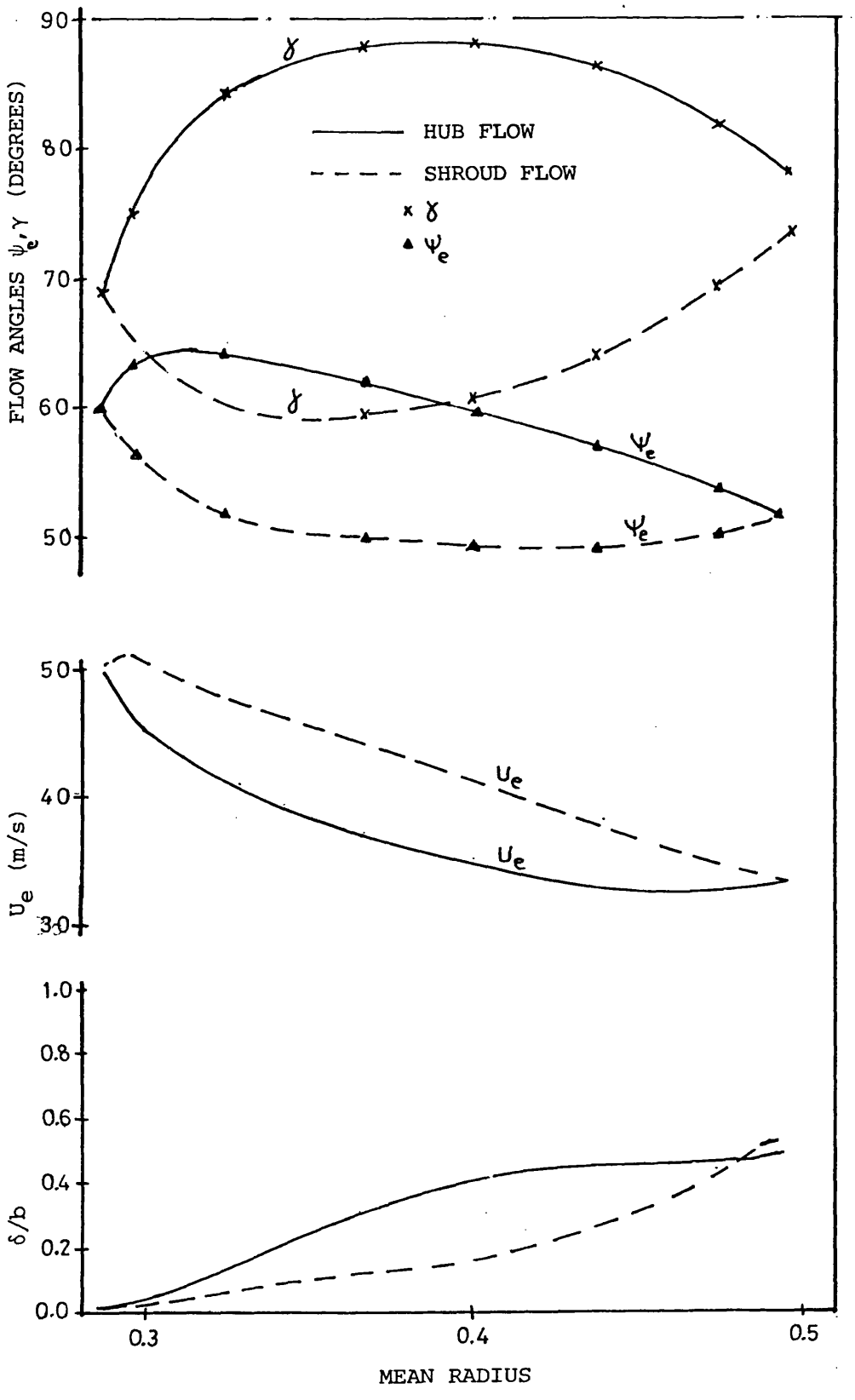

FIG.5.13 BOUNDARY LAYER DEVELOPMENT IN CONICAL DIFFUSER

CHAPTER 6 : CONCLUSIONS AND RECOMMENDATIONS

6.1 Conclusions

Of the two diffusers studied it has been clearly demonstrated that the curved diffuser is superior to the conical diffuser in both performance and stability. Various inlet flow conditions affected mainly the internal flow behaviour of the two diffusers but had a little effect on the overall performance. The introduction of the jet-wake flow pattern had little effect on the pressure recovery of the two diffusers. This suggests that the performance maps obtained under steady inlet conditions can be used as a guide for the design of the centrifugal compressor diffusers.

The conical diffuser exhibited a flow reversal on the hub surface which increased in depth and magnitude as the mass flow rate was reduced. At low mass flow rates the flow through the conical diffuser was very unsteady with a strong low frequency pulsations. This flow pulsation was accommpanied by flow reversal on the hub which extended from inlet to outlet of the diffuser. The pulsating flow is considered to be caused by a rotating stall of the type reported by Jansen (65). The introduction of the jet-wake flow pattern had little effect on the flow behaviour through the conical diffuser.

The curved diffuser, on the other hand, showed no reverse flow initially and only by reducing the flow rate was it possible to detect small areas of flow reversals on the hub surface. The introduction of the unsteady jet-wake flow significantly modified the flow pattern through the curved diffuser with the initial zone of reverse flow on the hub switching to the shroud surface at discharge. No flow pulsation was experienced nor was a flow reversal which extended from inlet to outlet on one wall detected at any test condition.

The flow behaviour after the point of separation showed common features through both of the diffusers tested of rotation of the energy and the angular momentum profile. For non-separated flow this phenomena was not observed.

The direct analytical solution of the inviscid flow equations has been

shown to agree well with other numerical methods despite its simplicity. The predicted results showed good agreement with those obtained experimentally. The points of separation could be well predicted but any predictions after separation were not satisfactory. The main reason for this is the inability of the inviscid flow analysis to predict the rotation of energy and angular momentum profiles. Because of the simplicity of this direct solution and its satisfactory performance up to the point of separation it can be applied to the assessment of diffuser design by studying the effect on flow behaviour of different geometric and inlet flow parameters. For example, the direct solution showed the beneficial effect of wall contraction and curvature on delaying separation. This simple solution also demonstrated clearly the major role played by the inlet gradients of energy and angular momentum in flow separation.

The simultaneous interactive boundary layer-inviscid core computation method gave reasonable prediction of unseparated flow and proved to be fast. However, the method needs further development to deal with more complicated flow situations which usually arise in real machines such as flow separation, variable flow wise and cross flow velocity profiles and flow after the boundary layer merged.

6.2 Recommendation for Future Work

The experimental work should be extended to include a straight radial diffuser typical of those used with centrifugal compressors. This will then complete the geometric range of diffusers commonly used. Due to the importance of the stability of the diffuser on the operating range of the compressor, the pulsating flow phenomenon encountered in the case of the conical diffuser needs to be fully investigated to reveal its nature and initiation. A study of the possibility of initiation of the same phenomenon in curved and radial diffuser will then establish a stability limit for each geometry and help to understand its causes. For this unsteady flow it will be essential to use rapid response instrumentation such as hot wire anemometries and at least two wall static pressure transducers.

Due to the importance of inlet gradients of energy and angular

momentum on flow behaviour inside annular diffusers, a test rig modification is needed to create different enthalpy gradients at inlet to study their effect. Any possible modifications in compressor design to give better overall stability and performance could then be developed. While model diffusers are helpful in developing understanding of their behaviour, it is necessary to move eventually from these models to direct studies of alternative turbocharger diffusers using more sophisticated instrumentation techniques such as hot-wire anemometers and Laser doppler velocimeters.

Due to the limitations and lack of generality of most boundary layer theoretical approaches, further consideration should be given to current developments in the direct solution of the Navier-Stokes equations using finite difference or finite element techniques. However, since it is not expected to obtain this full Navier-Stokes solution in the near future, further improving of the already existing boundary layer methods will still be helpful. The inclusion of the effects of wall curvature and an ability to accommodate separatedand re-attached flow in the boundary layer methods are main areas needing to be improved.

APPENDIX A

DERIVATION OF THE INVISCID FLOW EQUATIONS IN THE DIFFUSER

The equations of motion governing the inviscid flow in a vaneless diffuser in a fixed cylindrical co-ordinate system, r, θ, x (see Fig. A.1a) are :

$$\frac{dC_r}{dt} - \frac{C_\theta^2}{r} = -\frac{1}{\rho}\frac{\partial P}{\partial r} \qquad \text{A.1}$$

$$\frac{dC_\theta}{dt} + \frac{C_r . C_\theta}{r} = 0 \qquad \text{A.2}$$

$$\frac{dC_x}{dt} = -\frac{1}{\rho}\frac{\partial P}{\partial x} \qquad \text{A.3}$$

Assuming the flow to be steady and axisymmetric equations A.1, A.2 and A.3 become

$$C_r \frac{\partial C_r}{\partial r} + C_x \frac{\partial C_r}{\partial x} - \frac{C_\theta^2}{r} = -\frac{1}{\rho}\frac{\partial P}{\partial r} \qquad \text{A.4}$$

$$C_r \frac{\partial C_\theta}{\partial r} + C_x \frac{\partial C_\theta}{\partial x} + \frac{C_r C_\theta}{r} = 0 \qquad \text{A.5}$$

$$C_r \frac{\partial C_x}{\partial r} + C_x \frac{\partial C_x}{\partial x} = -\frac{1}{\rho}\frac{\partial P}{\partial x} \qquad \text{A.6}$$

By reference to the flow geometry fig. A.1a the following relations are obtained

$$C_r = C_m \sin = C_m \frac{\partial r}{\partial m} \qquad \text{A.7}$$

$$C_x = C_m \cos = C_m \frac{\partial x}{\partial m} \qquad \text{A.8}$$

where m refers to the meridional direction.

Introducing and expanding $\frac{dC_r}{dm}$, $\frac{dC_\theta}{dm}$ and $\frac{dC_x}{dm}$ and substituting from A.7 and A.8 the components of absolute velocity are related as follows

$$C_m \frac{dC_r}{dm} = C_r \frac{\partial C_r}{\partial r} + C_x \frac{\partial C_r}{\partial x} \qquad A.9$$

$$C_m \frac{dC_\theta}{dm} = C_r \frac{\partial C_\theta}{\partial r} + C_x \frac{\partial C_\theta}{\partial x} \qquad A.10$$

$$C_m \frac{dC_x}{dm} = C_r \frac{\partial C_x}{\partial r} + C_x \frac{\partial C_x}{\partial x} \qquad A.11$$

substituting these expressions into A.4, A.5 and A.6 yields

$$C_m \frac{dC_r}{dm} - \frac{C_\theta^2}{r} = -\frac{1}{\rho} \frac{\partial P}{\partial r} \qquad A.12$$

$$C_m \frac{dC_\theta}{dm} + \frac{C_r . C_\theta}{r} = 0 \qquad A.13$$

$$C_m \frac{dC_x}{dm} = -\frac{1}{\rho} \frac{\partial P}{\partial x} \qquad A.14$$

Equations A.7 and A.8 can be differentiated to yield.

$$C_m \frac{dC_r}{dm} = C_m \frac{d(C_m . \sin\alpha)}{dm} = C_m \left(C_m \cos\alpha \frac{d\alpha}{dm} + \sin\alpha \frac{dC_m}{dm}\right) \qquad A.15$$

$$C_m \frac{dC_x}{dm} = C_m \frac{d(C_m . \cos\alpha)}{dm} = C_m \left(- C_m \sin\alpha \frac{d\alpha}{dm} + \cos\alpha \frac{dC_m}{dm}\right) \qquad A.16$$

Substituting A.15, A.16 and A.17 into equations A.12 and A.14 and noting that the radius of curvature, R_c is defined by

$$\frac{d\alpha}{dm} = \frac{1}{R_c} \qquad A.17$$

leads to

$$\frac{C_m^2}{R_c} \cos\alpha + C_m \sin\alpha \frac{dC_m}{dm} - \frac{C_\theta^2}{r} = -\frac{1}{\rho} \frac{\partial P}{\partial r} \qquad A.18$$

$$-\frac{C_m^2}{R_c} \sin\alpha + C_m \cos\alpha \frac{dC_m}{dm} = -\frac{1}{\rho} \frac{\partial P}{\partial x} \qquad A.19$$

The pressure gradient normal to a streamline can be expressed by (see fig. A.1b)

$$\frac{1}{\rho}\frac{\partial P}{\partial n} = \frac{1}{\rho}\frac{\partial P}{\partial r}\cos\alpha - \frac{1}{\rho}\frac{\partial P}{\partial x}\sin\alpha \qquad \text{A.20}$$

substituting equations A.18 and A.19 into A.20 yields

$$\frac{1}{\rho}\frac{\partial P}{\partial n} = -\frac{C_m^2}{R_c}\cos^2\alpha - C_m \sin\alpha\cos\alpha\frac{dC_m}{dm} - \frac{C_m^2}{R_c}\sin^2\alpha + C_m\cos\alpha\sin\alpha\frac{dC_m}{dm} + \frac{C_\theta^2}{r}\cos\alpha$$

and hence

$$\frac{C_m^2}{R_c} - \frac{C_\theta^2}{r}\cos\alpha + \frac{1}{\rho}\frac{\partial P}{\partial n} = 0 \qquad \text{A.21}$$

The stagnation enthalpy can be expressed as

$$h_o = h + \frac{C^2}{2} \qquad \text{A.22}$$

By reference to fig. A.1a

$$C^2 = C_m^2 + C_\theta^2$$

Differentiating equation A.22 with respect to n gives :

$$\frac{dh_o}{dn} = \frac{dh}{dn} + C_m\frac{dC_m}{dn} + C_\theta\frac{dC_\theta}{dn} \qquad \text{A.23}$$

where $\frac{dh_o}{dm} = 0$ (adiabatic flow)

For isentropic flow of perfect gas

$$dh = \frac{dP}{\rho} \qquad \text{A.24}$$

Substituting equations A.23 and A.24 into equation A.21 gives

$$\frac{dC_m}{dn} = \frac{C_m}{R_c} - \frac{C_\theta}{C_m}\left(\frac{dC_\theta}{dn} + \frac{C_\theta}{r}\cos\alpha\right) + \frac{1}{C_m}\frac{dh_o}{dn} \qquad \text{A.25}$$

This is the main equation which must be solved to obtain the meridional velocity C_m as a function of the normal direction n. The tangential velocity component C_θ is derived through equation A.13, which when combined with equation A.7 yields

$$C_r \frac{dC_\theta}{dr} = -\frac{C_r . C_\theta}{r}$$

$$\frac{dC_\theta}{C} = -\frac{dr}{r}$$

hence

$$C_\theta\, r = \text{constant} = \lambda \qquad \text{A.26}$$

This final expression relates the tangential component of velocity C to the radius r by the free vortex relationship along a streamline.

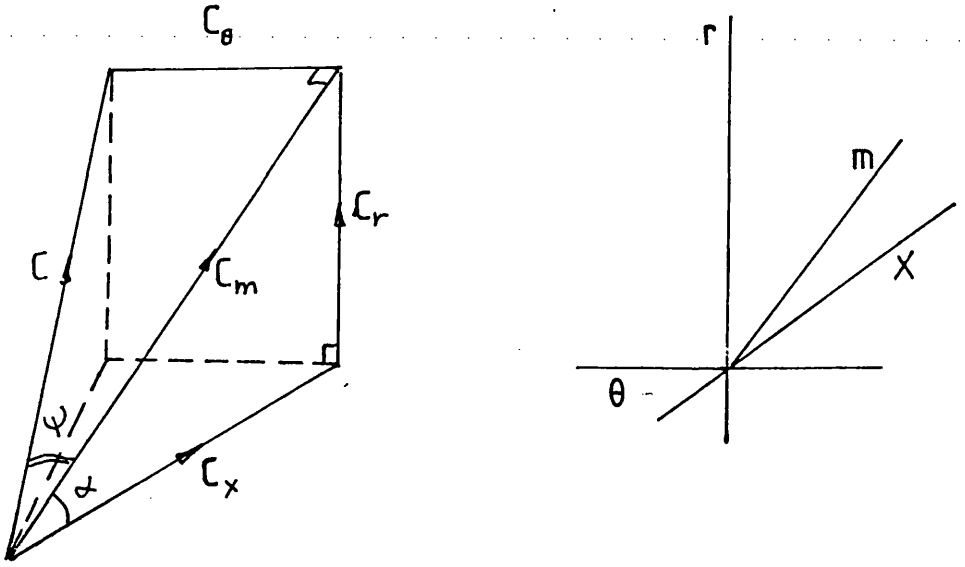

FIG. A.1a THREE DIMENSIONAL FLOW GEOMETRY

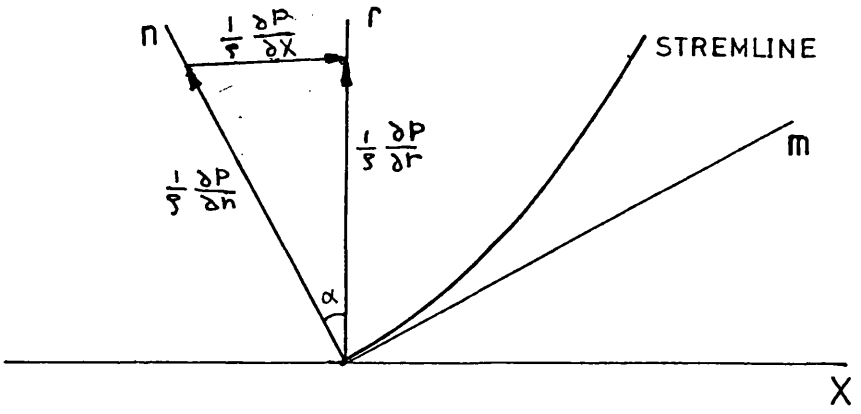

FIG. A.1b RELATION BETWEEN PRESSURE FORCE COMPONENTS

APPENDIX B

The Navier-Stokes Equations in Curvilinear Co-ordinates

The equation of motion of a fluid for steady incompressible flow is

$$\text{grad}\left(\frac{1}{2}\vec{V}^2\right) - \vec{V} \times \text{curl}\ \vec{V} = -\frac{1}{\rho}\,\text{grad}\ p + \nu\,\nabla^2\vec{V} \qquad \text{B.1}$$

where $\vec{V}$ is the vectorial velocity, and p the pressure

The continuity equation is

$$\text{div}\ \vec{V} = 0 \qquad \text{B.2}$$

For a general triply - orthogonal curvilinear coordinate system in which the coordinates of a point in space are X, Y, Z and h_1, h_2 and h_3 are the metrical coefficients, the length δs of a line element is given by :

$$(\delta S)^2 = (h_1\delta X)^2 + (h_2\delta Y)^2 + (h_3\delta Z)^2 \qquad (B.3)$$

If u, v and w are the velocity components in X, Y and Z directions, the continuity equation (B.2) becomes

$$\frac{1}{h_1h_2h_3}\left[\frac{\partial}{\partial X}(h_2h_3u) + \frac{\partial}{\partial Y}(h_3h_1v) + \frac{\partial}{\partial Z}(h_1h_2w)\right] = 0 \qquad (B.4)$$

The Navier-Stokes equations, which express the conservation of momentum in the X, Y, Z directions, are

$$\frac{\partial u}{\partial t} + \frac{u}{h_1}\frac{\partial u}{\partial x} + \frac{v}{h_2}\frac{\partial u}{\partial y} + \frac{w}{h_3}\frac{\partial u}{\partial Z} + \left(\frac{u}{h_1h_2}\frac{\partial h_1}{\partial Y} - \frac{v}{h_2h_1}\frac{\partial h_2}{\partial X}\right)v$$

$$+\left(\frac{u}{h_1h_3}\frac{\partial h_1}{\partial Z} - \frac{w}{h_3h_1}\frac{\partial h_3}{\partial X}\right)w + \frac{1}{h_1}\frac{\partial}{\partial X}\frac{P}{\rho} - \nu\,(\nabla^2\vec{V})_X = 0 \qquad (B.5)$$

$$\frac{\partial v}{\partial t} + \frac{u}{h_1}\frac{\partial v}{\partial X} + \frac{v}{h_2}\frac{\partial v}{\partial Y} + \frac{w}{h_3}\frac{\partial v}{\partial Z} + \left(\frac{v}{h_2h_3}\frac{\partial h_2}{\partial Z} - \frac{w}{h_3h_2}\frac{\partial h_3}{\partial Y}\right)w$$

$$+\left(\frac{v}{h_2h_1}\frac{\partial h_2}{\partial X} - \frac{u}{h_1h_2}\frac{\partial h_1}{\partial Y}\right)u + \frac{1}{h_2}\frac{\partial}{\partial Y}\frac{P}{\rho} - \nu(\nabla^2\vec{V})_Y = 0 \qquad (B.6)$$

$$\frac{\partial w}{\partial t} + \frac{u}{h_1}\frac{\partial w}{\partial X} + \frac{v}{h_2}\frac{\partial w}{\partial Y} + \frac{w}{h_3}\frac{\partial w}{\partial Z} + \left(\frac{w}{h_3 h_1}\frac{\partial h_3}{\partial X} - \frac{u}{h_1 h_3}\frac{\partial h_1}{\partial Z}\right) u$$

$$+\left(\frac{w}{h_3 h_2}\frac{\partial h_3}{\partial y} - \frac{v}{h_2 h_3}\frac{\partial h_2}{\partial Z}\right) v + \frac{1}{h_3}\frac{\partial}{\partial Z}\frac{P}{\rho} - \nu(\nabla^2 \vec{v})_Z = 0 \qquad (B.7)$$

where t = time P = pressure ρ = density

ν = kinematic viscosity

The viscosity terms $\nu(\nabla^2 \vec{v})_{X,Y,Z}$ are complicated and lengthy and in the interest of brevity they will be kept in their vector components.

The laplacian operator $\nabla^2$is defined by

$$\nabla^2 = \frac{1}{h_1 h_2 h_3}\left\{\frac{\partial}{\partial X}\left(\frac{h_2 h_3}{h_1}\frac{\partial}{\partial X}\right) + \frac{\partial}{\partial Y}\left(\frac{h_3 h_1}{h_2}\frac{\partial}{\partial Y}\right) + \frac{\partial}{\partial Z}\left(\frac{h_1 h_2}{h_3}\frac{\partial}{\partial Z}\right)\right\} \qquad (B.8)$$

with the following definitions

$$K_{11} = \frac{1}{h_1^2}\frac{\partial h_1}{\partial X} \qquad K_{21} = \frac{1}{h_2 h_1}\frac{\partial h_2}{\partial X} \qquad K_{31} = \frac{1}{h_3 h_1}\frac{\partial h_3}{\partial X}$$

$$K_{12} = \frac{1}{h_1 h_2}\frac{\partial h_1}{\partial Y} \qquad K_{22} = \frac{1}{h_2^2}\frac{\partial h_2}{\partial Y} \qquad K_{32} = \frac{1}{h_3 h_2}\frac{\partial h_3}{\partial Y} \qquad (B.9)$$

$$K_{13} = \frac{1}{h_1 h_3}\frac{\partial h_1}{\partial Z} \qquad K_{23} = \frac{1}{h_2 h_3}\frac{\partial h_3}{\partial Z} \qquad K_{33} = \frac{1}{h_3^2}\frac{\partial h_3}{\partial Z}$$

and the conditions of orthogonality of Lamé (91), the continuity and Navier-Stokes equations can be written as

$$\frac{1}{h_1}\frac{\partial u}{X} + \frac{1}{h_2}\frac{\partial v}{\partial Y} + \frac{1}{h_3}\frac{\partial w}{\partial Z} + (K_{21} + K_{31})u + (K_{32} + K_{12})v$$

$$+ (K_{13} + K_{23})w = 0 \qquad (B.10)$$

$$\frac{\partial u}{\partial t} + \frac{u}{h_1}\frac{\partial u}{\partial X} + \frac{v}{h_2}\frac{\partial u}{\partial Y} + \frac{w}{h_3}\frac{\partial u}{\partial Z} + (K_{12}u - K_{21}v)v +$$

$$(K_{13}u - K_{31}w)w + \frac{1}{h_1}\frac{\partial}{\partial X}\frac{P}{\rho} - \nu(\nabla^2\vec{V})_X = 0 \qquad \text{(B.11)}$$

$$\frac{\partial v}{\partial t} + \frac{u}{h_1}\frac{\partial v}{\partial X} + \frac{v}{h_2}\frac{\partial v}{\partial Y} + \frac{w}{h_3}\frac{\partial v}{\partial Z} + (K_{23}v - K_{32}w)w +$$

$$(K_{21}v - K_{12}u)u + \frac{1}{h_2}\frac{\partial}{\partial Y}\frac{P}{\rho} - \nu(\nabla^2\vec{V})_Y = 0 \qquad \text{(B.12)}$$

$$\frac{\partial w}{\partial t} + \frac{u}{h_1}\frac{\partial w}{\partial X} + \frac{v}{h_2}\frac{\partial w}{\partial Y} + \frac{w}{h_3}\frac{\partial w}{\partial Z} + (K_{31}w - K_{13}u)u +$$

$$(K_{32}w - K_{23}v)v + \frac{1}{h_3}\frac{\partial}{\partial Z}\frac{P}{\rho} - \nu(\nabla^2\vec{V})_Z = 0 \qquad \text{(B.13)}$$

For turbulent flow, the instantaneous values of the three component of velocity and of pressure may be written as

$$u + u', \quad v + v', \quad W + w' \text{ and } P + P',$$

where u, v, w and p are the time mean values and u', v', w' and P' are the turbulent fluctuations.

Introducing the mean and fluctuating components of velocity into the continuity equation (B.10), and time averaging, leads to the continuity equation of the mean flow which will be typically as equation (B.10) with u, v and w now as the time mean value since

$$\bar{u}' = \bar{v}' = \bar{w}' = \bar{P}' = 0$$

If this form (equation B.10) is subtracted from the equation obtained before the time averages are taken, then

$$\frac{1}{h_1}\frac{\partial u'}{\partial X} + \frac{1}{h_2}\frac{\partial v'}{\partial Y} + \frac{1}{h_3}\frac{\partial w'}{\partial Z} + (K_{21} + K_{31})u' + (K_{32} + K_{12})\,v'$$

$$+ (K_{13} + K_{23})w' = 0 \qquad \text{(B.14)}$$

If it is assumed that the Navier-Stokes equations remain valid at all instants of time, corresponding equations of mean motion for turbulent flow can be obtained by introducing the mean and fluctuating components of velocity and pressure into equations (B.11), (B.12) and (B.13), taking time average and using equation (B.14). The resultant equations for incompressible turbulent flow are :-

$$\frac{U}{h_1}\frac{\partial u}{\partial X} + \frac{v}{h_2}\frac{\partial u}{\partial Y} + \frac{w}{h_3}\frac{\partial u}{\partial Z} + (K_{12}u - K_{21}v)v + (K_{13}u - K_{31}w)w$$

$$+ \frac{1}{h_1}\frac{\partial}{\partial X}\left(\frac{P}{\rho} + \overline{u'^2}\right) + \frac{1}{h_2}\frac{\partial}{\partial Y}\left(\overline{u'v'}\right) + \frac{1}{h_3}\frac{\partial}{\partial Z}\left(\overline{u'w'}\right)$$

$$+ (2K_{12} + K_{32})\overline{u'v'} + (2K_{13} + K_{23})\,\overline{u'w'} + (K_{21} + K_{31})\overline{u'^2}$$

$$- K_{21}\,\overline{v'^2} - K_{31}\,\overline{w'^2} - \nu(\nabla^2\vec{V})_X = 0 \qquad \text{(B.15)}$$

$$\frac{u}{h_1}\frac{\partial v}{\partial X} + \frac{v}{h_2}\frac{\partial v}{\partial Y} + \frac{w}{h_3}\frac{\partial v}{\partial Z} + (K_{23}v - K_{32}w)w + (K_{21}v - K_{12}u)u$$

$$+ \frac{1}{h_1}\frac{\partial}{\partial X}\left(\overline{u'v'}\right) + \frac{1}{h_2}\frac{\partial}{\partial Y}\left(\frac{P}{\rho} + \overline{v'^2}\right) + \frac{1}{h_3}\frac{\partial}{\partial Z}\left(\overline{v'w'}\right) + (2\,K_{21} + K_{31})\overline{u'v'}$$

$$+ (2\,K_{23} + K_{13})\overline{v'w'} - K_{12}\,\overline{u'^2} + (K_{32} + K_{12})\overline{v'^2} - K_{32}\,\overline{w'^2} - \nu(\nabla^2\vec{V})_Y = 0$$

$$\text{(B.16)}$$

and

$$\frac{u}{h_1}\frac{\partial w}{\partial X} + \frac{v}{h_2}\frac{\partial w}{\partial Y} + \frac{w}{h_3}\frac{\partial w}{\partial Z} + (K_{31}w - K_{13}u)u + (K_{32}w - K_{23}v)v$$

$$+ \frac{1}{h_1}\frac{\partial}{\partial X}\left(\overline{u'w'}\right) + \frac{1}{h_2}\frac{\partial}{\partial Y}\left(\overline{u'w'}\right) + \frac{1}{h_3}\frac{\partial}{\partial Z}\left(\frac{P}{\rho} + \overline{w'^2}\right)$$

$$+ (2\,K_{31} + K_{21})\overline{u'w'} + (2\,K_{32} + K_{12})\,\overline{u'w'} - K_{13}\,\overline{u'^2} - K_{23}\,\overline{v'^2}$$

$$+ (K_{13} + K_{23})\,\overline{w'^2} - \nu(\nabla^2 V)_Z = 0 \qquad \text{(B.17)}$$

Equations (B.15), (B.16) and (B.17) are the equations for conservation

of mean flow momentum in turbulent incompressible flow in curvilinear coordinates system X, Y, Z. A full account of these equations with their viscous terms can be found in reference (91).

These equations are exact and involve besides the three mean velocity components and pressure another six additional unknowns, the Reynolds stresses namely, $\rho\overline{u'v'}$, $\rho\overline{u'w'}$, $\rho\overline{v'w'}$, $\rho\overline{u'^2}$, $\rho\overline{v'^2}$ and $\rho\overline{w'^2}$. The continuity condition and the three momentum equations are not sufficient to determine the mean flow and an exact mathematical solution is therefore impossible.

In order to close the system of mean flow equations, it becomes necessary to apply simplifying approximations to the equations and to introduce some empirical relations. One of the various approaches used to close the system of equations (B.14), (B.15) and (B.16) is the boundary layer approximation which is described in the following appendix and employed in a prediction method used in this thesis.

APPENDIX C

Derivation of the Momentum Integral Equations

C.1 Boundary Layer Equations

Starting from equations (B.14), (B.15) and (B.16) from the previous appendix and assuming that the boundary layer is thin compared with the principle radii of curvature of the body surface i.e. $\delta/R_c \ll 1$, and that the curvilinear co-ordinate y is to correspond identically with the physical distance from the body i.e. the metric coefficient h_2 can be set to unity, then applying an order of magnitude analysis to the equations derived in Appendix B, the following boundary layer equations can be developed

$$\frac{u}{h_1}\frac{\partial u}{\partial X} + v\frac{\partial u}{\partial Y} + \frac{w}{h_3}\frac{\partial u}{\partial Z} + (K_{13}u - K_{31}w)w + \frac{1}{h_1}\frac{\partial}{\partial X}\frac{P}{\rho} - \frac{\partial}{\partial Y}\left(\nu\frac{\partial u}{\partial Y} - \overline{u'v'}\right) = 0 \qquad (C.1)$$

$$\frac{\partial}{\partial Y}\left(\frac{P}{\rho} + \overline{v'^2}\right) = 0 \qquad (C.2)$$

$$\frac{u}{h_1}\frac{\partial w}{\partial X} + v\frac{\partial w}{\partial Y} + \frac{w}{h_3}\frac{\partial w}{\partial Z} + (K_{31}w - K_{13}u)u + \frac{1}{h_3}\frac{\partial}{\partial Z}\frac{P}{\rho} - \frac{\partial}{\partial X}\left(\nu\frac{\partial w}{\partial Y} - \overline{v'w'}\right) = 0 \qquad (C.3)$$

$$\frac{1}{h_1 h_3}\left(\frac{\partial}{\partial X}(h_3 u) + h_1 h_3\frac{\partial v}{\partial Y} + \frac{\partial}{\partial Z}(h_1 w)\right) - \frac{1}{h_1}\frac{\partial u}{\partial X} + \frac{\partial v}{\partial Y} + \frac{1}{h_3}\frac{\partial w}{\partial Z} + K_{31}u + K_{13}w = 0 \qquad (C.4)$$

A detailed account of this order of magnitude analysis applied to the Navier-Stokes equations is given in reference (91).

C.2 Momentum Integral Equations

The momentum integral equations were obtained by integrating equations (C.1), (C.2), and (C.3) with respect to Y from the wall (Y = O) to a point at the edge of the boundary layer in the potential flow (Y = δ).

By examining Equation (C.2), it can be seen that the static pressure variation across the boundary layer is of small order since the turbulence component $\overline{v'^2}$ was found from the order of magnitude analysis to be of small order, hence the static pressure across the boundary layer can be assumed to remain constant and equal to the value of static pressure of the potential flow at the boundary layer edge. This assumption is used to eliminate the pressure terms in the boundary layer equations by substituting for their values from the equations of motion at the boundary layer edge, where viscosity and turbulence has negligible effect and where the component of velocity v normal to the wall is negligible compared to the u and w components. Thus at the edge of the boundary layer equations (C.1), (C.2) and (C.3) simplify to

$$\frac{U_e}{h_1}\frac{\partial U_e}{\partial X} + \frac{W_e}{h_3}\frac{\partial U_e}{\partial Z} + (K_{13}\,U_e - K_{31}\,W_e)W_e + \frac{1}{h_1}\frac{\partial}{\partial X}\frac{P}{\rho} = 0 \qquad \text{(C.5)}$$

$$\frac{\partial}{\partial Y}\frac{P}{\rho} = 0 \qquad \text{(C.6)}$$

$$\frac{U_e}{h_1}\frac{\partial W_e}{\partial X} + \frac{W_e}{h_3}\frac{\partial W_e}{\partial Z} + (K_{31}\,W_e - K_{13}\,U_e)\,U_e + \frac{1}{h_3}\frac{\partial}{\partial Z}\frac{P}{\rho} = 0 \qquad \text{(C.7)}$$

Where a subscript e denotes conditions at the edge of the boundary layer.

Eliminating the pressure terms between equations (C.1) through (C.3) and (C.5) through (C.7) gives

$$\frac{U_e}{h_1}\frac{\partial U_e}{\partial X} + \frac{W_e}{h_3}\frac{\partial U_e}{\partial Z} + (K_{13}\,U_e - K_{31}\,W_e)W_e - \frac{u}{h_1}\frac{\partial u}{\partial X} - v\frac{\partial u}{\partial Y} - \frac{w}{h_3}\frac{\partial u}{\partial Z} - (K_{13}\,u - K_{31}\,w)w + \frac{\partial}{\partial Y}\left(\nu\frac{\partial u}{\partial Y} - \overline{u'v'}\right) = 0 \qquad \text{(C.8)}$$

$$\frac{U_e}{h_1}\frac{\partial W_e}{\partial X} + \frac{W_e}{h_3}\frac{\partial W_e}{\partial Z} + (K_{31} W_e - K_{13} U_e)U_e - \frac{u}{h_1}\frac{\partial w}{\partial X}$$

$$- v\frac{\partial w}{\partial Y} - \frac{w}{h_3}\frac{\partial w}{\partial Z} - (K_{31} w - K_{13} u)\, u + \frac{\partial}{\partial Y}\left(\nu\frac{\partial w}{\partial Y} - \overline{u'w'}\right) = 0 \qquad (C.9)$$

By multiplying the continuity equation (C.4) by $(U_e - U)$, adding it to equation (C.8), and then to equation (C.9) leads to

$$\frac{1}{h_1}\frac{\partial}{\partial X}\left[(U_e-u)u\right] + (U_e-u)\frac{1}{h_1}\frac{\partial U_e}{\partial X} - \left[\frac{\partial}{\partial Y}(uv)\right.$$

$$\left. - U_e\frac{\partial v}{\partial Y}\right] + \frac{1}{h_3}\frac{\partial}{\partial Z}\left[(U_e-u)w\right] + (W_e-w)\frac{1}{h_3}\frac{\partial U_e}{\partial Z}$$

$$+ K_{13}\left[(U_e-u)w + (W_e-w)u + (U_e-u)W_e\right]$$

$$+ K_{31}\left[(U_e-u)u - (W_e-w)w - (W_e-w)W_e\right] + \frac{\partial}{\partial Y}\left(\nu\frac{\partial u}{\partial Y} - \overline{u'v'}\right) = 0 \qquad (C.10)$$

and

$$\frac{1}{h_1}\frac{\partial}{\partial X}\left[(W_e-w)u\right] + (U_e-u)\frac{1}{h_1}\frac{\partial W_e}{\partial X} - \left[\frac{\partial}{\partial Y}\left(wv - W_e\frac{\partial v}{\partial Y}\right)\right]$$

$$+ \frac{1}{h_3}\frac{\partial}{\partial Z}\left[(W_e-w)w\right] + (W_e-w)\frac{1}{h_3}\frac{\partial W_e}{\partial Z}$$

$$+ K_{31}\left\{(W_e-w)u + (U_e-u)w - (W_e-w)U_e\right\} + K_{13}\left[(W_e-w)w - (U_e-u)u\right.$$

$$\left. - (U_e-u)U_e\right] + \frac{\partial}{\partial y}\left[\nu\frac{\partial w}{\partial y} - \overline{v'w'}\right] = 0 \qquad (C.11)$$

If the parametric curves Z = constant and X = constant on the surface of the body are chosen to coincide with the projections of the external flow streamlines on the surface and their orthogonal trajectories respectively (see fig. 2.13a) it follows that

$$W_e = 0, \qquad h_1 dX = dS, \qquad h_3 dZ = dN$$

substituting with the above relations into equations (C.10) and (C.11) and integrating with respect to Y from Y = 0 to Y = δ where

$v = 0 \qquad \overline{u'v'} = 0 \qquad$ at $Y = 0$

$v = 0 \qquad \overline{u'v'} = 0 \qquad$ at $Y = \delta$

incompressible momentum integral equations in streamline coordinates are obtained as

$$\frac{\partial}{\partial s}(U_e^2 \theta_{11}) + U_e \frac{\partial U_e}{\partial s} \delta_1^* + \frac{\partial}{\partial N}(U_e^2 \theta_{12})$$

$$+ U_e \frac{\partial U_e}{\partial Z} \delta_2^* + K_1 U_e^2 (\theta_{11} - \theta_{12})$$

$$+ K_3 U_e^2 (\theta_{21} + \theta_{12}) = \frac{\tau_{ws}}{\rho} \qquad \text{(C.12)}$$

and

$$\frac{\partial}{\partial S}(U_e^2 \theta_{21}) + \frac{\partial}{\partial N}(U_e^2 \theta_{22}) + U_e^2 K_1 (\theta_{21} + \theta_{12})$$

$$+ U_e^2 K_3 (\theta_{22} - \theta_{11}) + U_e^2 (K_1 \delta_2^* - K_3 \delta_1^*) = \frac{\tau_{wN}}{\rho} \qquad \text{(C.13)}$$

where

$K_1 = K_{31}$ and $K_3 = K_{13}$

$$\delta_1^* = \int_o^\delta (1 - \frac{u}{U_e})\, dy \qquad \theta_{21} = -\int_o^\delta \frac{uw}{U_e 2}\, dy$$

$$\delta_2^* = -\int_o^\delta \frac{w}{U_e}\, dy \qquad \theta_{22} = -\int_o^\delta \frac{w^2}{U_e 2}\, dy$$

$$\theta_{11} = \int_o^\delta \frac{u}{U_e}(1 - \frac{u}{U_e})\, dy$$

$$\theta_{12} = \int_o^\delta \frac{w}{U_e}(1 - \frac{u}{U_e})\, dy$$

Equations (C.12) and (C.13) are the principal momentum integral boundary layer equations to be solved in terms of the boundary layer parameters of boundary layer thickness δ and skew angle β providing that conditions at the boundary layer edge of velocity and flow angle are known and the flow wise and cross-flow velocity profiles are assured, together with an expression for wall shear stress. Equations (c.12) and (C.13) provide

the starting point in the approach of Davis (84) which is used in this thesis and given in details in section 2.6.

APPENDIX D

DIFFUSER PERFORMANCE IN SWIRLING FLOW

D.1 Introduction

The procedure presented by Sovran and Klomp (1) to account for ideal pressure recovery and actual pressure recovery on the basis of a kinetic energy approach was extended to swirling flow by Schneider (2) and Barbotin (22). In this appendix, Barbotin's approach is reviewed and the resultant equation used to estimate annular diffuser performance.

D.2 Ideal pressure recovery for uniform swirling flow

The definition of pressure recovery coefficient as a measure of diffuser performance is

$$C_p = \frac{P_2' - P_1'}{\frac{1}{2}\rho C_1'^2} \qquad D.1$$

In the case of swirling uniform flow, if the assumptions of incompressible and isentropic flow is made, it can be shown that the ideal pressure recovery coefficient is given by:-

$$C_{p_i} = \cos^2 \psi_1' \left(1 - \frac{1}{AR^2}\right) + \sin^2 \psi_1' \left(1 - \frac{1}{RR^2}\right) \qquad D.2$$

where AR = area ratio RR = radius ratio

Equation D.2 can be re-arranged in the form

$$C_{p_i} = \left(1 - \frac{1}{AR^2}\right) + \sin^2 \psi_1' \left(\frac{1}{AR^2} - \frac{1}{RR^2}\right) \qquad D.3$$

It can be seen that if the inlet swirl angle ψ_1' is zero, or if the diffuser has parallel walls i.e. AR = RR equation D.3 reduces to

$$C_{p_i} = 1 - \frac{1}{AR^2} \quad (\text{for } \psi_1' = 0° \text{ or } AR = RR) \qquad D.4$$

Equation D.3 is plotted in fig. D.1 for any swirl angle ψ_1. The abscissa represents the term $(1 - \frac{1}{RR^2})$ while the ordinate represents $(1 - \frac{1}{AR^2})$ i.e. they represent the radius ratio and the area ratio in non-linear scale. The rays constructed from the origin make an angle ψ_1 with the ordinate. A circle having its centre at the origin will represent a constant C_{p_i} equal to the radius. A specific diffuser performance C_{p_i} is represented by a curve connecting its area ratio (i.e. its C_{p_i} at $\psi = 0°$) with its radius ratio (i.e. its C_{p_i} at $\psi_1' = 90°$) through different C_{p_i} values for different $\psi 1'$. The ideal pressure recovery of that diffuser at a particular inlet flow angle is the length of the line measured from the origin to the intersection of its curve with the ray making that swirl angle with the ordinate. Line X-X for example represents a diffuser of AR = 3.0 and RR = 2.0.

From Fig. D.1 it can be seen that for typical centrifugal compressor discharge swirl angles, of the order of 70 degrees, the ideal pressure recovery coefficient C_{p_i}, cannot be significantly increased by increasing the area ratio for any fixed radius ratio.

D.3 Velocity distortion and actual pressure recovery for swirling non-uniform flow

In the case of a real flow, the velocity and the static pressure profiles can be non-uniform across the diffuser passage, and losses cannot be neglected, hence an expression had to be developed for the actual pressure recovery. In this case average values were used and since three conservation relations exist for mass, angular momentum, and energy, average velocity which will satisfy one relation will not necessarily satisfy the other two.

For the case of non-swirling flow Sovran and Klomp (1) used a kinetic energy flux coefficient α to allow for the difference caused by this averaging technique in the eenrgy equation. This is referred to as the kinetic energy approach.

For non-swirling flow the coefficient of kinetic energy flux α is

defined as :-

$$\alpha = \frac{1}{A} \frac{\int C^3 \, dA}{\bar{C}^3} \qquad D.5$$

where $\bar{C} = \frac{\dot{m}}{\rho A}$.

In the case of swirling flow, the angular momentum equation had to be satisfied as well. Barbotin (22) suggested averaging the meridional velocity component using the continuity equation to give

$$\bar{C}_m = \frac{1}{A} \int_A C_m \, dA \qquad D.6$$

and averaging the tangential velocity component using the conservation of angular momentum relation :-

$$\bar{C} = \frac{1}{\bar{R}A} \int_A r.C_\theta.C_m. \, dA \qquad D.7$$

where $\bar{R}$ = area average radius = $\frac{1}{A} \int_A r \, dA$

The mean flow angle is then given by

$$\bar{\psi} = \tan^{-1} \frac{\bar{C}_m}{\bar{C}_\theta} \qquad D.8$$

The coefficient of kinetic energy flux is given by

$$\alpha = \frac{1}{A} \frac{\int_A C^2.C_m.dA}{\bar{C}^2 \, \bar{C}_m} \qquad D.9$$

where $\bar{C}^2 = \bar{C}_m^2 + \bar{C}_\theta^2$ D.10

When flow distortions and losses are considered, the energy equation gives

$$\bar{P}_2' - \bar{P}_1' = \alpha_1' \tfrac{1}{2} \rho \bar{C}_1'^2 - \alpha_2' \tfrac{1}{2} \rho \bar{C}_2'^2 - (\bar{P}_{O1}' - \bar{P}_{O2}') \qquad D.11$$

which can be expanded as

$$\bar{P}_2' - \bar{P}_1' = \alpha_1' \rho \frac{\bar{C}_{m_1'}^2}{2} - \alpha_2' \rho \frac{\bar{C}_{m_2'}^2}{2} + \alpha_1' \rho \frac{\bar{C}_{\theta_1'}^2}{2} - \alpha_2' \rho \frac{\bar{C}_{\theta_2'}^2}{2}$$

$$- (\bar{P}_{O1}' - \bar{P}_{O2}') \qquad \text{D.12}$$

The pressure recovery coefficient is then given by

$$C_p = \frac{\bar{P}_2' - \bar{P}_1'}{\frac{1}{2}\rho \bar{C}_1'^2} = \alpha_1' \left(\frac{\bar{C}_{m_1'}}{\bar{C}_1'} \right)^2 \left[1 - \alpha_2'/\alpha_1' \left(\frac{\bar{C}_{m_2'}}{\bar{C}_{m_1'}} \right)^2 \right]$$

$$+ \alpha_1' \left(\frac{\bar{C}_{\theta_1'}}{\bar{C}_1'} \right)^2 \left[1 - \alpha_2'/\alpha_1' \left(\frac{\bar{C}_{\theta_2'}}{\bar{C}_{\theta_1'}} \right)^2 \right] - \bar{\omega} \qquad \text{D.13}$$

where $\bar{\omega} = \dfrac{\bar{P}_{O1}' - \bar{P}_{O2}'}{\frac{1}{2}\rho \bar{C}_1'^2}$ D.14

From equation D.6 and D.7

$$\frac{\bar{C}_{m_i}}{\bar{C}_{m_2'}} = AR \qquad \frac{\bar{C}_{\theta_1'}}{\bar{C}_{\theta_2'}} = \frac{\bar{R}_2'}{\bar{R}_1'} = \overline{RR}$$

Substituting in equation D.13 from the above relations together with equation D.8, equation D.13 becomes

$$C_p = \alpha_1' \cos^2 \bar{\psi}_1' \left[1 - \alpha_2'/\alpha_1' \frac{1}{AR^2} \right] + \alpha_2' \sin^2 \bar{\psi}_1' \left[1 - \alpha_2'/\alpha_1' \frac{1}{\overline{RR}} \right]$$

$$- \bar{\omega} \qquad \text{D.15}$$

if losses are ignored, then an expression for a non-uniform ideal pressure recovery coefficient is then

$$C_{p_{in}} = \alpha_1' \cos^2 \bar{\psi}_1' \left[1 - \alpha_2'/\alpha_1' \frac{1}{AR^2} \right] + \alpha_2' \sin^2 \bar{\psi}_1' \left[1 - \alpha_2'/\alpha_1' \frac{1}{\overline{RR}} \right]$$

D.16

Equation D.16 differs from equation D.2 by the introduction of the kinetic energy coefficients α_1' and α_2'. The pressure recovery

coefficient ideally attainable is then not only a function of the diffuser geometry but also the degree of flow distortion at inlet to the diffuser.

D.4 Measured Pressure Recovery

To calculate the actual or measured pressure recovery coefficient the static pressures and kinetic energy at inlet obtained from flow traverse were mass average, i.e.

$$(\bar{P}_1')_{\dot{m}} = \frac{1}{\dot{m}} \int_{A_1'} \rho \, P_1' \, C_{m_1'} \, dA \qquad \text{D.17}$$

$$(\bar{P}_2')_{\dot{m}} = \frac{1}{\dot{m}} \int_{A_2'} \rho \, P_2' \, C_{m_2'} \, dA \qquad \text{D.18}$$

$$\overline{KE}_{\dot{m}} = \frac{1}{\dot{m}} \int_{A_1'} \rho/2 \, C_1'^2 \, C_{m_1'} \, dA \qquad \text{D.19}$$

A measured pressure recovery coefficient is defined as

$$C_{p_m} = \frac{(\bar{P}_2')_{\dot{m}} - (\bar{P}_1')_{\dot{m}}}{\overline{KE}_{\dot{m}}} \qquad \text{D.20}$$

Wall pressure tappings provided another option for performance estimation. In this case the total pressure recorded by the probe was considered together with the mean static pressure of the two walls. In this case wall pressure based pressure recovery coefficient was defined as

$$C_{p_\omega} = \frac{\bar{P}_{2_\omega}' - \bar{P}_{1_\omega}'}{\bar{P}_{O_1}' - \bar{P}_{1_\omega}'} \qquad \text{D.21}$$

where

$$\bar{P}_{o_1}' = \frac{1}{\dot{m}} \int_{A_1'} \rho \, P_{O_1}' \, C_{m_1'} \, dA \quad , \quad \bar{P}_{i_\omega} = \frac{P_{hub} + P_{shroud}}{2} \quad (i=1,2)$$

D.5 Coefficient of Separation

During the execution of the experimental program a reversed flow condition was encountered. It was noted that this severe distortion was not reflected in certain cases in the value of the coefficient of kinetic energy flux (compare α at mid position test AS2 where no separation occurred and α at mid position test BJ3 where separation occupied 35% of diffuser width table 4.2). To indicate that sort of distortion and its extent a coefficient of separation K_s was defined as

$$K_s = \frac{\int_A C^2 |C_m| dA}{\int_A C^2 C_m dA} \qquad D.22$$

For non-separated flow $K_s = 1.0$ and $K_s > 1.0$ for separated flow. The K_s value will increase with an increase in separation.

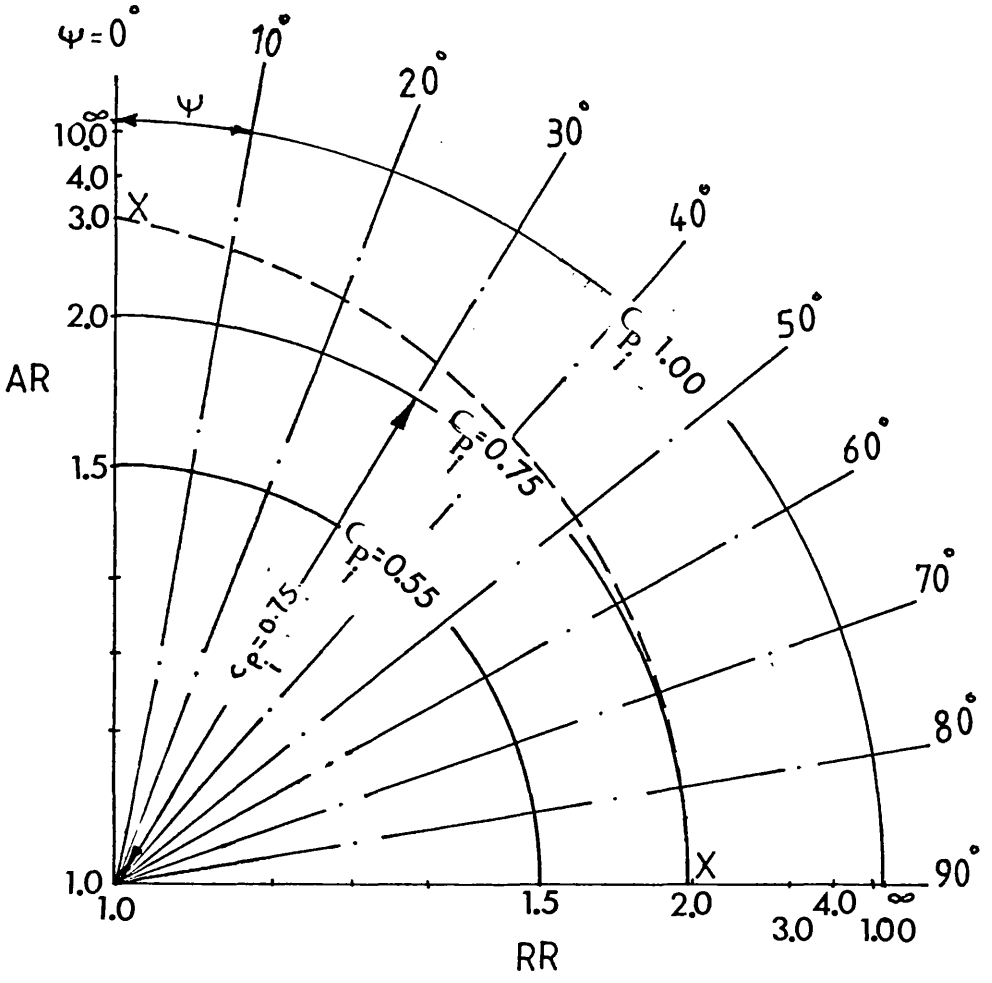

FIG. D.1. GRAPHICAL REPRESENTATION OF IDEAL PRESSURE RECOVERY RELATION (EQ. D.3)

REFERENCES

(1) Sovran, G., Klomp, E.D.
Experimentally Determined Optimum Geometries for Rectilinear Diffusers with Rectangular, Conical or Annular Cross-Section.
Fluid Mechanics of Internal Flow,
Sovran, G. Editor. Elsurier Publishing Co., 1967.

(2) Schneider, V.H.
Effect of Inlet Swirl on Annular Diffuser Performance
M.Sc. Thesis, University of Windsor, 1971.

(3) Wallace, F.J., Whitfield, A., Barbotin, D.
Experimental and Theoretical Evaluation of Flow Patterns in Curved Annular Diffusers.
Presented at the 1979 Israel Joint Gas Turbine Congress, Haifa, Israel.

(4) Reneau, L.R., Johnston, J.P., Kline, S.J.
Performance and Design of Straight, Two-Dimensional Diffusers.
Journal of Basic Engineering, March 1967 p.p. 141-150.

(5) Cockrell, D.J., Markland, E.
A Review of Incompressible Diffuser Flow.
Journal of Aircraft Engineering, Oct. 1963, p.p 286-292.

(6) Kline, S.J., Abbot, D.E., Fox, R.W.
Optimum Design of Straight Walled Diffusers.
Journal of Basic Engineering, Sept. 1959, p.p 321-331.

(7) McDonald, A.T., Fox, R.W.
An Experimental Investigation of Incompressible Flow in Conical Diffusers.
International Journal of Mechanical Science.
Vol. 8 1966 p.p 125-139.

(8) Runstadler, P.W., Dolan, F.X., Dean, R.C.
Diffuser Data Book
Creare Inc. Science and Technology, TN 186 May 1975.

(9) McDonald, A.T., Runstadler, P.W.Jr.
Behaviour of Diffusers with Distorted and Unsteady Inlet Conditions.
Fluid Dynamics of Unsteady Three-Dimensional and Separated Flows.
Proc. of a SQUID Workshop held at Georgia Institute of Technology June 1971 p.p 43-102.

(10) Howard, J.H.G., Henseller, H.J., Thornton-Trump, A.B.
Performance and Flow Regimes for Annular Diffusers.
ASME Paper 67-WA/FE-21

(11) Stevens, S.J., Fry, P.
Measurements of The Boundary-Layer Growth in Annular Diffusers.
Journal of Aircraft, Feb. 1973 p.p 73-80.

(12) Thayer, E.B.
Evaluation of Curved-Wall Annular Diffusers
ASME Paper 71-WA/FE-35

(13) Barina, F.J.
Comparative Performance of Two Vaneless Diffusers designed with Different Rates of Passage Curvature for Mixed-Flow Impellers.
NACA Technical Note No. 1490 Nov. 1947.

(14) Saki, T., Sanbe, M., Nakayama, T.
Experimental Study on Diffusers for Mixed-flow Machines.
ASME Paper 78-GT-120.

(15) Polyakov, V.Y., Bukatykh, A.F.
Calculation of Separation-free Vaneless Diffusers of Centrifugal Compressor Stages on a Digital Computer
Teploenergetika No.11 Nov. 1969 p.p 29-31
English Translation : Thermal Engineerinv Vol.16No.11 Nov. 1969, p.p 40-43.

(16) Brown, W.B., Bradshaw, G.R.
Method of Designing Vaneless Diffusers and Experimental Investigation of Certain Undetermined Parameters.
NACA Technical Note. No.1426 1947

(17) Sherstyuk, A.N., Kosmin, V.M.
The Effect of the Slope of Vaneless Diffuser Walls on the Characteristics of a Mixed-flow Compressor
Teploenergetika No. 8 Aug. 1969 p.p 77-80
English Translation : Thermal Engineering Vol.16 No.8 Aug. 1969 p.p 112-116

(18) Watson, N., Ingham, D.R.
Compressible Flow in a Radial Vaneless Diffuser
Symposium on Internal Flows, Apr. 1971
University of Salford, Paper 8.

(19) Volov, V.T., Shakhov, V.G.
Study of Radial Diffusers with Flow Swirl.
Soviet Aeronautics, Vol.21 No.3 1978, p.p 111-112

(20) Whitfield, A., Atkey, R.C., Wallace, F.J.
The Design and Performance of Vaneless Curved Annular Diffusers for Mixed Flow Turbocharger Compressors.
Presented at the 1979 Israel Joint Gas Turbine Congress, Haifa, Israel.

(21) Wallace, F.J., Atkey, R., Whitfield, A.
A Pseudo Three-Dimensional Analysis of Flows in Vaneless Diffusers for Mixed-Flow Compressors.
Journal of Mechanical Engineering Science Vol.17 No.6 1975 p.p 348-356

(22) Barbotin, D.
Experimental and Theoretical Evaluation of Flow Pattern in Curved Annular Diffusers.
M.Sc. Thesis Bath University 1977.

(23) Carlson, J.J., Johnston, J.P., Sagi, G.J.
Effects of Wall Shape on Flow Regimes and Performance in Straight Two-Dimensional Diffusers.
Journal of Basic Engineering, Mar. 1967 p.p 151-160.

(24) Fox, R.W., Kline, S.J.
Flow Regimes in Curved Subsonic Diffusers.
Journal of Basic Engineering, Sept. 1962 p.p 303-316

(25) Sagi, C.J., Johnston, J.P.
The Design and Performance of Two-Dimensional Curved Diffusers.
Journal of Basic Engineering, Dec. 1967 p.p 715-731.

(26) Waitman, B.A., Reneau, L.R., Kline, S.J.
Effects of Inlet Conditions on Performance of Two-Dimensional Subsonic Diffusers.
Journal of Basic Engineering, Sept. 1961 p.p 349-360.

(27) Moller, P.S.
A Radial Diffuser using Incompressible Flow between Narrowly Spaced Disks.
Journal of Basic Engineering, Mar. 1966 p.p 155-162.

(28) Coladipietro, R., Schneider, J.H., Sridhar, K.
Effects of Inlet Flow Conditions on the Performance of Equiangular Annular Diffusers.
CSME Paper No. 73-CSME-84.

(29) Bradshaw, P.
Performance of a Diffuser with Fully-Developed Pipe Flow at Entry.
Journal of the Royal Aeronautical Society, Vol. 67
Nov. 1963, p.p 733 -

(30) Cockrell, D.J., Markland, E.
The Effects of Inlet Conditions on Incompressible Fluid Flow through Conical Diffusers.
Journal of The Royal Aeronautical Society Vol.66
Jan. 1962 p.p 51-52.

(31) Johnston, J.P., Powers, C.A.
Some Effects of Inlet Blockage and Aspect Ratio on Diffuser Performance.
Journal of Basic Engineering, Sept. 1969 p.p 551-553.

(32) Eckert, T., Johnston, J.P., Simons, T.D., Mort, K.W., Page, V.R.
An Experimental Investigation of Two Large Annular Diffusers with Swirling and Distorted Inflow.
NASA Technical Paper 1628.
NACA Report N80-17984/9 Feb.1980.

(33) Tyler, R.A., Williamson, R.G.
Diffuser Performance with the Distorted Inflow New Line
Proceedings of the Institute of Mechanical Engineers
Vol. 2 No.4 Apr. 1961 p.p 251-266

(34) Masuda, S., Ariga, I., Watanabe, I.
On the Behaviour of Uniform Shear Flow in Diffusers and its Effect on Diffuser Performance.
Journal of Engineering for Power, Oct. 1971 p.p 377 - 385

(35) Quinn, B.
The Decay of Highly Skewed Flows in Ducts.
Journal of Engineering for Power, Jan. 1975, p.p 85-92.

(36) Viets, H.
Directional Effects in 3-D Diffusers.
AIAA Journal, Vol.13 No. Jan. 1975, p.p 823-825

(37) Ellis, G.O.
A Study of Induced Vorticity in Centrifugal Compressors.
Journal of Engineering for Power, Jan. 1964, p.p 63-76.

(38) Rebernik, B.
Investigation on Induced Vorticity in Vaneless Diffusers of Radial Flow Pumps.
Proc. of the Fourth Conference on Fluid Machinery,
Budapest 1972. p.p 1129 - 1140.

(39) Williams, G.J.
The Influence of Inlet Conditions on the Boundary Layer Growth and Overall Performance of Annular Diffusers.
Ph.D. Thesis, Loughborough University of Technology. Aug. 1972.

(40) Klein, A., Pucher, P., Rohlffs, M.
The Effect of Blade-Wakes on the Performance of Short Dump-Diffuser Type Combustor Inlets.
Journal of Fluids Engineering 1980, p.p 236-241.

(41) Wolf, S., Johnston, J.P.
Effects of Non-uniform Inlet Velocity Profiles on Flow Regimes and Performance in Two-Dimensional Diffusers.
Journal of Basic Engineering, Sept. 1969 p.p 462-474.

(42) Kaiser, K.F., McDonald, A.T.
Effect of Wake-Type Non-uniform Inlet Velocity Profiles on First Appreciable Stall in Plane-Wall Diffusers.
Journal of Fluids Engineering, Sept. 1980, p.p 283-288

(43) Hoadley, D.
Three-Dimensional Turbulent Boundary Layers in an Annular Diffuser.
Ph.D. Thesis, University of Cambridge, Feb. 1970.

(44) Srinath, T.
An Investigation of the Effect of Swirl on the Flow Regimes and Performance of Annular Diffusers with Equal Inner and Outer Cone Angle.
M.Sc. Thesis, University of Waterloo, July 1969.

(45) Kumar, D.S., Kumar, K.L.
Effect of Swirl on Pressure Recovery in Annular Diffusers.
Journal of Mechanical Engineering Science, Vol.22 No. 6
1980, p.p 305-313

(46) Jansen, W.
Steady Fluid Flow in a Radial Vaneless Diffuser.
Journal of Basic Engineering, Sept. 1964, p.p 607-619.

(47) James, R.C.
Swirl Flow in a Radial Vaneless Diffuser.
M.Sc. Thesis, University of Waterloo 1970.

(48) Japikse, D., Pampreen, R.
Annular Diffuser Performance for an Automotive Gas Turbine.
ASME Paper No. 78-GT-147.

(49) Gardow, E.B.
The Three-Dimensional Turbulent Boundary Layer in a Free Vortex Diffuser.
Gas Turbine Laboratory Report No. 42, Massachusetts Institute of Technology, Jan. 1958.

(50) Lohman, R.P., Markowski, S.J., Brookman, E.T.
Swirling Flow through Annular Diffusers with Conical Walls.
Journal of Fluids Engineering, Vol.101 June 1979, p.p 224-229

(51) Honami, S., Tsukagoshi, K., Sakai, T., Watanabe, I.
Investigation concerning the Fluid Flow in the Mixed-Flow Diffuser.
ASME Paper 71-GT-40.

(52) McDonald, A.T., Fox, R.W., Van Dewcestine, R.V.
Effects of Swirling Inlet Flow on Pressure Recovery in Conical Diffusers.
AIAA Journal, Vol.9 Oct. 1971, p.p2014-2018.

(53) Neve, R.S., Wirasinghe, N.E.A.
Change in Conical Diffuser Performance by Swirl Addition.
Aeronautical Quarterly, Aug. 1978, p.p131-143.

(54) Senoo, Y., Kawaguchi, N., Nagata, T.
Swirl Flow in Conical Diffusers.
Bull. of JSME, Vol.21 No.151, Jan.1975 p.p 112-119

(55) Dean, R.C., Senoo, Y.
Rotating Wakes in Vaneless Diffusers.
Journal of Basic Engineering, Sept. 1960, p.p 563-574.

(56) Johnson, J.P., Dean, R.C., Jr.
Losses in Vaneless Diffusers of Centrifugal Compressors and Pumps. Analysis, Experimental and Design.
Journal of Engineering for Power, Jan. 1966, p.p 49-62.

(57) Inoue, M.
Radial Vaneless Diffusers : A Re-examination of the Theories of Dean and Senoo and of Johnston and Dean.
ASME Paper 78-GT-186

(58) Inoue, M., Cumpsty, N.A.
Small Perturbation Analysis of Non-uniform Rotating Disturbances in a Vaneless Diffuser.
Journal of Engineering for Power, Oct. 1978, Vol.100 p.p 711-721

(59) Baade, K.H.
Unsteady Flow in the Vaneless Diffuser of a Radial Compressor Stage.
Proceedings of The Fourth Conference on Fluid Machinery, Budapest 1972. p.p 115-128.

(60) Mates, R.E.
Three-Dimensional Flow in the Diffuser of a Mixed Flow Compressor.
Ph.D. Thesis, Cornell University, Jan. 1963.

(61) Eckardt, D.
Instantaneous Measurements in the Jet-Wake Discharge Flow of a Centrifugal Compressor Impeller.
Journal of Engineering for Power, July 1975. p.p 337-346.

(62) Baghdadi, S.
The Effect of Rotor Blade Wakes on Centrifugal Compressor Diffuser Performance - A Comparative Experiment.
Journal of Fluids Engineering, Mar. 1977, p.p 45 - 52.

(63) Adenubi, S.O.
Performance and Flow Regime of Annular Diffusers with Axial Turbomachine Discharge Inlet Conditions.
Journal of Fluids Engineering, June 1976, p.p 236 - 243.

(64) Senoo, Y., Ishida, M.
Behaviour of Severely Asymmetric Flow in a Vaneless Diffuser.
Journal of Engineering for Power, July 1975, p.p 375 - 387.

(65) Jansen, W.
Rotating Stall in a Radial Vaneless Diffuser.
Journal of Basic Engineering, Dec. 1964, p.p 750 - 758.

(66) Abelhamid, A.N., Colwill, W.H., Harrows, J.F.
Experimental Investigation of Unsteady Phenomena in Vaneless Radial Diffusers.
Journal of Engineering for Power, Vol.101 Jan. 1979, p.p 52-60

(67) Imaichi, K., Tsurusaki, H.
Rotating Stall in Vaneless Diffuser of a Centrifugal Fan.
Proc. of ASME Annular Meeting, Dec. 1979, p.p 23-31.

(68) Abdelhamid, A.N., Bertrand, J.
Distinction between two Types of Self-Excited Gas Oscillations in Vaneless Radial Diffusers.
Canadian Aeronautics and Space Journal, Vol.26 No.2
Second Quarter 1980, p.p 105-117

(69) Senoo, Y., Kinoshita, Y.
Limits of Rotating Stall and Stall in Vaneless Diffuser of Centrifugal Compressors.
ASME Paper 78-GT-19.

(70) Abdelhamid, A.N.
Analysis of Rotating Stall in Vaneless Diffusers of Centrifugal Compressors.
Canadian Aeronautical and Space Journal, Vol.26 No.2
Second Quarter 1980, p.p 118-128

(71) Runstadler, P.W.,Jr., Dolan, F.X.
Further Data on the Pressure Recovery Performance of Straight-Channel, Plane-Divergence Diffusers at High Subsonic Mach Numbers.
Journal of Fluids Engineering Sept.1973, p.p 373-384.

(72) Runstadler, P.W.,Jr., Dean, R.C.,Jr.
Straight-Channel Diffuser Performance at High Inlet Mach Numbers.
Journal of Basic Engineering, Sept. 1969, p.p 397-422.

(73) Stevens, S.J., Williams, G.J.
The Influence of Inlet Conditions on the Performance of Annular Diffusers.
Journal of Fluids Engineering, Sept. 1980, Vol.102,
p.p 357-363.

(74) Bradley, C.I., Cockrell, D.J.
The Response of Diffusers to Flow Conditions at their Inlet.
Proc. Symp. on Internal Flows, Salford University,
Paper 5, p.p A32 - A41.

(75) Norbury, J.F.
Some Measurements of Boundary-Layer Growth in a Two-Dimensional Diffuser.
Journal of Basic Engineering, Sept. 1959, p.p 285-296.

(76) Livesey, J.L., Turner, J.T.
The Dependence of Diffuser Performance upon Inlet Flow Conditions.
Journal of the Aero.Soc. Vol.69, Nov. 1965, p.p 794-795.

(77) Davis, W.R., Millar, O.A.J.
A Comparison of the Matrix and Streamline Curvature Methods of Axial Turbomachinery Analysis from Allser's Point of View.
Journal of Engineering for Power, Oct. 1975, p.p 549-560.

(78) Marsh, H.
A Digital Computer Program for the Through-Flow Fluid Mechanics in an Arbitrary Turbomachine, using a Matrix Method.
N.G.T.E. Report No. R282 A.R.C.R. & M.3509 1968.

(79) Hirsch, C.H., Warzee, G.
A Finite Element Method for Through-Flow Calculations in Turbomachines.
Journal of Fluids Engineering, Sept. 1976, p.p 403 - 421.

(80) Bammert, K., Rautenberg, M., Wittekindt, W.
Vaneless Diffuser Flow with extremely distorted Inlet Profile.
ASME Paper No. 78-GT-47.

(81) Senoo, Y., Kinoshita, Y., Ishida, M.
Asymmetric Flow in Vaneless Diffusers of Centrifugal Blowers.
Journal of Fluids Engineering, Mar. 1977, p.p 104 - 112.

(82) Atkey, R.
Computer Aided Design of Radial and Mixed Flow Compressors.
Ph.D. Thesis, University of Bath, 1975.

(83) Voorde, C.B.v.d., Bos, J.
Measurement and Calculated Turbulent Boundary Layer Flow in a Vaneless Radial Diffuser.
AGARD-AG-164 Boundary Layer Effects in Turbomachines,
Institute T.N.O. for Mechanical Constructions, Delft Paper II-2
p.p 293-310.

(84) Davis, W.R.
Three-Dimensional Boundary-Layer Computation on the Stationary End-Walls of Centrifugal Turbomachinery.
Journal of Fluids Engineering, Sept. 1976, p.p 431-442.

(85) Kawaguchi, T., Furuya, Y.
The Rotating Flows in a Vaneless Diffuser having two Parallel Discs.
Bull. of JSME, Vol.9 No.36 1966, p.p 711 - 718

(86) Antonia, R.A.
Radial Diffusion with Swirl.
Australia Mechanical and Chemical Engineering Trans.
May 1968, p.p. 127 - 132.

(87) Mager, A.
Generalization of Boundary Layer Momentum Integral Equations to Three-Dimensional Flows including those of Rotating Systems.
NACA Report 1067, 1952.

(88) Stastny, M., Feistauer, M.
Flow in an Annular Axial-Radial Diffuser.
ASME Paper No. 78-GT-133,

(89) Ghoose, S., Kline, S.J.
The Computation of Optimum Pressure Recovery in Two-Dimensional Diffusers.
Journal of Fluids Engineering, Dec. 1978, Vol.100
p.p 419 - 426.

(90) Ayres, F.,Jr.
Differential Equations
Schaum's Outline Series, McGraw-Hill Book Company.

(91) Nash, J.F., Patel, V.C.
Three-Dimensional Turbulent Boundary Layers
SBC Technical Books, 1972.

(92) Ludwieg, H., Tillman, W.
Untersuchungen uber die Wandschub-Spannung in Turbulenten Reibungsschichten
Ing. Arch. 17, P.288

(93) Wheeler, A.J., Johnston, J.P.
Three-Dimensional Turbulent Boundary Layers Data Sets for Two-Space Coordinate Flows.
Report NASA-CR-138962 N74-29653.
Stanford University Thermoscience Div. August 1972.

(94) Bryer, D.W., Pankhurst, R.C.
Pressure-Probe Methods for determining Wind Speed and Flow Direction.
National Physical Laboratory.

(95) So, R.M.C., Mellor, G.L.
An Experimental Investigation of Turbulent Boundary Layer along Curved Surfaces.
NASA CR-1940 Report, April 1972.

(96) Yeh, H.
Boundary Layer along Annular Walls in a Swirling Flow
Trans. ASME, May 1958/767

(97) Meroney, R.N., Bradshaw, P.
Turbulent Boundary Layer Growth over a Longitudinally Curved Surface
AIAA Journal, Vol.13, No.11 p.1448

(98) Marris, A.W.
Radial Distribution of Temporal-Mean Peripheral Velocity and Pressure for fully developed Turbulent Flow in Curved Channels.
Journal of Basic Engineering, Sept.1966, p.p 528-538.